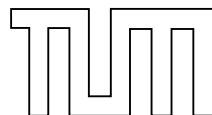


**Shape fluctuations of crystal facets
and surface growth in one dimension**

PATRIK L. FERRARI

SUPERVISED BY

PROF. DR. H. SPOHN



June 2004

Zentrum Mathematik
Technische Universität München

**Shape fluctuations of crystal facets
and surface growth in one dimension**

PATRIK L. FERRARI

Vollständiger Abdruck der von der Fakultät für Mathematik der Technischen Universität München zur Erlangung des akademischen Grades eines

Doktors der Naturwissenschaften (Dr. rer. nat.)

genehmigten Dissertation.

Vorsitzender: Univ.-Prof. Dr. Rupert Lasser
Prüfer der Dissertation: 1. Univ.-Prof. Dr. Herbert Spohn
2. Univ.-Prof. Dr. Franz Merkl,
Ludwig-Maximilians-Universität München
3. Univ.-Prof. Dr. Wolfgang König,
Universität Leipzig

Die Dissertation wurde am 07.06.2004 bei der Technischen Universität München eingereicht und durch die Fakultät Mathematik am 02.11.2004 angenommen.

Acknowledgments

I am very grateful to my supervisor Herbert Spohn for his guidance, his availability for discussions, his valuable advice, and for teaching me the importance of combining physical problems with mathematical rigor. Special thanks go to Michael Prähofer who explained me patiently their previous works facilitating my understanding of the subject. During our discussions I very much appreciated his critical thinking as well as his physical intuition. I have profited from discussions with other people too, in particular, with Tomohiro Sasamoto whose work turned out to be linked with my own, with Kurt Johansson and Richard Kenyon explaining to me their work, and Craig Tracy giving me some advice on random matrices. My thanks go also to Jani Lukkarinen for several technical discussions.

In the preparation of the manuscript, I have benefited from the advice of Herbert Spohn, and from the careful reading of Michael Prähofer who helped in reducing the number of mistakes. My thanks go also to József Lőrinczi for reading part of the manuscript and for his very good advice on English, as well as Jani Lukkarinen and Jonas Gustavsson who also read part of the thesis.

I am very grateful to Christian for being a great brother, for teaching me climbing, and for taking me to the 4000s! He also encouraged me to gain experience abroad, thus I left Lausanne for diploma work. This happened to be a decisive step on my way to Munich, for which I also thank very much my diploma adviser Joel Lebowitz. I also wish to thank Danilo and Remo of the CERFIM, my parents Giulio and Renata, and all my friends for the “healthy distractions”. In particular, Gianluca Panati with whom I could, among other things, enjoy speaking in my mother tongue!, and Stefan Großkinsky with whom I did a lot of sports and who involved me in the activities of his Wohnheim, where I could practice my German! Special thanks go to József for the (non-academic) discussions and for being an excellent guide for me and Jani to the (extended) region around Munich. I enjoyed the friendly atmosphere in Herbert’s group and, on top of those already mentioned, I wish to thank Hans Mittermeier for playing a part in it. Finally I would like to thank my first landlady Gerti Hegendörfer and her family for the nice welcome.

I also wish to thank the institutions providing the financial support. Initially, my work was supported by the “Sunburst Fonds” and the “Graduiertenkolleg Mathematik im Bereich ihrer Wechselwirkung mit der Physik”. After this the financial support was coming from the “Deutsche Forschungsgemeinschaft” under the research project SP 181/17-1.

Zusammenfassung

In dieser Dissertation betrachten wir zwei Modelle der statistischen Mechanik, eines im Nichtgleichgewicht und das andere im Gleichgewicht. Die Verbindung zwischen den Modellen liegt in den mathematischen Methoden, die für ihre Untersuchung benutzt werden.

Als erstes betrachten wir das *Polynukleare Wachstumsmodell* (PNG) in einer Raumdimension, das der KPZ-Universalitätsklasse angehört, wobei KPZ für Kardar, Parisi und Zhang steht. Für Wachstumsmodelle erwartet man, dass für grosse Wachstumszeit t die statistischen Eigenschaften nur von qualitativen Eigenschaften der Dynamik und von Symmetrien abhängen, aber nicht von den Details des Modells. Im PNG-Modell skalieren die Höhenfluktuationen für grosse Wachstumszeit t wie $t^{1/3}$ und die Korrelationslänge wie $t^{2/3}$. Prähofer und Spohn haben bewiesen, dass die statistischen Eigenschaften einer tropfenförmigen Oberfläche vom Airy-Prozess beschrieben werden. Dieses Ergebnis wurde durch die Erweiterung der Oberfläche zu einem Multi-layer-Modell erhalten. In dieser Dissertation betrachten wir den translationsinvarianten Fall und bestimmen den asymptotischen Punktprozess an einer festen Stelle. Wir beweisen, dass dieser Punktprozess der Skalierung von Eigenwerten am Rand des Spektrums einer Zufallsmatrix des Gausschen Orthogonalen Ensembles (GOE) entspricht.

Zweitens betrachten wir ein vereinfachtes Modell einer Kristallecke: die *3D-Ising-Ecke* für tiefe Temperaturen. Die Ecke besteht aus drei Facetten, die durch eine gerundete Fläche verbunden sind, siehe Abbildung 1.1 in der Einleitung. Wir analysieren die Begrenzungslinie einer der Facetten. Wenn die Kristallecke eine typische Ausdehnung der Länge L hat, dann haben die Fluktuationen der Begrenzungslinie die Grössenordnung $L^{1/3}$, und die longitudinalen Korrelationen skalieren wie $L^{2/3}$. Wir beweisen, dass die richtig skalierte Begrenzungslinie vom Airy-Prozess gut beschrieben wird. Das ist auch der Fall für das “terrace-ledge-kink”-Modell (TLK) und deshalb erwarten wir, dass der Airy-Prozess die Facettenbegrenzungen für die Modelle beschreibt, die der Universalitätsklasse mit kurzreichweitigen Wechselwirkungen angehören.

Obwohl die zwei Modelle physikalisch sehr unterschiedliche Systeme beschreiben, werden für ihre Untersuchung ähnliche mathematische Methoden benutzt. Beide Modelle können auf eine Menge von sich nicht überkreuzenden Linien abgebildet werden, die man auch als Trajektorien von Fermionen interpretieren kann. Für diese Linien definiert man einen Punktprozess. Für die 3D-Ising-Ecke besteht er in einem erweiterten deterministischen Punktprozess, dessen Kern gegen den erweiterten Airy-Kern konvergiert. Der Airy-Kern erscheint auch in der Randskalierung von Dysons Brownscher Bewegung für GUE-Zufallsmatrizen. Der Prozess für das PNG-Modell ist ein Pfaffscher Punktprozess (an einer festen Stelle) und sein 2×2 -Matrixkern konvergiert gegen den der GOE-Zufallsmatrizen. In der Dissertation diskutieren wir auch die Verbindung zu einigen anderen Modellen: das Problem der längsten steigenden Teilfolgen, gerichtete Polymere, “last passage percolation”, der total asymmetrische Ausschlussprozess, zufällige Parkettierungen und 3D-Young-Diagramme.

Abstract

In this thesis we consider two models, the first belonging to non-equilibrium and the second one to equilibrium statistical mechanics. The two models are connected the mathematical methods used to their analysis.

The first model analyzed is the *polynuclear growth model* (PNG) in one dimension, which belongs to the KPZ (Kardar-Parisi-Zhang) universality class. For growth processes, when the growth time t is large, the statistical properties of the surface are expected to depend only on qualitative properties of the dynamics and on symmetries, but not on the details of the models. In the case of the PNG, for large growth time t the surface height fluctuations scale as $t^{1/3}$ and the spatial correlation length as $t^{2/3}$. For boundary conditions inducing a droplet shaped surface, it was shown by Prähofer and Spohn that the statistics of the surface is described by the Airy process. This result was obtained by extending the surface line to a multi-layer model. In this thesis we consider the space-translation invariant case and determine the limit point process of the multi-layer model at fixed position. The process coincides with the edge scaling of eigenvalues of the Gaussian orthogonal ensemble (GOE) of random matrices.

The second model we study is the *3D-Ising corner* at zero temperature. The corner of the crystal is composed by three facets (flat pieces) and a rounded piece interpolating between them, see Figure 1.1 in the Introduction for an illustration. We analyze the border line between the rounded and a flat piece. When the corner defect size is large, say of linear length L , the fluctuations of the border line are of order $L^{1/3}$ and the spatial correlation length scales as $L^{2/3}$. We prove that the (properly rescaled) border line is well described by the Airy process. This is also the case for the terrace-ledge-kink (TLK) model, a simple model used to describe surfaces close to the high symmetry ones. We expect that the Airy process describes the border of the facets in the class of surface models with short range interactions.

Although the two models describe physically very different systems, the mathematical methods employed for their investigation are similar. Both models can be mapped into some non-intersecting line ensembles, which can also be viewed as trajectories of fermions. One can associate some point processes to the line ensembles. For the 3D-Ising corner it is an extended determinantal point process, whose kernel converges to the extended Airy kernel. The Airy kernel appears also in the edge scaling of Dyson's Brownian motion for GUE random matrices. The process for the PNG is a Pfaffian point process (at fixed position) and the 2×2 matrix kernel converges to the one of GOE random matrices. In the thesis we also discuss the connection with some other models: the longest increasing subsequence problem, directed polymers, last passage percolation, totally asymmetric exclusion process, random tiling, 3D-Young diagrams, and indirectly, Gaussian ensembles of random matrices.

Versione abbreviata

Premessa: la versione italiana dell'abstract è rivolta al lettore "comune" e non propriamente ai fisici e/o matematici. A quest'ultimi si consiglia di leggere la versione inglese e l'introduzione, dove il lavoro è presentato in modo più dettagliato.

In questo lavoro di dottorato studiamo due problemi di meccanica statistica, il primo riguarda un modello di crescita (fuori equilibrio) e il secondo descrive un sistema in equilibrio (termodinamico).

Innanzitutto abbiamo considerato un modello che descrive la crescita di una "superficie" su di un substrato unidimensionale, dunque la superficie è una linea. Si pensi ad un materiale poroso fine, ad esempio un foglio di carta, che viene messo a contatto con un liquido. Con il passar del tempo il bordo tra la parte bagnata e quella asciutta cresce globalmente in modo regolare, pur presentando alcune irregolarità. In altre parole, se prendiamo due campioni diversi per fare lo stesso esperimento e osserviamo la linea che delimita la parte bagnata dopo un lasso di tempo uguale, vedremo piccole differenze, fluttuazioni. Nel nostro modello, chiamato *modello di crescita polinuclere*, abbiamo posto l'attenzione sulle proprietà statistiche della superficie in crescita, come le fluttuazione sopraccitate.

Il secondo è un modello semplificato di un angolo di un cristallo, chiamato *3D-Ising corner*. L'angolo consiste in tre facce lisce e una parta arrotondata che le interpola, vedi Figura 1.1 a pagina 2 dell'introduzione. Abbiamo posto la nostra attenzione sulla linea che separa la regione arrotondata da una delle facce lisce. Se "guardata da lontano" questa linea ha una forma ben definita, ma facendo un ingrandimento ci si accorge che il dettaglio dipende dal campione preso in considerazione. Infatti ci sono delle fluttuazioni, le quali, assieme ad altre proprietà statistiche, sono state studiate in questo lavoro.

Apparentemente i due modelli non hanno un granché in comune. In effetti dal punto di vista fisico i sistemi presi in considerazione sono molto diversi. L'unica analogia immediata è che studiamo in entrambi i casi interfacce "unidimensionali", cioè delle linee. Ciononostante una connessione esiste ed è dovuta alla descrizione matematica dei due sistemi. Infatti, entrambi possono essere descritti da un insieme di linee che non si intersecano. A loro volta queste linee sono reinterpretate come traiettorie di particelle su una linea retta, le quali non vengono mai in contatto tra di loro. La conseguenza è che caratteristiche simili possono essere riscontrate nei due modelli analizzati. Ad esempio, le proprietà statistiche che abbiamo riscontrato nel "3D-Ising corner" sono le stesse precedentemente trovate da Prähofer e Spohn nel modello di crescita polinucleare nel caso in cui l'interfaccia prende la forma di una goccia.

Contents

1	Introduction	1
2	From directed polymers to polynuclear growth model and 3D-Ising corner	7
2.1	Directed polymers and longest increasing subsequence	7
2.1.1	The Poisson process	7
2.1.2	Directed polymers on Poisson points	8
2.1.3	Directed polymers and longest increasing subsequences	14
2.1.4	Young tableaux and increasing subsequences	15
2.1.5	Discrete analogous of directed polymers	17
2.2	Polynuclear growth model (PNG)	20
2.2.1	Polynuclear growth model and Poisson points	20
2.2.2	Longest directed polymers and surface height	21
2.2.3	Discrete time version of the polynuclear growth model	23
2.2.4	Recent developments on 1D polynuclear growth model	25
2.2.5	Universality	27
2.3	3D-Ising model at zero temperature	28
2.3.1	The model	28
2.3.2	3D-Ising corner and directed polymers	30
2.3.3	Bulk and edge scaling	31
2.3.4	Universality of shape fluctuations of crystal shapes	33
2.3.5	On general macroscopic facets	38
3	Line ensembles and point processes	41
3.1	Point processes	41
3.1.1	Determinantal point processes	41
3.1.2	Pfaffian point processes	45
3.2	Random matrices	47
3.2.1	Classical Gaussian random matrix ensembles	47
3.2.2	GUE eigenvalues: a determinantal process	51
3.2.3	GOE and GSE eigenvalues: Pfaffian processes	53
3.3	Extended determinantal point processes	56
3.3.1	Dyson's Brownian motion	56
3.3.2	Extended point process	58

3.3.3	Airy process	61
3.4	Description of the systems via line ensembles	62
3.4.1	Line ensemble for the polynuclear growth model	62
3.4.2	Line ensemble for 3D-Ising corner	65
4	Analysis of the flat PNG line ensemble	69
4.1	Formulation of the result	69
4.2	Line ensemble	71
4.2.1	Line ensemble for the \square symmetry	71
4.2.2	Flat PNG and line ensemble for \square symmetry	74
4.3	Correlation functions	75
4.4	Kernel for finite T	78
4.5	Edge scaling and asymptotics of the kernel	82
4.6	Proof of Theorem 4.1	86
4.A	Appendices	91
4.A.1	Bounds on the inverse of A	91
4.A.2	Some bounds and relation on Bessel functions	92
5	Analysis of the 3D Ising corner line ensemble	97
5.1	Formulation of the main result	97
5.2	Extended determinantal point process	98
5.2.1	Fermions	98
5.2.2	Correlation functions	103
5.3	Limit shape	104
5.4	Bulk scaling, local equilibrium	106
5.5	Edge scaling	111
5.6	Proof of Theorem 5.1	125
5.A	Appendix: fermionic correlations	126
5.A.1	Two-point function	126
5.A.2	Proof of (5.41)-(5.43)	127
	Appendix	129
A.1	Equilibrium crystal shape geometry	129
A.2	Fredholm determinant and Fredholm Pfaffian	130
A.2.1	Preliminaries	130
A.2.2	Fredholm determinant	131
A.2.3	Fredholm Pfaffian	133
A.3	Real quaternionic matrices	133
A.4	Gaussian ensembles via variational principle	134
A.5	Hermite polynomials	135
A.6	Kernel for $\beta = 2$ Dyson's Brownian motion	136
A.7	Convergence of the extended Hermite kernel to the extended Airy kernel	137
A.8	Numerical analysis	139
	Bibliography	141

Chapter 1

Introduction

The title of the thesis refers to two subjects. The first, *shape fluctuations of crystal facets*, belongs to equilibrium statistical mechanics. The studied system is a crystal and we are interested in the fluctuations of the flat pieces of the surface, called facets. The second, *surface growth in one dimension*, is part of non-equilibrium statistical mechanics. One considers a surface which grows above a one-dimensional substrate due to deposition of atoms. The two physical systems described are very different and at first sight there is no reason why they should share common features. However, as we will discover and explain in great detail in our work, the two problems are linked to each other.

A crystal in equilibrium at very low temperature consists essentially of facets (flat pieces) which are connected forming sharp angles. When the temperature is increased, the facets become smaller and are interpolated by some rounded surfaces of the crystal, and eventually all the facets have disappeared. On the other hand, if the temperature is above some T_M the crystal melts. The shape of the crystal is determined by the surface free energy, and the solid-liquid transition by the total free energy. We just introduced the term *facet* to designate an intuitive quantity, but due to thermal fluctuations it might not be always a well defined object. For a surface with a fixed orientation, the free energy per unit length of a step in the surface decreases as the temperature is increased, and vanishes above some temperature T_R . In the latter case, there is no longer any mechanism preventing the formation of extra steps, and the surface becomes rough. T_R is called roughening temperature and depends on the orientation of the surface. For high-symmetry surfaces, e.g. (1 0 0) or (1 1 1) for a cubic lattice, the roughening temperature is larger than the melting temperature T_M for most materials. The situation changes for the surfaces whose orientations are close to a high-symmetry one, called vicinal surfaces. For example, consider the surface (0 0 1) and their vicinal surfaces (1 1 n) for large n . They consist of a succession of (0 0 1) terraces separated by steps. Those steps that are not at equal distance have to pay an energy ε for each atom of the step. When ε is small enough, a vicinal surface can be rough already at fairly low temperature compared with T_M , i.e., $T_R \ll T_M$. To the reader interested in the physical background we suggest for further details the book *Physics of Crystal Growth* by Pimpinelli and Villain [73].

We are interested in the statistics of the facets' borders in the temperature range where

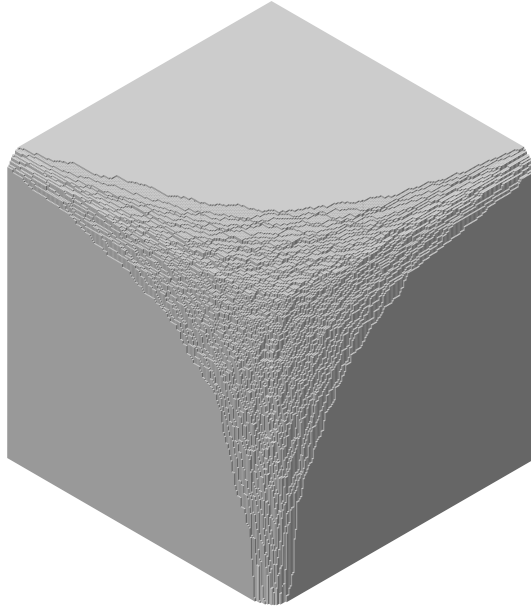


Figure 1.1: Crystal corner viewed from the (111) direction.

they live on a mesoscopic scale, large with respect to the atomic scale, but small with respect to the macroscopic one. Therefore we consider temperatures not too small but also (considerably) less than T_R , since above T_R the facets are no longer recognizable. In this temperature range, the facets are macroscopically flat and well localized, but on a microscopic scale irregularities still occur due to thermal fluctuations. This happens also close to the borders of the facets, which are then not uniquely defined. Nevertheless one can define a coarse-grained border of the facets, because the irregularities are relevant only on the atomic scale. Depending on the material and on the facet orientations, the facets are smooth up to some hundreds of kelvins, thus also at room temperature. Figure 1.1 is a computer-generated image of the model we actually study. It is called the 3D-Ising corner. The facets are perfectly flat and their borders are easily recognizable.

We consider large crystals at equilibrium with fixed number of atoms N . This is the fixed volume constraint, under which there is a Gibbs measure on the possible crystal configurations. The equilibrium crystal shape is the expected shape under the measure. It is determined by minimizing the surface free energy under the volume constraint. The formation of facets with a specific orientation depends on the energy of interactions between the atoms and the structure of the crystal. Since we are interested in the statistical properties of the (coarse-grained) border of the facets induced by the Gibbs measure, we consider N sufficiently large so that the border fluctuations are in an intermediate scale between the atomic distance and the macroscopic one. When N becomes very large, the width of the fluctuations is expected to become independent of the details of the microscopic model and depend only on some qualitative properties, like whether the interactions have short or long range. This is universality hypothesis. The models which show the same fluctuations

are said to be in the same universality class. For example, the model studied in this thesis belongs to the class of models with short range interactions.

Growth processes belong to non-equilibrium statistical mechanics, whose aim is to explain the macroscopic and mesoscopic properties from (simple) microscopic laws. There are different types of growth to be distinguished. A solid can grow in a solution (or in a vapor) and the growth depends on the concentration (or on the partial pressure) of the atoms of the growing solid. Another way of growth, put at actual use in laboratories, is molecular beam epitaxy (MBE). It consists of ejecting single atoms (or molecules) onto the surface under ultra-high vacuum conditions. What happens to the atoms when they reach the surface? At very low temperature they essentially stick to the location where they arrive. At higher temperatures the atoms diffuse for a while on the surface until meet a preexisting step and stay there, or they meet another diffusing atom and stick together forming a dimer. The mobility of a dimer is much reduced and other atoms attach to it forming a growing island. If the temperature is high enough, small clusters are not stable and break up time and again. Therefore the atoms diffuse until they meet a preexisting step. Another phenomenon which can occur when a crystal is growing by deposition are instabilities. For example, a diffusing atom reaching the boundary of an island has a tendency to be reflected and thus remains on the island. In this case, islands grow only when atoms moving on a lower level attach to it. This creates a surface which resembles to an ensemble of steep mountains with deep valleys. Instabilities can occur also in growth from a liquid, mainly for two-dimensional systems, in which case the shape is not convex but lots of spikes appear. Growth occurs also in the atmosphere where water molecules form hailstones or snow flakes. Let us finally note that growth processes can include also other phenomena, like the spread of a liquid in a porous medium, where the growing quantity is the wetted region, or even the spread of a fire line in a forest. The border of the surface can be one or two dimensional, or even have (on a certain scale) a fractal dimension. To the reader interested in the physical background we suggest the books *Physics of Crystal Growth* by Pimpinelli and Villain [73], *Fractal Concepts in Surface Growth* by Barabási and Stanley [15], and *Islands, Mounds and Atoms* by Michely and Krug [63].

In our work we consider a surface growth model on a one dimensional substrate. We are interested in statistical properties of the growing surface for large growth times. They are expected to be independent on the details of the model and depend uniquely on qualitative properties like conservation laws and symmetries (phenomenon of universality). In particular, one can try to find the scale invariant quantities, that is, those showing the same quantitative law under the appropriate rescaling of space and time. A growth is said to be local if the new material added to the surface depends only on local properties of the surface. A smoothening mechanism prevents the surface from producing, for example, spikes. This is the case of local diffusion of atoms from the high to the low parts of the surface. When growth is local and has a smoothening mechanism, the growing cluster has a well defined interface and on the macroscopic level its growth is deterministic, thus it has a macroscopic limit shape. The fluctuations with respect to the mean macroscopic shape are relevant only on a mesoscopic level. This is the observable we are mainly in-

terested in. The most studied class of local growth models is KPZ universality class. In one dimension, it is characterized by the extra requirement that the speed of growth as a function of the slope of the tangent surface has a non-zero curvature. The KPZ model was introduced by Kardar, Parisi, and Zhang where they described a random surface growth by a stochastic differential equation. It is the simplest equation for the dynamics of an interface which includes irreversibility, nonlinearity, randomness, and locality. It contains a Laplacian term which smoothes the surface and contrasts a local noise term, and a non-linear term, the square of the surface gradient, which expands the hills laterally. In our thesis we study a model in the KPZ universality class in one dimension.

Now that the class of models are explained we can come back to the question of the similarities between growth in one dimension and border facets of equilibrium crystals. On a macroscopic level, that is for large growth time t , a one dimensional growing surface having a limit shape can be parameterized by a single-valued height function. This is also the case of the border of a facet at equilibrium. In the example of Figure 1.1 we fix the coordinate axis so that the facets are in the surfaces with (001) , (010) , (100) directions meeting at the origin. Then the boundary of the (001) facet is a curve in the xy -plane described as a height function. The distance to the origin scales as L if the missing volume of the corner scales as L^3 . On a microscopic scale we still can describe the growing surface and the border of the facet by a height function if we do a coarse graining. Therefore both models can be described in a similar way. Of course, this does not yet mean that the models have any relevant statistical property in common. For KPZ growth in one dimension, the height fluctuation above a fixed position scales as $t^{1/3}$ and the height at two different points are correlated on a distance of order $t^{2/3}$. This is exactly what happens for the case of the 3D-Ising corner too, where the role of t is taken over by L . Moreover, in the growth model we consider, when initial conditions create a growing droplet, the height profile is described by an Airy process. This process also describes the border of the facet in the 3D-Ising corner! The reason of these similarities lies in the underlying mathematical description of the two models. In fact both models can be mapped into some non-intersecting line ensembles having the same mathematical structure.

Finally a note on the structure of the thesis. Instead of starting immediately from the study of the above models, we first introduce directed polymers. The reason is that directed polymers are directly connected to the models, they are the link between them. We begin by describing the problem of the longest length of directed polymers in a Poisson point process. This model is directly related to the longest increasing subsequence in a random permutation. We also present a discrete analogue, that is, directed polymers on \mathbb{Z}^2 . This is made in the first part of Chapter 2. The second part is devoted to the surface growth model we study: the polynuclear growth (PNG) model. It is known that the height of the surface is the same as the longest length of directed polymers on Poisson points. The PNG droplet is obtained when the surface grows above a single spreading island. An important result of Prähofer and Spohn on the PNG droplet is that the fluctuations of the surface height are described by the Airy process. We also present a discrete version of the PNG model and

shortly discuss the question of universality. In the third part of Chapter 2 we consider the model of a crystal which we actually study: the 3D-Ising corner. The border of the facets can be expressed via the lengths of some directed polymers on \mathbb{Z}^2 . Our new result is that the fluctuations of the facet boundary are described by the Airy process. With this result we then discuss the question of universality of the fluctuations of the facet borders.

Chapter 3 is devoted to the explanation of the point processes which occur in our analysis. First we review the concept of point processes with particular focus on determinantal and Pfaffian ones. Secondly we introduce the Gaussian ensembles of random matrices, whose eigenvalues are point processes. Of particular interest are point processes of top eigenvalues when the size of the matrices goes to infinity, and the distribution of the largest eigenvalue. These point processes are also the limiting ones of our models. Dyson's Brownian motion describes an evolution of the eigenvalues of the Gaussian ensembles. Starting from it we then discuss the generalization of the point processes when they are subject to an evolution. In the last part of the chapter we go back to the PNG and 3D-Ising corner models. We explain how they are mapped to some set of non-intersecting line ensembles. The position of the lines form an extended point process. For the 3D-Ising corner they are an extended determinantal point process. This is also the case for the PNG droplet and is the reason why both models are described by the Airy process. Also the evolution of the largest eigenvalue in Dyson's Brownian motion for hermitian matrices is described by the Airy process. If the constraint that the surface grows only above one island is suppressed, then the surface is statistically translation invariant. This is called the flat PNG and only its one-point distribution is known. The space correlations are not yet known, but the conjecture is that it is the same as the evolution of the largest eigenvalue for Dyson's Brownian motion in the case of symmetric matrices. For fixed position, the line ensemble of the flat PNG is a point process. Our novel finding is that this point process, in the limit of large growth time, is the same as the point process for fixed time of the eigenvalues of Dyson's Brownian motion for symmetric matrices, in the limit of large matrix size. This is a step towards the just explained conjecture.

Chapter 4 contains our new result on the flat PNG as well as its rigorous derivation. Similarly, in Chapter 5 we present our new result on the 3D-Ising corner model and analyze it. In the Appendix we include various results completing the discussions of Chapters 2 and 3.

Chapter 2

From directed polymers to polynuclear growth model and 3D-Ising corner

2.1 Directed polymers and longest increasing subsequence

To describe the problem considered in this section we first have to introduce the Poisson process. Then we define the directed polymers on Poisson points, give some known results and connections with other problems, in particular with the longest increasing subsequence.

2.1.1 The Poisson process

Consider a Borel set \mathcal{D} of \mathbb{R}^2 which can either be bounded or unbounded. The Poisson process on \mathcal{D} is a point process $(\Omega, \mathcal{F}, \mathbb{P})$ defined as follows. Let ω be a countable configuration of points in \mathcal{D} . For any compact subset B of \mathcal{D} , denote the number of points of ω in B by $n(B)(\omega)$. Then

$$\Omega = \{\omega | n(B)(\omega) < \infty, \forall \text{ compact } B \subset \mathcal{D}\} \quad (2.1)$$

is the set of all locally finite configurations of points in \mathcal{D} . Let \mathcal{F} be the σ -algebra of events on Ω .

Definition 2.1. A Poisson process of intensity $\varrho > 0$ in \mathcal{D} is given by setting the probability \mathbb{P} such that, for all compact $B \subset \mathcal{D}$,

$$\mathbb{P}(\{n(B) = k\}) = \frac{(\varrho|B|)^k}{k!} e^{-\varrho|B|} \quad (2.2)$$

and events on disjoint subsets of \mathcal{D} are independent: for all $m \in \mathbb{N}$, $k_1, \dots, k_m \in \mathbb{N}$, and $B_1, \dots, B_m \subset \mathcal{D}$, if $B_i \cap B_j = \emptyset$ for $i \neq j$, then

$$\mathbb{P}\left(\bigcap_{i=1}^m \{n(B_i) = k_i\}\right) = \prod_{i=1}^m \mathbb{P}(\{n(B_i) = k_i\}). \quad (2.3)$$

More generally one can fix a locally integrable intensity $\varrho : \mathcal{D} \rightarrow \mathbb{R}_+$. Then the Poisson process with density $\varrho(x)$ is defined as before up to the following modification of (2.2). Let

$$\bar{\varrho}(B) = |B|^{-1} \int_B dx \varrho(x), \quad (2.4)$$

then (2.2) is replaced by

$$\mathbb{P}(\{n(B) = k\}) = e^{-\bar{\varrho}(B)} \bar{\varrho}(B)^k / k!. \quad (2.5)$$

2.1.2 Directed polymers on Poisson points

Point-to-point problem

We introduce a partial ordering \prec as follows. For $x, y \in \mathbb{R}^2$ we say that $x \prec y$ if both coordinates of x are strictly less than those of y . Consider a Poisson process with intensity ϱ in \mathbb{R}^2 .

Definition 2.2. A directed polymer on Poisson points *starting at S and ending at E* is a piecewise linear path π connecting $S \prec q_1 \prec \dots \prec q_{l(\pi)} \prec E$, $q_i \in \omega$ Poisson points. The length $l(\pi)$ of the directed polymer π is the number of Poisson points visited by π .

We denote by $\Pi(S, E)(\omega)$ the set of directed polymers from S to E . The maximal length of $\pi \in \Pi(S, E)(\omega)$ is

$$L(S, E)(\omega) = \max_{\pi \in \Pi(S, E)(\omega)} l(\pi). \quad (2.6)$$

A directed polymer of maximal length is also called *maximizer* and the set of maximizers is denoted by $\Pi_{\max}(S, E)(\omega)$. This is the *point-to-point* setting because both initial and final points are fixed. Figure 2.1 is a realization of the Poisson process with intensity 1 in the square $[0, 15]^2$. The highest and lowest maximizers are visualized.

Some questions one would like to answer are:

- a) What is the distribution of the maximal length?
- b) How does this distribution depend on the relative positions of S and E ?
- c) Where are typically located the points of the maximizers?

The answer to question b) is simple. Take as starting point $S = (0, 0)$ and the two following end-points, $E_1 = (t, t)$ and $E_2 = (\gamma t, \gamma^{-1} t)$ for some $\gamma \geq 1$. Denote by R_1 , resp. R_2 , the rectangle with opposite corners S and E_1 , resp. E_2 . Consider the bijective mapping $\Phi : \mathbb{R}^2 \rightarrow \mathbb{R}^2$ defined by $\Phi(x, y) = (\gamma x, \gamma^{-1} y)$. Φ preserves the distribution on points and $\Phi(R_1) = R_2$. Moreover, a directed polymer in R_1 is mapped into a directed polymer in R_2 . Consequently the distribution of $L(S, E)$ depends only on the area of the rectangle with opposite corners S and E . Therefore we consider $S = (0, 0)$, $E = (t, t)$, and denote the maximal length by $L(t) = L(S, E)$.

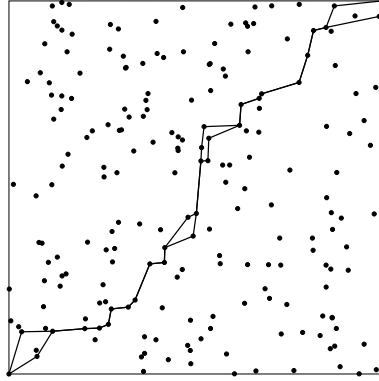


Figure 2.1: A realization of Poisson points with density $\rho = 1$ in the square of edge-length 15. The highest and lowest directed polymers of maximal length are shown.

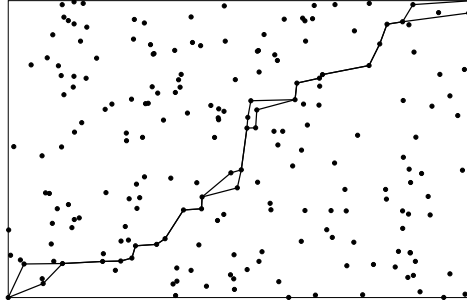


Figure 2.2: Realization of Figure 2.1 transformed by Φ with $\gamma = 1.25$.

Question a), in the $t \rightarrow \infty$ limit, was settled by Baik, Deift, and Johansson in their already famous paper [10]. Their result reads

$$\lim_{t \rightarrow \infty} \mathbb{P} \left(\frac{L(t) - 2t}{t^{1/3}} \leq s \right) = F_2(s) \quad (2.7)$$

where F_2 is the GUE Tracy-Widom distribution [100]. In other words for large t

$$L(t) \simeq 2t + t^{1/3} \zeta_{\text{GUE}} \quad (2.8)$$

with ζ_{GUE} a random variable F_2 -distributed. The *length fluctuation exponent* $1/3$ in (2.8) is denoted by χ .

Question c) has an answer in terms of the *transversal fluctuation exponent* ξ defined as follows. Denote by $C_\gamma(t)$ the cylinder of width t^γ around the segment $(0, 0) \rightarrow (t, t)$,

$$C_\gamma(t) = \{(x, y) \in \mathbb{R}^2 \mid 0 \leq x + y \leq 2t, |y - x| \leq \sqrt{2}t^\gamma\}. \quad (2.9)$$

Consider the set of configurations ω such that all the maximizers are contained in $C_\gamma(t)$,

$$A_\gamma(t) = \{\omega \in \Omega \mid \pi \subseteq C_\gamma(t) \text{ for all } \pi \in \Pi_{\max}(t)(\omega)\} \quad (2.10)$$

where $\Pi_{\max}(t)(\omega) \equiv \Pi_{\max}((0, 0), (t, t))(\omega)$. Then ξ is defined by

$$\xi = \inf\{\gamma > 0 \mid \liminf_{t \rightarrow \infty} \mathbb{P}(A_\gamma(t)) = 1\}. \quad (2.11)$$

Johansson proves [44] that for this model $\xi = 2/3$. Since $\xi > 1/2$, the directed polymers are *superdiffusive*.

The previous results, $\chi = 1/3$ and $\xi = 2/3$, implies that the scaling identity

$$\chi = 2\xi - 1 \quad (2.12)$$

holds for this model. (2.12) is expected to hold in any dimensions for a large class of related models, like growing surfaces, first and directed last passage percolation. We discuss it further in section 2.1.5 for directed last passage percolation on \mathbb{Z}^d . An heuristic argument leading to the scaling relation (2.12) is the following. The length of a typical path from $(0, 0)$ to (x, y) is $\sim 2\sqrt{xy}$. Hence, a maximal path from $(0, 0)$ to (t, t) that passes through $(t(\alpha - \delta), t(\alpha + \delta))$, $0 < \alpha < 1$, δ small, is shorter by the amount

$$2t\sqrt{(\alpha + \delta)(\alpha - \delta)} + 2t\sqrt{(1 - \alpha - \delta)(1 - \alpha + \delta)} - 2t \simeq \frac{t\delta^2}{\alpha(1 - \alpha)} \quad (2.13)$$

which should be of the same order of the fluctuations t^χ . Therefore $\delta^2 \sim t^{\chi-1}$, and $t^\xi \sim t\delta \sim t^{(\chi+1)/2}$.

Point-to-line problem

A modification of the problem consists in considering the set of directed polymers starting from $(0, 0)$ and ending in the segment of line $U_t = \{(x, y) \in \mathbb{R}_+^2 \mid x + y = 2t\}$. This is called the *point-to-line* problem. The fluctuation exponent is still $\chi = 1/3$, but the fluctuation of the maximal length, $L_\ell(t)$, is governed by the GOE Tracy-Widom distribution [101] $F_1(s)$,

$$\lim_{t \rightarrow \infty} \mathbb{P}\left(\frac{L_\ell(t) - 2t}{t^{1/3}} \leq 2^{-2/3}s\right) = F_1(s), \quad (2.14)$$

that is, $L_\ell(t) \simeq 2t + 2^{-2/3}t^{1/3}\zeta_{\text{GOE}}$ for large t , with ζ_{GOE} a random variable F_1 -distributed. This result follows from related problems [13, 77]: the longest increasing subsequence, see Section 2.1.3, and the polynuclear growth model which is discussed in Section 2.2.

For the point-to-line problem, some other questions arise. The first we discuss is about the (non-)uniqueness of the end-point of the maximizers. Consider the set of directed polymers of maximal length from $O = (0, 0)$ to U_t , denoted by $\Pi_{\max}(O, U_t)$. For any $\pi \in \Pi_{\max}(O, U_t)$, denote by $E(\pi) \in U_t$ the closest point on U_t to the last Poisson point of π . The question is to know whether typically the directed polymers of maximal length ends in a unique point or not. Denote by $\text{deg}(\omega)$ the number of such points. Some numerical studies indicates that deg has a distribution which is not reduced to a point mass. For large t ,

$$\mathbb{P}(\text{deg}(\omega) = k) \simeq (q^{-1} - 1)q^k, \quad k \geq 1, \quad (2.15)$$

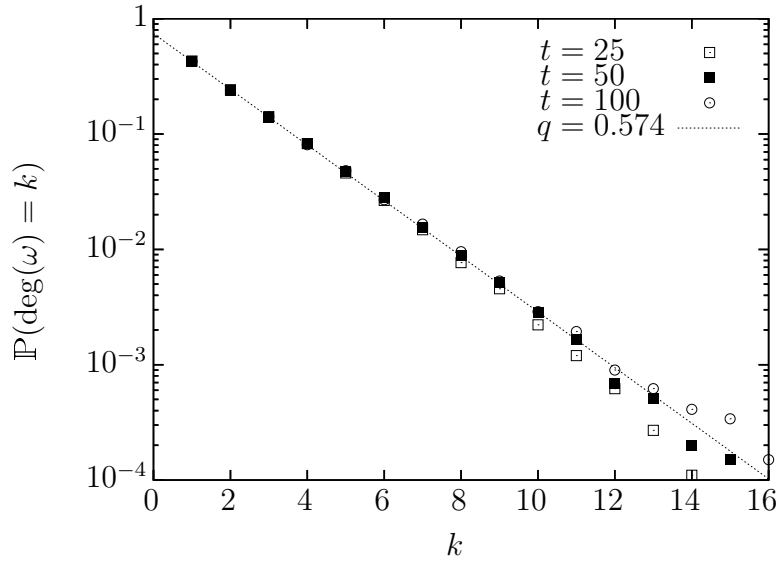


Figure 2.3: Probability distribution deg for $t = 25, 50, 100$ over 10^5 runs for each t , and the fit obtained for $q = 0.574$.

with $q = 0.574 \pm 0.005$, i.e., $\mathbb{E}(\text{deg}) \simeq 2.35 \pm 0.03$, see Figure 2.3. We run a simulation up to $t = 1000$ but only over 10^3 runs. The average value of end points was about 2.4 ± 0.1 . We then made the simulation for $t = 25, 50, 100$ for 10^5 runs, and the fit of these results is $q = 0.574 \pm 0.005$, which means that the average number is 2.35 ± 0.03 .

Since $E(\pi)$ is typically not unique, we investigate a second random variable: the maximal distance between the $E(\pi)$'s. Let π_+ , resp. π_- , be in $\Pi_{\max}(O, U_t)$ such that the distance $d(t) = |E(\pi_+) - E(\pi_-)|$ is maximal. The simulations for $t = 25, 50, 100$ over 10^5 runs show the following behaviors.

- 1) There is a frequency of $a = 42.6\% \pm 0.5\%$ that the end point is unique, i.e., that $d = 0$. Therefore the distribution of d has the form $a\delta(x) + \rho_t(x)$.
- 2) For small distances, ρ_t has a limit behavior without needing to be rescaled in t , see Figure 2.4, but when d is increased ρ_t shows the t -dependence, see Figure A.6 in Appendix A.8.
- 3) The density ρ_t extends over an interval $\mathcal{O}(t^{2/3})$ and then has (super-)exponential cutoff. Define the rescaled density $\rho_r(\xi) = \rho_t(x = \xi t^{2/3})t^{2/3}$. If we plot $\xi \mapsto t^{1/3}\rho_r(\xi)$ then we have a good collapse of the functions for different values of t , see Figures 2.5 and A.7.

Now consider the distribution of $d_r = d/t^{2/3}$. The above results imply that it has a delta peak at the origin plus a density ρ_r . For large t , the contributions of small distance, 2), much smaller than $\mathcal{O}(t^{2/3})$, sum up with the frequency a and create the delta peak at zero, $a_t\delta(\xi)$. For the density, define $f(\xi) = \lim_{t \rightarrow \infty} t^{1/3}\rho_r(\xi)$. For large t , the probability measure μ of the rescaled distance d_r is

$$\mu(\xi) \simeq a_t\delta(\xi) + t^{-1/3}f(\xi). \quad (2.16)$$

$x \mapsto f(\xi)$ is a continuous function which has a polynomial decay at the beginning and is

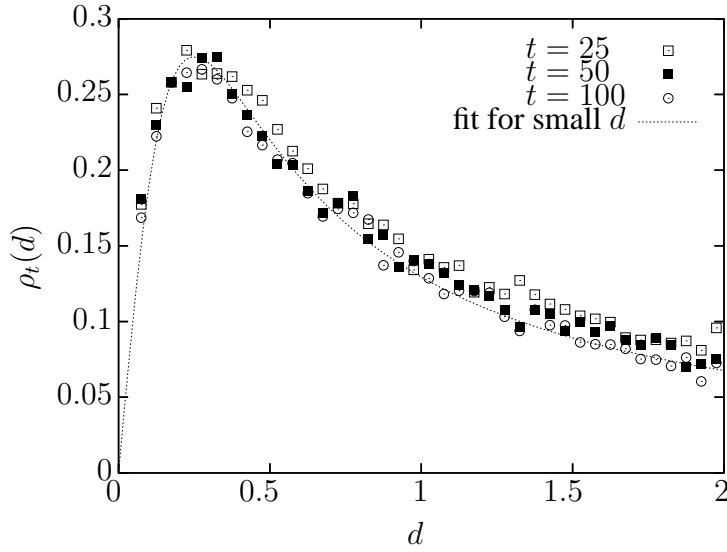


Figure 2.4: Probability density of the distribution of the distance d for $t = 25, 50, 100$ and small d . The fit is best for $t = 50, 100$ and is $\rho = 2.2d(1 + 16d^2)^{-1}$.

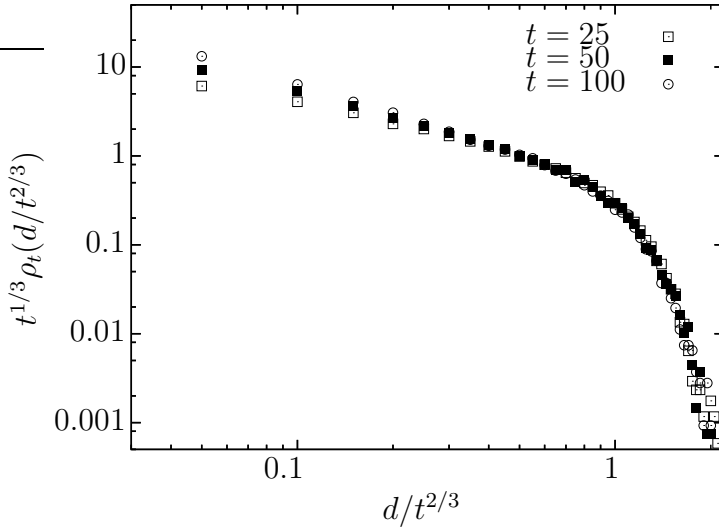


Figure 2.5: Rescaled probability density of the distribution of the distance d for $t = 25, 50, 100$.

followed by a (super-)exponential decay which becomes important close to $\xi = 1$. Our data do not permit to obtain the precise power-law decay, but they indicate that it should be $\sim \xi^{-1}$.

The normalization condition implies $a_t \simeq 1 - t^{-1/3} \int_{\mathbb{R}_+} f(\xi) d\xi$. Thus the weight of the distribution is concentrated in the central peak except for a fraction of order $t^{-1/3}$. A measure of the form (2.16) for the rescaled distance d_r implies that the moments of the

distance d are given by

$$\mathbb{E}(d^k) = t^{2k/3} \mathbb{E}(d_r^k) \simeq t^{(2k-1)/3} \int_{\mathbb{R}_+} f(\xi) \xi^k d\xi \quad (2.17)$$

for $k \geq 1$. The simulations for $t = 25, 50, 100$ leads to

$$\mathbb{E}(d)/t^{1/3} \simeq 0.55, \quad \text{Var}(d^2)/t \simeq 0.23. \quad (2.18)$$

We also made simulations also for larger values of t , up to $t = 1000$, but with only 1000 runs. The results agree with (2.17) and (2.18), see Table A.1.

A second question concerns the position of the branching of directed polymers. Consider for all points $E \in U_t$ the set of directed polymers of maximal length from $O = (0, 0)$ to E , $\Pi_{\max}(O, E)$. Take two end points E_1 and E_2 on U_t such that $|E_2 - E_1| \simeq t^\nu$, $0 < \nu \leq 1$. We say that two directed polymers π_1 and π_2 intersect at $x \in \mathbb{R}^2$ if x is a Poisson point visited by both π_1 and π_2 . Then the problem of last branching of directed polymers is the following. Define the set

$$I(E_1, E_2)(\omega) = \{x \in \omega \mid \exists \pi_1 \in \Pi_{\max}(O, E_1), \pi_2 \in \Pi_{\max}(O, E_2), x \in \pi_1 \cap \pi_2\} \quad (2.19)$$

and let $J(E_1, E_2)$ be the closest element of $I(E_1, E_2)$ to U_t . Then $J(E_1, E_2)$ is called the *last branching point* of directed polymers with end-points in E_1 and E_2 . We would like to know something about the random variable $J(E_1, E_2)$. One would expect that the branching is governed by the transverse exponent $2/3$. If $\nu = 2/3$, the last branching point should have a distance of order t from U_t with some distribution, on that scale, not reduced to a point mass. On the other hand if $\nu > 2/3$ the branching will be close to the root and if $\nu < 2/3$ the branching will be close to U_t . We give a partial answer to this problem in [30], where we prove the following estimates for the position of $J(E_1, E_2)$.

Theorem 2.3. *Let $E_1 = (t, t)$ and $E_2 = E_1 + yt^\nu(-1, 1)$ with $y \in \mathbb{R}$ fixed.*

i) For $\nu > 2/3$, there exists a $C(y) < \infty$ such that for all $\sigma > 5/3 - \nu$,

$$\lim_{t \rightarrow \infty} \mathbb{P}(\{d(O, J(E_1, E_2)) \leq C(y)t^\sigma\}) = 1. \quad (2.20)$$

ii) For $\nu \leq 2/3$ and for all $\mu < 2\nu - 1/3$ one has

$$\lim_{t \rightarrow \infty} \mathbb{P}(\{d(J(E_1, E_2), U_t) \leq t^\mu\}) = 0. \quad (2.21)$$

In particular for $\nu = 2/3$, one can choose any $\mu < 1$.

Figure 2.6 shows the set of maximizers from $(0, 0)$ to (a part of) U_t for a realization with $t = 2000$.

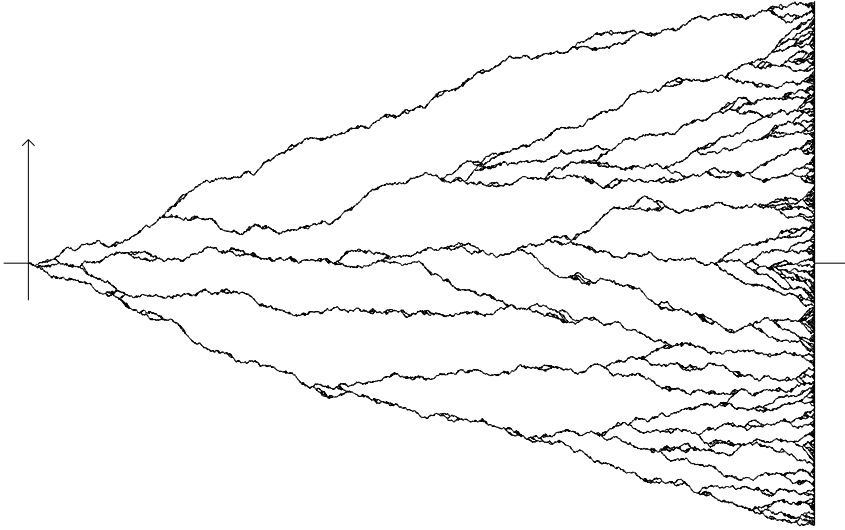


Figure 2.6: Set of all maximizers from the origin to the line U_t . The sample uses $\sim 8 \cdot 10^6$ Poisson points, which in our units correspond to $t = 2000$ and $\varrho = 2$. Only the section $[0, 1] \times [-1/6, 1/6]$ is shown. The picture is rotated of -45 degrees.

2.1.3 Directed polymers and longest increasing subsequences

As we will explain, the directed polymers on Poisson points is closely related to the following combinatorial problem. Let \mathcal{S}_N denote the permutation group of the set $\{1, \dots, N\}$. For each permutation $\sigma \in \mathcal{S}_N$ the sequence $(\sigma(1), \dots, \sigma(N))$ has an increasing subsequence of length k , (n_1, \dots, n_k) , if $1 \leq n_1 < n_2 < \dots < n_k \leq N$. Denote by $L_N(\sigma)$ the length of the longest increasing subsequence for the permutation σ . The problem of finding the asymptotic law for L_N for uniform distribution on \mathcal{S}_N is also called Ulam's problem (1961). Ulam conjectured [106] on the basis of Monte Carlo simulations that asymptotically $\mathbb{E}(L_N) \simeq c\sqrt{N}$, that is the limit $c = \lim_{N \rightarrow \infty} N^{-1/2} \mathbb{E}(L_N)$ exists. Some other numerical analysis by Baer and Brock [9] suggested $c = 2$. The proof of the existence of c was obtained by Hammersley [39]. Then Logan and Sheep [61] proved that $c \geq 2$, and Vershik and Kerov [108] showed that $c = 2$, thus settling Ulam's problem. Other proofs are due to Aldous and Diaconis [5], Seppäläinen [89], and Johansson [41]. The proofs in [61, 108] use Young tableaux representation, see below, where an asymptotic analysis is carried out for *fixed* large N . Another approach is used by Hammersley in [39], where he considers the length of the permutation to be Poisson distributed with mean value N . This point of view is equivalent to the directed polymers on Poisson points. The subsequent works [5, 89, 41] are also in this framework. For more details, see the review by Diaconis and Aldous [6].

The next step is to analyze the fluctuations. Some Monte Carlo simulation of Odlyzko and Rains (1993), see also [68], indicated that asymptotically $\text{Var}(L_N) \simeq c_0 N^{1/3}$ with $c_0 \simeq 0.819$, and also $\mathbb{E}(L_N) \simeq 2\sqrt{N} + c_1 N^{1/6}$ with $c_1 \simeq -1.758$. The final answer is

given by Baik, Deift and Johansson [10]. They proved that

$$\lim_{N \rightarrow \infty} \mathbb{P}(L_N \leq 2\sqrt{N} + sN^{1/6}) = F_2(s), \quad s \in \mathbb{R} \quad (2.22)$$

where F_2 is the GUE Tracy-Widom distribution. From this result it follows that $c_0 = 0.8132\dots$ and $c_1 = -1.7711\dots$. To obtain (2.22) they use the Poissonized version of the problem. Instead of fixing the length of the permutations to N , they consider the set $\mathcal{S} = \cup_{n \geq 0} \mathcal{S}_n$ and assign the probability $e^{-N} k^N / k!$ that a permutation is in \mathcal{S}_k . They first prove that (2.22) holds for this problem, and secondly obtain the result via a de-Poissonization method, consisting in bounding from above and below the distribution of L_N in terms of the Poissonized one.

The problem of the longest increasing subsequence of length N is equivalent to the problem of finding the longest directed polymer from $(0, 0)$ to (t, t) when N points are distributed uniformly in the square $[0, t]^2$, and the directed polymers on Poisson points is the Poissonized version. In statistical physics the problem with fixed N corresponds to the canonical ensemble, the one with Poisson distributed length to the grand canonical ensemble, and the $N \rightarrow \infty$ limit is the thermodynamical limit.

2.1.4 Young tableaux and increasing subsequences

On a more combinatorial point of view, the longest increasing subsequence can be seen via the Young tableaux associated to a permutation. The Young tableaux are defined as follows. Take a partition $\lambda = (\lambda_1, \lambda_2, \dots, \lambda_k)$ of an integer N , i.e., satisfying $\lambda_1 \geq \lambda_2 \geq \dots \geq \lambda_k \geq 1$ and $\sum_{i=1}^k \lambda_i = N$. A Young tableau of *shape* $\lambda = (\lambda_1, \lambda_2, \dots)$ is a diagram with k rows and λ_i cells for row i , $i = 1, \dots, k$, where the cells are occupied by the numbers $1, 2, \dots, N$ increasingly in each row and column (or, by symmetry, decreasingly). The Robinson-Schensted correspondence is a *bijection* between permutations $\sigma \in \mathcal{S}_N$ and *pairs* of Young tableaux $(\mathcal{P}(\sigma), \mathcal{Q}(\sigma))$ with N cells and the same shape. The algorithm leading to $(\mathcal{P}(\sigma), \mathcal{Q}(\sigma))$ is the following [88]:

\mathcal{P} -tableau: for $i = 1$ to N :

Place $\sigma(i)$ in the top row of the \mathcal{P} -tableau as follows: a) if $\sigma(i)$ is higher than all numbers in the first row of the \mathcal{P} -tableau, then append to the right of them, b) otherwise put it at the place of the smallest higher element of the first row of \mathcal{P} .

If an element was replaced in row j , take it and apply the same procedure in row $j + 1$.

\mathcal{Q} -tableau: for $i = 1$ to N :

Place i in the position where a number appeared the first time at step i in the \mathcal{P} -tableau.

As an illustration we show the construction of the Young tableaux for the permutation $\sigma = (6, 2, 5, 1, 4, 8, 7, 3)$, whose shape is $\lambda = (3, 3, 1, 1)$.

i	1	2	3	4	5	6	7	8
\mathcal{P}	6	2 6	2 5 6	1 5 2 6	1 4 2 5 6	1 4 8 2 5 6	1 4 7 2 5 8 6	1 3 7 2 4 8 5 6
\mathcal{Q}	1	1 2	1 2 3	1 2 2 4	1 2 3 5 4	1 2 6 3 5 4	1 2 6 3 5 7 4	1 2 6 3 5 7 4 8

The shapes of the Young tableaux $\mathcal{P}(\sigma)$ and $\mathcal{Q}(\sigma)$ are the same by construction. In particular, the length of the longest increasing subsequence of σ equals the length of the first row [6]

$$L_N(\sigma) = \lambda_1(\sigma). \quad (2.23)$$

Thus a way to determine the asymptotic behavior of L_N is via the analysis of the length of the first row on Young tableaux. The measure on λ induced by the uniform measure on \mathcal{S}_N is the *Plancherel* measure: let d_λ denote the number of Young tableaux of shape λ , then

$$\text{Pl}_N(\lambda) = \frac{d_\lambda^2}{\sum_{\mu \in Y_N} d_\mu^2}, \quad \lambda \in Y_N \quad (2.24)$$

with Y_N denoting the set of partitions of $\{1, \dots, N\}$.

Finally we discuss the interpretation of all λ_i 's. Consider a Poisson process in $[0, t]^2$ and ω a configuration with N points. Let (x_i, y_i) , $i = 1, \dots, N$, be the points of ω , where the index is defined by the rule $x_i \leq x_{i+1}$, and the permutation $\sigma \in \mathcal{S}_N$ by $y_{\sigma(i)} < y_{\sigma(i+1)}$. Clearly the length of the longest increasing subsequence of σ , $L_N(\sigma)$, equals the length of the longest directed polymer from $(0, 0)$ to (t, t) for the configuration ω , which is the λ_1 of $\mathcal{P}(\sigma)$. The interpretation of the other λ_i 's follows from a theorem of Greene. Let $\sigma \in \mathcal{S}_N$ and $\lambda = (\lambda_1, \dots, \lambda_m)$ be a the shape of $\mathcal{P}(\sigma)$. Let, for $k \leq m$, $a_k(\sigma)$ be the length of the longest subsequence of σ consisting of k disjoint increasing subsequences. Greene proves [36] that

$$a_k(\sigma) = \lambda_1 + \dots + \lambda_k. \quad (2.25)$$

In terms of directed polymers (2.25) means that a_k is the maximal sum of the lengths of k non-intersecting directed polymers from $(0, 0)$ to (t, t) , where non-intersecting means without common Poisson points.

2.1.5 Discrete analogues of directed polymers

We describe a discrete analogue on \mathbb{Z}^2 of the directed polymers problem, because it leads to a discrete analogue of the polynuclear growth model discussed in Section 2.2. It is also linked with the totally asymmetric exclusion process, TASEP.

Let $\omega(i, j), (i, j) \in \mathbb{Z}_+^2$ be independent geometrically distributed random variables,

$$\mathbb{P}(\omega(i, j) = k) = (1 - q)q^k, \quad k \in \mathbb{Z}_+ \quad (2.26)$$

with $q \in (0, 1)$. The directed polymers from $(0, 0)$ to (M, N) is the set of up/right paths π from $(0, 0)$ to (M, N) , i.e., sequences of points $(i_k, j_k), k = 0, \dots, M + N$, of sites in \mathbb{Z}_+^2 with $(i_0, j_0) = (0, 0)$, $(i_{M+N}, j_{M+N}) = (M, N)$, and $(i_{k+1}, j_{k+1}) - (i_k, j_k) \in \{(1, 0), (0, 1)\}$. We denote by $\Pi_{M,N}$ the set of directed polymers from $(0, 0)$ to (M, N) . The length of the directed polymer is defined by the sum of the $\omega(i, j)$ visited by the directed polymer, and we are interested in the length of the longest directed polymers in $\Pi_{M,N}$ given by

$$L_{N,M} = \max_{\pi \in \Pi_{M,N}} \sum_{(i,j) \in \pi} \omega(i, j). \quad (2.27)$$

$\Pi_{M,N}^{\max}$ denote the set of directed polymers in $\Pi_{M,N}$ of maximal length. This model was considered by Johansson in [43], where he obtained the following results. For the asymptotic expected value of the length of directed polymers he proved that, for each $q \in (0, 1)$ and $\gamma \geq 1$,

$$m(\gamma, q) \equiv \lim_{N \rightarrow \infty} \frac{1}{N} \mathbb{E}(L_{[\gamma N], N}) = \frac{(1 + \sqrt{\gamma q})^2}{1 - q} - 1, \quad (2.28)$$

$[\cdot]$ denotes the integer part. The fluctuations around the mean value are described by the GUE Tracy-Widom distribution F_2 as follows. For each $q \in (0, 1)$ and $\gamma \geq 1$, and $s \in \mathbb{R}$, write

$$\sigma(\gamma, q) = \frac{q^{1/6} \gamma^{-1/6}}{1 - q} (\sqrt{\gamma} + \sqrt{q})^{2/3} (1 + \sqrt{\gamma q})^{2/3}, \quad (2.29)$$

then

$$\lim_{N \rightarrow \infty} \mathbb{P}(L_{[\gamma N], N} \leq m(\gamma, q)N + \sigma(\gamma, q)N^{1/3}s) = F_2(s). \quad (2.30)$$

A generalization of this model consists in taking $\omega(i, j), (i, j) \in \mathbb{Z}_+^2$ be independent geometrically distributed random variables with

$$\mathbb{P}(\omega(i, j) = k) = (1 - a_i b_j)(a_i b_j)^k, \quad k \in \mathbb{N} \quad (2.31)$$

with the a_i 's and the b_i 's in $[0, 1)$. The 3D-Ising corner problem introduced in Section 2.3 will be closely related to this generalization.

Question of universality

Consider the more general case of directed polymers where the i.i.d. random variables $\omega(i, j)$ are *positive* and have a distribution F (not reduced to a point mass) satisfying $\mathbb{E}(\omega) < \infty$ and $\text{Var}(\omega) < \infty$. The random variable

$$L_N^* = L_{N,N} - \omega(N, N) \quad (2.32)$$

is superadditive, i.e., $L_{N+M}^* \geq L_N^* + L_M^*$. The subadditive ergodic theorem ensures the existence of the limit

$$\lim_{N \rightarrow \infty} \frac{L_N^*}{N} = \mu(0) \quad (2.33)$$

with probability one, from which follows that $\lim_{N \rightarrow \infty} N^{-1} L_{N,N} = \mu(0)$ too. Similarly, we can consider the end-point $P(\alpha) = (N - [N \tan(\alpha)], N + [N \tan(\alpha)])$, with α the angle to the diagonal (the straight line passing by $(0, 0)$ and (N, N)). Then for some $\mu(\alpha)$, $\lim_{N \rightarrow \infty} N^{-1} L_{P(\alpha)} = \mu(\alpha)$ a.s. too. As for the directed polymers on Poisson points, we define the length fluctuation exponent χ_α such that

$$\chi_\alpha = \lim_{N \rightarrow \infty} \frac{\ln \text{Var}(L_{P(\alpha)})}{2 \ln N} \quad (2.34)$$

and the lateral fluctuation exponent ξ_α as follows. Let C_γ be the cylinder of width N^γ with axis passing by $(0, 0)$ and $P(\alpha)$. Then

$$\xi_\alpha = \inf\{\gamma > 0 | \mathbb{P}(\pi \in \Pi_{P(\alpha)}^{\max} \cap C_\gamma) = 1\}. \quad (2.35)$$

There are quantities, like the function $\mu(\alpha)$, that depend on the distribution F . But other quantities like the exponents ξ and χ are expected to be independent of the details of F , i.e., to be *universal* within a class of models. It is known that the scaling relation $\chi_\alpha = 2\xi_\alpha - 1$ is not always satisfied if $\mu''(\alpha) = 0$. From scaling theory and the results of some solvable models it is known that in dimension two the universal exponents are $\xi = 2/3$ and $\chi = 1/3$. Assume the condition that μ'' exists and

$$\mu''(\alpha) \neq 0. \quad (2.36)$$

Then the conjecture is that, if (2.36) is satisfied, then $\chi_\alpha = 2\xi_\alpha - 1$ holds with $\chi_\alpha = \chi = 1/3$ and $\xi_\alpha = \xi = 2/3$ independent of α . In the above model, (2.36) does not hold for $\alpha = \pm\pi/4$, but this is a point where (2.36) does not apply since μ'' does not exist. For $\alpha = \pm\pi/4$, $\xi = 0$ because the directed polymers can not fluctuate laterally at all, and $\chi = 1/2$ since the length is a sum of i.i.d. random variables. It is not clear if the condition of finite second moment is enough or if one needs to assume the existence of exponential moments. Even in the discrete model studied above there is not a rigorous proof of $\xi = 2/3$. The strategy used to prove $\xi = 2/3$ for the Poisson case [44] can be easily adapted to the discrete case, but a large deviation estimate for one of the tails is missing.

Several attempts of proving the scaling relation (2.12), $2\xi - 1 = \chi$, have been made over the past years with some partial but rigorous results, the most relevant can be found in [65, 60, 74]. In these papers some of the rigorous results involve modified versions of ξ and χ .

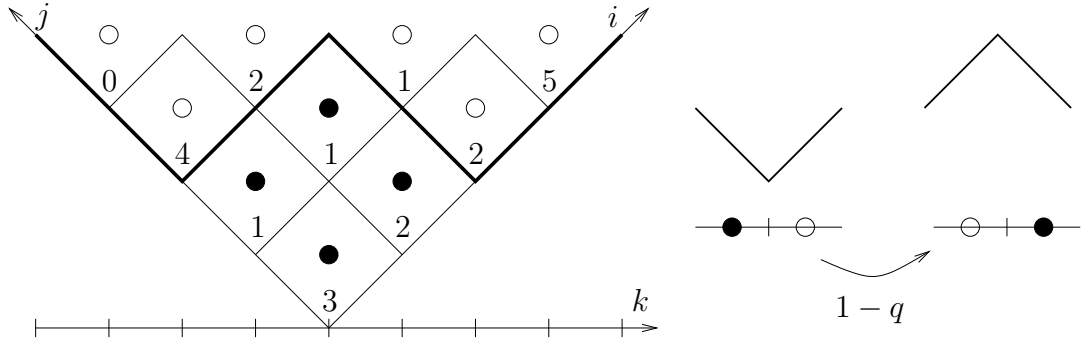


Figure 2.7: Directed polymers and TASEP. The bold line passes by the points of B_6 , the black dots are $\tilde{\mathcal{D}}_6$, and the numbers are the $\omega(i, j)$. The right shows how the jump of a particle is reflected by B_t .

Poisson points and TASEP limits

There are two limits which are of particular interest:

a) The $q \rightarrow 0$ limit leads to the Poisson points case as follows. Define $N = t\sqrt{\varrho/q}$ and take the limit $q \rightarrow 0$ with t fixed. Then $m(\gamma, q)N \rightarrow \sqrt{\varrho\gamma}t$, and $\sigma(\gamma, q)N^{1/3} \rightarrow (\sqrt{\gamma\varrho}t)^{1/3}$. In particular, for $\varrho = 1$ and $\gamma = 1$, $m(\gamma, q)N \rightarrow 2t$ and $\sigma(\gamma, q)N^{1/3} \rightarrow t^{1/3}$, compare with equation (2.7). The picture of Poisson points with intensity ϱ is directly obtained in the $q \rightarrow 0$ limit if, for fixed t , the lattice spacing is $\sqrt{q/\varrho}$.

b) The second limit is $q \rightarrow 1$, which leads to the totally asymmetric exclusion process, TASEP [43, 78]. Let us call $L(i, j)$ the waiting time from $(0, 0)$ to (i, j) , and define the domain

$$\mathcal{D}_t = \{(i + \frac{1}{2}, j + \frac{1}{2}) \in (\mathbb{N} + \frac{1}{2})^2 | L(i, j) \leq t\}. \quad (2.37)$$

Now rotate the picture by $\pi/4$, denote by \mathcal{L} the image of the lattice \mathbb{Z}_+^2 and by $\tilde{\mathcal{D}}_t$ the one of \mathcal{D}_t . Let $k = i - j$ and B_t the lowest set of points in \mathcal{L} which are above $\tilde{\mathcal{D}}_t$, see figure 2.7. At each time t , we associate a set of random variables $\{\eta_k(t), k \in \mathbb{Z}\}$ to each bond $(B_t(k), B_t(k+1))$ by setting $\eta_k(t) = 1$ if $B_t(k+1) - B_t(k) = (1, -1)$ and $\eta_k(t) = 0$ if $B_t(k+1) - B_t(k) = (1, 1)$. $\eta_k(t)$ represents the state of the site k , it is 1 if there is a particle at k at time t and zero if it is empty. For $t = -1$, the initial configuration of particles is $\eta_k(t) = 1$ for $k < 0$ and $\eta_k(t) = 0$ for $k \geq 0$. If at time t a particle occupies site k and is followed by an empty space, at time $t + 1$ it will be at site $k + 1$ with probability $1 - q$. Moreover each particle jumps independently. This is the discrete time TASEP with geometrical distributed waiting times. Now consider the $q \rightarrow 1$ limit. Let the unit time interval be $1 - q$. Then the waiting time $\tau(i, j) = (1 - q)\omega(i, j)$ is in the limit exponentially

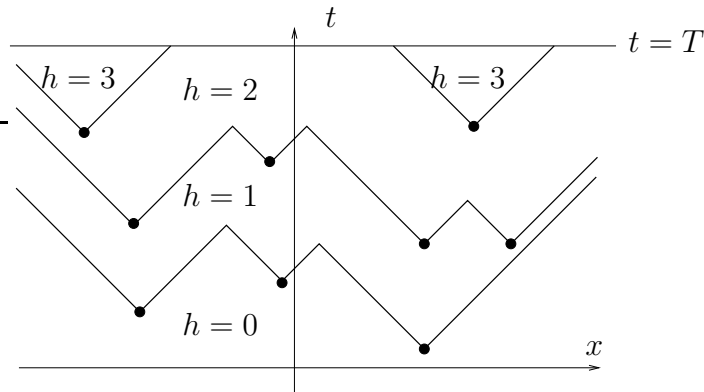


Figure 2.8: Graphical construction generating the surface height from the Poisson points.

distributed. In fact,

$$\begin{aligned} \mathbb{P}(\tau(i, j) \leq s) &= \sum_{t \in \mathbb{N} \cap [0, s/(1-q)]} \mathbb{P}(\omega(i, j) = t) \\ &= \sum_{t' \in (1-q)\mathbb{N} \cap [0, s]} \mathbb{P}(\omega(i, j) = t'/(1-q)) \xrightarrow{q \rightarrow 1} \int_0^s e^{-t} dt. \quad (2.38) \end{aligned}$$

2.2 Polynuclear growth model (PNG)

The first model we consider which is related with the directed polymers on Poisson points is the polynuclear growth model (PNG) in one spatial dimension.

2.2.1 Polynuclear growth model and Poisson points

The PNG model in $1+1$ dimension is a growth model for a one dimensional surface, which at time t and position x is described by a height function $x \mapsto h(x, t) \in \mathbb{Z}$. It is a local random growth model. Space and time are continuous and the height is discrete (given in “atomic units”). First we consider the case of flat initial condition $h(x, 0) = 0$ for all $x \in \mathbb{R}$, the case of non-flat initial condition is discussed later. Fix a $T > 0$, then for each configuration of Poisson points $\omega \in \Omega$ we define the height function $h(x, t)(\omega)$, $(x, t) \in \mathbb{R} \times [0, T]$, by the following graphical construction. Because of flat initial conditions, we set $h(x, 0)(\omega) = 0$ and we call *nucleation events* the points of ω . Each nucleation event generates two lines, with slope $+1$ and -1 along its forward light cone. A line ends upon crossing another line. In Figure 2.8 the dots are the nucleation events and the lines follow the forward light cones. The height $h(x, t)(\omega)$ is then the number of lines crossed along the straight path from $(x, 0)$ to (x, t) . Since ω is locally finite, it follows that $x \mapsto h(x, t)(\omega)$, $t \in [0, T]$, is locally bounded and the number of discontinuities is locally finite.

The interpretation of the graphical construction in terms of a growing surface is the following. The surface height at position $x \in \mathbb{R}$ and time $t \geq 0$ is $h(x, t) \in \mathbb{Z}$. The initial condition is $h(x, 0) = 0$ for all $x \in \mathbb{R}$. For fixed time t , consider the height profile $x \mapsto h(x, t)$. We say that there is an up-step (of height one) at x if $h(x, t) = \lim_{y \uparrow x} h(y, t) + 1$ and a down-step (of height one) at x if $h(x, t) = \lim_{y \downarrow x} h(y, t) + 1$. A nucleation event which occurs at position x and time t is a creation of a pair of up- and down-step at x at time t . The up-steps move to the left with unit speed and the down-steps to the right with unit speed. When a pair of up- and down-step meet, they simply merge. In Figure 2.8 the dots are the nucleation events, the lines with slope -1 (resp. $+1$) are the positions of the up-steps (resp. down-steps). In the case that the initial surface profile is not flat, the surface height at some later time t is obtained similarly. The only difference is the following. To the lines generated by the Poisson points we need to add additional lines starting from the $t = 0$ axis with slope -1 , resp. $+1$, if initially at x there is an up-step, resp. a down-step. Moreover, the number of lines crossed along the straight path from $(x, 0)$ to (x, t) is the height difference $h(x, t) - h(x, 0)$. Varying the density on Poisson points ϱ in the space, different geometries are obtained, see below.

2.2.2 Longest directed polymers and surface height

We explain the connection between the longest directed polymers on Poisson points and the surface height.

The PNG droplet

The PNG droplet is obtained when the density of Poisson points is constant (here we choose $\varrho = 2$) in the forward light cone of the origin and zero outside, i.e., for $(x, t) \in \mathbb{R} \times \mathbb{R}_+$

$$\varrho(x, t) = \begin{cases} 2 & \text{if } |x| \leq t, \\ 0 & \text{if } |x| > t, \end{cases} \quad (2.39)$$

and the initial height profile is flat, $h(x, 0) = 0$ for $x \in \mathbb{R}$. The height above the origin at time t , $h(0, t)$, equals the number of times that we enter in a light cone when we follow any path from $(0, 0)$ to $(0, t)$ with “speed” between -1 and $+1$, i.e., with absolute slope bigger than one in the (x, t) graph. Notice that $h(0, t)$ depends only on the Poisson points in the diamond $\{(x', t') \mid |x'| \leq t', |x'| \leq t - t'\}$. In particular, consider the paths which enter in the light cones only at the nucleation points and that consists in straight segments between these points. These paths are the *point-to-point* directed polymers of maximal length rotated by $\pi/4$, see Figure 2.9. Therefore $h(0, t)$ equals the length of the longest directed polymer from $(0, 0)$ to $(t/\sqrt{2}, t/\sqrt{2})$ on Poisson points with *intensity two*, which, by rescaling, is equal to the length $L(t)$ of the longest directed polymer from $(0, 0)$ to (t, t) on Poisson points with *intensity one*. Thus by (2.7) the asymptotic behavior of $h(0, t)$ is

$$\lim_{t \rightarrow \infty} \mathbb{P}(h(0, t) \leq 2t + t^{1/3}s) = F_2(s), \quad (2.40)$$

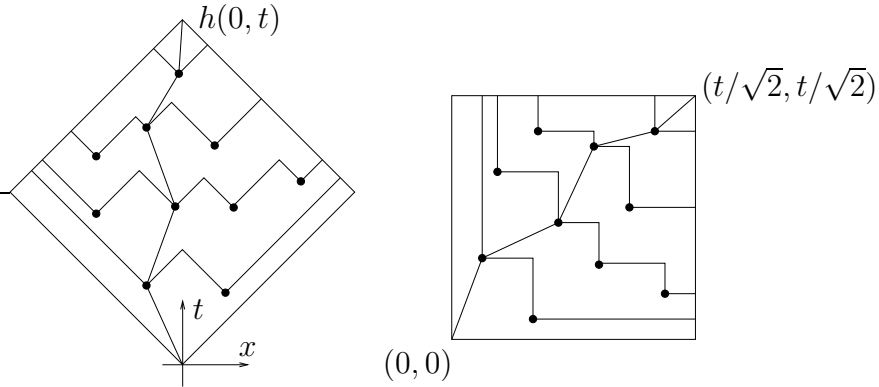


Figure 2.9: Height and directed polymers for the droplet geometry

with F_2 the GUE Tracy-Widom distribution. By invariance of the directed polymers and Poisson process under the mapping $\Phi : \mathbb{R}^2 \rightarrow \mathbb{R}^2$,

$$\Phi(x, t) = \left(\frac{\gamma - \gamma^{-1}}{2} t - \frac{\gamma + \gamma^{-1}}{2} x, \frac{\gamma + \gamma^{-1}}{2} t - \frac{\gamma - \gamma^{-1}}{2} x \right), \quad (2.41)$$

it follows that, for fixed $\tau \in (-1, 1)$,

$$\lim_{t \rightarrow \infty} \mathbb{P}(h(\tau t, t) \leq 2t\sqrt{1 - \tau^2} + t^{1/3}(1 - \tau^2)^{1/6}s) = F_2(s). \quad (2.42)$$

For this model also the spatial correlations are known. Consider the height function at time T , $x \mapsto h(x, T)$. For large T the fluctuations scales as $T^{1/3}$ and it turns out that the spatial correlations scales as $T^{2/3}$. The limit shape of the PNG droplet, $\lim_{T \rightarrow \infty} T^{-1}h(\tau T, T)$, is $2\sqrt{1 - \tau^2}$. Then the rescaled surface height is given by

$$\xi \mapsto h_T^{\text{edge}}(\xi) = T^{-1/3}(h(\xi T^{2/3}) - (2T - \xi^2 T^{1/3})). \quad (2.43)$$

In [81] it is proven that, in the sense of finite dimensional distribution,

$$\lim_{T \rightarrow \infty} h_T^{\text{edge}}(\xi) = \mathcal{A}(\xi) \quad (2.44)$$

where \mathcal{A} is the *Airy process*, whose precise definition and properties are given in Section 3.3.3.

Recently Borodin and Olshanski showed [19] that the Airy process describes the space-time correlations along any *space-like* (and *light-like*) path in the droplet geometry. They work with Young diagrams. To each point $(u, v) \in \mathbb{R}_+^2$, they consider the random Young diagram (the shape of Young tableaux) $Y(u, v)$ obtained by RSK correspondence. Then for each space-like path in \mathbb{R}_+^2 they construct a Markov chain which describes the evolution of the Young diagram Y . The case $u + v = T$ is the one analyzed by Prähofer and Spohn [81]. The case $uv = \text{const}$ correspond to the terrace-ledge-kink (TLK) model which was used, together with the 3D-Ising model, to determine universality for the fluctuations of a crystal around the equilibrium shape, see Section 2.3.4 and [29]. For *time-like* paths no result is known. The major difficulty lies on the lack of the Markov property.

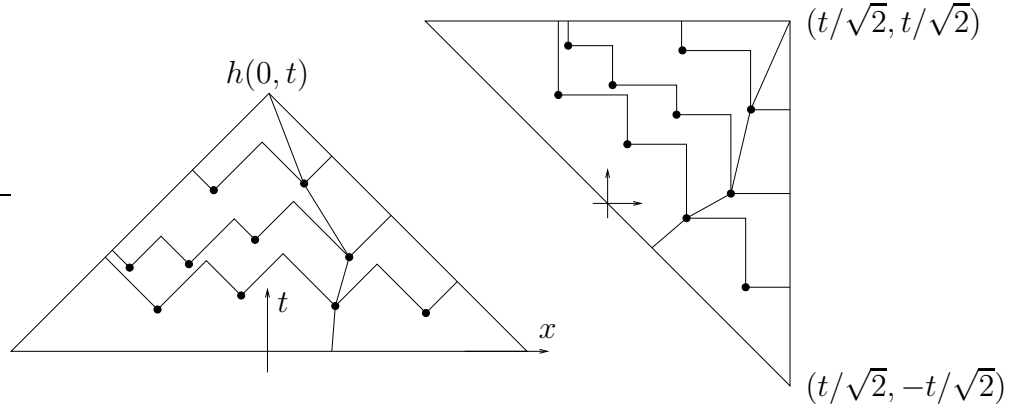


Figure 2.10: Height and directed polymers for the flat geometry

The flat PNG

With flat PNG we mean the surface obtained when the density of Poisson points is constant in $\mathbb{R} \times \mathbb{R}_+$ (as before we choose $\rho = 2$). In this case, since no other constraint is fixed, the surface height $h(x, t)$ is statistically translation-invariant, thus we consider $x = 0$. The height $h(0, t)$ depends only on the Poisson points in the intersection of the backwards light cone of $(0, t)$ and $\mathbb{R} \times \mathbb{R}_+$, namely in the triangle $\{(x', t') \mid t' \geq 0, |x'| \leq t - t'\}$. $h(0, t)$ is the number of times that any path from $(0, t)$ to the $t = 0$ axis “speed” between -1 and $+1$ exits a light cone. In particular, consider the paths that exit the light cones only at the nucleation points and that consist in straight segments between these points. Let us apply a rotation of $\pi/4$, see Figure 2.10. Then the rotated paths are the *point-to-line* (or better *line-to-point*) directed polymers of maximal length on Poisson points with intensity two. Rescaling to intensity one, we obtain $h(0, t) = L_\ell(t)$ where $L_\ell(t)$ is the one of (2.14). Thus for large t ,

$$\lim_{T \rightarrow \infty} \mathbb{P}(h(0, t) \leq 2t + t^{1/3}2^{-2/3}s) = F_1(s), \quad (2.45)$$

with F_1 the GOE Tracy-Widom distribution.

For this model the spatial correlations are still unknown. In [28] we do a first step in the understanding of it. We will explain it extensively in Section 3.4 and Chapter 4.

2.2.3 Discrete time version of the polynuclear growth model

We now consider a discrete time version of the polynuclear growth model. It is closely related to the discrete version of the directed polymers introduced in Section 2.1.5. Here the space is \mathbb{Z} and the time is \mathbb{N} . We consider only flat initial conditions, i.e., $h(x, -1) = 0$ for all $x \in \mathbb{Z}$. The discrete PNG model is defined by

$$h(x, t) = \max\{h(x-1, t-1), h(x, t-1), h(x+1, t-1)\} + \tilde{\omega}(x, t), \quad (2.46)$$

for $t \geq 0$, where $\tilde{\omega}(x, t) \in \mathbb{Z}_+$, $(x, t) \in \mathbb{Z} \times \mathbb{N}$, are independent random variables.

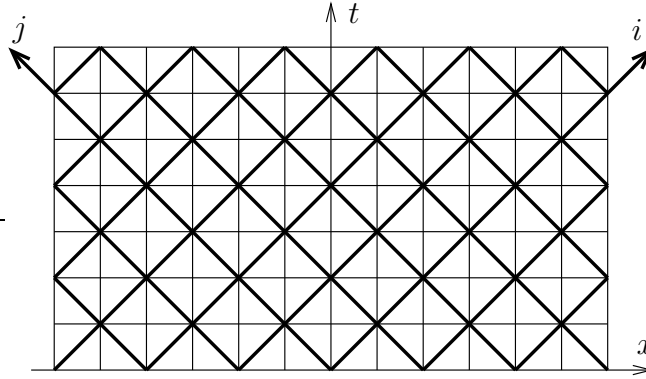


Figure 2.11: \mathbb{Z}^2 and the lattice \mathcal{L} (bold lines). $x = i - j$ and $t = i + j$.

Remark: One could also consider $h(x, 0) = 0$ for all $x \in \mathbb{Z}$ and start nucleations at time $t = 1$, or nucleate only at semi-integer times $\mathbb{N} + \frac{1}{2}$.

The discrete PNG can be seen directly in the framework of the continuous PNG as follows. Consider continuous space-time with nucleations occurring independently only in $(x, t) \in \mathbb{Z} \times \mathbb{N}$. The important difference is that the nucleations generate steps of height $\tilde{\omega}(x, t)$ and not only of unit height. Therefore the picture of Figure 2.8 has to be also slightly modified. Each nucleation generate $\tilde{\omega}(x, t)$ lines which follow the forward light cone. Moreover, the lines merge as follows. Let us consider $m \leq n$: if at some point in space-time m lines with slope $+1$ meet n lines of slope -1 , the m first lines merge and the remaining $n - m$ lines with slope -1 continue.

Of particular interest is the case where $\tilde{\omega}(x, t) = 0$ if $x - t$ is odd, in which case there is a direct correspondence to the directed polymers. $\tilde{\omega}(x, t)$ is therefore non zero in the lattice \mathcal{L} (rotated by $\pi/4$), see Figure 2.11. We denote its vertices by $i = (x + t)/2$ and $j = (t - x)/2$. Denote also $\omega(i, j) = \tilde{\omega}(i - j, i + j)$. We discuss the two geometries already considered in the continuum.

The discrete PNG droplet

For the droplet geometry, the extra condition to be imposed is $\tilde{\omega}(x, t) = 0$ if $|x| > t$, meaning that $\omega(i, j) = 0$ for $i < 0$ or $j < 0$. The height $h(x, t)$, for $x - t$ even, is equal to the length of the longest directed polymer from $(0, 0)$ to $((x + t)/2, (t - x)/2)$ on the lattice \mathcal{L} . Some results are known in the case that $\omega(i, j)$ is a geometric random variable with parameter $a_i b_j$, i.e., $\mathbb{P}(\omega(i, j) = k) = (1 - a_i b_j)(a_i b_j)^k$, $k \in \mathbb{Z}_+$. In particular for $a_i = b_i = \sqrt{q}$, $0 < q < 1$, $i \geq 0$,

$$h(x, t) = L_{(x+t)/2, (t-x)/2} \quad (2.47)$$

with L the one defined in (2.27). A point $([\gamma N], N)$, $\gamma \geq 1$, $N \in \mathbb{N}$, in the lattice \mathcal{L} , corresponds to $(x, t) = ((\gamma - 1)N, [(\gamma + 1)N])$. We want to know $h(\tau T, T)$

with $\tau \in (-1, 1)$. By symmetry consider $\tau \in [0, 1)$, take $\gamma = (1 - \tau)/(1 + \tau)$ and $N = T(1 - \tau)/2 = T/(1 + \gamma)$. Then

$$\mu(\tau, q) = \frac{m(\gamma, q)}{(1 + \gamma)} = \frac{1}{1 + \gamma} \left(\frac{(1 + \sqrt{\gamma q})^2}{1 - q} - 1 \right) \quad (2.48)$$

with $m(\gamma, q)$ given in (2.28). Define also

$$\tilde{\sigma}(\tau, q) = \frac{\sigma(\gamma, q)}{(1 + \gamma)^{1/3}} = \frac{q^{1/6} \gamma^{-1/6}}{(1 - q)(1 + \gamma)^{1/3}} (\sqrt{\gamma} + \sqrt{q})^{2/3} (1 + \sqrt{\gamma q})^{2/3} \quad (2.49)$$

with $\sigma(\gamma, q)$ given in (2.29). Then the asymptotics of $h(x, t)$ follows from (2.30) and writes

$$\lim_{T \rightarrow \infty} \mathbb{P}(h([\tau T], T) \leq \mu(\tau, q)T + \tilde{\sigma}(\tau, q)T^{1/3}s) = F_2(s). \quad (2.50)$$

Moreover, for large T , the height is described by the Airy process \mathcal{A} as proven by Johansson in [46]. He shows that, for $\tau = 0$, the process \mathfrak{h}_T given by

$$\xi \mapsto \kappa_1 T^{-1/3} (h(\xi \kappa_2 T^{2/3}, T) - \mu(1, q)T) \quad (2.51)$$

converges to $\mathcal{A}(\xi) - \xi^2$ as $T \rightarrow \infty$, where $\kappa_1 = 2^{1/3} \sigma(1, q)^{-1}$ and $\kappa_2 = 2^{1/3} \sigma(1, q)^{-1} (1 + \sqrt{q})(1 - \sqrt{q})^{-1}$. The convergence is in the weak*-topology of probability measures on $C([-M, M])$ for an arbitrarily fixed $M > 0$, that is, for any $f \in C([-M, M])$, one has $\lim_{T \rightarrow \infty} \int_{-M}^M dx \mathfrak{h}_T(x) f(x) = \int_{-M}^M dx (\mathcal{A}(\xi) - \xi^2) f(x)$.

In the limit $q \rightarrow 0$ and with lattice spacing $\sqrt{q/\varrho}$, the continuum version of the PNG droplet is recovered (ϱ the Poisson points intensity), and in the limit $q \rightarrow 1$ with unit time equal $1 - q$, the TASEP is obtained, see Section 2.1.5.

Discrete flat PNG

The connection with discrete directed polymers on \mathbb{Z}^2 implies that height $h(x, t)$, for $x - t$ even, is equal to the length of the longest directed polymer from the set (line) $\{(i, j) \in \mathcal{L} | i + j = 0\}$ to $((x + t)/2, (t - x)/2)$ on the lattice \mathcal{L} .

2.2.4 Recent developments on 1D polynuclear growth model

It is in [77] that Prähofer and Spohn obtained the one-point distribution function for the surface height in both the PNG droplet and the flat PNG geometries. Their results are achieved by identifying the surface height with the longest directed polymers, for which Baik and Rains already analyzed the asymptotics [13, 12]. The joint-distribution of the height profile is obtained in [81] using a multilayer generalization of the PNG, see Section 3.4, which is also used in our analysis. The idea of the multilayer comes from the work of Johansson on the Aztec diamond [45], where a rhombus-shaped (checkerboard) table is tiled with dominos, see Figure 2.12. On the tiling one can introduce a set of lines

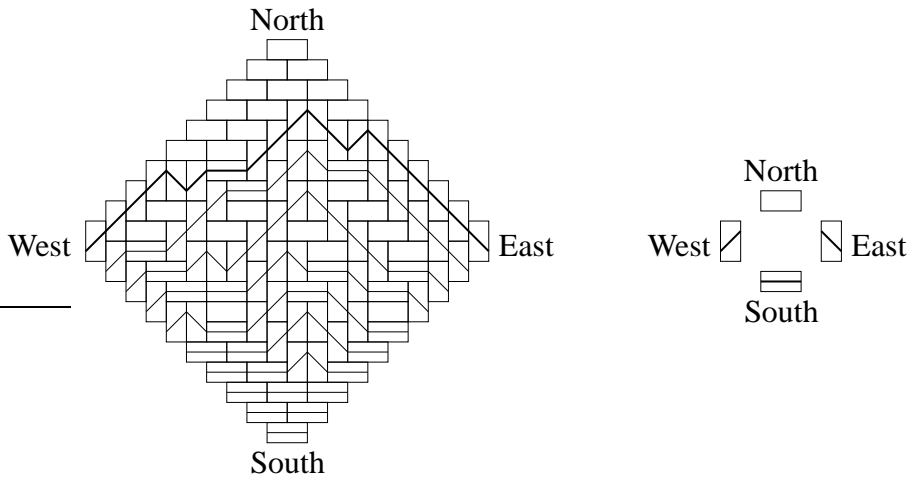


Figure 2.12: A dominos tiling for an Aztec diamond with 50 dominos. The border line between the regular and the North regular tiling is the center of the top line.

with initial and final points in the lower half diamond as shown in the figure. The only rule is the following. In vertical dominos the lines have slope $+1$ or -1 and in the horizontal ones the lines can only be horizontal. The dominos are classified into four types, North, South, East, and West, depending on how the lines fill them. The names are so chosen because for large tables, close to the North, South, East, and West corners there is a regular tiling of the corresponding dominos. In the central region the tiling is “disordered”. The border line between the regular and the disordered region is described by the Airy process as proven in [47].

More recently Sasamoto and Imamura study the (discrete) half-droplet PNG geometry, which consists in allowing nucleations only in positive x and $x \leq t$ [40]. They prove that the rescaled height is GUE distributed away from the $x = 0$ axis and there is a transition to GSE at $x = 0$. If extra nucleations are added at the origin with intensity $\gamma \geq 0$, the distribution above $x = 0$ has a transition for $\gamma = 1$. For $\gamma < 1$ it is still GSE, for $\gamma = 1$ it is GOE distributed, and for $\gamma > 1$ the fluctuations become Gaussian because the contribution of the nucleation at the origin dominates. The one-point distribution asymptotics follows from [13, 12] too.

A modification of the PNG droplet consists in adding sources at the boundaries, which means that extra nucleations with fixed (linear) density α_+ and α_- are independently added in the forward light cone of the origin, i.e., in (x, t) such that $|x| = t$. This model was introduced by Prähofer and Spohn [77, 78]. Then Baik and Rains analyzed it in details [11] with the following results. For α_{\pm} small, the effects coming from the edges are small and the fluctuations are still GUE distributed. On the other hand, if $\alpha_+ > 1$ or $\alpha_- > 1$, then the boundary effects are dominant the fluctuations become Gaussian. The cases where $\alpha_+ = 1$ and/or $\alpha_- = 1$ are also studied and other statistics arise. Of particular interest is when $\alpha_+ \alpha_- = 1$ for $1 - \alpha_{\pm} = \mathcal{O}(T^{-1/3})$, in which case the PNG growth is stationary and has a flat limit shape.

2.2.5 Universality

The PNG model explained above is in the $(1 + 1)$ -dimensional KPZ universality class. We do not enter into details, which can be found, together with some discussion of higher dimensional cases, in the thesis of Michael Prähofer [76], Chapters 2 and 3, see also [79].

KPZ equation

The $(d+1)$ -dimensional KPZ equation was introduced by Kardar, Parisi, and Zhang in [48] as a continuum description of a d -dimensional stochastic surface growth, which is parameterized by a height function $h(x, t)$, $x \in \mathbb{R}^d$, relative to a substrate. The KPZ equation writes

$$\partial_t h(x, t) = v_0 + \nu \Delta h(x, t) + \frac{1}{2} \lambda (\nabla h(x, t))^2 + \eta(x, t). \quad (2.52)$$

v_0 is a deterministic growth which can be eliminated by changing the frame of the observer. The Laplace term $\nu \Delta h(x, t)$, $\nu \neq 0$, represents the surface tension, smooths the surface and contrasts the noise term $\eta(x, t)$ which is assumed to be local. The surface hills expand laterally if the non-linear term $\lambda \neq 0$.

KPZ universality class

Now let us restrict to $d = 1$. The conditions for a surface growth model on a one-dimensional substrate to be in the KPZ universality class are the following:

- 1) the evolution is local, i.e., $h(x, t + dt)$ depends on the values of $h(y, t)$ only for $|y - x| \lesssim \mathcal{O}(dt)$,
- 2) the randomness is local, i.e., $\eta(x, t)$ and $\eta(y, t)$ are not correlated in time and for same time they are correlated only if $|y - x| \leq C$ for some $C > 0$ fixed,
- 3) let $v(u)$ be the growth velocity of the stationary surface $h_u(x, t)$ with *fixed slope* $u = \partial_x h$, then the KPZ condition is $v''(u) \neq 0$.

Some explanation on 3) are needed. Assume that a growth mechanism is given, like the PNG rules. For a finite system of size L , impose chiral boundary conditions (periodic up to a vertical shift) such that the surface grows with fixed mean slope u . The height process is also required to be ergodic, i.e., the mean of observables of $h(x, t)$ on the state space for a fixed time t and the mean over the evolution for fixed x agree in the large time limit. In the thermodynamic limit, $L \rightarrow \infty$, one expects to have a unique limiting process, $h_u(x, t)$, whose gradient is stationary in space and time. If this is the case, then $v = v(u)$ denotes the growth velocity of $h_u(x, t)$.

Condition 3) is the same as the condition on the curvature (2.36) in the last passage percolation, where one can define a growing random set $B(t) = \{x \in \mathbb{Z}^d | L_x \leq t\}$. Then the mean speed of growth of $B(t)$ in the direction α is $v(\alpha) = 1/\mu(\alpha)$, from which the equivalence of the two conditions.

The PNG model is in the KPZ universality class

The first two conditions are satisfied, because $h(x, t + dt)$ depends only on $h(y, t)$ with $|y - x| \leq dt$, and the noise is a Poisson process in space-time, thus completely uncorrelated. Thus one need to verify condition 3).

Let $x \mapsto h_u(x, 0)$ be a two-sided random walk of mean slope u , i.e., the up-steps and down-steps, are two independent Poisson processes on \mathbb{R} with densities ρ_+ and ρ_- satisfying the condition $\rho_+ - \rho_- = u$. Moreover, the nucleations have to be counterbalanced by the annihilation, so in a time interval dt , $\varrho Ldt = 2\rho_+\rho_-Ldt$, i.e., $\rho_+\rho_- = \frac{1}{2}\varrho$, with $\varrho = 2$ is the space-time density of nucleations. Next one verify that the PNG evolution does not modify the up- and down-steps processes. The last step is to determine $v(u) = \partial_t \mathbb{E}(h_u(x, t))$. In an interval dt , each up- and down-step moves of dt , thus the area under $h_u(x, t)$ is typically increased by $(\rho_+ + \rho_-)Ldt$. The annihilation and the nucleation contributions compensate in average. Thus $v = \rho_+ + \rho_-$, and, using the previous relations with u and ϱ , the velocity is given by

$$v(u) = \sqrt{4 + u^2}. \quad (2.53)$$

Thus condition 3) is satisfied which indicates that the PNG model is in the KPZ universality class.

2.3 3D-Ising model at zero temperature

The second model we consider that belongs to the same framework is the 3D-Ising corner at zero temperature. First we explain the model, secondly we show the correspondence of the Ising corner with a particular case of the (discrete) directed polymers, and finally we explain our results. The detailed analysis is then carried out in Chapter 5.

2.3.1 The model

As a very common phenomenon, crystals are faceted at sufficiently low temperatures with facets joined through rounded pieces. Of course, on the atomic scale the crystal surface must be stepped. These steps meander through thermal fluctuations. On a facet the steps are regularly arranged except for small errors, whereas on a rounded piece the steps have more freedom to fluctuate. Our aim is to understand the precise step statistics, where the step bordering the crystal facet is of particular interest. To gain some insight we will study a simplified statistical mechanics model of a cubic crystal. Its equilibrium shape has three facets, each consisting of a part of one of the coordinate planes. The facets do not touch each other and there is an interpolating rounded piece, see Figure 1.1 in the Introduction. For this model the step statistics will be analyzed in great detail. In section 2.3.4 we explain how our results relate to the predictions of universal properties of crystals with short range step-step interactions.

Let us first explain our model for the corner of a crystal. The crystal is assumed to be simple cubic with lattice \mathbb{Z}^3 . We use lattice gas language and associate to each site $x \in \mathbb{Z}_+^3$, the occupation variable $n_x = 0, 1$ with 1 standing for site x occupied by an atom and 0 for site x empty. Up to a chemical potential the binding energy of the configuration n is

$$H(n) = J \sum_{|x-y|=1} (n_x - n_y)^2, \quad J > 0. \quad (2.54)$$

We consider very low temperatures, meaning that all allowed configurations have the same energy, i.e., the same number of broken bonds. To define properly, we introduce the reference configuration n^{ref} in which only the octant \mathbb{Z}_+^3 is occupied,

$$n_x^{\text{ref}} = \begin{cases} 1 & \text{for } x \in \mathbb{Z}_+^3, \\ 0 & \text{for } x \in \mathbb{Z}^3 \setminus \mathbb{Z}_+^3. \end{cases} \quad (2.55)$$

n is an allowed configuration if for a sufficiently large box Λ one has

$$n_x = n_x^{\text{ref}} \text{ for all } x \in \mathbb{Z}_+^3 \setminus \Lambda \text{ and } H(n) - H(n^{\text{ref}}) = 0. \quad (2.56)$$

The set of allowed configurations is denoted by Ω . By construction Ω is countable. To favor a crystal corner, we introduce the fugacity q , $0 < q < 1$, and assign to each $n \in \Omega$ the weight

$$q^{V(n)}, \quad (2.57)$$

where $V(n)$ is the number of atoms removed from n^{ref} , i.e.

$$V(n) = \sum_{x \in \mathbb{Z}_+^3} (1 - n_x). \quad (2.58)$$

A configuration $n \in \Omega$ can uniquely be represented by a height function \mathbf{h} over \mathbb{Z}_+^2 . For the column at $(i, j) \in \mathbb{Z}_+^2$, all sites below $\mathbf{h}(i, j)$, excluding $\mathbf{h}(i, j)$, are empty and all sites above $\mathbf{h}(i, j)$ are filled. $n \in \Omega$ if and only if

$$\mathbf{h}(i+1, j) \leq \mathbf{h}(i, j), \quad \mathbf{h}(i, j+1) \leq \mathbf{h}(i, j), \quad \mathbf{h}(i, j) \rightarrow 0 \text{ for } (i, j) \rightarrow \infty. \quad (2.59)$$

By abuse of notation, the set of height functions satisfying (2.59) is also denoted by Ω . For $\mathbf{h} \in \Omega$ let $V(\mathbf{h}) = \sum_{(i,j) \in \mathbb{Z}_+^2} \mathbf{h}(i, j)$ be the volume in \mathbb{Z}_+^3 below \mathbf{h} . Then the weight for the height \mathbf{h} is $q^{V(\mathbf{h})}$.

There is an alternative way to describe configurations $n \in \Omega$, which we just mention for completeness, but will not use later on. One builds the crystal out of unit cubes and projects its surface along the (111)-direction, which results in a tiling of the plane \mathbb{R}^2 with lozenges (rhombi) oriented along $0, 2\pi/3$, and $4\pi/3$. With the orientation of Figure 2.13 there are three sectors of the plane corresponding to the polar angle θ with $-\pi/6 < \theta < \pi/2, \pi/2 < \theta < 7\pi/6, 7\pi/6 < \theta < 11\pi/6$. $n \in \Omega$ if and only if the tiling in each sector becomes regular sufficiently far away from the origin.

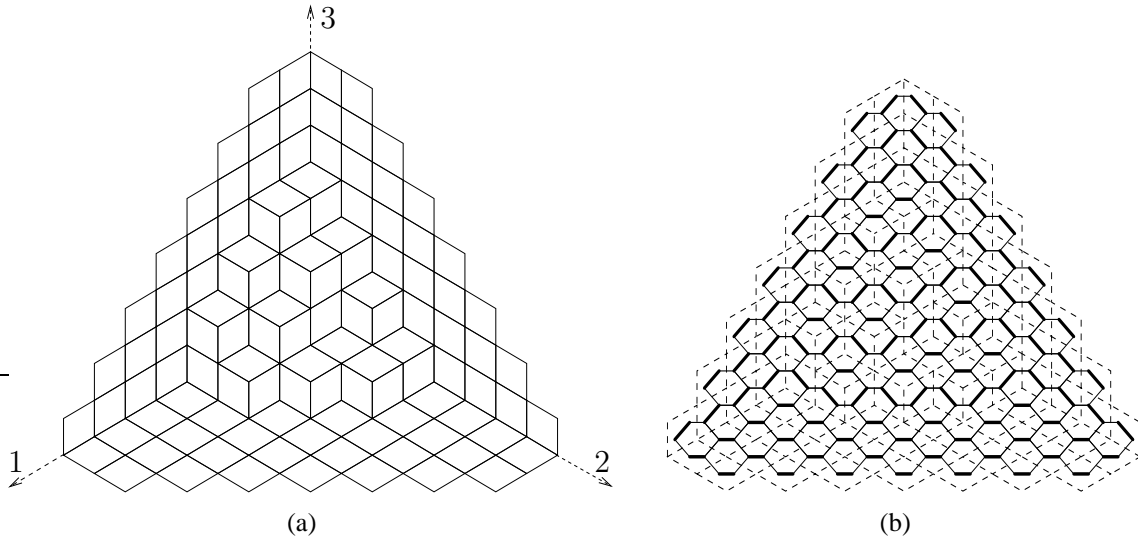


Figure 2.13: (a) The (111)-projection of a configuration $n \in \Omega$. In each of the three sectors the tiling becomes regular far away from the origin. (b) The corresponding perfect matching on the honeycomb lattice.

Instead of tilings, if preferred, one can also think of covering the dual honeycomb lattice by dimers such that every site is covered. In computer science this is called perfect matching. Equivalently, to have a more statistical mechanics flavor, one can consider the fully frustrated antiferromagnetic Ising model on a triangular lattice, i.e., for an allowed spin configuration every triangle must have exactly two spins of the same sign. Erasing all bonds connecting equal sign spins yields a lozenge tiling, and vice versa.

2.3.2 3D-Ising corner and directed polymers

Our main goal is to describe the line bordering the facet and the rounded part of the crystal corner. We are therefore interested in the line $i \mapsto \mathbf{h}(0, i)$, $i \in \mathbb{Z}_+$. We now give the connection between the 3D-Ising corner and the generalization (2.31) of the directed polymers on \mathbb{Z}_+^2 introduced in Section 2.1.5. Consider independent random variables $\omega(i, j)$, $(i, j) \in \mathbb{Z}_+^2$, geometrically distributed with mean value q^{i+j+1} , $q \in (0, 1)$ as above:

$$\mathbb{P}(\omega(i, j) = k) = (1 - q^{i+j+1})q^{(i+j+1)k}, \quad k \in \mathbb{Z}_+. \quad (2.60)$$

Denote by $L(i, j)$ the length of the longest directed polymer from (i, j) to (∞, ∞) . This quantity is well defined because $q < 1$. In fact, consider the random variable $\alpha(m) = \sum_{i+j \geq m} \omega(i, j)$. Then

$$\mathbb{P}(\alpha(m) \geq 1) \leq \mathbb{E}(\alpha(m)) \leq \frac{mq^m}{(1-q)} \rightarrow 0, \quad m \rightarrow \infty. \quad (2.61)$$

Therefore when a directed polymer goes to infinity, with probability one it only passes a finite number of sites (i, j) with $\omega(i, j) > 0$. By symmetry $L(i, j)$ is also the maximal length of directed polymers from infinity to (i, j) , i.e., with down-left steps. From Section 2.2.3 we know the relation between directed polymers and PNG growth. The connection between directed polymers and 3D-Ising corner is

$$\mathbf{h}(i, 0) = L(i, 0), \quad \mathbf{h}(0, i) = L(0, i), \quad (2.62)$$

for $i \in \mathbb{Z}_+$ in law. On the other hand, there is not a simple connection between $L(i, j)$, $i, j > 0$, and the heights $\mathbf{h}(i, j)$. The best way to explain this correspondence is via a multilayer extension of the PNG. It is introduced in Section 3.4 and in Section 3.4.2 we will derive the correspondence of the whole 3D-Young diagrams with the directed polymers (via PNG growth) described above.

2.3.3 Bulk and edge scaling

The step statistics is studied in the limit $q \rightarrow 1$, which means that the typical missing volume from the corner is large, since $\mathbb{E}(V(h)) \simeq 2\zeta(3)(1-q)^{-3}$, ζ the Riemann's zeta function. Thus it is convenient to set

$$q = 1 - \frac{1}{T}, \quad T \rightarrow \infty. \quad (2.63)$$

Let \mathbf{h}_T denote the random height function distributed according to

$$\frac{1}{Z_T} \exp[\ln(1 - \frac{1}{T})V(\mathbf{h}_T)] \quad (2.64)$$

relative to the counting measure on Ω , Z_T the normalizing partition function. For large T the heights are $\mathcal{O}(T)$. Thus one expects a limit shape on the scale T . In fact, as proved in [20, 69],

$$\lim_{T \rightarrow \infty} \frac{1}{T} \mathbf{h}_T([uT], [vT]) = \mathbf{h}_{\text{ma}}(u, v) \quad (2.65)$$

in probability. Here $(u, v) \in \mathbb{R}_+^2$ and $[\cdot]$ denotes the integer part. Let $\mathcal{D} = \{(u, v) \in \mathbb{R}_+^2, e^{-u/2} + e^{-v/2} > 1\}$. On \mathcal{D} , \mathbf{h}_{ma} is strictly decreasing in both coordinates and $\mathbf{h}_{\text{ma}} > 0$, whereas $\mathbf{h}_{\text{ma}} = 0$ on $\mathbb{R}_+^2 \setminus \mathcal{D}$. The analytic form of \mathbf{h}_{ma} is given in Section 5.3. If r denotes the distance to $\partial\mathcal{D} = \{(u, v) \in \mathbb{R}_+^2, e^{-u/2} + e^{-v/2} = 1\}$, it follows that \mathbf{h}_{ma} vanishes as $r^{3/2}$. This is the Pokrovsky-Talapov law [75].

Our interest here is to zoom to the atomic scale. There are mainly two interesting limits. The first is the to focus in the bulk of the 3D-Ising corner, i.e., in the rounded part. Consider a macroscopic point $(u, v) \in \mathcal{D}$ and the local height statistics $\{\mathbf{h}_T([uT] + i, [vT] + j), (i, j) \in \mathbb{Z}^2\}$. In the limit $T \rightarrow \infty$, locally the height profile is planar and one expects that the height statistics corresponds to a random tiling of the plane with the three types of lozenges from Figure 2.13, such that the relative fraction of lozenges yields the average slope $\nabla \mathbf{h}_{\text{ma}}(u, v)$. This property will be proven in Section 5.3 and we refer

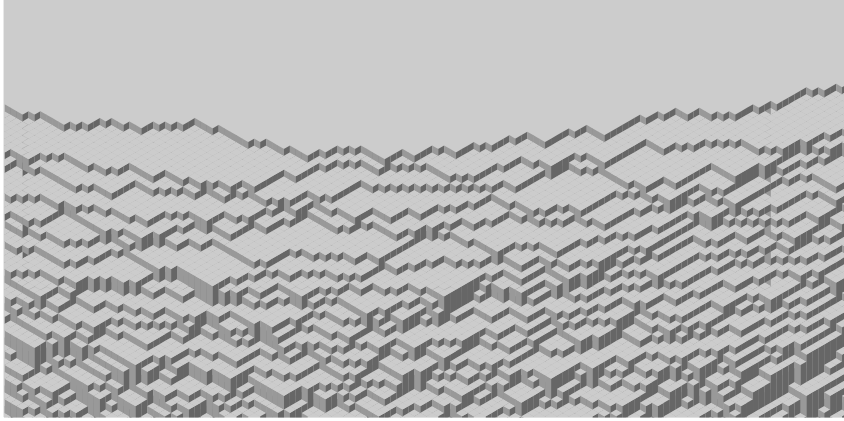


Figure 2.14: Zoom to the facet edge in Figure 1.1.

to it as *local equilibrium*: as $T \rightarrow \infty$, locally one has a translation invariant, spatially ergodic Gibbs measure for the lozenges with their chemical potentials determined through $\nabla \mathbf{h}_{\text{ma}}(u, v)$.

An even more intriguing limit is to zoom to the facet edge, which means to take $(u, v) \in \partial \mathcal{D}$, see Figure 2.14. Since the step density vanishes at $\partial \mathcal{D}$, typically there will be only a few steps in focus. Thus it is more natural to consider directly the crystal step bordering the facet. By symmetry we can choose the border step lying in the 2 – 3 plane. Then the border step is given as the graph of the function

$$t \mapsto b_T(t) = \mathbf{h}_T(0, t), \quad t \in \mathbb{N}. \quad (2.66)$$

From (2.59) we have $b_T(t+1) \leq b_T(t)$ and $\lim_{t \rightarrow \infty} b_T(t) = 0$. For large T , b_T is $\mathcal{O}(T)$, and there is a limiting shape according to

$$\lim_{T \rightarrow \infty} T^{-1} b_T([\tau T]) = b_\infty(\tau), \quad (2.67)$$

where

$$b_\infty(\tau) = -2 \ln(1 - e^{-\tau/2}), \quad \tau > 0. \quad (2.68)$$

(2.68) tells us only the rough location of the step. For the step statistics the relevant quantity is the size of the fluctuations of $b_T([\tau T]) - T b_\infty(\tau)$. As will be shown they are of order $T^{1/3}$ which is very different from steps inside the rounded piece of the crystal which are allowed to fluctuate only as $\ln T$ [93]. On a more refined level one would like to understand correlations, e.g., the joint height statistics at two points t and t' . They have a systematic part corresponding to $T b_\infty(\tau)$. Relative to it the correlation length along the border step scales as $T^{2/3}$, which reflects that on short distances the border step looks like a Brownian motion. Thus b_∞ has to be expanded including the curvature term and the

correct scaling for the border step is

$$A_T(s) = T^{-1/3} \left\{ b_T([\tau T + sT^{2/3}]) - (b_\infty(\tau)T + b'_\infty(\tau)sT^{2/3} + \frac{1}{2}b''_\infty(\tau)s^2T^{1/3}) \right\}. \quad (2.69)$$

Here $\tau > 0$ is a fixed macroscopic reference point and $s \in \mathbb{R}$ with $sT^{2/3}$ the longitudinal distance. $s \mapsto A_T(s)$ is regarded as a stochastic process in s . In Chapter 5 we prove the convergence

$$\lim_{T \rightarrow \infty} A_T(s) = \kappa \mathcal{A}(s\kappa/2) \quad (2.70)$$

in the sense of convergence of finite dimensional distributions. The limit process $\mathcal{A}(s)$ is the stationary Airy process. Its scale is determined by the local curvature via $\kappa = \sqrt[3]{2b''_\infty(\tau)}$.

2.3.4 Universality of shape fluctuations of crystal shapes

Equilibrium crystal shapes typically consist of various flat facets connected by rounded surfaces. For a microscopically flat facet there must be an atomic ledge bordering the facet. This border step could be blurred because of thermal excitations, but is clearly visible at sufficiently low temperatures [97, 67, 66]. While in the interior of the rounded piece of the crystal the step line density is of order one on the scale of the lattice constant, it decays to zero as the edge of a high symmetry facet is approached. If r denotes the distance from the facet edge, according to Pokrovsky-Talapov [75] the step line density vanishes as \sqrt{r} . Thus there is a lot of space for the border ledge to meander, in sharp contrast to steps in the rounded part which are so confined by their neighbors that they fluctuate only logarithmically [93]. Now we discuss the statistics of border ledge fluctuations. In the 3D-Ising corner model, the border ledge is b_T .

In this section we follow the outline of our paper [29]. First we present the terrace-ledge-kink (TLK) model and obtain a form for the universality of the border ledge fluctuations. In the TLK model spatial translation invariance is imposed, therefore it might seem somewhat artificial, we therefore compare the result with the 3D-Ising corner analyzing the consequences of (2.70). By universality we expect our result to be valid for short-range step-step crystal interactions. To obtain the form which properly distinguishes between model-dependent and universal properties we have to rely on a few notions from the thermodynamics of equilibrium crystal shapes [3].

TLK model

We first consider the terrace-ledge-kink (TLK) model, which serves as a description of a vicinal surface, i.e., a crystal cut at a small angle relative to a high symmetry crystal plane. The surface is made up of an array of ledges which on the average run in parallel and are separated by terraces. The ledges are not perfectly straight and meander through kink excitations, only constrained not to touch a neighboring ledge. One can think of these ledges also as discrete random walks constrained not to cross, i.e., with a purely entropic

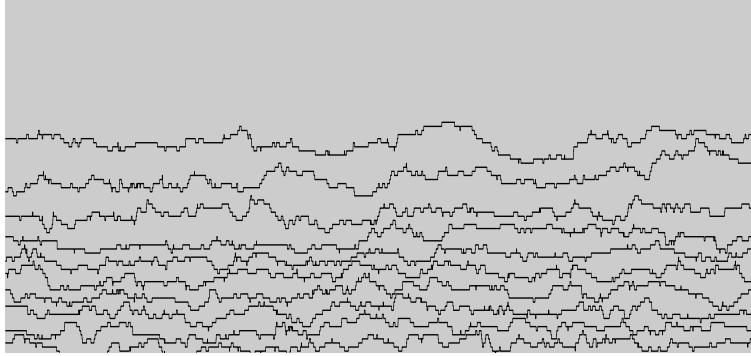


Figure 2.15: Top lines for a TLK model with volume constraint.

repulsion. Such a line ensemble is very closely related to Dyson’s Brownian motion, in which the random walks are replaced by continuum Brownian motions. As discussed in [49, 23], the location of the steps at fixed random walk time t have the same distribution as the eigenvalues of a GUE ($\beta = 2$) random matrix. On this basis it is expected that the ledge-ledge distance is governed by the GUE level spacing [25]. This prediction is verified experimentally [26], however with deviations from $\beta = 2$ which are attributed to long range elastic forces mediated through the bulk of the crystal and not included in the TLK model.

If in the TLK model one retains the lattice structure in the transverse direction and makes the continuum approximation in the direction along the ledges, then the ledges can be regarded as the world lines of free fermions in space-time $\mathbb{Z} \times \mathbb{R}$ [109]. The world lines are piecewise constant and have jumps of only one lattice spacing. Consequently the transfer matrix has a nearest neighbor hopping term and the Pauli exclusion principle guarantees entropic repulsion in the sense that ledges do not meet.

The TLK model, in the version as just explained, has no facet. The crystalline surface has a constant average slope. Slope variations can be enforced through a *volume constraint*. For this purpose we introduce the “occupation” variables $\eta_j(t)$, $|j| \leq N$, $|t| \leq T$, in the surface patch $[-N, -N + 1, \dots, N] \times [-T, T]$: $\eta_j(t) = 1$ if there is some ledge passing through (j, t) , and $\eta_j(t) = 0$ otherwise. In these variables, up to an overall constant, the crystal volume is given by

$$A_v = \int_{-T}^T dt \sum_{j=-N}^N j \eta_j(t) \quad (2.71)$$

and volume constraint means to have an ensemble of ledges where the action A_v is kept fixed.

Without volume constraint the transfer matrix is generated by a free fermion Hamiltonian with nearest neighbor hopping [109]. Imposing the volume constraint grand-canonically adds to the fermionic action the term $\lambda^{-1} A_v$ with a suitable Lagrange mul-

multiplier λ^{-1} . Thereby the nearest neighbor hopping Hamiltonian is modified to

$$H_F = \sum_{j \in \mathbb{Z}} \left(-a_j^* a_{j+1} - a_{j+1}^* a_j + 2a_j^* a_j + \frac{j}{\lambda} a_j^* a_j \right). \quad (2.72)$$

a_j , resp. a_j^* , is the annihilation, resp. creation, operator at lattice site $j \in \mathbb{Z}$. They satisfy the anticommutation relations $\{a_i, a_j^*\} = \delta_{ij}$, $\{a_i, a_j\} = 0 = \{a_i^*, a_j^*\}$. In (2.72) we have taken already the limit $N \rightarrow \infty$. The transfer matrix is e^{-tH_F} , $t \geq 0$, and in the limit $T \rightarrow \infty$ one has to compute the ground state expectations for H_F . A macroscopic facet emerges as $\lambda \rightarrow \infty$. In Figure 2.15 we display a typical ledge configuration for the TLK model with volume constraint. There is no further ledge above the one shown and for $j \rightarrow -\infty$ ledges are perfectly flat and densely packed.

Since a ledge corresponds to a fermionic world line, the average step density $\mathbb{E}_\lambda(\eta_j(t)) = \rho_\lambda(j)$ is independent of t and given by $\mathbb{E}_\lambda(\eta_j(t)) = \mathbb{E}_\lambda(a_j^* a_j)$ with \mathbb{E}_λ on the right denoting the ground state expectation for H_F . By the linear potential in (2.72) steps are suppressed for large j . Hence the average surface height $h_j^\lambda(t)$ at (j, t) , relative to the high symmetry plane, equals

$$h_j^\lambda(t) = - \sum_{k=j}^{\infty} \mathbb{E}_\lambda(\eta_k(t)). \quad (2.73)$$

$\mathbb{E}_\lambda(a_j^* a_j)$ can be computed in terms of the Bessel function $J_j(z)$ of integer order j and its derivative $L_j(z) = \frac{dJ_j(z)}{dz}$ with the result [81]

$$\rho_\lambda(j) = \mathbb{E}_\lambda(a_j^* a_j) = \lambda(L_{j-1+2[\lambda]}(2\lambda)J_{j+2[\lambda]}(2\lambda) - L_{j+2[\lambda]}(2\lambda)J_{j-1+2[\lambda]}(2\lambda)) \quad (2.74)$$

where $[\cdot]$ denotes the integer part. For large λ the height $h_j^\lambda(t)$ is of order λ . Therefore we rescale the lattice spacing by $1/\lambda$. Then the macroscopic equilibrium crystal shape defined by

$$h_{\text{eq}}(r, t) = \lim_{\lambda \rightarrow \infty} \lambda^{-1} h_{[\lambda r]}^\lambda(\lambda t) \quad (2.75)$$

is given by

$$h_{\text{eq}}(r - 2, t) = \begin{cases} r & \text{for } r \leq -2, \\ \frac{1}{\pi}(r \arccos(r/2) - \sqrt{4 - r^2}) & \text{for } -2 \leq r \leq 2, \\ 0 & \text{for } r \geq 2. \end{cases} \quad (2.76)$$

Thus under volume constraint the TLK model has two facets, one with slope 1, the other one with slope 0, joined by a rounded piece. The upper facet edge is located at $r = 0$. It has zero curvature. Expanding near $r = 0$ results in $h_{\text{eq}}(r, t) \cong -\frac{2}{3\pi}(-r)^{3/2}$, consistent with the Pokrovsky-Talapov law.

With the exact result (2.74) it becomes possible to refine the resolution. The appropriate step size is $\lambda^{1/3}$ lattice constants. For the step density $\rho_\lambda(j) = \mathbb{E}_\lambda(a_j^* a_j)$ close to $r = 0$ one finds

$$\lim_{\lambda \rightarrow \infty} \lambda^{1/3} \rho_\lambda(\lambda^{1/3} x) = -x \text{Ai}(x)^2 + \text{Ai}'(x)^2, \quad (2.77)$$

As the Airy function, (2.77) has the asymptotics

$$\begin{aligned} & \frac{1}{\pi} \sqrt{|x|} \quad \text{for } x \rightarrow -\infty, \\ & \frac{1}{8\pi x} \exp(-4x^{3/2}/3) \quad \text{for } x \rightarrow \infty. \end{aligned} \quad (2.78)$$

Our real interest are the border ledge fluctuations. Clearly the border ledge is the top fermionic world line which we denote by $b_\lambda(t)$. $b_\lambda(t)$ takes integer values and is piecewise constant with unit size kinks. Since, at fixed t , the steps in the bulk have approximately the same statistics as a GUE random matrix, one would expect that the transverse fluctuations of the border ledge equal those of the largest eigenvalue. Indeed, using the fermionic transfer matrix combined with an asymptotic analysis [81], one finds that

$$u \mapsto \lambda^{-1/3} b_\lambda(\lambda^{2/3} u) \quad (2.79)$$

converges to the Airy process in the $\lambda \rightarrow \infty$ limit. Therefore the one-point distribution is the GUE Tracy-Widom distribution F_2 ,

$$\lim_{\lambda \rightarrow \infty} \mathbb{P}(b_\lambda(0) \leq \lambda^{1/3} s) = F_2(s), \quad s \in \mathbb{R}. \quad (2.80)$$

In our context an experimentally more accessible quantity is the ledge wandering $\mathbb{E}((b_\lambda(t) - b_\lambda(0))^2)$. In the limit of large λ it has been computed in [81] with the result

$$\text{Var}(b_\lambda(t) - b_\lambda(0)) \simeq \lambda^{2/3} g(\lambda^{-2/3} t). \quad (2.81)$$

Thus the transverse fluctuations are on the scale $\lambda^{2/3}$. In particular, for small s the scaling function $g(s)$ is linear in s , $g(s) \simeq 2|s|$, indicating that for small, on the scale $\lambda^{2/3}$, separations the border ledge has random walk statistics. On the other hand $g(s)$ saturates for large s , $g(s) \simeq g(\infty) - 2/s^2$, reflecting that the border ledge fluctuations are stationary (on the scale $\lambda^{2/3}$). For more details on the Airy process, see Section 3.3.3.

An alternative proof of the convergence of (2.79) to the Airy process follows from the recent work [19]. Their proof involves Markov dynamics on Young diagrams.

Thermodynamics

The border ledge of the TLK model and the 3D Ising corner have the same scaling behavior, which suggests the scaling to hold in greater generality. To obtain the form which properly distinguishes between model-dependent and universal properties we have to rely on a few notions from the thermodynamics of equilibrium crystal shapes [3]. Let us denote by $h(x, y)$ the height of a vicinal surface relative to the high symmetry reference plane. We find it convenient to measure h in number of atomic layers, whereas x, y are measured in a suitable macroscopic unit. Thus h is dimensionless and x, y have the dimension $[length]$. Further let $k_B T f(\mathbf{u})$ be the surface free energy per unit projected area depending on the

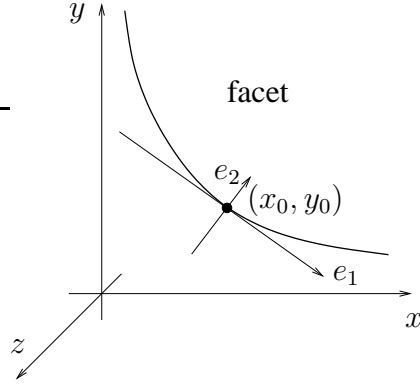


Figure 2.16: The original coordinate axis is $x - y$ and the tangential one is $e_1 - e_2$. The crystal lies in the region with negative z .

local slope $\mathbf{u} = \nabla h$. Below the roughening transition f has a cone at $\mathbf{u} = 0$ and for small \mathbf{u} behaves as

$$f(\mathbf{u}) \simeq \gamma(\theta)|\mathbf{u}| + B(\theta)|\mathbf{u}|^3 \quad (2.82)$$

with θ the polar angle of \mathbf{u} [37, 107]. The *line stiffness* $\tilde{\gamma}$ is defined through $\tilde{\gamma}(\theta) = \gamma(\theta) + \gamma''(\theta)$. As argued in [4], for short range surface models the Gaussian curvature of the equilibrium crystal shape has a universal jump across the facet edge, which implies the relation

$$\tilde{\gamma}(\theta)B(\theta) = \pi^2/6. \quad (2.83)$$

Let us denote by \hat{f} the Legendre transform of f . If $\int dx dy f(\nabla h(x, y))$ is minimized under the constraint of fixed volume, then the resulting equilibrium surface is given by $h(x, y) = \ell \hat{f}(\ell^{-1}x, \ell^{-1}y)$, where ℓ is the Lagrange multiplier adjusted so to give the correct volume [8]. h is convex downwards and has a convex facet lying in the x - y plane. The facet boundary is determined by $\gamma(\theta)$ alone. Close to the facet edge, $h \simeq -\frac{2}{3}\gamma_{PT}d^{3/2}$ with d the normal distance to the facet edge, which defines the *Pokrovsky-Talapov coefficient* γ_{PT} . Under Legendre transformation the angle θ becomes the angle between the x -axis and the outer normal to the facet and, correspondingly, γ_{PT} , the local curvature κ_0 , and the distance r of a point on the edge to the origin are parametrized through this angle θ . The relationship between $\tilde{\gamma}$ and B implies, see Appendix A.1,

$$\gamma_{PT}^2 \kappa_0 = 2\ell^{-2}\pi^{-2}. \quad (2.84)$$

We return to the border ledge fluctuations close to a given angle θ_0 . For this purpose it is convenient to use a preferred axis coordinate system $e_1 - e_2$, see Figure 2.16, centered at $r(\theta_0)$ with the e_1 -axis tangential and the e_2 -axis along the inner normal to the facet. In this frame, we denote by $x_2 = b(x_1)$ the fluctuating border step, where (x_1, x_2) are the coordinate of the points in $e_1 - e_2$. Then $\mathbb{E}(b(x_2)) = \frac{1}{2}\kappa_\perp(\theta_0)x_1^2$, in approximation. For sufficiently small $|x_1|$, still large on the scale of the lattice, $b(x_1)$ is like a random

walk and $\text{Var}(b(x_1) - b(0)) \cong \sigma_\perp^2 |x_1|$, which defines the local wandering coefficient σ_\perp^2 . Following [3] it is natural to equate $\sigma_\perp(\theta)^2$ with the inverse stiffness $\tilde{\gamma}(\theta)^{-1}$. This implies

$$\sigma_\perp^2 = \kappa_\perp \ell, \quad \kappa_\perp = \pi^2 \gamma_{PT,\perp}^2 \sigma_\perp^4 / 2 \quad (2.85)$$

valid for any point on the facet edge.

The general scaling form is obtained now by using the TLK model as benchmark. Locally the border ledge performs a random walk with nearest neighbor hopping rate 1, see (2.72), thus $\sigma^2 = 2$. From (2.76) the PT coefficient is $\gamma_{PT} = 1/\pi\sqrt{\ell}$ in our units. Using these two as model-dependent parameters yields the scaling form

$$\text{Var}(b(x_1) - b(0)) \simeq (\pi\gamma_{PT,\perp})^{-4/3} g((\pi\gamma_{PT,\perp})^{4/3} \sigma_\perp^2 x_1 / 2). \quad (2.86)$$

Of course, through (2.84), (2.85), any other pair of model-dependent parameter can be used to reexpress (2.86).

3D-Ising corner model

Within the volume-constrained TLK model we arrived at an interesting prediction for the border ledge fluctuations. This can be compared with the result of the 3D-Ising corner, where we prove that the border ledge is described by the Airy process too. Then from (2.70) it follows, for large T ,

$$\text{Var}(b_T(\tau T + t) - b_T(\tau T)) \simeq \kappa^2 T^{2/3} g(\kappa T^{-2/3} t / 2) \quad (2.87)$$

with $\kappa = \sqrt[3]{2b''_\infty(\tau)}$. As we have seen, the (111)-projection of the 3D-Ising corner gives a lozenge tiling. The free-energy of the lozenge tiling is the logarithm of the partition function computed in [111, 16] using Kasteleyn's method [50]. From this it follows that the ‘‘natural’’ limit shape is $\hat{f}(0, y) = -\ln(1 - e^{-y})$, which is the half of the one computed by the parameter T , compare with (2.68). Thus the first relation is

$$\ell = 2T. \quad (2.88)$$

Then explicit computations leads to

$$\begin{aligned} \kappa_\perp &= (2T)^{-1} \sigma_\perp^2, \\ \sigma_\perp^2 &= 2b''_\infty(\tau) (1 + b'_\infty(\tau)^2)^{-3/2}, \\ \gamma_{PT,\perp} &= (2b''_\infty(\tau))^{-1/2} T^{-1/2} \pi^{-1} (1 + b'_\infty(\tau)^2)^{3/4}. \end{aligned} \quad (2.89)$$

The terms $1 + b'_\infty(\tau)^2$ come from the particular orientation of the $e_1 - e_2$ axis, see (A.9) in Appendix A.1.

2.3.5 On general macroscopic facets

In this section we discuss the macroscopic equilibrium crystal shapes, one of which is the limit shape of the 3D-Ising corner. The macroscopic shape which minimize the surface free energy can be determined by the Wulff construction. For a more extended description see [73].

The surface tension

First we define the surface tension σ . Consider a macroscopic three-dimensional crystal and a plane Π with normal direction \mathbf{u} . To break the crystal into two parts along the plane Π and create two surfaces of area A , a work $W(\mathbf{u})$ is needed. The surface tension $\sigma(\mathbf{u})$ is the surface free energy per unit area, which is then given by $\sigma(\mathbf{u}) = W(\mathbf{u})/2A$ in the limit of large crystals. Let Σ be the surface of a crystal, the total free energy of Σ is given by

$$\mathcal{F} = \int_{\Sigma} \sigma dS \quad (2.90)$$

where dS is the surface element. (2.90) assumes already that the crystal is large (negligible border effects) and incompressible.

Equilibrium crystal shape

Equilibrium crystal shapes results from the minimization of the surface free energy. Given the surface tension σ , there is a geometrical construction which leads to the unique convex crystal shape minimizing the surface free energy (up to a global scaling fixed by the volume), the

Wulff construction: Fix the origin O , and for each direction \mathbf{u} define the point H on the spherical plot of σ given by $OH = \sigma(\mathbf{u})\mathbf{u}$. Construct the plane $\Pi_{\mathbf{u}}$ passing by H and orthogonal to \mathbf{u} . Then surface crystal shape is the inner envelope of all the planes $\Pi_{\mathbf{u}}$.

Facets in equilibrium crystal shapes appear only when the surface tension has non-differentiable points/lines.

Random surfaces and random tilings

Now we consider a particular class of random surfaces, the ones which can be mapped to random tilings. One example is the 3D-Ising corner described above. The surface tension can also be computed by microscopic models, the free energy being $-\ln Z$ with Z the partition function. For the 3D-Ising corner, the limit shape was obtained already in [16] using the mapping to the random tiling explained above, for which the free energy was known [111]. Moreover, in [20] a law of large numbers is proven for the microscopic model and shown that the limit shape obtained by the Wulff construction agrees using the free energy $-\ln Z$.

A first variation of the rhombus tiling of Figure 2.13 consists in giving different weights to the orientations of the rhombi. In this case a new facet F shows up with normal direction $(1, 1, 1)$ as proven by Blöte, Hilhorst, and Nienhuis in [17]. The border of the facet F shows the Pokrovsky-Talapov law too.

Recently Kenyon, Okounkov, and Sheffield [53] studied random surfaces which arise as height functions of random tilings on weighted, bipartite lattices with periodic boundary conditions. Among others, they shows (Theorem 5.5 in [53]) that inside any of the rounded

pieces the second derivative has constant determinant. This result would imply that (2.82) holds for these models too, thus also the PT-law.

Airy process: an open question

Consider for example the facet F . Macroscopically it is flat, but on a microscopic scale some irregularities exist. The border line between the rounded part and the facet F is not uniquely defined. One can define it as the border of the first macroscopic island without including eventual spikes on the atomic scale. Therefore, up to some coarse graining of order one, the different possible definitions should agree. From the argument explained above, the Pokrovsky-Talapov law should hold for all the facets like F . Therefore we can conjecture that the border line of these facets are also described by the Airy process, but the question remains open.

Chapter 3

Line ensembles and point processes

In this chapter we first introduce the notion of point process and two of its classes, the determinantal and the Pfaffian point processes. Then we consider the Gaussian ensembles of random matrix theory. Their eigenvalues form some determinantal/Pfaffian point processes. An edge scaling at the border of the spectrum of eigenvalues leads to some limiting point processes which show up in our results on the 3D-Ising corner and on the flat PNG. The eigenvalues of the Gaussian ensembles can be seen as positions of particles subjected to some random evolution. This is known as Dyson's Brownian motion and leads to a natural extension of the determinantal point process. In the last part of the chapter we turn back to our models and we map them to some non-intersecting line ensembles. In the subsequent two chapters we study the point processes defined by the positions of the lines.

3.1 Point processes

3.1.1 Determinantal point processes

Definitions

A point process is a measurable mapping from a probability space to a measurable space [64]. First let us construct the probability space. Denote by X a one-particle space, which we take to be \mathbb{R}^d , \mathbb{Z}^d , or some subset of them. Let Γ be the space of finite or countable configurations of particles in X , where the particles are ordered in some natural way and *each configuration* $\xi = (x_i)$, $x_i \in X$, $i \in \mathbb{Z}$ (or \mathbb{N} if $d > 1$) is *locally finite*, i.e., for every compact $B \subset X$, the number of $x_i \in B$, denoted $n(B)(\xi)$, is finite. Next we define the σ -algebra on Γ via the cylinder sets. For any bounded Borel set $B \subset X$ and $n \geq 0$, $C_n^B = \{\xi \in \Gamma, n(B)(\xi) = n\}$ is a cylinder set. Then we define \mathcal{F} as the σ -algebra generated by all cylinder sets and denote by \mathbb{P} a probability measure on (Γ, \mathcal{F}) .

Secondly we define the measurable space of the *point measures*. Let $\mathcal{B}(X)$ be the Borel σ -algebra of X . A point measure on X is a positive measure ν on the space $(X, \mathcal{B}(X))$ which is a locally finite sum of Dirac measures, i.e., for $x \in X$, $\nu(x) = \sum_{i \in I} \delta(x - x_i)$ with $x_i \in X$, $I \subset \mathbb{N}$, and for any bounded subset $B \subset X$, $x_i \in B$ for a finite number of

$i \in I$. Then denote by $M_p(X)$ the space of point measures defined on X and $\mathcal{M}_p(X)$ the σ -algebra generated by the applications $\nu \rightarrow \nu(f)$ of $M_p(X)$ to $\mathbb{N} \cup \{\infty\}$ obtained when f span $\mathcal{B}(X)$.

Definition 3.1. A point process η on X is a measurable mapping from $(\Gamma, \mathcal{F}, \mathbb{P})$ into $(M_p(X), \mathcal{M}_p(X))$. The probability law of this point process is the image of \mathbb{P} by η .

Moments of random variables (observables) can be expressed in terms of correlation functions which are defined as follows.

Definition 3.2. Let μ be a reference measure on X . The n -point correlation function of point process on $(\Gamma, \mathcal{F}, \mathbb{P})$ is a locally integrable function $\rho^{(n)} : X^n \rightarrow \mathbb{R}_+$ such that:
a) if μ is absolutely continuous with respect to the Lebesgue measure: for any disjoint infinitesimally small subsets $[x_i, x_i + dx_i]$, $i = 1, \dots, n$,

$$\mathbb{P}(\{n([x_i, x_i + dx_i]) = 1, i = 1, \dots, n\}) = \rho^{(n)}(x_1, \dots, x_n) \mu(dx_1) \dots \mu(dx_n), \quad (3.1)$$

where $\mu(dx)$ denotes $\mu([x, x + dx])$.

b) if μ is supported on a discrete sets of points: for any distinct points x_1, \dots, x_n of X ,

$$\mathbb{P}(\{n(x_i) = 1, i = 1, \dots, n\}) = \rho^{(n)}(x_1, \dots, x_n) \mu(x_1) \dots \mu(x_n). \quad (3.2)$$

Obviously the n -point correlation functions have to be symmetric in their arguments. The first question is to know whether the n -point correlation functions defines uniquely the point process or not. A first sufficient condition found by Ruelle, chapters 4.7 and 7 in [87], writes $\rho^{(n)}(x_1, \dots, x_n) \leq c^n$ a.s. for some $c > 0$ uniformly in (x_1, \dots, x_n) . Lenard studied the problem again and obtained a weaker condition. Let us define, for $A \subset X$,

$$m_k^A = \frac{1}{k!} \int_{A^k} \rho^{(k)}(x_1, \dots, x_k) d\mu(x_1) \dots d\mu(x_k). \quad (3.3)$$

If for all bounded measurable subset $A \subset X$

$$\sum_{k=1}^{\infty} (m_k^A)^{-1/k} = \infty, \quad (3.4)$$

then the point process is uniquely defined [58, 91].

Since $m_k^A \leq m_k^B$ if $A \subset B$, then to verify (3.4) it is enough to analyze the behavior of m_k^A for large A . In particular, for $X = \mathbb{R}$ it is enough to check (3.4) for $A = [-M, M]$ for all $M \in \mathbb{R}$. Remark also that no uniformity in M is required. In terms of correlation functions, if

$$\rho^{(n)}(x_1, \dots, x_n) \leq n^{2n} c^n \quad \text{a.s.} \quad (3.5)$$

for some $c > 0$, then (3.4) is satisfied. There is a stronger condition than (3.4) but easy to verify in some concrete situations [58], namely $\liminf_{k \rightarrow \infty} (m_k^A)^{-1/k} > 0$ for every bounded $A \subset X$.

The second question analyzed by Lenard [59] is to know under which conditions a set of locally integrable functions $\rho_n : X^n \rightarrow \mathbb{R}_+$ are correlation functions of some point process. The first condition is the *symmetry condition*

$$\rho_n(x_1, \dots, x_n) = \rho_n(x_{\sigma(1)}, \dots, x_{\sigma(n)}) \quad (3.6)$$

for all permutation $\sigma \in \mathcal{S}_n$, which is obviously necessary. To state the second condition, we first have to introduce a few definitions. We denote by K the space of *finite sequences* of points in X : $K = \bigcup_{n \geq 0} X^n$ where X^0 denotes the empty sequence. A subset $H \subseteq K$ is compact if and only if it is of the form $H = \bigcup_{n=0}^m H_n$ with $H_n \subset X^n$ compact and $m \geq 0$ *finite*. Consider any real valued function f on K with compact support and denote by f_k the restriction of f to X^k . Define a real function Sf on Γ by

$$(Sf)(\xi) = \sum_{k \geq 0} \sum_{i_1 \neq \dots \neq i_k} f_k(x_{i_1}, \dots, x_{i_k}). \quad (3.7)$$

The sum over k is finite because f is of compact support. The *positivity condition* is the following. If $f : K \rightarrow \mathbb{R}$ is a bounded measurable function such that $(Sf)(\xi) \geq 0$ for all $\xi \in \Gamma$, then

$$\mathbb{E}(Sf) = \sum_{k \geq 0} \int_{X^k} f_k(x_1, \dots, x_k) \rho_n(x_1, \dots, x_k) d\mu(x_1) \cdots d\mu(x_k) \geq 0 \quad (3.8)$$

holds if ρ_n are correlation functions, μ being the reference measure on X .

Correlation functions are important in the computation of expected values of observables. Some random variables of interest are often called *linear statistics* and are of the form

$$\sum_i f(x_i) \quad (3.9)$$

for some real function f . Define the function $u = 1 - e^f$. Then

$$\begin{aligned} \mathbb{E}\left(\exp\left(\sum_j f(x_j)\right)\right) &= \mathbb{E}\left(\prod_j (1 - u(x_j))\right) = \sum_{n=0}^{\infty} (-1)^n \mathbb{E}\left(\sum_{j_1 < \dots < j_n} \prod_{k=1}^n u(x_{j_k})\right) \\ &= \sum_{n=0}^{\infty} \frac{(-1)^n}{n!} \mathbb{E}\left(\sum_{j_1 \neq \dots \neq j_n} \prod_{k=1}^n u(x_{j_k})\right) \\ &= \sum_{n=0}^{\infty} \frac{(-1)^n}{n!} \int_{X^n} d^n \mu(x) \rho^{(n)}(x_1, \dots, x_n) \prod_{j=1}^n u(x_j). \end{aligned} \quad (3.10)$$

An interesting class of point processes which will be considered in the rest of the section are the determinantal point processes, also called *fermionic* since the probability that two points are at the same position is zero.

Definition 3.3. A point process is called *determinantal* if the n -point correlation functions are given by

$$\rho^{(n)}(x_1, \dots, x_n) = \text{Det}(K(x_i, x_j))_{1 \leq i, j \leq n} \quad (3.11)$$

where $K(x, y)$ is a kernel of an integral operator $K : L^2(X, \mu) \rightarrow L^2(X, \mu)$, non-negative and locally trace class.

The positivity is required because the n -point correlation functions are positive, and locally trace class because each configuration is locally finite. For a determinantal point process, (3.11) in (3.10) leads to

$$\begin{aligned} \mathbb{E} \left(\prod_j (1 - u(x_j)) \right) &= \sum_{n=0}^{\infty} \frac{(-1)^n}{n!} \int_{X^n} \text{Det}(K(x_i, x_j))_{1 \leq i, j \leq n} \prod_{j=1}^n u(x_j) d^n \mu(x) \\ &\equiv \text{Det}(\mathbb{1} - uK)_{L^2(X, \mu)} \end{aligned} \quad (3.12)$$

where for each $\varphi \in L^2(X, \mu)$,

$$[(uK)\varphi](x) = \int_X u(x)K(x, y)\varphi(y)d\mu(y). \quad (3.13)$$

The last determinant in (3.12) is called *Fredholm determinant* of the operator uK on the space $L^2(X, \mu)$, see also Appendix A.2. Note that uK in (3.12) can be replaced by the symmetrized $u^{1/2}Ku^{1/2}$, where with $u^{1/2}$ we mean the multiplication operator by $u(x)^{1/2}$.

A special but important observable which can be computed via a Fredholm determinant is the *hole probability*. For a subset B of X the probability that it is empty is

$$\mathbb{P}(\{n(B) = 0\}) = \mathbb{E} \left(\prod_j (1 - \chi_B(x_j)) \right) = \text{Det}(\mathbb{1} - K)_{L^2(B, \mu)}. \quad (3.14)$$

In particular for a determinantal point process on \mathbb{R} or \mathbb{Z} which has a *last particle* whose position is denoted by x_{\max} , the distribution of x_{\max} writes

$$\mathbb{P}(x_{\max} \leq t) = \mathbb{P}(n((t, \infty)) = 0) = \text{Det}(\mathbb{1} - K)_{L^2((t, \infty), \mu)}. \quad (3.15)$$

The next question is to know whether a given point process is determinantal or not. Borodin (Prop. 2.2 of [18], see also Tracy and Widom for the GUE case [102]) determined the following class of determinantal point process.

Theorem 3.4. *If we have a measure of the form*

$$\frac{1}{Z_N} \text{Det}(\varphi_j(x_k))_{j, k=1, \dots, N} \text{Det}(\psi_j(x_k))_{j, k=1, \dots, N} d^N \mu(x), \quad (3.16)$$

then it is a determinantal process with kernel

$$K_N(x, y) = \sum_{i, j=1}^N \psi_i(x)[A^{-1}]_{i, j} \varphi_j(y) \quad (3.17)$$

where

$$A = [A_{i,j}]_{i,j=1,\dots,N}, \quad A_{i,j} = \int_X \psi_j(t) \varphi_i(t) d\mu(t) \quad (3.18)$$

Unfortunately, although an explicit formula is given, it is not always easy (feasible) to invert the matrix A as $N \rightarrow \infty$. A particular case is when $A = \mathbb{1}$ in a particular basis. In this case the kernel $K_N(x, y)$ becomes of simple form and the limiting distribution can be analyzed.

Some important kernels: sine and Airy kernel

Let $x, x' \in \mathbb{R}$, the *sine kernel* is defined by

$$S_\varrho(x, x') = \frac{\sin(\varrho\pi(x - x'))}{\pi(x - x')}, \quad (3.19)$$

with ϱ the density of points. By rescaling, ϱ can be always be set to one, but we prefer to keep the parameter in general. The *Airy kernel* writes

$$A(x, x') = \frac{\text{Ai}(x) \text{Ai}'(x') - \text{Ai}'(x) \text{Ai}(x')}{x - x'} \quad (3.20)$$

where $\text{Ai}(x)$ is the Airy function [1]. In some models appears the *discrete sine kernel*, which means only that $x, x' \in \mathbb{Z}$.

In Section 3.2.2 we will see that the asymptotics in the bulk of the spectrum of GUE random matrices leads to the sine kernel, and in the edge of the spectrum to the Airy kernel.

3.1.2 Pfaffian point processes

A generalization of determinantal point process are the *Pfaffian point processes*. First we define the Pfaffian. Let $A = [A_{i,j}]_{i,j=1,\dots,2N}$ be an *antisymmetric* matrix, then its Pfaffian is defined by

$$\text{Pf}(A) = \sum_{\substack{\sigma \in S_{2N} \\ \sigma_{2i-1} < \sigma_{2i}}} (-1)^{|\sigma|} \prod_{i=1}^N A_{\sigma_{2i-1}, \sigma_{2i}}, \quad (3.21)$$

where S_{2N} is the set of all permutations of $\{1, \dots, 2N\}$. Notice that the Pfaffian depends only on the upper triangular part of A . For an antisymmetric matrix the identity $\text{Pf}(A)^2 = \text{Det}(A)$ holds.

Definition 3.5. *A point process is Pfaffian if the n -point correlation functions are given by*

$$\rho^{(n)}(x_1, \dots, x_n) = \text{Pf}[K(x_i, x_j)]_{i,j=1,\dots,n}, \quad (3.22)$$

where $K(x, y)$ is a 2×2 antisymmetric matrix kernel.

With the notation $[K(x_i, x_j)]_{i,j=1,\dots,n}$ we mean the $2n \times 2n$ matrix composed by n^2 matrix blocks $K(x_i, x_j)$ of size 2×2 .

A class of Pfaffian point process is introduced in [82], see also [92]. Let (X, μ) be a measurable space, f_1, \dots, f_{2N} complex-valued functions on X and $\varepsilon(x, y)$ be an *antisymmetric kernel*, and define by

$$p(x_1, \dots, x_{2N}) = \frac{1}{Z_{2N}} \text{Det}[f_j(x_k)]_{j,k=1,\dots,2N} \text{Pf}[\varepsilon(x_j, x_k)]_{j,k=1,\dots,2N} \quad (3.23)$$

the density of a $2N$ -dimensional probability distribution on X^{2N} with respect to $\mu^{\otimes 2N}$, the product measure generated by μ . The normalization constant is given by

$$Z_{2N} = \int_{X^{2N}} d^{2N} \mu \text{Det}[f_j(x_k)]_{j,k=1,\dots,2N} \text{Pf}[\varepsilon(x_j, x_k)]_{j,k=1,\dots,2N} = (2N)! \text{Pf}[M] \quad (3.24)$$

where the matrix $M = [M_{i,j}]_{i,j=1,\dots,2N}$ is defined by

$$M_{i,j} = \int_{X^2} f_i(x) \varepsilon(x, y) f_j(y) d\mu(x) d\mu(y). \quad (3.25)$$

The point process with measure (3.23) is Pfaffian with the antisymmetric kernel $K(x, y)$ given by

$$K(x, y) = \begin{pmatrix} K_{1,1}(x, y) & K_{1,2}(x, y) \\ K_{2,1}(x, y) & K_{2,2}(x, y) \end{pmatrix}, \quad (3.26)$$

where

$$\begin{aligned} K_{1,1}(x, y) &= \sum_{i,j=1}^{2N} f_i(x) M_{j,i}^{-1} f_j(y), \\ K_{1,2}(x, y) &= \sum_{i,j=1}^{2N} f_i(x) M_{j,i}^{-1} (\varepsilon f_j)(y), \\ K_{2,1}(x, y) &= \sum_{i,j=1}^{2N} (\varepsilon f_i)(x) M_{j,i}^{-1} f_j(y), \\ K_{2,2}(x, y) &= -\varepsilon(x, y) + \sum_{i,j=1}^{2N} (\varepsilon f_i)(x) M_{j,i}^{-1} (\varepsilon f_j)(y), \end{aligned} \quad (3.27)$$

provided that M is invertible, and $(\varepsilon f_i)(x) = \int_X \varepsilon(x, y) f_i(y) d\mu(y)$. $M_{j,i}^{-1}$ means the (j, i) component of the inverse of the matrix M . Note the order of indices in $M_{j,i}^{-1}$. Similarly to the determinantal processes, the linear statistics of Pfaffian processes is given by the Fredholm Pfaffian of the kernel K . Let $u = 1 - e^f$, then

$$\mathbb{E}_N \left(\exp \left(\sum_j f(x_j) \right) \right) = \mathbb{E}_N \left(\prod_{j=1}^{2N} (1 - u(x_j)) \right) = \text{Pf}(J - Ku) = \sqrt{\text{Det}(\mathbb{1} + JKu)} \quad (3.28)$$

with the matrix kernel $J(x, y) = \delta_{x,y} \begin{pmatrix} 0 & 1 \\ -1 & 0 \end{pmatrix}$. For Fredholm Pfaffian see Appendix A.2.

Finally notice that the determinantal point processes are included in the Pfaffian ones. In fact if K is of the form $K = \begin{pmatrix} \varepsilon & K_0 \\ -K_0 & 0 \end{pmatrix}$, then for arbitrary ε the point process is determinantal with kernel K_0 . In fact, $\text{Pf}(J + K) = \text{Det}(\mathbb{1} + K_0)$ in this case [82].

3.2 Random matrices

3.2.1 Classical Gaussian random matrix ensembles

In this section we explain some results on the classical Gaussian random matrix ensembles which are linked with our problems. Of particular interest for our work are the edge statistics of the eigenvalues, which lead to the Tracy-Widom distributions [103]. The standard reference on classical random matrices is Mehta's book [62]. The reader interested in a shorter discussion on random matrices in physics can read [56]. For more recent reviews see for example [71, 72].

Gaussian Orthogonal, Unitary, Symplectic Ensembles

Usually the spectrum of an hamiltonian contains both continuum and discrete part. If we are interested in the discrete spectrum we restrict the Hilbert space to a finite subspace where the hamiltonian is represented as a hermitian matrix. Moreover, if there exists some constants of motion, then the matrix is decomposed into blocks. Consider one of these blocks, say a $N \times N$ hermitian matrix H . If the only constraints are space-time symmetries, then there are three important cases of random matrices [24]

- $\beta = 1$: if the system is invariant with respect to time-inversion and the total angular momentum is integer or the system is rotational invariant, then the matrix H can be taken *real symmetric*. Since it can be diagonalized by an orthogonal transformation, the corresponding random matrix ensemble is called *orthogonal*.
- $\beta = 2$: if the system is not invariant with respect to time-inversion (for example, systems with external magnetic field), then the matrix H is *complex hermitian*. It can be diagonalized by a unitary transformation, so the random matrix ensemble is called *unitary*.
- $\beta = 4$: if the system is invariant with respect to time-inversion but with half-integer total angular momentum, then the matrix H is *real quaternionic*. It can be diagonalized by a symplectic unitary transformation and the random matrix ensemble is called *symplectic* (see Appendix A.3).

The meaning of β will be clear at the level of the distribution of eigenvalues. The eigenvalues are real for all these three ensembles. The classical Gaussian ensembles are obtained setting the probability distribution on matrices as

$$p(H)dH = \frac{1}{Z'} e^{-\text{Tr}(H^2)/2N} dH \quad (3.29)$$

where dH is the Lebesgue product measure on the independent elements of H and Z' is the normalization. The ensembles of random matrices obtained are called *Gaussian Orthogonal* (GOE), *Unitary* (GUE), and *Symplectic* (GSE) *Ensembles* for $\beta = 1$, $\beta = 2$, and $\beta = 4$ respectively.

Remark: the factor $1/2N$ in (3.29) is somewhat unusual, but it turns out to be convenient for the comparison with the results on the PNG and the 3D-Ising corner.

The distribution (3.29) is also recovered by taking the independent elements of H as Gaussian random variables with mean zero and variance N for the diagonal terms, $N/2$ for the non-diagonal terms (since in $\text{Tr}(H^2)$ they appears twice).

Another way to obtain (3.29) is to maximize the functional “entropy” [14]

$$S(p) = - \int p(H) \ln p(H) dH \quad (3.30)$$

under the condition $\mathbb{E}(\text{Tr}(H^2)/2N) = \frac{1}{2}n$, where $n = N + \frac{1}{2}\beta N(N-1)$ is the number of independent elements of the matrix H , see also Appendix A.4. This is the same method used to derive the canonical and grand-canonical measures in statistical mechanics.

Distribution of eigenvalues

One interesting quantity of random matrices is the distribution of eigenvalues, because they are the energy of the system with Hamiltonian H . The probability distribution (3.29) depends only on the eigenvalues of the matrices, reflecting the requirement that (3.29) has to be independent of the choice of the basis used to describe the physical system. This means that (3.29) is invariant under the symmetry group, i.e., orthogonal group $G = O(N)$ for GOE, unitary group $G = U(N)$ for GUE, and unitary symplectic group $G = USp(2N)$ for GSE.

We can diagonalize H by a transformation of the group G , $H = g\Lambda g^{-1}$ for some $g \in G$, with $\Lambda_{i,j} = \lambda_i \delta_{i,j}$, λ_i the eigenvalues of H . The infinitesimal transformation is

$$\delta H = g\delta H'g^{-1}, \quad \delta H' = \delta\Lambda + [g^{-1}\delta g, \Lambda], \quad (3.31)$$

which implies that the jacobian of the change of variable from H to H' is one. On the other hand,

$$\delta H'_{i,j} = \delta\lambda_i \delta_{i,j} + \delta\Omega_{i,j}(\lambda_i - \lambda_j), \quad \delta\Omega = g^{-1}\delta g, \quad (3.32)$$

then the jacobian from H' to (Λ, g) is given by $\prod_{1 \leq i < j \leq N} |\lambda_j - \lambda_i|^\beta$. The variations $\delta\Omega$ can be described by parameterizing the group G , and give as volume element the Haar measure dG . It then follows that $dH = |\Delta_N(\lambda)|^\beta d\lambda dG$, with $d\lambda = \prod_{k=1}^N d\lambda_k$ and

$$\Delta_N(\lambda) = \text{Det}(\lambda_i^{j-1})_{i,j=1}^N = \prod_{1 \leq i < j \leq N} (\lambda_j - \lambda_i). \quad (3.33)$$

$\Delta_N(\lambda)$ is called the Vandermonde determinant. Finally integrating over the symmetry group G , the joint probability distribution of the eigenvalues is

$$\mathbb{P}_{\beta,N}(\lambda_1, \dots, \lambda_N) d\lambda_1 \cdots d\lambda_N = \frac{1}{Z_{\beta,N}} |\Delta_N(\lambda)|^\beta \prod_{j=1}^N e^{-\lambda_j^2/2N} d\lambda_j, \quad (3.34)$$

with $Z_{\beta,N}$ the normalization constant.

Now we review some results on the distribution of eigenvalues in the $N \rightarrow \infty$ limit.

Wigner semi-circle law

Denote by $\rho_{\beta,N}(\lambda)$ the expected density of eigenvalues at λ . For large N this density vanishes outside the interval $[-2N, 2N]$ and has a semi-circle shape (if the eigenvalues are rescaled by $2N$). This is the *Wigner semi-circle law*, and in our setting writes

$$\rho_{\beta,N}(\lambda) \simeq \frac{1}{\pi} \sqrt{(1 - (\lambda/2N)^2)_+} \quad (3.35)$$

for large N , where $x_+ = \max\{0, x\}$.

In [42] the *global* fluctuations properties of the eigenvalues is studied. The case for general confining potential $V(x)$ (in the Gaussian ensembles $V(x) = x^2/2N$) so that the weight on random matrices is $e^{-\text{Tr}(V(H))}$ and for all β is studied. In our setting the result is the following. For continuous function $f : [-1, 1] \rightarrow \mathbb{R}$ which increases at most as the potential V ,

$$\ln \mathbb{E} \left(e^{\sum_{j=1}^N f(\lambda_j/2N)} \right) - \int_{-2N}^{2N} d\lambda \rho_{\beta,\infty}(\lambda) f(\lambda/2N) \longrightarrow B(f) \quad (3.36)$$

as $N \rightarrow \infty$ where $B(f)$ is an explicit quadratic functional of f . Remark that no factor $1/\sqrt{N}$ is needed.

Fluctuations in the bulk for GUE

In a recent preprint, Gustavsson considers the distribution of the k -th largest eigenvalue of GUE [38]. He proves that if $k \rightarrow \infty$ as $N \rightarrow \infty$ (and by symmetry, $N - k \rightarrow \infty$ too), then it converges to a normal distribution when properly rescaled. First consider k such that λ_k is in the bulk. Let $k = k(N)$ be chosen such that $k/N \rightarrow a \in (0, 1)$ as $N \rightarrow \infty$. Let t be the value such that $\mathbb{E}_N(\lambda_k) = 2Nt$. Then, for large N ,

$$\lambda_k \simeq 2Nt + \left(\frac{\ln N}{2(1-t^2)} \right)^{1/2} \xi_G \quad (3.37)$$

with ξ_G a random variable with normal distribution $N(0, 1)$. Next he considered k such that $k \rightarrow \infty$ as $N \rightarrow \infty$ but with $k/N \rightarrow 0$, thus still close to the edge. Then, for large N ,

$$\lambda_{N-k} \simeq 2N \left(1 - \left(\frac{3\pi}{4\sqrt{2}} \right)^{2/3} (k/N)^{2/3} \right) + \left(\frac{2}{(12\pi)^{2/3}} \frac{\ln k}{(k/N)^{2/3}} \right)^{1/2} \xi_G. \quad (3.38)$$

He also determines a convergence of the joint-distribution functions of m eigenvalues.

Largest eigenvalue: Tracy-Widom distributions

The Wigner semi-circle law tells us that the largest eigenvalue $\lambda_{N,\max}$ is located close to $2N$. Tracy and Widom study the distribution of $\lambda_{N,\max}$ in the limit $N \rightarrow \infty$ for $\beta = 1, 2, 4$

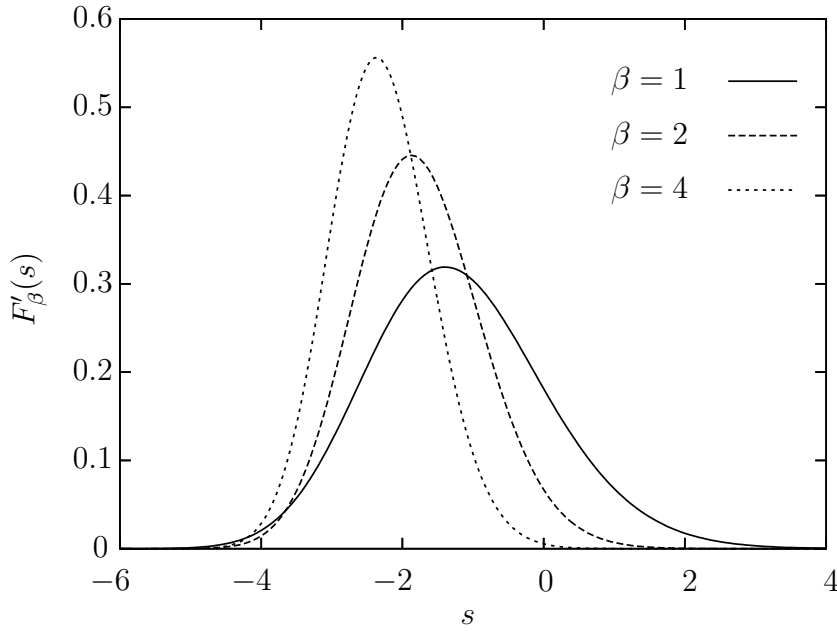


Figure 3.1: Probability densities of the Tracy-Widom distributions generated using [80].

with the following result [100, 101], see also their review paper [103]. Let $F_{\beta,N}(t) = \mathbb{P}_{\beta,N}(\lambda_{N,\max} \leq t)$, then $F_{\beta}(s)$ defined by

$$F_{\beta}(s) = \lim_{N \rightarrow \infty} F_{\beta,N}(2N + sN^{1/3}) \quad (3.39)$$

exists for $\beta = 1, 2, 4$. For $\beta = 2$, it is given by

$$F_2(s) = \exp\left(-\int_s^{\infty} (x-s)q^2(x)dx\right) \quad (3.40)$$

where q is the unique solution of the Painlevé II equation $q'' = sq + 2q^3$ satisfying the asymptotic condition $q(s) \sim \text{Ai}(s)$ for $s \rightarrow \infty$. F_2 is called the *GUE Tracy-Widom distribution*. For $\beta = 1$ the *GOE Tracy-Widom distribution* reads

$$F_1(s) = \exp\left(-\frac{1}{2}\int_s^{\infty} q(x)dx\right)F_2(s)^{1/2} \quad (3.41)$$

and for $\beta = 4$ the *GSE Tracy-Widom distribution* reads

$$F_4(s/\sqrt{2}) = \cosh\left(\frac{1}{2}\int_s^{\infty} q(x)dx\right)F_2(s)^{1/2}. \quad (3.42)$$

Remark: $F_2(s)$ can also be rewritten as a Fredholm determinant of the Airy operator, see Section 3.2.2, and $F_1(s)$, $F_4(s)$ as Fredholm Pfaffians, see Section 3.2.3.

Some characteristics of these distributions are reported in the following table.

β	Mean	Variance	Skewness	Kurtosis
1	-1.20653	1.6078	0.293	0.165
2	-1.77109	0.8132	0.224	0.094
4	-2.30688	0.5177	0.166	0.049

We remind that, if χ is a random variable, then the skewness is defined by $\mathbb{E}((\chi - \mathbb{E}(\chi))^3)/\mathbb{E}((\chi - \mathbb{E}(\chi))^2)^{3/2}$ and measures the degree of asymmetry of the distribution of χ . The kurtosis is defined by $\mathbb{E}((\chi - \mathbb{E}(\chi))^4)/\mathbb{E}((\chi - \mathbb{E}(\chi))^2)^2 - 3$ and measures the degree to which a distribution is flat or peaked (for normal distribution is 0).

Moreover the tails of the distributions are, for $x \rightarrow -\infty$,

$$\ln(F_1'(x)) \simeq -\frac{1}{24}|x|^3, \quad \ln(F_2'(x)) \simeq -\frac{1}{12}|x|^3, \quad \ln(F_4'(x)) \simeq -\frac{1}{24}|\sqrt{2}x|^3, \quad (3.43)$$

and for $x \rightarrow \infty$,

$$\ln(F_1'(x)) \simeq -\frac{2}{3}x^{3/2}, \quad \ln(F_2'(x)) \simeq -\frac{4}{3}x^{3/2}, \quad \ln(F_4'(x)) \simeq -\frac{2}{3}(\sqrt{2}x)^{3/2}. \quad (3.44)$$

3.2.2 GUE eigenvalues: a determinantal process

Consider the case of $N \times N$ hermitian matrices and let $V(x)$ be an *even degree* polynomial with positive leading coefficient. Define a measure on random matrices by

$$\frac{1}{Z_N} e^{-\text{Tr} V(M)} dM \quad (3.45)$$

with $dM = \prod_{i=1}^N dM_{i,i} \prod_{1 \leq i < j \leq N} d\text{Re} M_{i,j} d\text{Im} M_{i,j}$. The GUE ensemble is recovered by setting $V(x) = x^2/2N$. The same procedure used for the GUE case leads to the distribution of eigenvalues

$$\frac{1}{Z_N} \Delta_N(\lambda)^2 \prod_{j=1}^N e^{-V(\lambda_j)} d\lambda_j. \quad (3.46)$$

We denote by ζ_N the point process of the eigenvalues $\lambda_1, \dots, \lambda_N$ of the random matrices, i.e.,

$$\zeta_N(x) = \sum_{j=1}^N \delta(x - \lambda_j), \quad x \in \mathbb{R}. \quad (3.47)$$

In particular the point process of $N \times N$ GUE random matrices is denoted by ζ_N^{GUE} .

ζ_N is a determinantal point process. For GUE random matrices this is an old result of Gaudin, Mehta, and Dyson, see Chapter 5 of [62]. Let $p_k(x)$, $k = 0, 1, \dots$ be the orthogonal polynomials with respect to the weight $e^{-V(x)} dx$, normalized as $\int_{\mathbb{R}} p_i(x) p_j(x) e^{-V(x)} dx = \delta_{i,j}$. Then the eigenvalue process ζ_N is determinantal with correlation kernel

$$K_N(x, y) = \sum_{k=0}^{N-1} p_k(x) p_k(y) e^{-\frac{1}{2}(V(x)+V(y))}. \quad (3.48)$$

Using the Christoffel-Darboux formula [99], (3.48) can be rewritten as

$$K_N(x, y) = \frac{u_{N-1} p_N(x) p_{N-1}(y) - p_{N-1}(x) p_N(y)}{u_N (x - y)} e^{-\frac{1}{2}(V(x)+V(y))}. \quad (3.49)$$

where u_k is the leading coefficient of p_k . (3.48) can be recovered by Theorem 3.4 as follows. Let the reference measure μ be the Lebesgue measure. Consider the vector space W_N with basis $B_1 = \{\varphi_j(x) = \psi_j(x) = x^{j-1} e^{-V(x)/2}, j = 1, \dots, N\}$, and with the scalar product $\langle g, f \rangle = \int_{\mathbb{R}} f(x)g(x)dx$. After a change of basis (Gram-Schmidt orthonormalization) one obtains an orthonormal basis $B_2 = \{b_j(x), j = 1, \dots, N\}$. If we denote by M the matrix with elements $M_{j,k} = \varphi_j(x_k)$, then the measure (3.16) is $\text{Det}(M)d^N x$. Let S be the basis transformation matrix from B_1 to B_2 and \tilde{M} be the matrix with entries $\tilde{M}_{j,k} = b_j(x_k)$. Then $\tilde{M} = S^{-1}M$ and then the measure (3.16) is $\text{Det } \tilde{M} \text{Det } S d^N x$. $\text{Det } S$ is a number which can be included in the normalization and $A = \mathbb{1}$ in the basis of the $b_j(x) \equiv p_{j-1}(x)e^{-V(x)/2}$'s.

Random matrices are therefore connected with orthogonal polynomials, which are also linked among others to the corner growth model, the PNG droplet, non-colliding random processes. For a review on these connections, see [54].

GUE kernel and its asymptotics

For GUE random matrices $V(x) = x^2/2N$ and the kernel K_N is the *Hermite kernel* given by

$$\begin{aligned} K_N^{\text{H}}(x, y) &= \sum_{k=0}^{N-1} p_k(x)p_k(y)e^{-(x^2+y^2)/4N} \\ &= N \frac{p_N(x)p_{N-1}(y) - p_{N-1}(x)p_N(y)}{x - y} e^{-(x^2+y^2)/4N}, \end{aligned} \quad (3.50)$$

where $p_k(x) = (2\pi N)^{-1/4} (2^k k!)^{-1/2} p_k^{\text{H}}(x/\sqrt{2N})$ with the (standard) Hermite polynomials

$$p_k^{\text{H}}(x) = e^{x^2} \frac{d^k}{dx^k} e^{-x^2}. \quad (3.51)$$

See Appendix A.5 for more details on Hermite polynomials.

First we focus in the bulk of the spectrum. The density of eigenvalues close to $2Na$, $|a| < 1$, is $u(a) = \frac{1}{\pi} \sqrt{1 - a^2}$. The asymptotics of the Hermite polynomials (A.43) with $x = 2Na + t/u(a)$ leads to $\sqrt{N} p_{N-h}(x) e^{-x^2/4N} \simeq \pi^{-1/2} \sin(\alpha_0 N + \pi t + \alpha_h h) / \gamma(a)$ for large N , with α_0 a constant, $\alpha_h = \frac{\pi}{2} - \arcsin(a)$, and $\gamma(a) = (1 - a^2)^{1/4}$. Applying this with $h = 0$ and $h = 1$ to the kernel (3.50) we conclude that in the bulk the Hermite kernel converges to the sine kernel,

$$\lim_{N \rightarrow \infty} \frac{1}{u(a)} K_N^{\text{H}} \left(2Na + \frac{t}{u(a)}, 2Na + \frac{t'}{u(a)} \right) = S_1(t, t'), \quad (3.52)$$

for any $a \in (-1, 1)$.

Now we focus at the edge of the spectrum $2N$. Since the fluctuations of the largest eigenvalues are of order $N^{1/3}$, the edge scaling of the point process ζ_N^{GUE} is

$$\eta_N^{\text{GUE}}(\xi) = N^{1/3} \zeta_N^{\text{GUE}}(2N + \xi N^{1/3}). \quad (3.53)$$

Thus the kernel of the determinantal point process η_N^{GUE} reads

$$K_N^{\text{GUE}}(\xi, \xi') = N^{1/3} K_N^{\text{H}}(2N + \xi N^{1/3}, 2N + \xi' N^{1/3}). \quad (3.54)$$

From the asymptotic (A.42) we obtain $p_{N-h}(x)e^{-x^2/4N} \simeq N^{-1/3} \text{Ai}(\xi + N^{-1/3}(h - \frac{1}{2}))$ for large N , where $x = 2N + \xi N^{1/3}$. Using this for $h = 0$ and $h = 1$ we obtain that the limit of (3.54) as $N \rightarrow \infty$ is the Airy kernel (3.20),

$$\lim_{N \rightarrow \infty} K_N^{\text{GUE}}(\xi, \xi') = A(\xi, \xi'). \quad (3.55)$$

From the asymptotics at the edge of the spectrum, the Tracy-Widom distribution $F_2(s)$ is given also by

$$F_2(s) = \text{Det}(\mathbb{1} - A)_{L^2((t, \infty), dx)} \quad (3.56)$$

with A the Airy kernel. To be precise, the convergence of (3.55) obtained above is uniformly for ξ, ξ' is a bounded set. To obtain (3.56) one need some uniform bound for $\xi \rightarrow \infty$ too. This follows from the super-exponential decay of $p_{N-h}(x)e^{-x^2/4N}$ for x larger than the last maximum.

3.2.3 GOE and GSE eigenvalues: Pfaffian processes

In this section we consider the point processes of the GOE and GSE eigenvalues which are Pfaffian point processes [92]. For example, in the GOE case the distribution of the eigenvalues is given by (3.23) with $f_j(x) = x^{j-1}$ and $\varepsilon(x, y) = \text{sgn}(x - y)$. Here we want to describe the edge scaling of the GOE and GSE point processes. If the weight is $e^{-V(x)}$ instead of $e^{-x^2/2N}$, with V an even degree polynomial with positive leading coefficient then, by (3.23)-(3.27), the GOE and GSE eigenvalues are still Pfaffian point processes for a different kernel.

GOE random matrices

We denote by ζ_N^{GOE} the point process of the eigenvalues $\lambda_1, \dots, \lambda_N$ of a $N \times N$ GOE random matrix, i.e.,

$$\zeta_N^{\text{GOE}}(x) = \sum_{j=1}^N \delta(x - \lambda_j), \quad x \in \mathbb{R}. \quad (3.57)$$

At the edge of the spectrum, $2N$, the eigenvalues are order $N^{1/3}$ apart, see (3.39). The edge rescaled point process is then given by

$$\eta_N^{\text{GOE}}(\xi) = N^{1/3} \zeta_N^{\text{GOE}}(2N + \xi N^{1/3}), \quad (3.58)$$

and for f a test function of compact support,

$$\eta_N^{\text{GOE}}(f) = \int_{\mathbb{R}} d\xi f(\xi) \eta_N^{\text{GOE}}(\xi) = \sum_{j=1}^N f((\lambda_j - 2N)/N^{1/3}). \quad (3.59)$$

We denote by η^{GOE} the limit of η_N^{GOE} as $N \rightarrow \infty$.

The limit point process η^{GOE} is characterized by its correlation functions as follows. Let us denote by $\rho_{\text{GOE}}^{(n)}(\xi_1, \dots, \xi_n)$ the n -point correlation functions of η^{GOE} , i.e., the joint density of having eigenvalues at ξ_1, \dots, ξ_n . Then

$$\rho_{\text{GOE}}^{(n)}(\xi_1, \dots, \xi_n) = \text{Pf}[G^{\text{GOE}}(\xi_i, \xi_j)]_{i,j=1,\dots,n} \quad (3.60)$$

where Pf is the Pfaffian and G^{GOE} is the 2×2 antisymmetric matrix kernel with elements

$$\begin{aligned} G_{1,1}^{\text{GOE}}(\xi_1, \xi_2) &= \int_0^\infty d\lambda \text{Ai}(\xi_1 + \lambda) \text{Ai}'(\xi_2 + \lambda) - (\xi_1 \leftrightarrow \xi_2), \\ G_{1,2}^{\text{GOE}}(\xi_1, \xi_2) &= \int_0^\infty d\lambda \text{Ai}(\xi_1 + \lambda) \text{Ai}(\xi_2 + \lambda) + \frac{1}{2} \text{Ai}(\xi_1) \int_0^\infty d\lambda \text{Ai}(\xi_2 - \lambda), \\ G_{2,1}^{\text{GOE}}(\xi_1, \xi_2) &= -G_{1,2}^{\text{GOE}}(\xi_2, \xi_1) \\ G_{2,2}^{\text{GOE}}(\xi_1, \xi_2) &= \frac{1}{4} \int_0^\infty d\lambda \int_\lambda^\infty d\mu \text{Ai}(\xi_1 - \lambda) \text{Ai}(\xi_2 - \mu) - (\xi_1 \leftrightarrow \xi_2), \end{aligned} \quad (3.61)$$

Ai is the Airy function [1] and the notation $(\xi_1 \leftrightarrow \xi_2)$ means that the previous term is repeated with ξ_1 and ξ_2 interchanged. The GOE kernel was studied in [101]. It is not uniquely defined, for example the one reported in [32, 40] differs slightly from the one written here, but they are equivalent because they yield the same point process. The point process η^{GOE} is uniquely determined by its correlation functions, see the discussion in Section 3.1.1.

Finally let us remark that F_1 can be written in terms of a Fredholm Pfaffian. First we consider the $N \times N$ matrices.

$$\begin{aligned} F_{1,N}(\xi) &= \mathbb{E} \left(\prod_{j=1}^N (1 - \mathbb{1}_{[\xi, \infty)}((\lambda_j - 2N)/N^{1/3})) \right) \\ &= \sum_{n=0}^{N-1} \frac{(-1)^n}{n!} \int_{(\xi, \infty)^n} d^n \xi \text{Pf}[G_N^{\text{GOE}}(\xi_i, \xi_j)]_{i,j=1,\dots,n}, \end{aligned} \quad (3.62)$$

where G_N^{GOE} is the kernel of the rescaled point process η_N^{GOE} . Then $F_1(\xi) = \lim_{N \rightarrow \infty} F_{1,N}(\xi)$ is given by

$$\begin{aligned} F_1(\xi) &= \sum_{n=0}^{\infty} \frac{(-1)^n}{n!} \int_{(\xi, \infty)^n} d^n \xi \text{Pf}[G^{\text{GOE}}(\xi_i, \xi_j)]_{i,j=1,\dots,n} \\ &= \text{Pf}(J - G^{\text{GOE}}) = \sqrt{\text{Det}(\mathbb{1} + JG^{\text{GOE}})} \end{aligned} \quad (3.63)$$

where J is the matrix kernel $J(x, y) = \delta_{x,y} \begin{pmatrix} 0 & 1 \\ -1 & 0 \end{pmatrix}$. The Fredholm Pfaffian and determinant are on the measurable space $((\xi, \infty), dx)$, i.e.,

$$\text{Pf}(J - G^{\text{GOE}}) = \sum_{n=0}^{\infty} \frac{(-1)^n}{n!} \int_{(\xi, \infty)^n} d\xi_1 \cdots d\xi_n \text{Pf} [G^{\text{GOE}}(\xi_k, \xi_l)]_{k,l=1,\dots,n} \quad (3.64)$$

and

$$\text{Det}(\mathbb{1} - K^{\text{GOE}}) = \sum_{n=0}^{\infty} \frac{(-1)^n}{n!} \int_{(\xi, \infty)^n} d\xi_1 \cdots d\xi_n \sum_{i_1, \dots, i_n \in \{1,2\}} \text{Det} [K_{i_k, i_l}^{\text{GOE}}(\xi_k, \xi_l)]_{k,l=1,\dots,n} \quad (3.65)$$

with $K^{\text{GOE}} = -JG^{\text{GOE}}$.

Remark: One can also consider instead of $\text{Det}(\mathbb{1} - K^{\text{GOE}})$ the determinant $\text{Det}(\mathbb{1} - \hat{K}^{\text{GOE}})$ with \hat{K}^{GOE} the operator with kernel K^{GOE} . \hat{K}^{GOE} is not trace-class on $L^2((\xi, \infty), dx) \oplus L^2((\xi, \infty), dx)$ because it is not even Hilbert-Schmidt. Nevertheless it is possible to make sense of it as follows. \hat{K}^{GOE} is Hilbert-Schmidt in the space $L^2((\xi, \infty), \theta dx) \oplus L^2((\xi, \infty), \theta^{-1} dx)$ where θ is any positive weight function with $\theta^{-1} \in L^1(\xi, \infty), dx$ which grows at most polynomially at $x \rightarrow \infty$. Moreover $\tilde{\text{Tr}}(\hat{K}^{\text{GOE}})$ the sum of the diagonal terms is absolutely integrable. Then the modified Fredholm determinant is defined by $\text{Det}(\mathbb{1} - \hat{K}^{\text{GOE}}) = e^{-\tilde{\text{Tr}}(\hat{K}^{\text{GOE}})} \text{Det}_2(\mathbb{1} - \hat{K}^{\text{GOE}})$ with Det_2 the regularized determinant [34]. This is made in [105] where they actually prove the $N \rightarrow \infty$ convergence of the kernel and of the modified Fredholm determinant, leading thus to (3.65).

GSE random matrices

As for GOE, we denote by ζ_N^{GSE} the point process of the eigenvalues $\lambda_1, \dots, \lambda_N$ of $N \times N$ GSE random matrices, i.e.,

$$\zeta_N^{\text{GSE}}(x) = \sum_{j=1}^N \delta(x - \lambda_j), \quad x \in \mathbb{R}. \quad (3.66)$$

The edge rescaled point process is then given by

$$\eta_N^{\text{GSE}}(\xi) = N^{1/3} \zeta_N^{\text{GSE}}(2N + \xi N^{1/3}), \quad (3.67)$$

and η^{GSE} is the limit of η_N^{GSE} as $N \rightarrow \infty$.

The limit point process η^{GSE} is characterized by its correlation functions as follows. Let us denote by $\rho_{\text{GSE}}^{(n)}(\xi_1, \dots, \xi_n)$ the n -point correlation functions of η^{GSE} , i.e., the joint density of having eigenvalues at ξ_1, \dots, ξ_n . Then

$$\rho_{\text{GSE}}^{(n)}(\xi_1, \dots, \xi_n) = \text{Pf}[G^{\text{GSE, TW}}(\xi_i, \xi_j)]_{i,j=1,\dots,n} \quad (3.68)$$

where Pf is the Pfaffian and $G^{\text{GSE, TW}}$ is a 2×2 antisymmetric matrix kernel with elements

$$G_{i,j}^{\text{GSE, TW}}(\xi_1, \xi_2) = 2^{1/4} G_{i,j}^{\text{GSE}}(\xi_1/\sqrt{2}, \xi_2/\sqrt{2}), \quad i, j \in \{1, 2\}, \quad (3.69)$$

where

$$\begin{aligned}
G_{1,1}^{\text{GSE}}(\xi_1, \xi_2) &= \int_0^\infty d\lambda \int_\lambda^\infty d\mu \text{Ai}(\xi_1 + \lambda) \text{Ai}(\xi_2 + \mu) - (\xi_1 \leftrightarrow \xi_2), \quad (3.70) \\
G_{1,2}^{\text{GSE}}(\xi_1, \xi_2) &= \int_0^\infty d\lambda \text{Ai}(\xi_1 + \lambda) \text{Ai}(\xi_2 + \lambda) - \frac{1}{2} \text{Ai}(\xi_2) \int_0^\infty d\lambda \text{Ai}(\xi_1 + \lambda), \\
G_{2,1}^{\text{GSE}}(\xi_1, \xi_2) &= -G_{1,2}^{\text{GSE}}(\xi_2, \xi_1) \\
G_{2,2}^{\text{GSE}}(\xi_1, \xi_2) &= \frac{1}{4} \int_0^\infty d\lambda \text{Ai}(\xi_2 - \lambda) \text{Ai}'(\xi_1 - \lambda) - (\xi_1 \leftrightarrow \xi_2).
\end{aligned}$$

We have chosen to write $G^{\text{GSE}, \text{TW}}$ in terms of G^{GSE} to keep more evident the analogies and differences with the GOE kernel. The kernel G^{GSE} is the one of the point process with last particle distribution given by $F_4(s/\sqrt{2})$. The GSE kernel was studied in [101].

3.3 Extended determinantal point processes

3.3.1 Dyson's Brownian motion

Dyson [23] noticed that the distribution of eigenvalues (3.34) is identical to the *equilibrium* probability distribution of the *positions* of N point charges, free to move in \mathbb{R} under the forces deriving from the potential W at inverse temperature β , with

$$U(x_1, \dots, x_N) = - \sum_{1 \leq i < j \leq N} \ln |x_i - x_j| + \frac{1}{2N\beta} \sum_{i=1}^N x_i^2. \quad (3.71)$$

In the attempt to interpret the Coulomb gas as a dynamical system Dyson considered the positions of the particles in Brownian motion subjected to the interaction forces $-\nabla U$ and a frictional force f (which fixes the rate of diffusion, or equivalently, the time scale).

Let $\rho_N(x_1, \dots, x_N; t)$ be the time-dependent probability density of finding the particles at positions x_j at time t . ρ_N satisfies the Smoluckowski equation

$$\frac{\partial \rho_N}{\partial t} = \sum_{i=1}^N \left[\frac{1}{2} \frac{\partial^2 \rho_N}{\partial x_i^2} + \frac{\beta}{2} \frac{\partial}{\partial x_i} \left(\frac{\partial U}{\partial x_i} \rho_N \right) \right] \quad (3.72)$$

which has as unique stationary solution (3.34) (we fixed the parameters of [23] as $f = 2/\beta$ and $a^2 = \beta N$). In other words, the set $\{x_1, \dots, x_N\}$ satisfies the set of stochastic differential equations

$$dx_j(t) = \left(-\frac{1}{2N} x_j(t) + \frac{\beta}{2} \sum_{\substack{i=1, \\ i \neq j}}^N \frac{1}{x_j(t) - x_i(t)} \right) dt + db_j(t), \quad j = 1, \dots, N, \quad (3.73)$$

with $\{b_j(t), j = 1, \dots, N\}$ a collection of N independent standard Brownian motions. We refer to the *stationary process of (3.73)* as *Dyson's Brownian motion*. Note that for $\beta \geq 1$

the process is well defined because there is no crossing of the eigenvalues, as proved by Rogers and Shi [86].

Moreover, Dyson showed that in term of random matrices, this is equivalent to the evolution of the eigenvalues when the $n = N + \frac{1}{2}N(N-1)\beta$ independent elements of M , $\{M_\mu, \mu = 1, \dots, n\}$, evolve as independent Ornstein-Uhlenbeck processes. More precisely, let $P(M_1, \dots, M_n; t)$ denote the time-dependent probability density of the M_μ , then

$$\frac{\partial P}{\partial t} = \sum_{\mu=1}^n \left[\frac{\kappa_\mu}{2} \frac{\partial^2 P}{\partial M_\mu^2} + \frac{1}{2N} \frac{\partial}{\partial M_\mu} (M_\mu P) \right] \quad (3.74)$$

with $\kappa_\mu = 1$ if M_μ is a diagonal term and $\kappa_\mu = 1/2$ otherwise.

Let $M(0)$ be the initial condition of a matrix evolving according to (3.74). Then the matrix distribution at time t is given by

$$P(M(t) = M) dM = \frac{1}{Z_N} (1 - q^2)^{-n/2} \exp \left(-\frac{\text{Tr}(M - qM(0))^2}{2N(1 - q^2)} \right) dM \quad (3.75)$$

with $q = \exp(-t/2N)$.

For $\beta = 2$ Dyson's Brownian motion, the properly rescaled largest eigenvalue converges to the Airy process in the $N \rightarrow \infty$ limit, see Section 3.3.3.

Finally we remark that it is connected with the Calogero-Sutherland model in one dimension [98]. It describes a system of N particles moving on \mathbb{R} , whose Hamiltonian is

$$H^{\text{CS}} = -\sum_{k=1}^N \frac{\partial^2}{\partial x_k^2} + \frac{\beta(\beta-2)}{2} \prod_{1 \leq k < l \leq N} \frac{1}{(x_k - x_l)^2} + \omega^2 \sum_{k=1}^N x_k^2. \quad (3.76)$$

Set the external potential strength as $\omega = 1/2N$. The ground state Ω_0 has energy $E_0 = \omega n$, $n = N + \frac{1}{2}N(N-1)\beta$ and is given, without normalization, by

$$\Omega_0(x_1, \dots, x_N) = e^{-\frac{1}{2}\omega \sum_{k=1}^N x_k^2} \prod_{1 \leq k < l \leq N} |x_k - x_l|^{\beta/2}. \quad (3.77)$$

The connection with Dyson's Brownian motion is via the ground state transformation as follows. Let $X_t = (x_1(t), \dots, x_N(t)) \in \mathbb{R}^N$ be an Ito diffusion with infinitesimal generator L given by

$$L f = -\Omega_0^{-1}(\tilde{H}\Omega_0 f), \quad \tilde{H} = \frac{1}{2}(H^{\text{CS}} - E_0), \quad (3.78)$$

for $f \in C_0^2(\mathbb{R}^N)$. Some simple computations leads to

$$L = \sum_{j=1}^N \frac{1}{2} \frac{\partial^2}{\partial x_j^2} + \sum_{j=1}^N a(x_j) \frac{\partial}{\partial x_j}, \quad a(x_j) = \frac{\beta}{2} \sum_{\substack{i=1, \\ i \neq j}}^N \frac{1}{x_j - x_i} - \frac{1}{2N} x_j. \quad (3.79)$$

L is the generator of a diffusion X_t which satisfies (see Chapter 7 of [70])

$$dX_t = A(X_t)dt + dB_t \quad (3.80)$$

with $A(X_t)_j = a(x_j(t))$ and dB_t an N -dimensional standard Brownian motion, which is identical to (3.73).

The careful reader has probably noticed that the system with Hamiltonian (3.76) is not well defined as soon as no domain is specified. Notice that the Hamiltonian is the same for β and $2 - \beta$, thus consider $\beta \geq 1$. Let us discuss the case $N = 2$. Defining the half-distance between the particles by $X = (x_2 - x_1)/2$ and the center of mass by $Y = (x_1 + x_2)/2$. One has $H_2^{\text{CS}} = H_{\text{CM}} + H_{\text{D}}$ with

$$H_{\text{CM}} = -\frac{1}{2} \frac{\partial^2}{\partial Y^2} + 2\omega^2 Y^2, \quad H_{\text{D}} = -\frac{1}{2} \frac{\partial^2}{\partial X^2} + \frac{\beta(\beta - 2)}{8X^2} + 2\omega^2 X^2. \quad (3.81)$$

The minimal domain of H_2^{CS} consists in smooth functions vanishing at $X = 0$. In this case, for $\beta \geq 3$ there is an unique self-adjoint extension because both $X = 0$ and the $X = \infty$ are in the limit point case, see Appendix to X.I of [84]. The ground state wave function is (3.77) (the solution with $\beta \leq -1$ is not in $L^2(\mathbb{R})$). For $\beta \in [1, 3)$, $X = \infty$ is still in the limit point case, but $X = 0$ is in the circle case, thus there exists a one-parameter family of self-adjoint extensions, but only for two of them $e^{-tH_2^{\text{CS}}}$ is a positive kernel (see [94] for a discussion of the singularity a/x^2). The ground states are given by (3.77) with β and $2 - \beta$. In particular for $\beta = 1$ there is only one-selfadjoint extension with positive transition kernel. A similar situation appears in Dyson's Brownian motion in a circle [95]. For general N we do not know rigorous results, but it is expected the same situation of before but with the $\beta \geq 3$ replaced by $\beta \geq 2 + 2/N$.

3.3.2 Extended point process

Definition

Consider a point process $\eta(x, 0)$ describing for example particles in a potential. It is natural to consider $\eta(x, 0) = \sum_i \delta(x - x_i(0))$ as the point process at time $t = 0$ and let the particles evolve in time according to some prescribed dynamics Φ_t , i.e., $x(t) = \Phi_t(x(0))$ with $x(t) = (x_1(t), x_2(t), \dots)$. For each time $t \geq 0$ define $\eta(x, t) = \sum_i \delta(x - x_i(t))$. We say that $\eta(x, t)$, $t \in [0, T]$ with $T \in \mathbb{R}_+$, is an *extended point process* if for each fixed $t \in [0, T]$ $\eta(x, t)$ is a point process. We thus exclude situations where there can be somewhere a condensation during $[0, T]$ of infinitely many particles. Otherwise the position of the particles would not be anymore a point process after some time.

Remark: The evolution is not restricted to continuous time, also discrete time evolution are allowed.

An example of an extended point process is Dyson's Brownian motion. As we shall see below, for $\beta = 2$ its *space-time* correlations are given by a determinantal form with a space-time kernel. The process is then called *extended determinantal point process* and the kernel is the *extended kernel*.

Extended Hermite kernel

Now we restrict to Dyson's Brownian motion with $\beta = 2$. (3.75) can be straightforwardly generalized to multi-time distributions, the so-called multi-matrix model. Let M_j be the matrix at time t_j . Let $0 = t_0 < t_1 < \dots < t_m$ and $q_j = \exp(-(t_{j+1} - t_j)/2N)$. Then the multi-time measure reads

$$\frac{1}{Z_{N,m}} \exp\left(-\frac{\text{Tr}(M_0^2)}{2N}\right) \prod_{j=0}^{m-1} \exp\left(-\frac{\text{Tr}(M_{j+1} - q_j M_j)^2}{2N(1 - q_j^2)}\right) dM_0 \dots dM_m. \quad (3.82)$$

For this multi-matrix model the joint-distribution of the eigenvalues reads (see e.g. [27])

$$\frac{1}{Z_{N,m}} \Delta_N(\lambda_0) \Delta_N(\lambda_m) \prod_{i=1}^N e^{-(\alpha_0 \lambda_{0,i}^2 + \alpha_{m-1} \lambda_{m,i}^2)} \prod_{k=0}^{m-1} \text{Det} \left[e^{\beta_k \lambda_{k,i} \lambda_{k+1,j}} \right]_{i,j=1,\dots,N} \prod_{k=0}^m d\lambda_k \quad (3.83)$$

where $\lambda_k = (\lambda_{k,j})$, $j = 1, \dots, N$, are the eigenvalues of the matrix M_k , $k = 0, \dots, m$,

$$\alpha_k = \frac{1}{(1 - q_k^2)2N}, \quad \beta_k = \frac{q_k}{(1 - q_k^2)N}. \quad (3.84)$$

We consider fixed initial and final eigenvalues (or matrices), so that the Vandermonde determinants in (3.83) can be absorbed by the normalization constant. For the same reason, we can replace α_0 and α_{m-1} by $\gamma_0 = \alpha_0 - 1/4N$ and $\gamma_{m-1} = \alpha_{m-1} - 1/4N$ without changing the distribution. In this case it is known [27] that the joint probability distributions of eigenvalues have a determinantal form. To obtain the kernel, a more useful form of (3.83) is the following. Define

$$q(t) = e^{-t/2N}, \quad \alpha(t) = \frac{1}{2N(1 - q(t)^2)}, \quad \gamma(t) = a(t) - \frac{1}{4N}, \quad \beta(t) = \frac{q(t)}{N(1 - q(t)^2)}, \quad (3.85)$$

and

$$\Phi_{t,t'}(\lambda, \lambda') = \begin{cases} e^{-\gamma(t'-t)(\lambda^2 + \lambda'^2)} e^{\beta(t'-t)\lambda\lambda'} \sqrt{\alpha(t'-t)/\pi} & \text{for } t' > t, \\ 0 & \text{for } t' \leq t. \end{cases} \quad (3.86)$$

$\Phi_{t,t'}$ is the transition function from time t to time t' . Then the joint-distribution of the eigenvalues $\lambda_{k,i}$, $k = 1, \dots, m-1$, $i = 1, \dots, N$, is given by

$$\frac{1}{Z'_{N,m}} \prod_{k=0}^{m-1} \text{Det} \left[\Phi_{t_k, t_{k+1}}(\lambda_{k,i}, \lambda_{k+1,j}) \right]_{i,j=1,\dots,N} d\lambda_1 \dots d\lambda_{m-1} \quad (3.87)$$

with λ_0 and λ_m fixed, and $Z'_{N,m}$ another normalization constant.

The following result of Johansson gives an explicit formula for the kernel of the extended determinantal point process with joint-distribution (3.87). For two transition functions φ and ψ their *convolution* is defined by

$$(\varphi * \psi)(x, y) = \int_{\mathbb{R}} \varphi(x, z) \psi(z, y) d\mu(z). \quad (3.88)$$

Define, for $t_0 < t_1 < \dots < t_m$,

$$\varphi_{t_i, t_j}(x, y) = \begin{cases} (\varphi_{t_i, t_{i+1}} * \dots * \varphi_{t_{j-1}, t_j})(x, y), & i < j \\ 0, & i \geq j. \end{cases} \quad (3.89)$$

The form (3.86) is chosen such that $\Phi_{t_1, t_3}(x_1, x_3) = \int_{\mathbb{R}} \Phi_{t_1, t_2}(x_1, x_2) \Phi_{t_2, t_3}(x_2, x_3) dx_2$. It is not necessary to include the normalization constant $\sqrt{\alpha(t' - t)}/\pi$, but it simplifies some computations.

Theorem 3.6 (Johansson [46]). *Consider a measure with joint density of the form*

$$\frac{1}{Z} \prod_{k=0}^{m-1} \text{Det}[\varphi_{t_k, t_{k+1}}(x_i(t_k), x_j(t_{k+1}))]_{i,j=1, \dots, N}. \quad (3.90)$$

If the configurations at time t_0 and time t_m , i.e., $x_i^0 = x_i(t_0)$ and $x_i^m = x_i(t_m)$ for $i = 1, \dots, N$, are fixed, then the measure (3.90) has determinantal correlation functions with extended kernel

$$K(x, t; x', t') = -\varphi_{t, t'}(x, x') + \sum_{i,j=1}^N \varphi_{t, t_m}(x, x_i^m) [A^{-1}]_{i,j} \varphi_{t_0, t'}(x_j^0, x') \quad (3.91)$$

where $A = [\varphi_{t_0, t_m}(x_i^0, x_j^m)]_{i,j=1, \dots, N}$.

The only problem in using Theorem 3.6 is that one needs to invert the matrix A , and this is not always a simple task.

Applying this theorem to the transition function Φ one obtains the kernel for Dyson's Brownian motion $\beta = 2$

$$K_N(x, t; x', t') = \begin{cases} \sum_{k=0}^{N-1} e^{k(t-t')/2N} p_k(x) p_k(y) e^{-(x^2+y^2)/4N}, & t \geq t' \\ -\sum_{k=N}^{\infty} e^{-k(t'-t)/2N} p_k(x) p_k(y) e^{-(x^2+y^2)/4N}, & t < t' \end{cases} \quad (3.92)$$

where $p_k(x) = p_k^H(x/\sqrt{2N})(\sqrt{2\pi N} 2^k k!)^{-1/2}$. The Hermite polynomials $p_k^H(x)$ are given in Appendix A.5. Since Dyson's Brownian motion is stationary, (3.92) is obtained in the limit $t_0 \rightarrow -\infty$ and $t_m \rightarrow \infty$. For the asymptotic analysis is convenient to modify slightly the form of the kernel. We will use the kernel defined by $K_N^H(x, t; x', t') = e^{-(t-t')/2} K_N(x, t; x', t')$ which gives the same correlation functions. It is called the *extended Hermite kernel* and reads

$$K_N^H(x, t; x', t') = \begin{cases} \sum_{k=-N}^{-1} e^{k(t-t')/2N} p_{N+k}(x) p_{N+k}(y) e^{-(x^2+y^2)/4N}, & t \geq t' \\ -\sum_{k=0}^{\infty} e^{k(t-t')/2N} p_{N+k}(x) p_{N+k}(y) e^{-(x^2+y^2)/4N}, & t < t' \end{cases} \quad (3.93)$$

For more details on the derivation of (3.92) see Appendix A.6.

Extended Airy kernel

An important extended kernel is the extended Airy kernel defined by

$$A(u, s; u', s') = \begin{cases} \int_{-\infty}^0 d\lambda e^{\lambda(s-s')} \text{Ai}(u - \lambda) \text{Ai}(u' - \lambda) & \text{for } s \geq s', \\ -\int_0^{\infty} d\lambda e^{\lambda(s-s')} \text{Ai}(u - \lambda) \text{Ai}(u' - \lambda) & \text{for } s < s'. \end{cases} \quad (3.94)$$

In particular for $s = s'$ (3.94) is equal to (3.20).

In the limit of large N , K_N^{H} converges in the edge scaling limit to the extended Airy kernel. The edge scaling is the following. Let $t = 2sN^{2/3}$, $x = 2N + uN^{1/3}$, and similarly rescale t' and x' . Then the edge-rescaled extended Hermite kernel converges to the extended Airy kernel,

$$\lim_{N \rightarrow \infty} N^{1/3} K_N^{\text{H}}(2N + uN^{1/3}, 2sN^{2/3}; 2N + u'N^{1/3}, 2s'N^{2/3}) = A(u, s; u', s'). \quad (3.95)$$

For the convergence, see Appendix A.7.

Extended GUE point process and its asymptotics

The extended GUE point process is the process which describes Dyson's Brownian motion with $\beta = 2$. Let the eigenvalues $\lambda_1(t), \dots, \lambda_N(t)$ evolve according to (3.73) and having the stationary distribution at $t = 0$. The extended GUE point process is defined by

$$\zeta_N^{\text{GUE}}(x, t) = \sum_{j=1}^N \delta(\lambda_j(t) - x) \quad (3.96)$$

and has the kernel (3.93). The edge scaling of ζ_N^{GUE} is

$$\eta_N^{\text{GUE}}(u, s) = N^{1/3} \zeta_N^{\text{GUE}}(2N + xN^{1/3}, 2uN^{2/3}). \quad (3.97)$$

In the sense of finite-dimensional distributions, $\eta_N^{\text{GUE}}(u, s)$ has a limit as $N \rightarrow \infty$, which we denote by $\eta^{\text{GUE}}(u, s)$. (3.95) implies that the kernel of $\eta^{\text{GUE}}(u, s)$ is the Airy kernel.

3.3.3 Airy process

The Airy process is the limiting process of the edge-rescaled largest eigenvalue of Dyson's Brownian motion with $\beta = 2$. Let $\lambda_1(t) < \dots < \lambda_N(t)$ the eigenvalues of GUE random matrices of Dyson's Brownian motion. The largest eigenvalue λ_N converges to the Airy process

$$\mathcal{A}(s) = \lim_{N \rightarrow \infty} N^{-1/3} (\lambda_N(sN^{-2/3}) - 2N) \quad (3.98)$$

in the sense of joint distributions.

The Airy process is defined by its finite-dimensional distribution [81, 47]. For given $a_1, \dots, a_n \in \mathbb{R}$ and $s_1 < \dots < s_n \in \mathbb{R}$, we define f on $\Lambda = \{s_1, \dots, s_n\} \times \mathbb{R}$ by $f(s_j, x) = \chi_{(a_j, \infty)}(x)$. Then

$$\mathbb{P}(\mathcal{A}(s_1) \leq a_1, \dots, \mathcal{A}(s_n) \leq a_n) = \text{Det}(\mathbb{1} - f^{1/2} A f^{1/2})_{L^2(\Lambda, dx)}$$

with A the extended Airy kernel.

The Airy process was first introduced by Prähofer and Spohn in their work on the PNG droplet [81]. They proved that $\mathcal{A}(t)$ is almost surely continuous, stationary in t , and invariant under time-reversal. Its single time distribution is given by the GUE Tracy-Widom distribution. In particular, for fixed t ,

$$\begin{aligned} \mathbb{P}(\mathcal{A}(t) > y) &\simeq e^{-y^{3/2} 4/3} \quad \text{for } y \rightarrow \infty, \\ \mathbb{P}(\mathcal{A}(t) < y) &\simeq e^{-|y|^3/12} \quad \text{for } y \rightarrow -\infty. \end{aligned} \quad (3.99)$$

Thus the Airy process is localized. Define the function g by

$$\text{Var}(\mathcal{A}(t) - \mathcal{A}(0)) = g(t). \quad (3.100)$$

From [81] we know that g grows linearly for small t and that the Airy process has long range correlations:

$$g(t) = \begin{cases} 2t + \mathcal{O}(t^2) & \text{for } |t| \text{ small,} \\ g(\infty) - 2t^{-2} + \mathcal{O}(t^{-4}) & \text{for } |t| \text{ large.} \end{cases} \quad (3.101)$$

with $g(\infty) = 1.6264\dots$. The coefficient 2 of the correlation's decay is determined in [2, 110]. The Airy process has been recently investigated and a set of PDE's [2] and ODE's [104] describing it are determined.

3.4 Description of the systems via line ensembles

Although physically the polynuclear growth model and the 3D-Ising corner at zero temperature are not connected, we have analyzed them using the same mathematical framework. The two systems are mapped to two different sets of non-intersecting line ensembles. The lines can be seen as the trajectories of particles which can not occupy simultaneously the same position (state), thus they are fermions. The idea of this mapping was already successfully applied by Johansson to the Aztec diamond problem [45], and by Prähofer and Spohn to the PNG droplet [81].

3.4.1 Line ensemble for the polynuclear growth model

The surface height at time T , $x \mapsto h(x, T)$, does not contain anymore the information of the position of the Poisson points, because when two islands merge, we lose information.

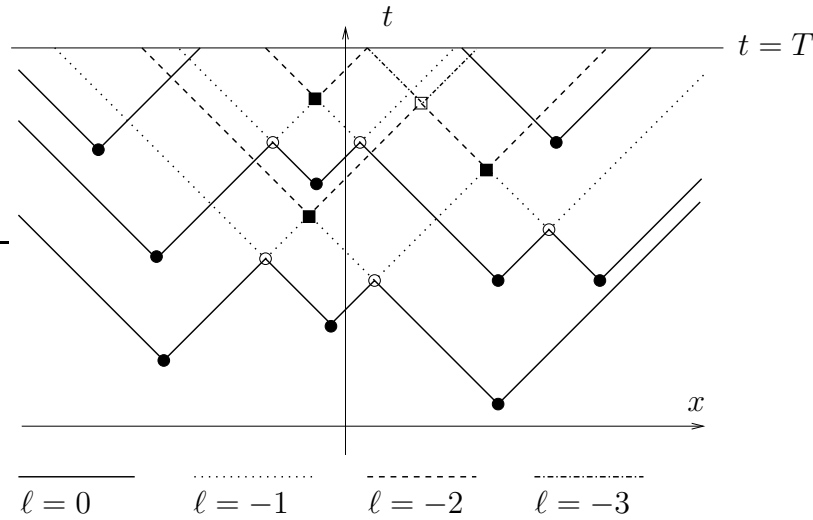


Figure 3.2: RSK construction up to time $t = T$.

Therefore the measure induced by the Poisson process on the set of heights is not easy to describe. A way of recording the lost information is to extend the model to a multilayer model. This is achieved using the Robinson-Schensted-Knuth (RSK) construction.

We first recall briefly the construction of the PNG surface height $h(x, t)$ of Section 2.2.1. Let $h(x, 0) = 0$ for all $x \in \mathbb{R}$ and fix a $T > 0$. Let $\omega \in \Omega$ be a configuration of Poisson points in $\mathbb{R} \times [0, T]$. Each Poisson point is a nucleation event which generate two lines, with slope $+1$ and -1 along its forward light cone. A line ends upon crossing another line. Then $h(x, t)(\omega)$, $(x, t) \in \mathbb{R} \times [0, T]$, is the number of lines crossed along the straight path from $(x, 0)$ to (x, t) . This construction is the level 0 of the RSK construction, which leads to a set of height functions $h_\ell(x, t)(\omega)$, $(x, t) \in \mathbb{R} \times [0, T]$, $\ell \leq 0$ as follows. At $t = 0$ we set $h_\ell(x, 0) = \ell$ with $\ell = 0, -1, \dots$, where ℓ denotes the level's height. The top height is defined by $h_0(x, t)(\omega) \equiv h(x, t)(\omega)$. The meeting points of the forward light cones generated by the points of ω are called the *annihilation events* of level 0. $h_{-1}(x, t)(\omega)$ is constructed as $h_0(x, t)(\omega)$ but the nucleation events for level -1 are the annihilation events of level 0 and $h_{-1}(x, t)(\omega) + 1$ equals the number of lines for level -1 crossed from $(x, 0)$ to (x, t) . In Figure 3.2 the nucleation events of level -1 are the empty dots, whose forward light cones are the dotted lines. Setting the annihilation events of level j as the nucleation events for level $j - 1$, the set of height functions $h_\ell(x, t)(\omega)$ is defined for all $\ell \leq 0$. By construction, the number of lines of level j along the path from $(x, 0)$ to (x, t) is greater than the one of level $j - 1$, for all $j \leq 0$. Therefore

$$h_j(x, t) \geq h_{j-1}(x, t) + 1 \quad (3.102)$$

for all $x \in \mathbb{R}$, $t \in [0, T]$, $j \leq 0$.

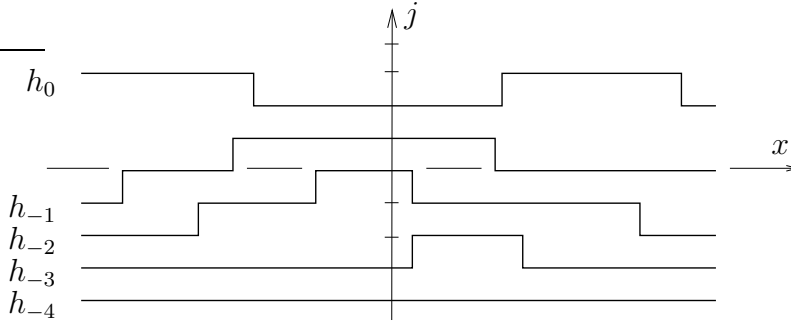


Figure 3.3: Line ensemble for $t = T$ for the point configuration of Figure 3.2.

Non-intersecting line ensembles for $t = T$

The RSK construction gives us the set of height functions $\{h_\ell, \ell \leq 0\}$. If we want to look at the PNG height at fixed time, say $t = T$, we consider the set of height functions $x \mapsto h_\ell(x, T)$, $\ell \leq 0$. By (3.102) $\{h_\ell(\cdot, T), \ell \leq 0\}$ is a set of non-intersecting line ensemble with $x \mapsto h_0(x, T)$ the surface profile at time T . Figure 3.3 shows this line ensemble for the Poisson points of Figure 3.2.

Non-intersecting line ensembles for other space-time cuts

In some situations, as in our work on the flat PNG, it can be convenient to analyze a line ensemble which corresponds to another cut in the space-time. Consider a continuous and piecewise differentiable path $\gamma : I \rightarrow \mathbb{R} \times [0, T]$, $I \subset \mathbb{R}$ an interval. Then the line ensemble corresponding to γ , denoted by $\{H_\ell, \ell \leq 0\}$, is given by $H_\ell(s) = h_\ell(\gamma(s))$, $s \in I$, $\ell \leq 0$. It is a non-intersecting line ensemble because of (3.102).

Discrete multilayer PNG

The multilayer generalization of the discrete PNG growth (2.46) is similar to the continuous one. As in Section 2.2.3 we consider the case $\tilde{\omega}(x, t) = 0$ for $x - t$ odd. The nucleations for the 0th level are simply the $\tilde{\omega}(x, t)$. When two islands of level $\ell + 1$ merge at (x, t) , we record the lost of information in the nucleation of level ℓ , $\omega_\ell(x, t)$. The multilayer growth then writes

$$h_\ell(x, t) = \max\{h_\ell(x - 1, t - 1), h_\ell(x, t - 1), h_\ell(x + 1, t - 1)\} + \omega_\ell(x, t), \quad (3.103)$$

where

$$\begin{aligned} \omega_0(x, t) &= \tilde{\omega}(x, t), \\ \omega_\ell(x, t) &= \min\{[h_{\ell+1}(x - 1, t - 1) - h_{\ell+1}(x, t - 1)]_+, \\ &\quad [h_{\ell+1}(x + 1, t - 1) - h_{\ell+1}(x, t - 1)]_+\}, \text{ for } \ell \leq -1, \end{aligned} \quad (3.104)$$

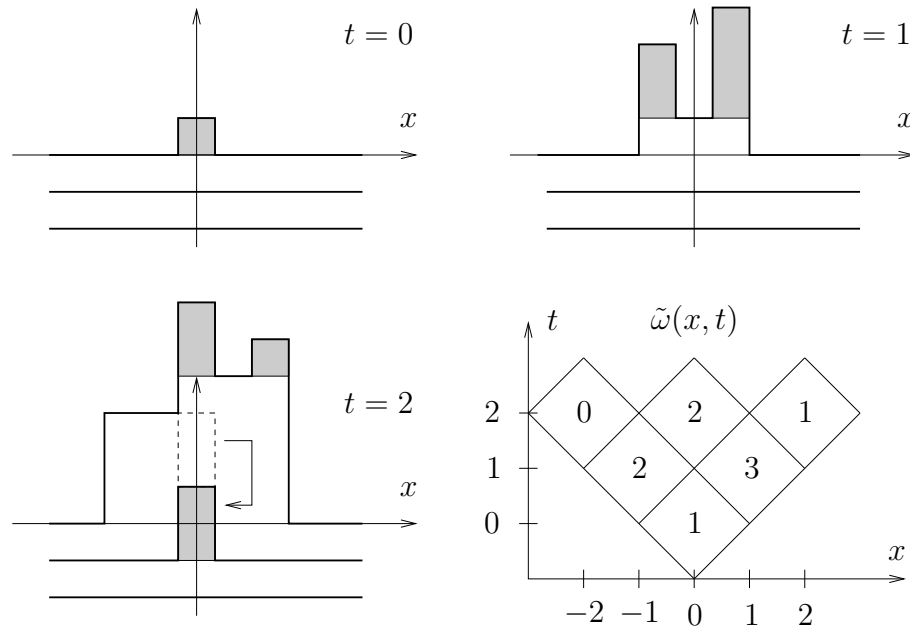


Figure 3.4: Line ensembles for nucleations $\tilde{\omega}$ (3.105). Each height is represented by a histogram of width one. The grey patterns indicated the new nucleations. In the last figure the nucleation for level -1 comes from the dashed region.

where $x_+ = \max\{0, x\}$. In Figure 3.4 we show the line ensemble for nucleations given by

$$\begin{aligned} \tilde{\omega}(0, 0) &= 1, \\ \tilde{\omega}(-1, 1) &= 2, \quad \tilde{\omega}(1, 1) = 3, \\ \tilde{\omega}(-2, 2) &= 0, \quad \tilde{\omega}(0, 2) = 2, \quad \tilde{\omega}(2, 2) = 1. \end{aligned} \tag{3.105}$$

Remark: If one prefers the framework with continuous space-time, then the line ensembles of Figure 3.4 are the ones taken at times $t = \frac{1}{2}$, $t = \frac{3}{2}$, and $t = \frac{5}{2}$.

3.4.2 Line ensemble for 3D-Ising corner

We have seen in Section 2.3.1 that the allowed configuration of the 3D-Ising corner are the 3D-Young diagrams. In view of Figure 2.13, it is natural to represent \mathbf{h} in terms of its level lines or, equivalently, the gradient lines as drawn in Figure 3.5(a). In Figure 3.5(b) the underlying lattice is distorted in such a way that the gradient lines become “trajectories” on a square lattice. It is this latter representation which will be used in the sequel. Clearly, the surface statistics can be reconstructed from the statistics of the line ensemble. More importantly, the border line between rounded and the $2 - 3$ facet is given directly by the top line $h_0(i)$, $i \geq 0$. As first noticed by Okounkov and Reshetikhin [69] the occupation number field corresponding to the line ensemble of Figure 3.5 has determinantal correlations. In Section 5.2 we rederive their results using the fermionic framework, which

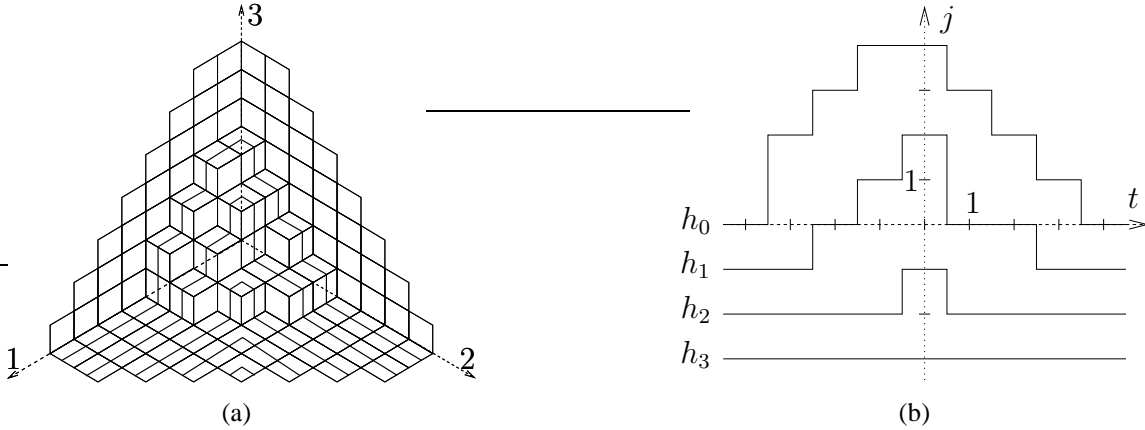


Figure 3.5: The gradient lines for the tiling of Figure 2.13: (a) on the (111)-projection, (b) as function of t .

is a convenient starting point for our asymptotic analysis. We could have chosen to describe the 3D-Young diagrams with the level lines. In this case we would have obtained the border line in the $1-2$ plane directly, but by symmetry they are equivalent.

The gradient lines of Figure 3.5 are defined through

$$t = j - i, \quad h_\ell(t) = \mathbf{h}(i, j) + \ell(i, j), \quad (3.106)$$

where

$$\ell(i, j) = -(i + j - |i - j|)/2 \quad (3.107)$$

labels the line, $(i, j) \in \mathbb{Z}_+^2$. h_ℓ is increasing for $t \leq 0$ and decreasing for $t \geq 0$,

$$h_\ell(t) \leq h_\ell(t + 1), \quad t \leq 0, \quad h_\ell(t) \geq h_\ell(t + 1), \quad t \geq 0, \quad (3.108)$$

with the asymptotic condition

$$\lim_{t \rightarrow \pm\infty} h_\ell(t) = \ell. \quad (3.109)$$

By construction the gradient lines satisfy the non-crossing constraint

$$h_{\ell-1}(t) < h_\ell(t - 1), \quad t \leq 0, \quad h_{\ell-1}(t) < h_\ell(t + 1), \quad t \geq 0. \quad (3.110)$$

Height configurations \mathbf{h} are mapped one-to-one to gradient lines satisfying (3.108), (3.109), and (3.110).

We extend h_ℓ to piecewise constant functions on \mathbb{R} such that the jumps are at mid-points, i.e., at points of $\mathbb{Z} + \frac{1}{2}$. For a given line, h_ℓ , let $t_{\ell,1} < \dots < t_{\ell,k(\ell)} < 0$ be the left jump times with jump heights $s_{\ell,1}, \dots, s_{\ell,k(\ell)}$ and let $0 < t_{\ell,k(\ell)+1} < \dots < t_{\ell,k(\ell)+n(\ell)}$ be the right jump times with jump heights $-s_{\ell,k(\ell)+1}, \dots, -s_{\ell,k(\ell)+n(\ell)}$. The volume of the

3D-Young diagram is simply given by the sum of the area below the lines h_j (of course with respect to the basis level j), that is

$$V(\mathbf{h}) = \sum_{j=1}^{k(\ell)+n(\ell)} s_{\ell,j} |t_{\ell,j}|. \quad (3.111)$$

Thus from (2.57), (2.58) follows that the weight for the line configuration $\{h_\ell\}_{\ell=0,-1,\dots}$ is

$$\prod_{\ell \in \mathbb{Z}_-} \exp \left[\ln(1 - 1/T) \left(\sum_{j=1}^{k(\ell)+n(\ell)} s_{\ell,j} |t_{\ell,j}| \right) \right]. \quad (3.112)$$

Connection with directed polymers

In Section 2.3.2 we anticipated that there is a connection between a discrete model of directed polymers and the 3D-Ising corner. Now all the notions needed to explain it are introduced. The directed polymers are on \mathbb{Z}_+^2 and generated by independent random variables $\omega(i, j)$, $(i, j) \in \mathbb{Z}_+^2$, geometrically distributed with mean value q^{i+j+1} , $q \in (0, 1)$. The role of the growth time $T \rightarrow \infty$ is now taken over by $q \rightarrow 1$. Let us denote by $L(i, j)$ the length of the longest directed polymer from $(i, j) \in \mathbb{Z}_+^2$ to the infinity. Then we want to show that

$$\mathbf{h}(i, 0) = L(i, 0), \quad \mathbf{h}(0, i) = L(0, i), \quad i \geq 0 \quad (3.113)$$

in law.

It would be natural to do the PNG growth starting from the corner and as in the discrete PNG growth explained above. But this does not give us the statistics of the $L(i, 0)$ all at the same time. Instead we do the backwards PNG growth, where growth starts from the infinity and come back to the origin. Since we want to fit in the previous framework of PNG growth, we invert the time axis. Thus we define $t = -(j + i)/2$, which then goes from $-\infty$ to 0. Moreover, denote $x = (j - i)/2$ and consider $\tilde{\omega}(x, t) = \omega(i, j)$ for $x - t$ even, $|x| \leq -t$, and $\tilde{\omega}(x, t) = 0$ otherwise. We apply the discrete PNG growth dynamics (3.103) with initial conditions $h_\ell(x, -\infty) = \ell$ for all $x \in \mathbb{Z}$, $\ell \leq 0$. The dynamics runs up to $t = 0$, see Figure 3.6 for an illustration.

Consider the set of line ensemble $\{H_\ell(j), j \in \mathbb{Z}, \ell \leq 0\}$ associated to the path expressed in the (x, t) coordinate axis by

$$\begin{aligned} \gamma : \mathbb{Z} &\rightarrow \mathbb{Z} \times \mathbb{Z}_- \\ k &\mapsto (k, -|k|). \end{aligned} \quad (3.114)$$

The correspondence between PNG and directed polymers implies $L(0, i) = H_0(i)$ and $L(i, 0) = H_0(-i)$ for $i \geq 0$. Thus we need to see that $H_0(\pm i) = \mathbf{h}(0, \pm i)$. This is obtained by proving that the gradient lines of the 3D-Ising corner and the set of line ensemble $\{H_\ell, \ell \leq 0\}$ are indeed identical. First let us check that the conditions (3.108), (3.109), and (3.110) are exactly satisfied by $\{H_\ell, \ell \leq 0\}$. (3.109) holds by definition of

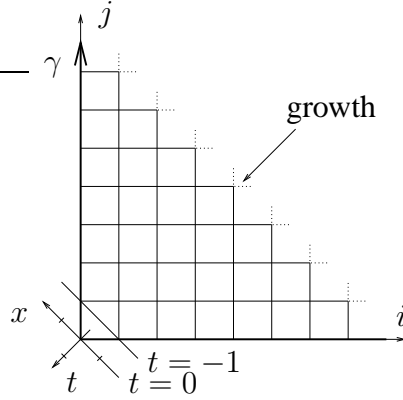


Figure 3.6: (Backwards) PNG growth and 3D-Ising corner. $(i, j) \in \mathbb{Z}_+^2$ and $x = (j - i)/2$, $t = -(i + j)/2$.

our initial conditions. For (3.108) consider $i \leq 0$, the case $i \geq 0$ is analogous. (3.108) is the only constraint between the heights of a level-line because

$$\begin{aligned} H_\ell(i) &= h_\ell(i, i) = \max\{h_\ell(i - 1, i - 1), h_\ell(i, i - 1), h_\ell(i + 1, i - 1)\} + \tilde{\omega}(i, i) \\ &\geq h_\ell(i - 1, i - 1) = H_\ell(i - 1). \end{aligned} \quad (3.115)$$

The third condition (3.110) reflects the non-intersecting constraint of the PNG growth, $h_\ell(i, i) > h_{\ell-1}(i, i)$, which implies

$$H_{\ell-1}(i) = h_{\ell-1}(i, i) < h_\ell(i, i) \leq h_\ell(i - 1, i - 1) = H_\ell(i - 1). \quad (3.116)$$

Next we show that the distribution of the gradient line ensemble and $\{H_\ell, \ell \leq 0\}$ coincide. A given configuration of lines $\{H_\ell(i), \ell \leq 0, i \in \mathbb{Z}\}$ carries the weight

$$\prod_{i, j \geq 0} q^{(i+j+1)\omega(i, j)}. \quad (3.117)$$

Consider the extension of $\{H_\ell(t), \ell \leq 0\}$ from $t \in \mathbb{Z}$ to $t \in \mathbb{R}$ defined by setting $\tilde{H}_\ell(t) = H_\ell(t)$ for $t \in \mathbb{Z}$ and with jumps only at $\mathbb{Z} + \frac{1}{2}$. In term of RSK lines, each $(i, j) \in \mathbb{Z}_+^2$ generates $\omega(i, j)$ pair of lines. Each RSK line originated at $(i, j) \in \mathbb{Z}_+^2$ which moves in the $(0, -1)$ direction (with slope -1 in PNG picture) generates an up-jump at $t = -(i + \frac{1}{2})$ in some level line and each line moving in the $(-1, 0)$ direction leads to a down-jump at $t = j + \frac{1}{2}$ in some level line. The weight of a couple of lines coming from $(i, j) \in \mathbb{Z}_+^2$ is q^{i+j+1} and can be divided by assigning the weight $q^{i+1/2}$ to each up-jump at $t = -(i + \frac{1}{2})$ and the weight $q^{j+1/2}$ to each down-jump at $t = j + \frac{1}{2}$. It then follows

$$\sum_{i, j \geq 0} (i + j + 1)\omega(i, j) = \sum_{\ell \leq 0} \int_{\mathbb{R}} (\tilde{H}_\ell(x) - \ell) dx = \sum_{\ell \leq 0} \sum_{i \in \mathbb{Z}} (H_\ell(i) - \ell), \quad (3.118)$$

which is the same weight of the line ensembles for the 3D-Ising corner configurations (3.112). Therefore the set of line ensembles $\{\tilde{H}_\ell, \ell \leq 0\}$ is identical to the gradient lines of the 3D-Ising corner.

Chapter 4

Analysis of the flat PNG line ensemble

This chapter is devoted to our result on the flat PNG model [28]. First we formulate our main result and then we prove it.

4.1 Formulation of the result

We consider the line ensemble introduced in section 3.4.1 for the flat PNG model at time $t = T$. It is statistically translation invariant. Define the point process on \mathbb{Z} describing the line ensemble at fixed position, say $x = 0$, by

$$\zeta_T^{\text{flat}}(j) = \begin{cases} 1 & \text{if a line passes at } (0, j), \\ 0 & \text{if no line passes at } (0, j). \end{cases} \quad (4.1)$$

The largest j such that $\zeta_T^{\text{flat}}(j) = 1$ is the PNG height and from the Baik and Rains result [13] we know that it fluctuates on a $T^{1/3}$ scale around $2T$. The edge rescaled point process is defined as follows. For any smooth test function f of compact support,

$$\eta_T^{\text{flat}}(f) = \sum_{j \in \mathbb{Z}} \zeta_T^{\text{flat}}(j) f((j - 2T)/(T^{1/3}2^{-2/3})), \quad (4.2)$$

where the factor $2^{-2/3}$ is the same as in (2.45). Notice that in (4.2) there is no prefactor to the sum. The reason is that close to $2T$, the points of ζ_T^{flat} are order $T^{1/3}$ apart and η_T^{flat} remains a point process in the limit $T \rightarrow \infty$. η_T^{flat} has a last particle, i.e., $\eta_T^{\text{flat}}(\xi) = 0$ for all ξ large enough, and even in the $T \rightarrow \infty$ limit has a finite density which increases as $\sqrt{-\xi}$ as $\xi \rightarrow -\infty$. Consequently the sum in (4.2) is effectively finite.

As our main result we prove that the point process η_T^{flat} converges weakly to the point process η^{GOE} as $T \rightarrow \infty$.

Theorem 4.1. *For any $m \in \mathbb{N}$ and smooth test functions of compact support f_1, \dots, f_m ,*

$$\lim_{T \rightarrow \infty} \mathbb{E}_T \left(\prod_{k=1}^m \eta_T^{\text{flat}}(f_k) \right) = \mathbb{E} \left(\prod_{k=1}^m \eta^{\text{GOE}}(f_k) \right). \quad (4.3)$$

\mathbb{E}_T refers to expectation with respect to the Poisson process measure \mathbb{P}_T . The expected value on the r.h.s. of (4.3) is computed via the correlation functions (3.60).

The result of Theorem 4.1 is a first step towards a conjecture on the self-similar statistics of the PNG with flat initial conditions. The starting observation is that, as for the PNG, also to random matrices one can introduce a line ensemble in a natural way. This is the Dyson's Brownian motion, see Section 3.3.1. The height statistics $x \mapsto h(x, t)$ for the PNG *droplet* is linked to the Airy process by

$$\lim_{T \rightarrow \infty} T^{-1/3} \left(h(\tau T^{2/3}, T) - 2\sqrt{T^2 - (\tau T^{2/3})^2} \right) = \mathcal{A}(\tau), \quad (4.4)$$

where the term subtracted from h is the asymptotic shape of the droplet [81]. To obtain this result, Prähofer and Spohn consider the line ensemble obtained by RSK and define a point process like (4.1) but extended to space-time. It is a determinantal point process and in the edge scaling it converges, as $T \rightarrow \infty$, to the point process associated with the extended Airy kernel. Thus they prove not only that the top line converges to the Airy process, but also that the top lines converges to the top lines of Dyson's Brownian motion with $\beta = 2$.

One can extend η_N^{GOE} of (3.58) to space-time as in (3.97), i.e., define

$$\eta_N^{\text{GOE}}(u, s) = N^{1/3} \zeta_N^{\text{GOE}}(2N + xN^{1/3}, 2uN^{1/3}), \quad \zeta_N^{\text{GOE}}(x, t) = \sum_{j=1}^N \delta(\lambda_j(t) - x) \quad (4.5)$$

where ζ_N^{GOE} is the extended point process of Dyson's Brownian motion with $\beta = 1$. The conjecture is that, under edge scaling, the process $x \mapsto h(x, T)$ for flat PNG is in distribution identical to the largest eigenvalue of Dyson's Brownian motion with $\beta = 1$. The result of Theorem 4.1 makes this conjecture more plausible. In fact we now know that, not only $h(0, T)$ in the limit $T \rightarrow \infty$ and properly rescaled is GOE Tracy-Widom distributed, but also that the complete point process η_T^{flat} converges to the edge scaling of Dyson's Brownian motion with $\beta = 1$ for fixed time. For $\beta = 1$ Dyson's Brownian motion one expects that under edge scaling the full stochastic process has a limit. More explicitly, one focuses at the space-time point $(2N, 0)$, rescales space by a factor $N^{1/3}$, time by $N^{2/3}$, and expects that the statistics of the lines has a limit for $N \rightarrow \infty$. It could be that this limit is again Pfaffian with suitably extended kernel. But even for $\beta = 1$ Dyson's Brownian motion this structure has not been unravelled.

The outline of the remainder of the chapter is the following. In section 4.2 we introduce an auxiliary point process, ζ_T^{sym} , from which ζ_T^{flat} can be recovered. ζ_T^{sym} derives from the end-points of a line ensemble with a relatively simple distribution. In section 4.3 we obtain a formula for the n -point correlation functions of ζ_T^{sym} . They are given by Pfaffians of a 2×2 matrix kernel. In section 4.4 we derive an explicit expression of the kernel and in section 4.5 we analyze its edge scaling. Finally in section 4.6 we first prove the same as Theorem 4.1 for the edge scaling of ζ_T^{sym} , and secondly using it we can prove Theorem 4.1. Appendix 4.A contains some bounds used in the asymptotic analysis.

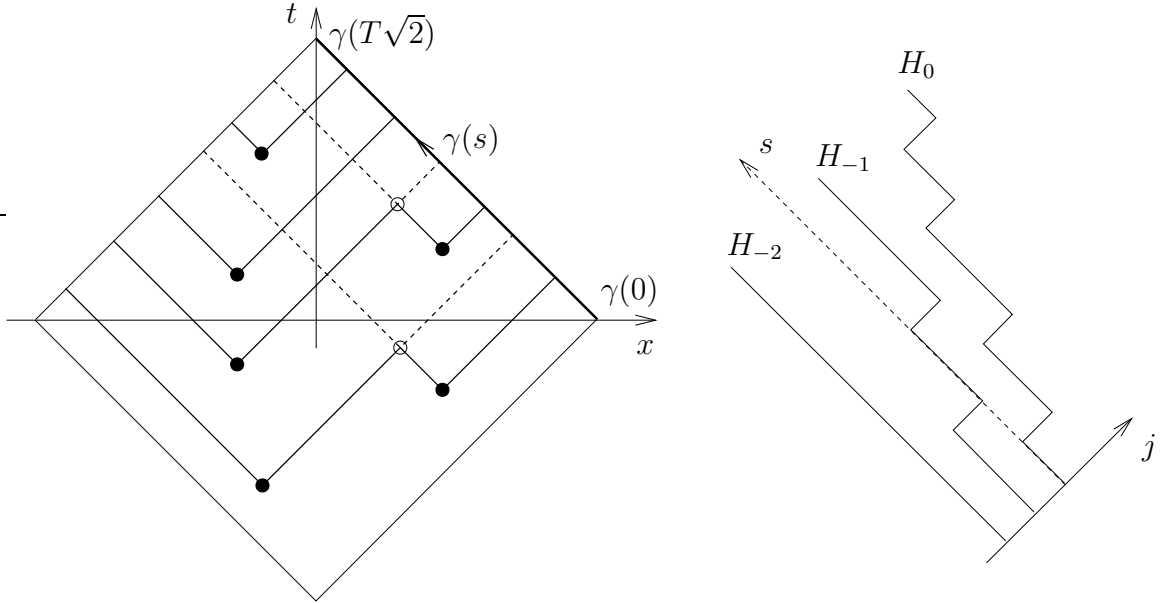


Figure 4.1: A configuration with three Poisson points in the triangle Δ_+ and their symmetric images with respect to the $t = 0$ axis. The path γ is the bold line. On the right we draw the top lines of the line ensemble associated to γ , $\{H_j(s), j \leq 0, s \in [0, T\sqrt{2}]\}$.

4.2 Line ensemble

4.2.1 Line ensemble for the \square symmetry

The line ensemble for flat PNG generated by RSK at time $t = T$ is not easy to analyze because there are non-local constraints on the line configurations. Instead, we start considering the point process ζ_T^{flat} . First remark that this point process depends only on the points in the triangle $\Delta_+ = \{(x, t) \in \mathbb{R} \times \mathbb{R}_+ | t \in [0, T], |x| \leq T - t\}$. We then consider the Poisson points only in Δ_+ and add their symmetric images with respect to the $t = 0$ axis, which are in $\Delta_- = \{(x, t) \in \mathbb{R} \times \mathbb{R}_- | (x, -t) \in \Delta_+\}$. We denote by ζ_T^{sym} the point process at $(0, T)$ obtained by RSK construction using the Poisson points and their symmetric images, see Figure 4.1. To study ζ_T^{sym} we consider a *different line ensemble*. Let us consider the path in space-time defined by $\gamma(s) = (T - s/\sqrt{2}, s/\sqrt{2})$, $s \in [0, T\sqrt{2}]$, and construct the line ensemble $\{H_j(s), j \leq 0, s \in [0, T\sqrt{2}]\}$, as follows. The initial conditions are $H_j(0) = j$ since the height at $t = 0$ is zero everywhere. Every times that γ crosses a RSK line corresponding to a nucleation event of level j , H_j has an up-jump. Then the point process ζ_T^{sym} is given by the points $\{H_j(T\sqrt{2}), j \leq 0\}$. In Proposition 4.3 we show that ζ_T^{flat} can be recovered by ζ_T^{sym} , in fact we prove that $h_j(0, T) = \frac{1}{2}(H_j(T\sqrt{2}) + j)$.

Next we have to determine the allowed line configurations and their distribution induced by the Poisson points. This is obtained as follows. We prove that the *particle-hole* transformation on the line ensemble $\{H_j(s), j \leq 0, s \in [0, T\sqrt{2}]\}$ is equivalent to a particular change of symmetry in the position of the nucleation events, and we connect with

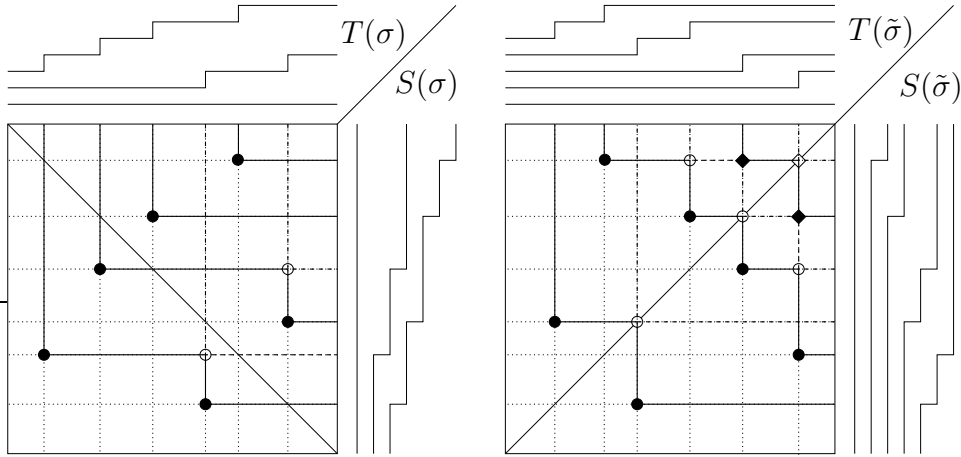


Figure 4.2: Line ensembles for $\sigma = (245163)$ and $\tilde{\sigma} = (361542)$. For the even levels, $\ell = 0, -2$, we use the solid lines and for the odd levels, $\ell = -1, -3$, the dashed lines. The line ensemble of $S(\sigma)$ corresponds to the line ensemble $\{H_j(s), j \leq 0, s \in [0, T\sqrt{2}]\}$ of Figure 4.1.

the half-droplet PNG problem studied by Sasamoto and Imamura [40].

Young tableaux

Let $\sigma = (\sigma(1), \dots, \sigma(2N))$ be a permutation of $\{1, \dots, 2N\}$ which indicate the order in which the Poisson points are placed in the diamond $\Delta_+ \cup \Delta_-$. More precisely, let (x_i, t_i) be the positions of the points with the index $i = 1, \dots, N$ such that $t_i + x_i$ is increasing with i , and σ is the permutation such that $t_{\sigma(i)} - x_{\sigma(i)}$ is increasing in i too. Let us construct the line ensembles along the paths $(T, 0) \rightarrow (0, T)$ and $(-T, 0) \rightarrow (0, T)$. The relative position of the steps on the line ensembles are encoded in the Young tableaux $S(\sigma)$ and $T(\sigma)$ constructed using Schensted's algorithm. If the k^{th} step occurs in line H_j , then in the Young tableau there is a k in row j , see Figure 4.2.

In our case the points are symmetric with respect to the axis $t = 0$ and we refer to it as the symmetry \boxtimes . In the case studied in [40], the points are symmetric with respect to the axis $x = 0$ and we call it the symmetry \boxminus . Consider a configuration of points with symmetry \boxtimes and let σ be the corresponding permutation. The RSK construction leads to the line ensembles of $T(\sigma)$ and $S(\sigma)$ as shown in the left part of Figure 4.2. If we apply the axis symmetry with respect to $x + t = 0$, then we obtain a configuration of points shown in the right part of Figure 4.2. The points have now the symmetry \boxminus and the corresponding permutation $\tilde{\sigma}$ is obtained simply by reversing the order of σ , that is, if $\sigma = (\sigma(1), \dots, \sigma(2N))$ then $\tilde{\sigma}(j) = \sigma(2N + 1 - j)$. By Schensted's theorem [88],

$$S(\tilde{\sigma}) = S(\sigma)^t, \quad (4.6)$$

Moreover, the positions of the steps in the line ensembles of $S(\sigma)$ and $S(\tilde{\sigma})$ occurs at the

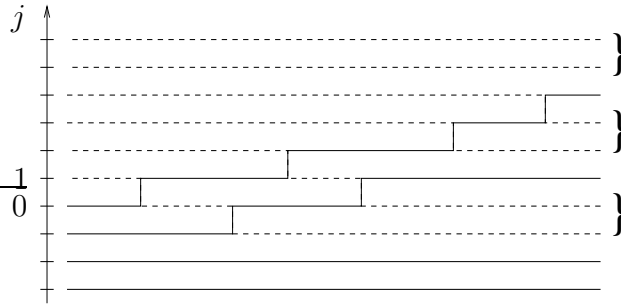


Figure 4.3: Particle (solid) and hole (dashed) line ensembles for the example of Figure 4.2. The particle line ensemble is the one associated with $S(\sigma)$, and the hole line ensemble is the one of $S(\tilde{\sigma})$ reflected with respect to the line $j = 1/2$. The pairing rule is shown by the brackets.

same positions, but of course in different line levels. Figure 4.2 shows an example with $\sigma = (2\ 4\ 5\ 1\ 6\ 3)$, for which the Young tableaux are

$$S(\sigma) = \begin{pmatrix} 1 & 3 & 5 & 6 \\ 2 & 4 & & \end{pmatrix}, \quad S(\tilde{\sigma}) = T(\tilde{\sigma}) = \begin{pmatrix} 1 & 2 \\ 3 & 4 \\ 5 & \\ 6 & \end{pmatrix}.$$

$$T(\sigma) = \begin{pmatrix} 1 & 2 & 3 & 5 \\ 4 & 6 & & \end{pmatrix},$$

Particle-hole transformation

At the level of line ensemble we can apply the particle-hole transformation, which means that a configuration of lines is replaced by the one with jumps at the same positions and the horizontal lines occupy the previous empty spaces, as shown in Figure 4.3. Let us start with the line ensemble corresponding to $S(\sigma)$, then the Young tableau for the *hole line ensemble* is given by $S(\sigma)^t$. In fact, the information encoded in $S(\sigma)$ tell us that the j^{th} particle has jumps at (relative) position $S(\sigma)_{j,k}$, $k \geq 1$, for $j \geq 1$. On the other hand, the j^{th} hole has jumps where the particles have their j^{th} jump. Therefore the particle-hole transformation is equivalent to the symmetry transformation $\square \rightarrow \square$.

Allowed line configurations and measure

Sasamoto and Imamura [40] study the half-droplet geometry for PNG, where nucleation events occurs symmetrically with respect to $x = 0$, i.e., with the \square symmetry. In particular, they prove that the point process at $x = 0$ converges to the point process of eigenvalues of the Gaussian Symplectic Ensemble (GSE). Its correlation functions have the same Pfaffian structure as GOE but with a different kernel. In a way the line ensemble they study is the hole line ensemble described above, thus their edge scaling focuses at the top holes, i.e., in the region where the lowest particles are excited. Notice that the change of focus between particles and holes changes the statistics from GSE to GOE. This differs from the case

of the PNG droplet [81] where for both holes and particles the edge statistics is GUE. Although the result of [40] cannot be applied directly to our symmetry, some properties derived there will be of use.

From [40] we know that for the symmetry \boxtimes a hole line configuration is allowed if: a) the lines do not intersect, b) have only down-jumps, c) they satisfy the *pairing rule*: $H_{2j}^{\text{hole}}(T\sqrt{2}) = H_{2j-1}^{\text{hole}}(T\sqrt{2})$ for all $j \geq 1$. This implies that for the symmetry \boxplus a line configuration $\{H_j\}$ is allowed if: a) the lines do not intersect, b) have only up-jumps, c) $H_j(T\sqrt{2}) - H_j(0)$ is *even* for each $j \leq 0$. Moreover, there is a one-to-one correspondence between allowed configurations and nucleation events. The probability measure for the line ensemble turns out to have a simple structure. Consider Poisson points with intensity ϱ and symmetry \boxplus . Each Poisson point $(x, t) \in \Delta_+$ has a probability $\varrho dx dt$ of being in $[x, x + dx] \times [t, t + dt]$. In the corresponding line ensemble this weight is carried by two jumps, therefore the measure induced by the points on a line configuration $\{H_j\}$ is given by $\sqrt{\varrho}^{\#\text{jumps in } \{H_j\}}$ times the uniform measure.

4.2.2 Flat PNG and line ensemble for \boxplus symmetry

The correspondence between the point process ζ_T^{flat} and ζ_T^{sym} is as follows. Let us consider a permutation σ with Young tableau $S(\sigma)$ of shape $(\lambda_1, \lambda_2, \dots, \lambda_m)$. Let, for $k \leq m$, $a_k(\sigma)$ be the length of the longest subsequence consisting of k disjoint increasing subsequences.

Theorem 4.2 (Greene [36]). *For all $k = 1, \dots, m$,*

$$a_k(\sigma) = \lambda_1 + \dots + \lambda_k. \quad (4.7)$$

The geometric interpretation is the following. Let σ be the permutation which corresponds to some configuration of Poisson points in $\Delta_+ \cup \Delta_-$. Then a_k is the maximal sum of the lengths of k non-intersecting (without common points) directed polymers from $(0, -T)$ to $(0, T)$.

Proposition 4.3. *Let π be a Poisson point configuration in Δ_+ and let the corresponding Young tableau $S(\pi)$ have shape $(\lambda_1, \lambda_2, \dots, \lambda_m)$. Let $\tilde{\pi}$ be the configuration of points on $\Delta_+ \cup \Delta_-$ with symmetry \boxplus which is identical to π in Δ_+ . Then $S(\tilde{\pi})$ has shape $(\tilde{\lambda}_1, \tilde{\lambda}_2, \dots, \tilde{\lambda}_m) = (2\lambda_1, 2\lambda_2, \dots, 2\lambda_m)$.*

Proof. To prove the proposition is enough to prove that $a_k(\tilde{\pi}) = 2a_k(\pi)$ for $k = 1, \dots, m$.

i) $a_k(\tilde{\pi}) \geq 2a_k(\pi)$: it is obvious since we can choose the k directed polymers on $\tilde{\pi}$ by completing the ones on π by symmetry.

ii) $a_k(\tilde{\pi}) \leq 2a_k(\pi)$: assume it to be false. Then there exists k directed polymers in Δ_+ and k in Δ_- such that the total length is strictly greater than $2a_k(\pi)$. This implies that at least one (by symmetry both) of the sets of k directed polymers has total length strictly greater than $a_k(\pi)$. But this is in contradiction with the definition of $a_k(\pi)$, therefore $a_k(\tilde{\pi}) \leq 2a_k(\pi)$. \square

Since $\lambda_{1-j} = h_j(0, T) - j$ and $\tilde{\lambda}_{1-j} = H_j(T\sqrt{2}) - j$, it follows from this proposition that

$$h_j(0, T) = \frac{1}{2}(H_j(T\sqrt{2}) + j) \quad (4.8)$$

for all $j \leq 0$.

4.3 Correlation functions

Non-intersecting lines can be viewed as trajectories of fermions in discrete space \mathbb{Z} and continuous time $[0, T\sqrt{2}]$. Let us start with a finite number of fermions, $2N$, which implies that only the information in the first $2N$ levels in the RSK construction is retained. For any configuration, the number of non perfectly flat lines, is obviously bounded by the number of Poisson points in Δ_+ . On the other hand for fixed T , the probability of having a number of Poisson points greater than $2N$ decreases exponentially fast for N large. First we derive an exact formula for the n -point correlation function for finite N , and then take the limit $N \rightarrow \infty$ so that, for any fixed T , each line configuration contains all the information of the Poisson points. Finally we consider the asymptotic for large T .

Let a_j^* and a_j , $j \in \mathbb{Z}$, be the creation and annihilation operator for the fermions and $|\emptyset\rangle$ be the state without fermions. The initial state is then given by

$$|\Omega_{\text{in}}\rangle = \prod_{j=-2N+1}^0 a_j^* |\emptyset\rangle, \quad (4.9)$$

and the final state is

$$|\Omega_{\text{fin}}\rangle = \sum_{\mathbf{n} \in C_N} \prod_{j=-2N+1}^0 a_{j+2n_j}^* |\emptyset\rangle \quad (4.10)$$

where $C_N = \{\{n_0, \dots, n_{-2N+1}\} | n_j \geq n_{j-1}, n_j \geq 0\}$. Let us define the up-jump operator as

$$\alpha_1 = \sum_{k \in \mathbb{Z}} a_{k+1}^* a_k, \quad (4.11)$$

which when applied on $|\Omega_{\text{in}}\rangle$ is actually a finite sum. Then the evolution from the initial state ($t = 0$) to the final one ($t = T\sqrt{2}$) is given by the transfer operator

$$\exp(\tilde{T}\alpha_1), \quad \tilde{T} = \sqrt{2}qT = 2T. \quad (4.12)$$

The linear statistics, i.e., for a bounded function $g : \mathbb{Z} \rightarrow \mathbb{R}$, is

$$\mathbb{E}_{N,T} \left(\prod_{j=-2N+1}^0 (1 - g(x_j^{\text{fin}})) \right) = \frac{\langle \Omega_{\text{fin}} | \prod_{y \in \mathbb{Z}} (1 - g(y) a_y^* a_y) e^{\tilde{T}\alpha_1} | \Omega_{\text{in}} \rangle}{\langle \Omega_{\text{fin}} | \prod_{y \in \mathbb{Z}} e^{\tilde{T}\alpha_1} | \Omega_{\text{in}} \rangle} \quad (4.13)$$

where the $x_j^{\text{fin}}, j \in \{-2N+1, \dots, 0\}$ are the position of the fermions at time $T\sqrt{2}$. Let us denote by $\rho^{(n)}(x_1, \dots, x_n)$ the n -point correlation function of ζ_T^{sym} . Then

$$\mathbb{E}_{N,T} \left(\prod_{j=-2N+1}^0 (1 - g(x_j^{\text{fin}})) \right) = \sum_{n \geq 0} \frac{(-1)^n}{n!} \sum_{x_1, \dots, x_n \in \mathbb{Z}} \rho^{(n)}(x_1, \dots, x_n) \prod_{j=1}^n g(x_j). \quad (4.14)$$

For finite N , $\rho^{(n)} = 0$ for $n > 2N$.

Proposition 4.4. *Let us define the matrix Φ with entries*

$$\Phi_{x,i} = \frac{1}{(x-i)!} \tilde{T}^{x-i} \Theta(x-i), \quad (4.15)$$

with Θ the Heaviside function, the antisymmetric matrices S and A

$$S_{x,y} = \frac{1 + \text{sgn}(x-y)(-1)^x}{2} \frac{1 - \text{sgn}(x-y)(-1)^y}{2} \text{sgn}(x-y), \quad (4.16)$$

$$A_{i,j} = \sum_{x,y \in \mathbb{Z}} \Phi_{i,x}^t S_{x,y} \Phi_{y,j} = [\Phi^t S \Phi]_{i,j}. \quad (4.17)$$

Then the n -point correlation function, for $n \in \{0, \dots, 2N\}$, are given by

$$\rho^{(n)}(x_1, \dots, x_n) = \text{Pf} [K(x_i, x_j)]_{i,j=1, \dots, n} \quad (4.18)$$

where K is a 2×2 matrix kernel, $K(x, y) = \begin{pmatrix} K_{1,1}(x, y) & K_{1,2}(x, y) \\ K_{2,1}(x, y) & K_{2,2}(x, y) \end{pmatrix}$, with

$$\begin{aligned} K_{1,1}(x, y) &= - \sum_{i,j=-2N+1}^0 \Phi_{i,x}^t A_{i,j}^{-1} \Phi_{j,y}^t \\ K_{1,2}(x, y) &= - \sum_{i,j=-2N+1}^0 \Phi_{i,x}^t A_{i,j}^{-1} [\Phi^t S^t]_{j,y} = -K_{2,1}(y, x) \\ K_{2,1}(x, y) &= - \sum_{i,j=-2N+1}^0 [\Phi^t S^t]_{i,x} A_{i,j}^{-1} \Phi_{j,y}^t \\ K_{2,2}(x, y) &= S_{x,y}^t - \sum_{i,j=-2N+1}^0 [\Phi^t S^t]_{i,x} A_{i,j}^{-1} [\Phi^t S^t]_{j,y}. \end{aligned} \quad (4.19)$$

When $N \rightarrow \infty$, (4.14) becomes a Fredholm Pfaffian, $\text{Pf}(J - Kg) = \sqrt{\text{Det}(\mathbb{1} - J^{-1}Kg)}$, where $J = \begin{pmatrix} 0 & 1 \\ -1 & 0 \end{pmatrix}$, see Section 8 of [82]. In this case, we consider bounded functions g with support bounded from below, so that the sum in (4.14) is well defined. From the point of view of operators, the determinant has to be thought as defined through the modified determinant like in the case of the GOE case, see discussion at the end of Section 3.2.3. Finally, note that A is invertible because $\text{Det}(A)$ is the partition function of the line ensemble.

Proof. Since it is often used, we denote the ordered set $I = \{-2N+1, \dots, 0\}$, and instead of writing a matrix $M = [M_{i,j}]_{i,j=-2N+1, \dots, 0}$ we write $M = [M_{i,j}]_{i,j \in I}$. Let $w(\{x^{\text{in}}\}) \rightarrow$

$\{x_{\mathbf{n}}^{\text{fin}}\}$), $\mathbf{n} \in C_N$ as given in (4.10), be the weight of fermions starting from positions $\{x^{\text{in}}\} = (x_i^{\text{in}})_{i \in I}$, $x_i^{\text{in}} = i$, and ending at $\{x_{\mathbf{n}}^{\text{fin}}\} = (x_j^{\text{fin}})_{j \in I}$, $x_j^{\text{fin}} = j + 2n_j$. The non-intersection constraint implies [49] that the weight can be expressed via determinants,

$$w(\{x^{\text{in}}\} \rightarrow \{x_{\mathbf{n}}^{\text{fin}}\}) = \text{Det}[\varphi_{i,j}]_{i,j \in I} \quad (4.20)$$

with

$$\varphi_{i,j} = \langle \emptyset | a_{j+2n_j} e^{\tilde{T}\alpha_1} a_i^* | \emptyset \rangle = [e^{\tilde{T}\alpha_1}]_{j+2n_j,i} = \Phi_{j+2n_j,i}. \quad (4.21)$$

Taking into account the even/odd initial position of the fermions, (4.20) can be rewritten as

$$w(\{x^{\text{in}}\} \rightarrow \{x_{\mathbf{n}}^{\text{fin}}\}) = \text{Det}[\Phi_i(x_j^{\text{fin}})]_{i,j \in I} \prod_{j=-N+1}^0 \mathbf{e}(x_{2j}^{\text{fin}}) \mathbf{o}(x_{2j-1}^{\text{fin}}) \quad (4.22)$$

with

$$\mathbf{e}(x) = \frac{1 + (-1)^x}{2}, \quad \mathbf{o}(x) = \frac{1 - (-1)^x}{2}. \quad (4.23)$$

Let us denote by $p(x_{-2N+1}, \dots, x_0)$ the probability that the set of end points $\{x_j^{\text{fin}}, j = -2N + 1, \dots, 0\}$ coincide with the set $\{x_{-2N+1}, \dots, x_0\}$. We want to show that this probability can be written as a determinant times a Pfaffian. Since the x_j 's do not have to be ordered, let π be the permutation of $\{-2N + 1, \dots, 0\}$ such that $x_{\pi(i)} < x_{\pi(i+1)}$, that is, $x_{\pi(i)} = x_i^{\text{fin}}, i \in I$. Moreover, define the matrix $\Xi = [\Xi_{i,j}]_{i,j \in I}$ by setting $\Xi_{i,j} = \delta_{i,\pi(j)}$. Then

$$[\Phi_i(x_j^{\text{fin}})]_{i,j \in I} = [\Phi_i(x_j)]_{i,j \in I} \Xi. \quad (4.24)$$

Now let us show that

$$\prod_{j=-N+1}^0 \mathbf{e}(x_{2j}^{\text{fin}}) \mathbf{o}(x_{2j-1}^{\text{fin}}) = \text{Pf}[S_{x_i^{\text{fin}}, x_j^{\text{fin}}}^t]_{i,j \in I}. \quad (4.25)$$

Since $x_i^{\text{fin}} < x_{i+1}^{\text{fin}}$, the components i, j ($i < j$) of the r.h.s. matrix are given by $\mathbf{o}(x_i^{\text{fin}}) \mathbf{e}(x_j^{\text{fin}})$. The Pfaffian of a matrix $M = [M_{i,j}]_{i,j \in I}$ is

$$\text{Pf}(M) = \sum_{\substack{\sigma \\ \sigma_{2i-1} < \sigma_{2i}}} (-1)^{|\sigma|} \prod_{i=-N+1}^0 M_{\sigma_{2i-1}, \sigma_{2i}}, \quad (4.26)$$

where the sum is on the permutations σ of $\{-2N + 1, \dots, 0\}$ with $\sigma_{2i-1} < \sigma_{2i}$. The identity permutation gives already l.h.s. of (4.25). Thus we have to show that all other terms cancels pairwise. Take a permutation σ such that $\sigma(2i-1) < \sigma(2j-1) < \sigma(2i) < \sigma(2j)$ and define the permutation σ' by setting $\sigma'(2j) = \sigma(2i)$, $\sigma'(2i) = \sigma(2j)$, and $\sigma'(k) = \sigma(k)$ otherwise. The term of the Pfaffian coming from σ and σ' are identical up to a minus sign because $(-1)^{|\sigma|} = -(-1)^{|\sigma'|}$. Moreover, the only permutation for which $\sigma(2i-1) < \sigma(2j-1) < \sigma(2i) < \sigma(2j)$ can not be satisfied for some i, j is the identity. Consequently (4.25) holds.

Finally, define the matrix $G = \Xi^t [S_{x_i, x_j}^t]_{i, j \in I} \Xi$. Replacing the definition of Ξ we obtain $G = [S_{x_i^{\text{fin}}, x_j^{\text{fin}}}^t]_{i, j \in I}$. Then

$$\begin{aligned} p(x_{-2N+1}, \dots, x_0) &= w(\{x^{\text{in}}\} \rightarrow \{x_n^{\text{fin}}\}) \\ &= \text{Det}[\Phi_i(x_j^{\text{fin}})]_{i, j \in I} \prod_{j=-N+1}^0 \mathbf{e}(x_{2j}^{\text{fin}}) \mathbf{o}(x_{2j-1}^{\text{fin}}) \\ &= \text{Det}[\Phi_i(x_j)]_{i, j \in I} \text{Det}(\Xi) \text{Pf}(\Xi^t [S_{x_i, x_j}^t]_{i, j \in I} \Xi) \\ &= \text{Det}[\Phi_i(x_j)]_{i, j \in I} \text{Pf}[S_{x_i, x_j}^t]_{i, j \in I} \end{aligned} \quad (4.27)$$

where we used the property of Pfaffians $\text{Pf}(\Xi^t T \Xi) = \text{Pf}(T) \text{Det}(\Xi)$, see e.g. [96], and $\text{Det}(\Xi) = (-1)^{|\pi|}$.

The probability (4.27) is of the form (3.23) with

$$\varepsilon(x, y) = S_{x, y}^t, \quad f_i(x) = \Phi_{x, i} \quad (4.28)$$

from which follows that

$$M_{i, j} = -A_{i, j}, \quad (\varepsilon f_i)(x) = -[S\Phi]_{x, i}, \quad (4.29)$$

and the kernel is given by

$$K'(x, y) = \begin{pmatrix} -K_{1,1}(x, y) & K_{1,2}(x, y) \\ K_{2,1}(x, y) & -K_{2,2}(x, y) \end{pmatrix}. \quad (4.30)$$

But K and K' are two equivalent kernels (they give the same correlation functions) since $K' = U^t K U$ with $U = i \begin{pmatrix} 1 & 0 \\ 0 & -1 \end{pmatrix}$ and $\text{Pf}[U^t K U] = \text{Det}[U] \text{Pf}[K]$. We use K instead of K' uniquely because another derivation of the kernel gave K and we already carried out the analysis. \square

4.4 Kernel for finite T

In this section we compute the components of the kernel given in (4.19). At this stage we take the limit $N \rightarrow \infty$. The justification of this limit is in the end of this section. The first step is to find the inverse of the matrix A . First we extend A to be defined for all $i, j \in \mathbb{Z}$ by using (4.17) to all i, j . Let us divide $\ell^2(\mathbb{Z}) = \ell^2(\mathbb{Z}_+^*) \oplus \ell^2(\mathbb{Z}_-)$, where $\mathbb{Z}_+^* = \{1, 2, \dots\}$ and $\mathbb{Z}_- = \{0, -1, \dots\}$. The inverse of A in (4.19) is the one in the subspace $\ell^2(\mathbb{Z}_-)$. Let us denote by P_- the projector on \mathbb{Z}_- and P_+ the one on \mathbb{Z}_+^* .

Lemma 4.5. *The inverse of A in subspace $\ell^2(\mathbb{Z}_-)$, which can be expressed as $P_-(P_- A P_- + P_+)^{-1} P_-$, is given by*

$$[A^{-1}]_{i, j} = [\alpha_{-1} e^{-\tilde{T}\alpha_{-1}} P_- e^{-\tilde{T}\alpha_1} - e^{-\tilde{T}\alpha_{-1}} P_- e^{-\tilde{T}\alpha_1} \alpha_1]_{i, j} \quad (4.31)$$

where $[\alpha_1]_{i, j} = \delta_{i, j+1}$ and $\alpha_{-1} \equiv \alpha_1^t$.

Proof. First we rewrite A as a sum of a Toeplitz matrix plus the remainder. Let α_e be the matrix with $[\alpha_e]_{i,j} = \delta_{i,j} \frac{1+(-1)^i}{2}$ and $\alpha_o = \mathbb{1} - \alpha_e$. Then

$$S = \sum_{k \geq 0} \alpha_1^{2k+1} \alpha_o - \sum_{k \geq 0} \alpha_{-1}^{2k+1} \alpha_e. \quad (4.32)$$

It is then easy to see that, for $V_e(x)$ an even polynomial of arbitrarily high order

$$V_e(\alpha_{\pm 1}) \alpha_e = \alpha_e V_e(\alpha_{\pm 1}), \quad V_e(\alpha_{\pm 1}) \alpha_o = \alpha_o V_e(\alpha_{\pm 1}) \quad (4.33)$$

and for $V_o(x)$ an odd polynomial of arbitrarily high order

$$V_o(\alpha_{\pm 1}) \alpha_e = \alpha_o V_o(\alpha_{\pm 1}), \quad V_o(\alpha_{\pm 1}) \alpha_o = \alpha_e V_o(\alpha_{\pm 1}). \quad (4.34)$$

Hence A can be written as

$$A = \exp(\tilde{T} \alpha_{-1}) \sum_{k \geq 0} (\alpha_1^{2k+1} \alpha_o - \alpha_{-1}^{2k+1} \alpha_e) (\cosh(\tilde{T} \alpha_1) + \sinh(\tilde{T} \alpha_1)). \quad (4.35)$$

We pull the last factor in (4.35) in front of the sum using the commutation relations (4.33) and (4.34), and, after some algebraic manipulations, we obtain

$$A = M + R \quad (4.36)$$

where $M = \frac{1}{2} \Phi^t (Q - Q^t) \Phi$, $R = \frac{1}{2} (Q + Q^t) (\alpha_o - \alpha_e)$, with $Q = \sum_{k \geq 0} \alpha_1^{2k+1}$ and $\Phi = \exp(\tilde{T} \alpha_1)$.

Let $B = [\Phi^{-1}]^t (\alpha_{-1} P_- - P_- \alpha_1) \Phi^{-1}$. We want to prove that it is the inverse of A in the subspace $\ell^2(\mathbb{Z}_-)$. First notice that $B_{i,j} = 0$ if $i \geq 1$ or $j \geq 1$, which implies $[A \cdot B]_{i,j} = [P_- A P_- \cdot B]_{i,j}$ for $i, j \leq 0$. Therefore, for $i, j \leq 0$,

$$[A \cdot B]_{i,j} = [(M + R) \cdot [\Phi^{-1}]^t U_0 \Phi^{-1}]_{i,j} \quad (4.37)$$

with

$$U_0 = \alpha_{-1} P_- - P_- \alpha_1, \quad (4.38)$$

and, expanding $M + R$, we have

$$\begin{aligned} [A \cdot B]_{i,j} &= \left[\left(e^{\tilde{T} \alpha_{-1}} \frac{Q - Q^t}{2} e^{\tilde{T} \alpha_1} + \frac{Q + Q^t}{2} (\alpha_o - \alpha_e) \right) \left(e^{-\tilde{T} \alpha_{-1}} U_0 e^{-\tilde{T} \alpha_1} \right) \right]_{i,j} \\ &= \left[e^{\tilde{T} \alpha_1} U_1 e^{-\tilde{T} \alpha_1} \right]_{i,j} + \left[e^{\tilde{T} \alpha_{-1}} U_2 e^{-\tilde{T} \alpha_1} \right]_{i,j} \end{aligned} \quad (4.39)$$

where $U_1 = \frac{1}{2} (Q - Q^t) U_0$ and $U_2 = \frac{1}{2} (Q + Q^t) (\alpha_o - \alpha_e) U_0$. The components of these matrices are given by

$$\begin{aligned} [U_1]_{n,m} &= \delta_{n,m} \mathbb{1}_{[n \leq 0]} + \frac{1}{2} \delta_{m,0} \operatorname{sgn}(n-1) \frac{1 + (-1)^n}{2}, \\ [U_2]_{n,m} &= \frac{1}{2} \delta_{m,0} \frac{1 + (-1)^n}{2}, \end{aligned} \quad (4.40)$$

and a simple algebraic computation leads then to $[A \cdot B]_{i,j} = \delta_{i,j}$ for $i, j \leq 0$. Finally, since A and B are antisymmetric, $[B \cdot A]_{i,j} = [A^t \cdot B^t]_{j,i} = [A \cdot B]_{j,i} = \delta_{i,j}$ too. Therefore B is the inverse of A in the subspace $\ell^2(\mathbb{Z}_-)$. \square

The second step is to find an explicit expression for the kernel's elements. Using the fact that $[A^{-1}]_{i,j}$ of Lemma 4.5 is zero for $i \geq 1$ or $j \geq 1$, we can extend the sum over all $i, j \in \mathbb{Z}$ and obtain

$$\begin{aligned} K_{1,1}(x, y) &= -[\Phi A^{-1} \Phi^t]_{x,y}, \\ K_{1,2}(x, y) &= -K_{2,1}(y, x), \\ K_{2,1}(x, y) &= -[S \Phi A^{-1} \Phi^t]_{x,y}, \\ K_{2,2}(x, y) &= S_{x,y}^t - [S \Phi A^{-1} \Phi^t S^t]_{x,y}. \end{aligned} \tag{4.41}$$

Put $\Psi = e^{\tilde{T}\alpha_1} e^{-\tilde{T}\alpha_{-1}}$. We write S as in (4.32), use the commutation relations (4.33) and (4.34), and after some straightforward algebra obtain

$$\begin{aligned} K_{1,1} &= -\Psi U_0 \Psi^t, \\ K_{2,1} &= -\Psi^t (S U_0 - U_1) \Psi^t - \Psi U_1 \Psi^t, \\ K_{2,2} &= S^t + S K_{1,1}^t, \end{aligned} \tag{4.42}$$

where U_1 is given by (4.40), and

$$\begin{aligned} [U_0]_{n,m} &= (\delta_{n,m-1} - \delta_{m,n-1}) \mathbb{1}_{[n,m \leq 0]} \\ [S U_0 - U_1]_{n,m} &= \frac{1}{2} \frac{1 + (-1)^n}{2} \delta_{m,0}. \end{aligned} \tag{4.43}$$

Using these relations we obtain the kernel elements, which are summed up in the following

Lemma 4.6.

$$K(x, y) = G(x, y) + R(x, y), \tag{4.44}$$

with

$$\begin{aligned} R_{1,1}(x, y) &= 0, \\ R_{1,2}(x, y) &= -\frac{(-1)^y}{2} J_{x+1}(2\tilde{T}), \\ R_{2,1}(x, y) &= \frac{(-1)^x}{2} J_{y+1}(2\tilde{T}), \\ R_{2,2}(x, y) &= -S(x, y) + \frac{1}{4} \operatorname{sgn}(x - y) \\ &\quad - \frac{(-1)^x}{2} \sum_{m \geq 1} J_{y+2m}(2\tilde{T}) + \frac{(-1)^y}{2} \sum_{n \geq 1} J_{2n+x}(2\tilde{T}), \end{aligned} \tag{4.45}$$

and

$$G_{1,1}(x, y) = - \sum_{n \geq 1} J_{x+n+1}(2\tilde{T}) J_{y+n}(2\tilde{T}) + \sum_{n \geq 1} J_{y+n+1}(2\tilde{T}) J_{x+n}(2\tilde{T}), \tag{4.46}$$

$$G_{1,2}(x, y) = \sum_{n \geq 1} J_{x+n}(2\tilde{T})J_{y+n}(2\tilde{T}) - J_{x+1}(2\tilde{T}) \left(\sum_{m \geq 1} J_{y+2m-1}(2\tilde{T}) - \frac{1}{2} \right), \quad (4.47)$$

$$G_{2,1}(x, y) = - \sum_{n \geq 1} J_{x+n}(2\tilde{T})J_{y+n}(2\tilde{T}) + J_{y+1}(2\tilde{T}) \left(\sum_{m \geq 1} J_{x+2m-1}(2\tilde{T}) - \frac{1}{2} \right), \quad (4.48)$$

$$\begin{aligned} G_{2,2}(x, y) &= \sum_{m \geq 1} \sum_{n \geq m} J_{x+2m}(2\tilde{T})J_{y+2n+1}(2\tilde{T}) - \sum_{n \geq 1} \sum_{m \geq n} J_{x+2m+1}(2\tilde{T})J_{y+2n}(2\tilde{T}) \\ &\quad - \frac{1}{2} \sum_{m \geq 1} J_{x+2m}(2\tilde{T}) + \frac{1}{2} \sum_{n \geq 1} J_{y+2n}(2\tilde{T}) - \frac{1}{4} \operatorname{sgn}(x - y), \end{aligned} \quad (4.49)$$

where $J_m(t)$ denotes the m^{th} order Bessel function.

Remark: this result could also be deduced starting from Section 5 of [82]. Now we justify the $N \rightarrow \infty$ limit. Let us first explain the idea. Denote the sets $I = \{-2N + 1, \dots, 0\}$ and $L = \{-N + 1, \dots, 0\}$. We consider the kernel's elements for $x, y \geq 0$. For $(i, j) \in I^2 \setminus L^2$, the inverse of A for finite N differs from the inverse for $N = \infty$ only by $\mathcal{O}(e^{-\mu N})$ with $\mu = \mu(\tilde{T}) > 0$. On the other hand, the contribution to $K_{\cdot, \cdot}(x, y)$ coming from $(i, j) \in (I \setminus L)^2$ are exponentially small in N . Therefore, replacing the inverse of A for finite N with the inverse obtained in Lemma 4.5 we introduce only an error exponentially small in N . The dependence of the kernel's elements on N is only via the extension of the sums in (4.19), which limit is the one we derived in Lemma 4.6.

In what follows we denote by A_N the $2N \times 2N$ matrix (4.17) and by A the $N = \infty$ one.

Lemma 4.7. *If we replace $[A_N^{-1}]_{i,j}$ by $A_{i,j}^{-1}$ in the kernel's elements (4.19), then for N large enough, the error made is $\mathcal{O}(e^{-\mu N})$ for some constant $\mu = \mu(\tilde{T}) > 0$. The error is uniform for $x, y \geq 0$.*

Proof. Here we use some results of Appendix 4.A.1. First, we define the matrix B by setting, $B_{i,j} = A_{i,j}^{-1}$ for $(i, j) \in I \times L$, and $B_{i,j} = -A_{-2N+1-i, -2N+1-j}^{-1}$ for $(i, j) \in I \times (I \setminus L)$. Since $[A_N]_{i,j} = -[A_N]_{-2N+1-i, -2N+1-j}$, by (4.107) follows that

$$A_N B = \mathbb{1} - C \quad (4.50)$$

for some matrix C with $\|C\| = \max_{i,j} |C_{i,j}| \leq \mathcal{O}(e^{-\mu_2 N})$. Therefore, for N large enough,

$$A_N^{-1} = B(\mathbb{1} + D), \quad D = \sum_{k \geq 1} C^k \quad (4.51)$$

with $\|D\| \leq \mathcal{O}(e^{-\mu_2 N})$ too. Thus, replacing A_N^{-1} with B we introduce an error in the kernel's elements of $\mathcal{O}(N^2 e^{-\mu_2 N})$.

If we replace $B_{i,j}$ with $A_{i,j}^{-1}$ also in $(i, j) \in L \times (I \setminus L)$ we introduce an error of $\mathcal{O}(N^2 e^{-\mu_3 N})$, with $\mu_3 = \min\{\mu_1, \mu_2/2\}$. This is achieved using (4.106) for $i < j + N/2$, and (4.104) otherwise.

The final step is to show, using only the antisymmetry of A_N^{-1} that the contribution of K_{\dots} coming from $(i, j) \in (I \setminus L)^2$ are also exponentially small in N . For $(i, j) \in (I \setminus L)^2$, it is easy to see that, uniformly in $x, y \geq 0$,

$$\begin{aligned} \Phi_{x,i} &= \mathcal{O}(e^{-\mu_1 N}) \\ (S\Phi)_{x,i} &= \mathcal{O}(e^{-\mu_1 N}), \text{ for odd } x, \\ (S\Phi)_{x,i} &= \sinh(\tilde{T}) + \mathcal{O}(e^{-\mu_1 N}), \text{ for even } x \text{ and even } i, \\ (S\Phi)_{x,i} &= \cosh(\tilde{T}) + \mathcal{O}(e^{-\mu_1 N}), \text{ for even } x \text{ and odd } i. \end{aligned} \quad (4.52)$$

Therefore, the contributions for $K_{1,1}$, $K_{1,2}$, and $K_{2,1}$ are $\mathcal{O}(N^2 e^{-\mu_1 N})$ because they contain at least a factor $\mathcal{O}(e^{-\mu_1 N})$ coming from $\Phi_{x,i}$ or $\Phi_{j,y}^t$. For $K_{2,2}$ there are terms without $\mathcal{O}(e^{-\mu_1 N})$, and containing only $\sinh(\tilde{T})$ and/or $\cosh(\tilde{T})$. These terms cancel exactly because A_N^{-1} is antisymmetric. Consequently, we can simply replace $B_{i,j}$ with $A_{i,j}^{-1}$ also in $(i, j) \in (I \setminus L)^2$ up to an error $\mathcal{O}(N^2 e^{-\mu_1 N})$. \square

4.5 Edge scaling and asymptotics of the kernel

In this section we define the edge scaling of the kernel, provide some bounds on them which will be used in the proofs of Section 4.6, and compute their $T \rightarrow \infty$ limit.

The edge scaling of the kernel is defined by

$$\begin{aligned} G_{T;1,1}^{\text{edge}}(\xi_1, \xi_2) &= \tilde{T}^{2/3} G_{1,1}([2\tilde{T} + \xi_1 \tilde{T}^{1/3}], [2\tilde{T} + \xi_2 \tilde{T}^{1/3}]) \\ G_{T;k}^{\text{edge}}(\xi_1, \xi_2) &= \tilde{T}^{1/3} G_k([2\tilde{T} + \xi_1 \tilde{T}^{1/3}], [2\tilde{T} + \xi_2 \tilde{T}^{1/3}]), \quad k = (1, 2), (2, 1) \\ G_{T;2,2}^{\text{edge}}(\xi_1, \xi_2) &= G_{2,2}([2\tilde{T} + \xi_1 \tilde{T}^{1/3}], [2\tilde{T} + \xi_2 \tilde{T}^{1/3}]), \end{aligned} \quad (4.53)$$

and similarly for $R_{T;k}^{\text{edge}}(\xi_1, \xi_2)$.

Next we compute some bounds on the kernel's elements such that, when possible, they are rapidly decreasing for $\xi_1, \xi_2 \gg 1$.

Lemma 4.8. *Write*

$$\Omega_0(x) = \begin{cases} 1, & x \leq 0 \\ \exp(-x/2), & x \geq 0 \end{cases}, \quad \Omega_1(x) = \begin{cases} 1 + |x|, & x \leq 0 \\ \exp(-x/2), & x \geq 0 \end{cases}, \quad (4.54)$$

$$\Omega_2(x) = \begin{cases} (1 + |x|)^2, & x \leq 0 \\ \exp(-x/2), & x \geq 0 \end{cases}. \quad (4.55)$$

Then there is a positive constant C such that for large \tilde{T}

$$\begin{aligned} |R_{T;1,2}^{\text{edge}}(\xi_1, \xi_2)| &\leq C\Omega_0(\xi_1), \\ |R_{T;2,1}^{\text{edge}}(\xi_1, \xi_2)| &\leq C\Omega_0(\xi_2), \\ |R_{T;2,2}^{\text{edge}}(\xi_1, \xi_2)| &\leq C(\Omega_1(\xi_1) + \Omega_1(\xi_2)), \end{aligned} \quad (4.56)$$

and

$$\begin{aligned}
|G_{T;1,1}^{\text{edge}}(\xi_1, \xi_2)| &\leq C\Omega_2(\xi_1)\Omega_2(\xi_2), \\
|G_{T;1,2}^{\text{edge}}(\xi_1, \xi_2)| &\leq C\Omega_1(\xi_1)(1 + \Omega_2(\xi_2)), \\
|G_{T;2,1}^{\text{edge}}(\xi_1, \xi_2)| &\leq C\Omega_1(\xi_2)(1 + \Omega_2(\xi_1)), \\
|G_{T;2,2}^{\text{edge}}(\xi_1, \xi_2)| &\leq C(1 + \Omega_1(\xi_1) + \Omega_1(\xi_2) + \Omega_1(\xi_1)\Omega_1(\xi_2)).
\end{aligned} \tag{4.57}$$

Proof. We use Lemma 4.13 and Lemma 4.14 to obtain the above estimate.

- 1) The bounds on $|R_{T;1,2}^{\text{edge}}(\xi_1, \xi_2)|$ and $|R_{T;2,1}^{\text{edge}}(\xi_1, \xi_2)|$ are implied by Lemma 4.13.
- 2) Bound on $|R_{T;2,2}^{\text{edge}}(\xi_1, \xi_2)|$.

$$|R_{T;2,2}^{\text{edge}}(\xi_1, \xi_2)| \leq \frac{5}{4} + \frac{1}{2} \sum_{M \in \mathbb{N}/\tilde{T}^{1/3}} |J_{[2\tilde{T}+(2M+\xi_2)\tilde{T}^{1/3]}(2\tilde{T})| + (\xi_1 \leftrightarrow \xi_2) \tag{4.58}$$

and

$$\sum_{M \in \mathbb{N}/\tilde{T}^{1/3}} |J_{[2\tilde{T}+(2M+\xi_2)\tilde{T}^{1/3]}(2\tilde{T})| \leq \sum_{M \in \mathbb{N}/\tilde{T}^{1/3}} |J_{[2\tilde{T}+(M+\xi_2)\tilde{T}^{1/3]}(2\tilde{T})|. \tag{4.59}$$

For $\xi_2 \leq 0$,

$$(4.59) \leq \sum_{M \in (\xi_2 + \mathbb{N}/\tilde{T}^{1/3}) \cap [\xi_2, 0]} |J_{[2\tilde{T}+M\tilde{T}^{1/3]}(2\tilde{T})| + \sum_{M \in \mathbb{N}/\tilde{T}^{1/3}} |J_{[2\tilde{T}+M\tilde{T}^{1/3]}(2\tilde{T})|. \tag{4.60}$$

By (4.108) the first term is bounded by a constant times $(1 + |\xi_2|)$ and by (4.109) the second term by a constant. For $\xi_2 \geq 0$,

$$(4.59) \leq \sum_{M \in \xi_2 + \mathbb{N}/\tilde{T}^{1/3}} |J_{[2\tilde{T}+M\tilde{T}^{1/3]}(2\tilde{T})| \tag{4.61}$$

which, by (4.109), is bounded by a constant times $\exp(-\xi_2/2)$. Therefore

$$\sum_{M \in \mathbb{N}/\tilde{T}^{1/3}} |J_{[2\tilde{T}+(M+\xi_2)\tilde{T}^{1/3]}(2\tilde{T})| \leq C\Omega_1(\xi_2). \tag{4.62}$$

for a constant C , from which follows the desired bound.

- 3) Bound on $|G_{T;1,1}^{\text{edge}}(\xi_1, \xi_2)|$. Let us define $\tilde{J}_n(t) = J_{n+1}(t) - J_n(t)$. Then

$$\begin{aligned}
G_{T;1,1}^{\text{edge}}(\xi_1, \xi_2) &= \tilde{T}^{2/3} \sum_{M \in \mathbb{N}/\tilde{T}^{1/3}} J_{[2\tilde{T}+(\xi_1+M)\tilde{T}^{1/3]}(2\tilde{T}) \tilde{J}_{[2\tilde{T}+(\xi_2+M)\tilde{T}^{1/3]}(2\tilde{T}) \\
&\quad - (\xi_1 \leftrightarrow \xi_2).
\end{aligned} \tag{4.63}$$

For large \tilde{T} , the sums are very close integrals and this time we use both Lemma 4.13 and Lemma 4.14, obtaining

$$\begin{aligned} |G_{T;1,1}^{\text{edge}}(\xi_1, \xi_2)| &\leq C \int_0^\infty dM \Omega_0(M + \xi_1) \Omega_1(M + \xi_2) \\ &\leq C \int_0^\infty dM \Omega_1(M + \xi_1) \Omega_1(M + \xi_2) \end{aligned} \quad (4.64)$$

for a constant $C > 0$. It is then easy to see that r.h.s. of (4.64) is bounded as follows: for $\xi_1 \leq \xi_2 \leq 0$ by $C(1 + |\xi_1|)^2$, for $\xi_1 \leq 0 \leq \xi_2$ by $C(1 + |\xi_1|)^2 \exp(-\xi_2/2)$, and for $0 \leq \xi_1 \leq \xi_2$ by $C \exp(-\xi_1/2) \exp(-\xi_2/2)$, for some other constant $C > 0$. Therefore $|G_{T;1,1}^{\text{edge}}(\xi_1, \xi_2)| \leq C \Omega_2(\xi_1) \Omega_2(\xi_2)$.

4) Bound on $|G_{T;1,2}^{\text{edge}}(\xi_1, \xi_2)|$.

$$\begin{aligned} G_{T;1,2}^{\text{edge}}(\xi_1, \xi_2) &= \sum_{M \in \mathbb{N}/\tilde{T}^{1/3}} J_{[2\tilde{T}+(\xi_1+M)\tilde{T}^{1/3}]}(2\tilde{T}) (\tilde{T}^{1/3} J_{[2\tilde{T}+(\xi_2+M)\tilde{T}^{1/3}]}(2\tilde{T})) \\ &\quad - \tilde{T}^{1/3} J_{[2\tilde{T}+(\xi_1+M)\tilde{T}^{1/3+1}]}(2\tilde{T}) \left(\sum_{M \in \mathbb{N}/\tilde{T}^{1/3}} J_{[2\tilde{T}+(\xi_1+2M)\tilde{T}^{1/3-1}]}(2\tilde{T}) - \frac{1}{2} \right). \end{aligned}$$

In the first sum, the term with ξ_2 is bounded by a constant and remaining sum was already estimated in (4.62). The second term is bounded by a constant times $\Omega_0(\xi_1) \Omega_2(\xi_2)$. Using $\Omega_0(\xi_1) \leq \Omega_1(\xi_1)$ we conclude that $|G_{T;1,2}^{\text{edge}}(\xi_1, \xi_2)| \leq C \Omega_1(\xi_1) (1 + \Omega_2(\xi_2))$.

5) Bound on $|G_{T;2,1}^{\text{edge}}(\xi_1, \xi_2)|$. The bound is the same as for $|G_{T;1,2}^{\text{edge}}(\xi_1, \xi_2)|$.

6) Bound on $|G_{T;2,2}^{\text{edge}}(\xi_1, \xi_2)|$. The terms with the double sums are estimated applying twice (4.62) and are then bounded by $\Omega_1(\xi_1) \Omega_1(\xi_2)$. The two terms with only one sum are bounded by $\Omega_1(\xi_1)$ and $\Omega_1(\xi_2)$ respectively, and the signum function by $1/4$. Therefore, for some constant $C > 0$, $|G_{T;2,2}^{\text{edge}}(\xi_1, \xi_2)| \leq C(1 + \Omega_1(\xi_1) + \Omega_1(\xi_2) + \Omega_1(\xi_1) \Omega_1(\xi_2))$. \square

Finally we compute the pointwise limits of the G 's since they remains in the weak convergence.

Lemma 4.9. For any fixed ξ_1, ξ_2 ,

$$\lim_{\tilde{T} \rightarrow \infty} G_{T;k}^{\text{edge}}(\xi_1, \xi_2) = G_k^{\text{GOE}}(\xi_1, \xi_2), \quad (4.65)$$

where the G_k^{GOE} 's are the ones in (3.61).

Proof. Let us consider ξ_1, ξ_2 fixed. In the proof of Lemmas 4.8, we have already obtained uniform bounds in T for $G_{T;k}^{\text{edge}}(\xi_1, \xi_2)$, so that dominated convergence applies. To obtain the limits we use (4.133), i.e.,

$$\lim_{T \rightarrow \infty} T^{1/3} J_{[2T+\xi T^{1/3}]}(2T) = \text{Ai}(\xi), \quad (4.66)$$

and

$$\lim_{T \rightarrow \infty} T^{2/3} (J_{[2T+\xi T^{1/3+1}]}(2T) - J_{[2T+\xi T^{1/3}]}(2T)) = \text{Ai}'(\xi). \quad (4.67)$$

The limit of $G_{T;1,1}^{\text{edge}}(\xi_1, \xi_2)$ follows from (4.63).

The limit of $G_{T;1,2}^{\text{edge}}(\xi_1, \xi_2)$ leads to

$$\int_0^\infty d\lambda \text{Ai}(\xi_1 + \lambda) \text{Ai}(\xi_2 + \lambda) - \frac{1}{2} \text{Ai}(\xi_1) \left(\int_0^\infty d\lambda \text{Ai}(\xi_2 + \lambda) - 1 \right) \quad (4.68)$$

which equals $G_{1,2}^{\text{GOE}}$ since $\int_0^\infty d\lambda \text{Ai}(\xi_2 + \lambda) - 1 = -\int_0^\infty d\lambda \text{Ai}(\xi_2 - \lambda)$.

The limit of $G_{T;2,1}^{\text{edge}}(\xi_1, \xi_2)$ is obtained identically.

Finally, the limit of $G_{T;2,2}^{\text{edge}}(\xi_1, \xi_2)$ is given by

$$\begin{aligned} & \frac{1}{4} \int_0^\infty d\lambda \int_\lambda^\infty d\mu \text{Ai}(\xi_1 + \lambda) \text{Ai}(\xi_2 + \mu) - (\xi_1 \leftrightarrow \xi_2) \\ & - \frac{1}{4} \int_0^\infty d\lambda \text{Ai}(\xi_1 + \lambda) + \frac{1}{4} \int_0^\infty d\mu \text{Ai}(\xi_2 + \mu) - \frac{1}{4} \text{sgn}(\xi_1 - \xi_2), \end{aligned} \quad (4.69)$$

which can be written in a more compact form. Since $\int_{\mathbb{R}} d\lambda \text{Ai}(\lambda) = 1$,

$$\int_0^\infty d\lambda \text{Ai}(\xi_1 + \lambda) = \int_0^\infty d\lambda \int_{-\infty}^\infty d\mu \text{Ai}(\xi_1 + \lambda) \text{Ai}(\xi_2 + \mu), \quad (4.70)$$

and the signum can be expressed as an integral of $\text{Ai}(\xi_1 + \lambda) \text{Ai}(\xi_2 + \mu)$

$$- \text{sgn}(\xi_1 - \xi_2) = \int_{\mathbb{R}} d\lambda \int_{\mathbb{R}} d\mu \text{Ai}(\xi_1 + \lambda) \text{Ai}(\xi_2 + \mu) \text{sgn}(\lambda - \mu). \quad (4.71)$$

In fact

$$\text{r.h.s. of (4.71)} = \int_{\mathbb{R}} d\lambda \int_{\mathbb{R}} d\mu \text{Ai}(\lambda) \text{Ai}(\mu) \text{sgn}(\lambda - \mu + \zeta) = b(\zeta) \quad (4.72)$$

with $\zeta = \xi_2 - \xi_1$. For $\zeta = 0$ it is zero by symmetry. Then consider $\zeta > 0$, the case $\zeta < 0$ follows by symmetry. By completeness of the Airy functions,

$$\frac{db(\zeta)}{d\zeta} = \int_{\mathbb{R}} d\mu \text{Ai}(\mu) \text{Ai}(\mu - \zeta) = \delta(\zeta). \quad (4.73)$$

Then using (4.70) and (4.71) we obtain the result. \square

Remark that the GOE kernel in [40] differs slightly from the one written here, but they are equivalent in the sense that they give the same correlation functions.

For the residual terms the limit does not exist, but exists in the even/odd positions. In particular

$$\lim_{T \rightarrow \infty} \sum_{m \geq 1} J_{[2\tilde{T}+\xi\tilde{T}^{1/3+2m}]}(2\tilde{T}) = \frac{1}{2} \int_0^\infty d\lambda \text{Ai}(\xi + \lambda). \quad (4.74)$$

4.6 Proof of Theorem 4.1

In this section we first prove the weak convergence of the edge rescaled point process of η_T^{sym} to η^{GOE} in the $T \rightarrow \infty$ limit. Secondly, using the equivalence of the point process ζ_T^{sym} and ζ_T^{flat} , we prove Theorem 4.1.

Theorem 4.10. *Let us define the rescaled point process*

$$\eta_{\tilde{T}}^{\text{sym}}(f) = \sum_{x \in \mathbb{Z}} f((x - 2\tilde{T})/\tilde{T}^{1/3}) \zeta_{\tilde{T}}^{\text{sym}}(x) \quad (4.75)$$

with $\tilde{T} = \sqrt{2\varrho}T = 2T$ and f a smooth test function of compact support. In the limit $T \rightarrow \infty$ it converges weakly to the GOE point process, i.e., for all $m \in \mathbb{N}$, and f_1, \dots, f_m smooth test functions of compact support,

$$\lim_{T \rightarrow \infty} \mathbb{E}_T \left(\prod_{k=1}^m \eta_T^{\text{sym}}(f_k) \right) = \mathbb{E} \left(\prod_{k=1}^m \eta^{\text{GOE}}(f_k) \right) \quad (4.76)$$

where the GOE kernel is given in 3.61.

Proof. Let f_1, \dots, f_m be smooth test functions of compact support and $\hat{f}_i(x) = f_i((x - 2\tilde{T})/\tilde{T}^{1/3})$, then

$$\begin{aligned} \mathbb{E}_T \left(\prod_{k=1}^m \eta_T^{\text{sym}}(f_k) \right) &= \sum_{x_1, \dots, x_m \in \mathbb{Z}} \hat{f}_1(x_1) \dots \hat{f}_m(x_m) \text{Pf}[K(x_i, x_j)]_{i,j=1, \dots, m} \\ &= \sum_{x_1, \dots, x_m \in \mathbb{Z}} \hat{f}_1(x_1) \dots \hat{f}_m(x_m) \text{Pf}[(X K X^t)(x_i, x_j)]_{i,j=1, \dots, m} / \text{Det}[X]^m \\ &= \frac{1}{\tilde{T}^{m/3}} \sum_{x_1, \dots, x_m \in \mathbb{Z}} \hat{f}_1(x_1) \dots \hat{f}_m(x_m) \text{Pf}[L(x_i, x_j)]_{i,j=1, \dots, m} \end{aligned} \quad (4.77)$$

where $X = \begin{pmatrix} \tilde{T}^{1/3} & 0 \\ 0 & 1 \end{pmatrix}$ and $L(x, y) = (X K X^t)(x, y)$, i.e., $L_{1,1}(x, y) = \tilde{T}^{2/3} K_{1,1}(x, y)$, $L_k(x, y) = \tilde{T}^{1/3} K_k(x, y)$, for $k = (1, 2), (2, 1)$, and $L_{2,2}(x, y) = K_{2,2}(x, y)$. Moreover, we define the edge scaling for the kernel elements as

$$L_{T;k}^{\text{edge}}(\xi_1, \xi_2) = L_k([2\tilde{T} + \xi_1 \tilde{T}^{1/3}], [2\tilde{T} + \xi_2 \tilde{T}^{1/3}]). \quad (4.78)$$

In what follows we denote by $\xi_i = (x_i - 2\tilde{T})/\tilde{T}^{1/3}$. To simplify the notations we consider $\tilde{T} \in \mathbb{N}$, but the same proof can be carried out without this condition, replacing for example $\mathbb{Z}/\tilde{T}^{1/3}$ by $(\mathbb{Z} - 2\tilde{T})/\tilde{T}^{1/3}$ in (4.79). Then

$$\mathbb{E}_T \left(\prod_{k=1}^m \eta_T^{\text{sym}}(f_k) \right) = \frac{1}{\tilde{T}^{m/3}} \sum_{\xi_1, \dots, \xi_m \in \mathbb{Z}/\tilde{T}^{1/3}} f_1(\xi_1) \dots f_m(\xi_m) \text{Pf}[L_T^{\text{edge}}(\xi_i, \xi_j)]_{i,j=1, \dots, m}. \quad (4.79)$$

Let us denote $\xi_i^I = [\xi_i \tilde{T}^{1/3}] / \tilde{T}^{1/3}$ the ‘‘integer’’ discretization of ξ_i . Then

$$\mathbb{E}_T \left(\prod_{k=1}^m \eta_T^{\text{sym}}(f_k) \right) = \int_{\mathbb{R}^m} d\xi_1 \cdots d\xi_m f_1(\xi_1^I) \cdots f_m(\xi_m^I) \text{Pf}[L_T^{\text{edge}}(\xi_i^I, \xi_j^I)]_{i,j=1,\dots,m}. \quad (4.80)$$

Using the definition in (4.53) we have

$$L_{T;k}^{\text{edge}}(\xi_1, \xi_2) = G_{T;k}^{\text{edge}}(\xi_1, \xi_2) + R_{T;k}^{\text{edge}}(\xi_1, \xi_2), \quad (4.81)$$

therefore (4.80) consists in one term with only $G_{T;k}^{\text{edge}}$ plus other terms which contain at least one $R_{T;k}^{\text{edge}}$.

First consider the contribution where only $G_{T;k}^{\text{edge}}$ occur. Let $M_f > 0$ be the smallest number such that $f_j(x) = 0$ if $|x| \geq M_f$, for all $j = 1, \dots, m$. We bound the product of the f_i 's by

$$|f_1(\xi_1^I) \cdots f_m(\xi_m^I)| \leq \prod_{j=1}^m \|f_j\|_{\infty} \mathbb{1}_{[-M_f, M_f]}(\xi_j) \quad (4.82)$$

and, in the same way as in Lemma 4.12 but with $K_{T;k}^{\text{edge}}$ replaced by $G_{T;k}^{\text{edge}}$, we conclude that this is uniformly integrable in T . We then apply dominated convergence and take the limit inside the integral obtaining

$$\begin{aligned} & \lim_{T \rightarrow \infty} \int_{\mathbb{R}^m} d\xi_1 \cdots d\xi_m f_1(\xi_1^I) \cdots f_m(\xi_m^I) \text{Pf}[G_T^{\text{edge}}(\xi_i^I, \xi_j^I)]_{i,j=1,\dots,m} \\ &= \int_{\mathbb{R}^m} d\xi_1 \cdots d\xi_m f_1(\xi_1) \cdots f_m(\xi_m) \text{Pf}[G^{\text{GOE}}(\xi_i, \xi_j)]_{i,j=1,\dots,m}. \end{aligned} \quad (4.83)$$

Next we have to show that whenever some $R_{T;k}^{\text{edge}}$ are present their contribution vanish in the limit $T \rightarrow \infty$. In (4.80) we have to compute the Pfaffian of E_T defined by

$$E_T(n, l) = \begin{cases} L_{T;1,1}^{\text{edge}}((n+1)/2, (l+1)/2), & n \text{ odd}, l \text{ odd}, \\ L_{T;1,2}^{\text{edge}}((n+1)/2, l/2), & n \text{ odd}, l \text{ even}, \\ L_{T;2,1}^{\text{edge}}(n/2, (l+1)/2), & n \text{ even}, l \text{ odd}, \\ L_{T;2,2}^{\text{edge}}(n/2, l/2), & n \text{ even}, l \text{ even}, \end{cases} \quad (4.84)$$

for $1 \leq n < l \leq 2m$, with $L_{T;k}^{\text{edge}}(a, b) \equiv L_{T;k}^{\text{edge}}(\xi_a, \xi_b)$. The Pfaffian of E_T is given by

$$\text{Pf}(E_T) = \sum_{\substack{\sigma \in S_{2m} \\ \sigma_{2i-1} < \sigma_{2i}}} (-1)^{|\sigma|} E_T(\sigma_1, \sigma_2) \cdots E_T(\sigma_{2m-1}, \sigma_{2m}). \quad (4.85)$$

Now we have to check that the product of residual terms does not contain twice the term $(-1)^x$ for the same x . This is implied by Lemma 4.11.

Let us decompose the sum in (4.79) into 2^m sums, depending on whether $\xi_i \tilde{T}^{1/3}$ is even or odd. Denote $\xi_i^e = [\xi_i \tilde{T}^{1/3}/2]2/\tilde{T}^{1/3}$ and $\xi_i^o = ([\xi_i \tilde{T}^{1/3}/2]2 + 1)/\tilde{T}^{1/3}$ the “even” and “odd” discretizations of ξ_i . Then

$$(4.79) = \frac{1}{2^m} \sum_{\substack{s_i=\{o,e\}, \\ i=1,\dots,m}} \int_{\mathbb{R}^m} d\xi_1 \cdots d\xi_m f_1(\xi_1^{s_1}) \cdots f_m(\xi_m^{s_m}) \text{Pf}[L_T^{\text{edge}}(\xi_i^{s_i}, \xi_j^{s_j})]_{i,j=1,\dots,m}. \quad (4.86)$$

With this subdivision, each term in the Pfaffian converges pointwise to a well defined limit. Moreover all the 2^m integrals, including $G_{T;k}^{\text{edge}}$'s and/or $R_{T;k}^{\text{edge}}$'s, are uniformly bounded in T . By dominated convergence we can take the limit inside the integrals.

Each time that there is a $R_{T;1,2}^{\text{edge}}(\xi_i, \xi_j)$, or $R_{T;2,1}^{\text{edge}}(\xi_j, \xi_i)$, the integral with $s_i = o$ and the one with $s_i = e$ only differs by sign, therefore they cancel each other. Each time that appears $R_{T;2,2}^{\text{edge}}(\xi_i, \xi_j)$, the part including coming from the $(-1)^{x_i}$ and the one with $(-1)^{x_j}$ simplifies in the same way. Finally we consider the second part, the one including the S and signum function. The sum of $s_i = \{o, e\}$ and $s_j = \{o, e\}$ of the terms with $-S(\xi_i \tilde{T}^{-1/3}, \xi_j \tilde{T}^{-1/3})$ equals minus the ones with $\frac{1}{4} \text{sgn}((\xi_i - \xi_j) \tilde{T}^{-1/3})$. Consequently all the terms including at least one time $R_{T;i}^{\text{edge}}$ have a contribution which vanishes in the $T \rightarrow \infty$ limit. \square

Lemma 4.11. *The following products do not appear in (4.85):*

$$\begin{aligned} (a) & L_{T;2,2}^{\text{edge}}(x_i, x_j) L_{T;1,2}^{\text{edge}}(x_k, x_i), & (b) & L_{T;2,2}^{\text{edge}}(x_i, x_j) L_{T;1,2}^{\text{edge}}(x_k, x_j), \\ (c) & L_{T;2,2}^{\text{edge}}(x_i, x_j) L_{T;2,1}^{\text{edge}}(x_i, x_k), & (d) & L_{T;2,2}^{\text{edge}}(x_i, x_j) L_{T;2,1}^{\text{edge}}(x_j, x_k) \\ (e) & L_{T;1,2}^{\text{edge}}(x_i, x_j) L_{T;2,1}^{\text{edge}}(x_j, x_k). \end{aligned} \quad (4.87)$$

Proof. We prove it by reductio ab absurdum. We assume that the product appear and we obtain a contradiction. (a) appears if there exist some $a < b$ and $c < d$ with a, b, d even and c odd, all different, such that $i = a/2, j = b/2, k = (c+1)/2, i = d/2$. But this is not possible since $d \neq a$. (b) appears if there exist some $a < b$ and $c < d$ with a, b, d even and c odd, all different, such that $i = a/2, j = b/2, k = (c+1)/2, j = d/2$. But this is not possible since $d \neq b$. (c) appears if there exist some $a < b$ and $c < d$ with a, b, c even and d odd, all different, such that $i = a/2, j = b/2, i = c/2, k = (d+1)/2$. But this is not possible since $c \neq a$. (d) appears if there exist some $a < b$ and $c < d$ with a, b, c even and d odd, all different, such that $i = a/2, j = b/2, j = c/2, k = (d+1)/2$. But this is not possible since $c \neq b$. (e) appears if there exist some $a < b$ and $c < d$ with b, c even and a, d odd, all different, such that $i = (a+1)/2, j = b/2, j = c/2, k = (d+1)/2$. But this is not possible since $c \neq b$. \square

Lemma 4.12. *There exists a constant $C > 0$ such that*

$$\mathbb{E}_T \left(|\eta_T^{\text{sym}}(\mathbb{1}_{[-M, \infty)})|^m \right) \leq C^m e^{Mm/2} (m)^{m/2} \quad (4.88)$$

uniformly in T .

Proof. The m -point correlation function $\rho^{(m)}(\xi_1, \dots, \xi_m)$ is a sum of product of $K_{T;k}^{\text{edge}}$'s which contains twice every ξ_i 's, $i = 1, \dots, m$, and only in $K_{T;k}^{\text{edge}}$ the two argument can be the same. From Lemma 4.8, for any $\xi_1, \xi_2 \in \mathbb{R}$,

$$\begin{aligned} |K_{T;1,1}^{\text{edge}}(\xi_1, \xi_2)| &\leq C \exp(-\xi_1/2) \exp(-\xi_2/2) \\ |K_{T;1,2}^{\text{edge}}(\xi_1, \xi_2)| &\leq C \exp(-\xi_1/2) \\ |K_{T;2,1}^{\text{edge}}(\xi_1, \xi_2)| &\leq C \exp(-\xi_2/2) \\ |K_{T;2,2}^{\text{edge}}(\xi_1, \xi_2)| &\leq C. \end{aligned} \quad (4.89)$$

For negative ξ we could replace $\exp(-\xi/2)$ by $(1 + |\xi|)^2$ where appears, but for our purpose this is not needed.

All the products in $\rho^{(m)}(\xi_1, \dots, \xi_m)$ contain at least one $\exp(-\xi_i/2)$ for each i . In fact, this holds if: $K_{T;2,2}^{\text{edge}}(\xi_1, \xi_2)$ is not multiplied by $K_{T;1,2}^{\text{edge}}(\xi_3, \xi_2)$, $K_{T;1,2}^{\text{edge}}(\xi_3, \xi_1)$, $K_{T;2,1}^{\text{edge}}(\xi_1, \xi_3)$, $K_{T;2,1}^{\text{edge}}(\xi_2, \xi_3)$, and if $K_{T;1,2}^{\text{edge}}(\xi_1, \xi_2)$ is not multiplied by $K_{T;2,1}^{\text{edge}}(\xi_2, \xi_3)$. This is already proven in Lemma 4.11.

Consequently,

$$\begin{aligned} \mathbb{E}_T \left(|\eta_T^{\text{sym}}(\mathbb{1}_{[-M, \infty)})|^m \right) &= \int_{[-M, \infty)^m} d\xi_1 \dots d\xi_m \rho_T^{(m)}(\xi_1, \dots, \xi_m) \\ &\leq (2m)^{m/2} \left(\int_{[-M, \infty)} C \exp(-\xi/2) d\xi \right)^m = 2^m C^m e^{Mm/2} (2m)^{m/2} \end{aligned} \quad (4.90)$$

uniformly in T . The term $(2m)^{m/2}$ comes from the fact that the absolute value of a determinant of a $n \times n$ matrix with entries of absolute value not exceeding 1 is bounded by $n^{n/2}$ (Hadamard bound). Finally resetting the constant as $C2\sqrt{2}$ the lemma is proved. \square

To prove Theorem 4.1 we use Theorem 4.10, Proposition 4.3, and Lemma 4.12.

Proof of Theorem 4.1. Let us denote by x_j , $j \leq 0$, the position of the j^{th} element of ζ_T^{flat} and x_j^{sym} , $j \leq 0$, the position of the j^{th} element of ζ_T^{sym} . Then define $\xi_{j,T}$ and $\xi_{j,T}^{\text{sym}}$ by

$$x_j = 2T + \xi_{j,T} T^{1/3} 2^{-2/3}, \quad x_j^{\text{sym}} = 4T + \xi_{j,T}^{\text{sym}} (2T)^{1/3}. \quad (4.91)$$

By Proposition 4.3, $x_j - j = \frac{1}{2}(x_j^{\text{sym}} - j)$, which implies

$$\xi_{j,T} = \xi_{j,T}^{\text{sym}} + \frac{j}{(2T)^{1/3}}. \quad (4.92)$$

Let f_1, \dots, f_m be test functions of compact support and denote by $M_f > 0$ the minimal value such that $f_j(x) = 0$ if $|x| \geq M_f$, $j = 1, \dots, m$. Then

$$\begin{aligned} \mathbb{E}_T \left(\prod_{k=1}^m \eta_T^{\text{flat}}(f_k) \right) &= \mathbb{E}_T \left(\prod_{k=1}^m \sum_{i \leq 0} f_k(\xi_{i,T}^{\text{sym}} + i/(2T)^{1/3}) \right) \\ &= \mathbb{E}_T \left(\sum_{i_1, \dots, i_m \leq 0} \prod_{k=1}^m f_k(\xi_{i_k, T}^{\text{sym}} + i_k/(2T)^{1/3}) \right). \end{aligned} \quad (4.93)$$

We bound the f_k 's by their supremum times $\mathbb{1}_{[-M_f, M_f]}$ as in (4.82), then

$$|\text{r.h.s. of (4.93)}| \leq \mathbb{E}_T \left(\prod_{j=1}^m \sum_{i \leq 0} \mathbb{1}_{[-M_f, M_f]}(\xi_{i,T}^{\text{sym}} + i/(2T)^{1/3}) \right) \prod_{j=1}^m \|f_j\|_\infty, \quad (4.94)$$

and, since $\mathbb{1}_{[-M_f, M_f]}(\xi_{i,T}^{\text{sym}} + i/(2T)^{1/3}) \leq \mathbb{1}_{[-M_f, \infty)}(\xi_{i,T}^{\text{sym}} + i/(2T)^{1/3}) \leq \mathbb{1}_{[-M_f, \infty)}(\xi_{i,T}^{\text{sym}})$, it follows that

$$|\text{r.h.s. of (4.93)}| \leq \mathbb{E}_T \left(\prod_{j=1}^m \eta_T^{\text{sym}}(\mathbb{1}_{[-M_f, \infty)}) \right) \prod_{j=1}^m \|f_j\|_\infty \quad (4.95)$$

which is uniformly bounded in T from Lemma 4.12. Therefore by Fubini's theorem,

$$\mathbb{E}_T \left(\prod_{k=1}^m \eta_T^{\text{flat}}(f_k) \right) = \sum_{i_1, \dots, i_m \leq 0} \mathbb{E}_T \left(\prod_{k=1}^m f_k(\xi_{i_k, T}^{\text{sym}} + i_k/(2T)^{1/3}) \right). \quad (4.96)$$

Moreover, $f_k(\xi_{i_k, T}^{\text{sym}} + i_k/(2T)^{1/3}) = f_k(\xi_{i_k, T}^{\text{sym}}) + f'_k(\tilde{\xi}_{i_k, T})i_k/(2T)^{1/3}$ for some $\tilde{\xi}_{i_k, T} \in [\xi_{i_k, T}^{\text{sym}} + i_k/(2T)^{1/3}, \xi_{i_k, T}^{\text{sym}}]$. Therefore (4.96) equals

$$\sum_{i_1, \dots, i_m \leq 0} \mathbb{E}_T \left(\prod_{k=1}^m f_k(\xi_{i_k, T}^{\text{sym}}) \right) = \mathbb{E}_T \left(\prod_{k=1}^m \eta_T^{\text{sym}}(f_k) \right) \quad (4.97)$$

plus $2^m - 1$ terms which contains some $f'_k(\tilde{\xi}_{i_k, T})i_k/(2T)^{1/3}$. Finally we have to show that these terms vanish as $T \rightarrow \infty$. First we bound the f_k 's and the f'_k 's by $\|f_k\|_\infty$ and $\|f'_k\|_\infty$ times $\mathbb{1}_{[-M_f, M_f]}$. Therefore each of the $2^m - 1$ terms is bounded by a

$$\frac{1}{T^{|J|/3}} \prod_{k \in I} \|f_k\|_\infty \prod_{k \in J} \|f'_k\|_\infty \sum_{i_1, \dots, i_m \leq 0} \prod_{k \in J} |i_k| \mathbb{E}_T \left(\prod_{k=1}^m \mathbb{1}_{[-M_f, \infty)}(\xi_{i_k, T}^{\text{sym}}) \right) \quad (4.98)$$

where I and J are subset of $\{1, \dots, m\}$ with $I \cup J = \{1, \dots, m\}$ and J is non-empty. Let $j_0 = \min\{i_1, \dots, i_m\}$, then

$$\begin{aligned} & \mathbb{E}_T \left(\prod_{k=1}^m \mathbb{1}_{[-M_f, \infty)}(\xi_{i_k, T}^{\text{sym}}) \right) = \mathbb{E}_T \left(\mathbb{1}_{[-M_f, \infty)}(\xi_{j_0, T}^{\text{sym}}) \right) \\ & = \mathbb{P}_T \left(\xi_{j_0, T}^{\text{sym}} \geq -M_f \right) \leq \mathbb{P}_T \left(\eta_T^{\text{sym}}(\mathbb{1}_{[-M_f, \infty)}) \geq j_0 \right) \\ & \leq \frac{\mathbb{E}_T \left(|\eta_T^{\text{sym}}(\mathbb{1}_{[-M_f, \infty)})|^{3m} \right)}{|j_0|^{3m}} \leq \frac{\mathcal{O}(C^{3m} e^{M_f 3m/2} (3m)^{3m/2})}{\prod_{k=1}^m |i_k|^3}, \end{aligned} \quad (4.99)$$

since $|j_0| \geq |i_k|$ for all $k = 1, \dots, m$. From (4.99) it follows that (4.98) is uniformly bounded in T and vanishes as $T \rightarrow \infty$. We have then proved that, for all f_1, \dots, f_m smooth test functions of compact support,

$$\lim_{T \rightarrow \infty} \mathbb{E}_T \left(\prod_{k=1}^m \eta_T^{\text{flat}}(f_k) \right) = \lim_{T \rightarrow \infty} \mathbb{E}_T \left(\prod_{k=1}^m \eta_T^{\text{sym}}(f_k) \right) = \mathbb{E} \left(\prod_{k=1}^m \eta^{\text{GOE}}(f_k) \right), \quad (4.100)$$

the last equality being Theorem 4.10.

4.A Appendices

4.A.1 Bounds on the inverse of A

Let us denote the finite matrix A by A_N and its inverse by A_N^{-1} . For the $N = \infty$ case we use the notations A and A^{-1} . Let us denote $I = \{-2N + 1, \dots, 0\}$ and $L = \{-N + 1, \dots, 0\}$. Using (4.36) we have

$$|A_{i,j}| \leq 1 + \frac{1}{2} \sum_{k \geq i} \sum_{l \geq j} \frac{\tilde{T}^{k-i}}{(k-i)!} \frac{\tilde{T}^{l-j}}{(l-j)!} = 1 + \frac{1}{2} e^{2\tilde{T}}. \quad (4.101)$$

To obtain some properties of A^{-1} , we first estimate $[e^{-\tilde{T}\alpha_{-1}} P_- e^{-\tilde{T}\alpha_1}]_{i,j}$.

$$\begin{aligned} [e^{-\tilde{T}\alpha_{-1}} P_- e^{-\tilde{T}\alpha_1}]_{i,j} &= \sum_{\max\{i,j\} \leq k \leq 0} \frac{(-\tilde{T})^{k-i}}{(k-i)!} \frac{(-\tilde{T})^{k-j}}{(k-j)!} \\ &= \sum_{l \geq 0} \frac{\tilde{T}^{2l} (-\tilde{T})^{|i-j|}}{l!(l+|i-j|)!} - \sum_{l > -\max\{i,j\}} \frac{\tilde{T}^{2l} (-\tilde{T})^{|i-j|}}{l!(l+|i-j|)!} \\ &= (-1)^{|i-j|} I_{|i-j|}(2\tilde{T}) - \sum_{l > -\max\{i,j\}} \frac{\tilde{T}^{2l} (-\tilde{T})^{|i-j|}}{l!(l+|i-j|)!}, \end{aligned} \quad (4.102)$$

where I_k is the modified Bessel function I of order k . From (4.102) and $(l+|i-j|)! \geq l!|i-j|!$ follows

$$|[e^{-\tilde{T}\alpha_{-1}} P_- e^{-\tilde{T}\alpha_1}]_{i,j}| \leq I_0(2\tilde{T}) \frac{\tilde{T}^{|i-j|}}{|i-j|!} \leq \frac{\tilde{T}^{|i-j|}}{|i-j|!} e^{2\tilde{T}}, \quad (4.103)$$

which implies

$$|A_{i,j}^{-1}| \leq 2 \frac{\tilde{T}^{|i-j|}}{|i-j|!} e^{2\tilde{T}} \leq c_1(\tilde{T}) e^{-\mu_2(\tilde{T})|i-j|}, \quad (4.104)$$

for some constants $c_1, \mu_2 > 0$.

The remainder sum in (4.102) is exponentially small in $-\max\{i, j\}$. In fact, for $n = -\max\{i, j\}$,

$$\begin{aligned} & |[e^{-\tilde{T}\alpha_{-1}} P_- e^{-\tilde{T}\alpha_1}]_{i,j} - (-1)^{|i-j|} I_{|i-j|}(2\tilde{T})| \\ & \leq \frac{\tilde{T}^{|i-j|}}{|i-j|!} \sum_{l > n} \frac{\tilde{T}^{2l}}{(l!)^2} \leq \frac{\tilde{T}^{|i-j|}}{|i-j|!} I_0(2\tilde{T}) e^{-\mu_1(\tilde{T})n} \end{aligned} \quad (4.105)$$

for some constant $\mu_1 > 0$. Thus, for all (i, j) such that $\max\{i, j\} \leq -N/2$,

$$|A_{i,j}^{-1} - \lim_{m \rightarrow \infty} A_{i-m, j-m}^{-1}| \leq c_2(\tilde{T}) e^{-\mu_1 N/2} \quad (4.106)$$

for some constant $c_2 > 0$, that is, in this region A^{-1} is exponentially close to a Toeplitz matrix.

For $j \in L$, using (4.101) and (4.104), we obtain

$$|[A_N A^{-1} - \mathbb{1}]_{i,j}| = \sum_{l \leq -2N} A_{i,l} A_{l,j}^{-1} \leq c_3(\tilde{T}) e^{-\mu_2 N} \quad (4.107)$$

with $c_3 > 0$ a constant.

4.A.2 Some bounds and relation on Bessel functions

Lemma 4.13. *For $N \geq 0$,*

$$|T^{1/3} J_{[2T+NT^{1/3}]}(2T)| \leq \exp(-N/2) \mathcal{O}(1) \quad (4.108)$$

uniformly in $T \geq T_0$ for some constant T_0 .

For $N \leq 0$ it follows from a result of Landau [57], see (4.134), that

$$|T^{1/3} J_{[2T+NT^{1/3}]}(2T)| \leq C \quad (4.109)$$

uniformly in T for a constant $C > 0$.

Proof. To obtain the bound we use 9.3.35 of [1], i.e., for $z \in [0, 1]$,

$$J_n(nz) = \left(\frac{4\zeta}{1-z^2} \right)^{1/4} \left[\frac{\text{Ai}(n^{2/3}\zeta)}{n^{1/3}} (1 + \mathcal{O}(n^{-2})) + \frac{\text{Ai}'(n^{2/3}\zeta)}{n^{5/3}} \mathcal{O}(1) \right] \quad (4.110)$$

where

$$\zeta(z) = (3/2)^{2/3} \left[\ln(1 + \sqrt{1-z^2}) - \ln(z) - \sqrt{1-z^2} \right]^{2/3}. \quad (4.111)$$

In our case, $n = 2T + NT^{1/3}$ and $z = (1 + \varepsilon)^{-1}$ with $\varepsilon = \frac{1}{2}NT^{-2/3} \geq 0$. This implies that $z \in [0, 1]$. In this interval the function $\zeta(z)$ is positive and decreasing. The prefactor is estimated using $4\zeta(z(\varepsilon))(1 - z(\varepsilon)^2)^{-1} 2^{-4/3} \leq 1 + \frac{4}{5}\varepsilon$ for all $\varepsilon > 0$. Moreover, for $x \geq 0$, $\text{Ai}(x) \leq \text{Ai}(x/2)$ and $|\text{Ai}'(x)| \leq \text{Ai}(x/2)$. Therefore

$$|T^{1/3} J_{[2T+NT^{1/3}]}(2T)| \leq \left(1 + \frac{4}{5}\varepsilon\right)^{1/4} \text{Ai}(n^{2/3}\zeta/2)(1 + \mathcal{O}(T^{-4/3})) \quad (4.112)$$

where we also used $(2T)^{1/3} \leq n^{1/3}$. Next we bound (4.112) separately for $N \leq \frac{1}{2}T^{2/3}$ and $N \geq \frac{1}{2}T^{2/3}$.

Case 1) $0 \leq N \leq \frac{1}{2}T^{2/3}$. In this case $\varepsilon \leq \frac{1}{4}$ and, for $\varepsilon \in [0, 1/3]$, $\zeta(z(\varepsilon)) \geq \varepsilon$ holds. Replacing n by $2T$ in the Airy function we have an upper bound since it is a decreasing function, consequently

$$|T^{1/3} J_{[2T+NT^{1/3}]}(2T)| \leq 2 \text{Ai}(N2^{-4/3})(1 + \mathcal{O}(T^{-4/3})). \quad (4.113)$$

Finally it is easy to verify that $2 \operatorname{Ai}(N2^{-4/3}) \leq \exp(-N/2)$, and obtain the bound of the lemma.

Case 2) $N \geq \frac{1}{2}T^{2/3}$. In this case $\varepsilon \geq \frac{1}{4}$ and $z(\varepsilon) \leq \frac{4}{5}$. In this interval $\zeta(z) \geq \frac{1}{4}(\ln(8\varepsilon))^{2/3}$ from which follows

$$|T^{1/3} J_{[2T+NT^{1/3}]}(2T)| \leq (NT^{-2/3})^{1/4} \operatorname{Ai}\left(\frac{1}{8}(n \ln(4NT^{-2/3}))^{2/3}\right) \mathcal{O}(1). \quad (4.114)$$

For $x \geq 0$, $\operatorname{Ai}(x) \leq \exp(-\frac{2}{3}x^{3/2})$, and $N \geq \frac{1}{2}T^{2/3}$ implies $\tilde{N} = 4NT^{-2/3} \geq 2$. Consequently,

$$\begin{aligned} |T^{1/3} J_{[2T+NT^{1/3}]}(2T)| &\leq \tilde{N}^{1/4} \exp(-c_1 T(1 + \tilde{N}/8)) \mathcal{O}(1) \\ &\leq \exp(-c_1 T) \exp(-2c_2 T \tilde{N}) \tilde{N}^{1/4} \mathcal{O}(1) \end{aligned} \quad (4.115)$$

with $c_1 = \ln(2)/3$, $c_2 = c_1/16$. For $T \geq 10$ and $\tilde{N} \geq 2$, $\tilde{N}^{1/4} \exp(-c_2 T \tilde{N}) \leq 1$, and $\exp(-c_2 T \tilde{N}) \leq \exp(-N/2)$ for T large enough. These two last inequalities imply

$$|T^{1/3} J_{[2T+NT^{1/3}]}(2T)| \leq \exp(-c_1 T) \exp(-N/2) \mathcal{O}(1) \quad (4.116)$$

for T large enough, and the lemma is proved. \square

Lemma 4.14. For all $N \geq 0$,

$$D_{T,N} = |T^{2/3}(J_{[2T+NT^{1/3+1}]}(2T) - J_{[2T+NT^{1/3}]}(2T))| \leq \exp(-N/2) \mathcal{O}(1) \quad (4.117)$$

uniformly in $T \geq T_0$ for some constant T_0 .

For $N \leq 0$, there is a constant $C > 0$ such that

$$D_{T,N} \leq C(1 + |N|) \quad (4.118)$$

uniformly in $T \geq 1$.

Proof. First we consider $N \geq 0$. Let $N' = N + T^{-1/3}$, then we have to subtract $J_{[2T+NT^{1/3}]}(2T)$ to $J_{[2T+N'T^{1/3}]}(2T)$. In term of $\varepsilon = \frac{1}{2}NT^{-2/3}$ the difference is $1/(2T)$. Let us define

$$q(\varepsilon) = \left(\frac{4\zeta(z(\varepsilon))}{1 - z(\varepsilon)^2} \right)^{1/4} (1 + \varepsilon)^{-1/3}, \quad p(\varepsilon) = (1 + \varepsilon)^{2/3} \zeta(z(\varepsilon)), \quad (4.119)$$

and

$$f(\varepsilon) = \frac{q(\varepsilon)}{(2T)^{1/3}} \operatorname{Ai}[(2T)^{2/3} p(\varepsilon)]. \quad (4.120)$$

With these notations,

$$\begin{aligned} J_{[2T+NT^{1/3}]}(2T) &= f(\varepsilon) + \frac{q(\varepsilon)}{(2T)^{1/3}} \operatorname{Ai}[(2T)^{2/3} p(\varepsilon)] \mathcal{O}(T^{-2}) \\ &\quad + \frac{q(\varepsilon)}{(2T)^{1/3}} \operatorname{Ai}'[(2T)^{2/3} p(\varepsilon)] \mathcal{O}(T^{-4/3}). \end{aligned} \quad (4.121)$$

Now we bound $D_{T,N}$ as follows.

Case 1) Let us consider $N \in [0, \frac{1}{2}T^{2/3}]$. The second and the third terms are simply bounded by their absolute value. Then

$$\begin{aligned} |D_{T,N}| &\leq T^{2/3} \left| f\left(\varepsilon + \frac{1}{2T}\right) - f(\varepsilon) \right| \\ &\quad + T^{2/3} \max_{x \in \{\varepsilon, \varepsilon + 1/2T\}} \frac{q(x)}{(2T)^{1/3}} \text{Ai}[(2T)^{2/3}p(x)] \mathcal{O}(T^{-2}) \\ &\quad + T^{2/3} \max_{x \in \{\varepsilon, \varepsilon + 1/2T\}} \frac{q(x)}{(2T)^{1/3}} |\text{Ai}'[(2T)^{2/3}p(x)]| \mathcal{O}(T^{-4/3}). \end{aligned} \quad (4.122)$$

The first term is bounded by

$$T^{2/3} \left| f\left(\varepsilon + \frac{1}{2T}\right) - f(\varepsilon) \right| \leq T^{2/3} \sup_{x \in [\varepsilon, \varepsilon + 1/2T]} |f'(x)| \frac{1}{2T}, \quad (4.123)$$

where

$$|f'(x)| \leq |q'(x)| \frac{|\text{Ai}[(2T)^{2/3}p(x)]|}{(2T)^{1/3}} + |q(x)p'(x)| \text{Ai}[(2T)^{2/3}p(x)] (2T)^{1/3}. \quad (4.124)$$

We are considering the case of $N \in [0, \frac{1}{2}T^{2/3}]$, which corresponds to $\varepsilon \in [0, 1/4]$. The functions q , q' , and $q \cdot p'$ behave modestly in this interval. They satisfy

$$q(x) \in [1.22, 1.26], \quad |q'(x)| \in [0.14, 0.17], \quad |q(x)p'(x)| \in [1.3, 1.6] \quad (4.125)$$

for $x \in [0, 1/4]$. The Airy function and its derivative are bounded as in Lemma 4.13. Therefore

$$|D_{T,N}| \leq \exp(-N/2)(1 + \mathcal{O}(T^{-2/3})). \quad (4.126)$$

Case 2) Let us consider $N \geq \frac{1}{2}T^{2/3}$. This case is simpler. We apply (4.116) and obtain the bound

$$|D_{T,N}| \leq T^{2/3} \exp(-c_1 T) \exp(-N/2) \mathcal{O}(1) \leq \exp(-N/2) \mathcal{O}(1) \quad (4.127)$$

for T large enough.

Secondly we consider $N \leq 0$. For $|N| \geq T^{1/3}$, using (4.134) we obtain

$$|D_{T,N}| \leq c_3 T^{1/3} \leq c_3 |N| \quad (4.128)$$

for some constant $c_3 > 0$. Next we consider $|N| \leq T^{1/3}$. Since N is negative, $z \geq 1$ and (4.110) holds with $\zeta(z)$ given by [1]

$$\zeta(z) = -(3/2)^{2/3} \left[\sqrt{z^2 - 1} - \arccos(1/z) \right]^{2/3}. \quad (4.129)$$

Recall that $z = (1 + \varepsilon)^{-1}$ and $\varepsilon = \frac{1}{2}NT^{-2/3}$. $|\varepsilon| \leq \frac{1}{2}T^{-1/3}$ is very close to zero. The estimate follows the same outline as for the case 1) for positive N . Take $T \geq 1$, then $\varepsilon \in [-\frac{1}{2}, 0]$ and

$$q(\varepsilon) \in [1.25, 1.37], \quad |q'(\varepsilon)| \in [0.16, 0.25], \quad |q(\varepsilon)p'(\varepsilon)| \in [1.5, 3.1]. \quad (4.130)$$

The difference is that now the Airy function is not rapidly decreasing since $p(\varepsilon) \leq 0$ and its derivative is even increasing. We use some simple bounds: $|\text{Ai}(x)| \leq 1$ and $|\text{Ai}'(x)| \leq 1 + |x|$ for all x , with the result

$$|D_{T,N}| \leq c_4(1 + |N|)(1 + \mathcal{O}(T^{-2/3})) \quad (4.131)$$

for a constant $c_4 > 0$. □

Some relations involving Bessel functions

Here we give some relation on Bessel function [1] which are used in the work. Bessel functions J_n are defined via the generating function by

$$\exp\left(\frac{1}{2}z(t - 1/t)\right) = \sum_{k \in \mathbb{Z}} t^k J_k(z), \quad (t \neq 0). \quad (4.132)$$

Then

1. for $n \in \mathbb{N}$, $J_{-n}(z) = (-1)^n J_n(z)$,
2. $J_0(z) + 2 \sum_{k \geq 1} J_{2k}(z) = 1$,
3. $J_0^2(z) + 2 \sum_{k \geq 1} J_k^2(z) = 1$,
4. for $n \geq 1$, $\sum_{k=0}^{2n} (-1)^k J_k(z) J_{2n-k}(z) + 2 \sum_{k=1}^{\infty} J_k(z) J_{2n+k}(z) = 0$.

Moreover the limit

$$\lim_{T \rightarrow \infty} T^{1/3} J_{[2T + \xi T^{1/3}]}(2T) = \text{Ai}(\xi) \quad (4.133)$$

holds. A useful result of Landau [57] is the following:

$$|J_n(x)| \leq c|x|^{-1/3}, \quad c = 0.785\dots \text{ for all } n \in \mathbb{Z}. \quad (4.134)$$

Chapter 5

Analysis of the 3D Ising corner line ensemble

This chapter is devoted to our results on the 3D-Ising corner [31]. Our main and new result is that the line bordering a flat facet and the rounded part is, in the thermodynamic limit, described by an Airy process. The precise statement of the main result is explained in the next section. The other results are precisely stated in the corresponding sections.

5.1 Formulation of the main result

The line ensemble explained in Section 2.3 can be thought of as world lines of “fermions” in discrete space, $j \in \mathbb{Z}$, and discrete time, $t \in \mathbb{Z}$. It is then natural to introduce the (extended) point process of occupation variables, $\eta(j, t)$, by

$$\eta(j, t) = \begin{cases} 1 & \text{if there is a line passing at } (j, t), \\ 0 & \text{otherwise.} \end{cases} \quad (5.1)$$

As explained in Section 5.2, η is an extended determinantal point process. In the thermodynamic limit, $q = 1 - 1/T \rightarrow 1$, we focus at two different regions of the crystal corner. In Section 5.4 we focus in the rounded part of the 3D-Ising corner, which corresponds to the bulk of the line ensemble, i.e., where the density of lines is away both from 0 and 1. In this case the kernel of the point process η is an extension of the sine kernel in the $T \rightarrow \infty$ limit.

Secondly we focus at the edge, where the density of lines vanishes. This is discussed in Section 5.5 where we prove that, properly rescaled, the kernel of η converges to the extended Airy kernel. In Section 2.3.3 we denoted by $b_T(t) = \mathbf{h}_T(0, t)$ the line bordering the 2 – 3 facet and the rounded piece, and by

$$b_\infty(\tau) = \lim_{T \rightarrow \infty} T^{-1} b_T([\tau T]) = -2(1 - e^{-\tau/2}) \quad (5.2)$$

its limit shape. Then we defined the edge scaling of b_T by (2.69), i.e.,

$$A_T(s) = T^{-1/3} \left\{ b_T([\tau T + sT^{2/3}]) - (b_\infty(\tau)T + b'_\infty(\tau)sT^{2/3} + \frac{1}{2}b''_\infty(\tau)s^2T^{1/3}) \right\}. \quad (5.3)$$

The convergence of η_T^{edge} to the extended Airy point process implies that the border step statistics, properly scaled as A_T converges to the Airy process. The result is also used in our discussion on the universality of the border step fluctuations, see Section 2.3.4.

Theorem 5.1. *Let $A_T(s)$ be the border step rescaled as in (5.3) and let $\mathcal{A}(s)$ be the Airy process. Then for any $m, s_i, a_i \in \mathbb{R}, i = 1, \dots, m$, the limit*

$$\lim_{T \rightarrow \infty} \mathbb{P}_T \left(\bigcap_{i=1}^m \{A_T(s_i) \leq a_i\} \right) = \mathbb{P} \left(\bigcap_{i=1}^m \{\mathcal{A}(s_i \kappa/2) \leq a_i/\kappa\} \right) \quad (5.4)$$

with $\kappa = \sqrt[3]{2b'_\infty(\tau)}$ holds.

With Theorem 5.1 we prove that the stochastic process $s \mapsto A_T(s)$ converges, as $T \rightarrow \infty$, to $s \mapsto \kappa \mathcal{A}(s\kappa/2)$ in the sense of finite dimensional distributions. Probabilistically, it would be natural to lift this theorem to the weak convergence of path measures. The missing piece is the tightness for the sequence of stochastic process $A_T(s)$. We have not attempted to fill this gap. The interested reader is referred to [47], where tightness for the edge scaling of the Aztec diamond is proved.

Theorem 5.1 will be proven in Section 5.6. This chapter ends with an appendix on fermionic correlations which are applied to show that η is an extended determinantal point process.

5.2 Extended determinantal point process

5.2.1 Fermions

The basic tool is the transfer matrix from t to $t + 1$, $t \in \mathbb{Z}$. A fermion is created (resp. annihilated) at the position $j \in \mathbb{Z}$ by the operator a_j^* (resp. a_j). The CAR algebra $\{a_j^*, a_j, j \in \mathbb{Z}\}$ over \mathbb{Z} is defined by the anticommutation relations

$$\{a_i, a_j\} = 0, \quad \{a_i^*, a_j^*\} = 0, \quad \{a_i, a_j^*\} = \delta_{i,j} \quad (5.5)$$

for $i, j \in \mathbb{Z}$. First we consider $t \leq -1$, in which case only up-steps can occur. To each unit up-step at time t we assign the weight $q_t = q^{|t+1/2|}$ which satisfy (3.112). The rule is that in a jump from i to $j, j \geq i$, one creates additional particles at sites m with $i + 1 \leq m \leq j$ and annihilates particles at sites m with $i \leq m \leq j - 1$. E.g. if a fermionic world line jumps from -1 to 3 , one creates particles at positions $0, 1, 2, 3$, and annihilates the particles at $-1, 0, 1, 2$. This rule ensures the non-crossing constraint (3.110), since, if two fermionic world lines would intersect, a fermion is created twice at the same position, which leads to a zero contribution. The corresponding rule applies to $t \geq 0$ with the difference that the jumps are downwards only.

Let us define the operators

$$b_l = \sum_{k \in \mathbb{Z}} a_{k+l}^* a_k. \quad (5.6)$$

The transfer matrix from t to $t + 1$ is a sum of the n -step transitions T_n as

$$\widehat{T}(t, t + 1) = \mathbb{1} + q_t T_1 + q_t^2 T_2 + \dots + q_t^n T_n + \dots, \quad (5.7)$$

where

$$T_n = \frac{(-1)^n}{n!} \sum_{k_1, \dots, k_n} a_{k_1} \dots a_{k_n} a_{k_n+1}^* \dots a_{k_1+1}^*. \quad (5.8)$$

The $(-1)^n$ prefactor results from the left ordering of the a_j and a_j^* 's.

We would like to reexpress T_n in terms of products of the b_i 's only. For $n, m > 0$ the commutators are

$$b_n a_k^* = a_k^* b_n + a_{k+n}^*, \quad b_n a_k = a_k b_n - a_{k-n}, \quad [b_n, b_m] = 0, \quad [b_{-n}, b_{-m}] = 0. \quad (5.9)$$

These relations lead to

$$T_n = \sum_{\substack{d_1, \dots, d_n \geq 1 \\ d_1 + 2d_2 + \dots = n}} \prod_{j=1}^n \left(\frac{b_j}{j} \right)^{d_j} \frac{1}{d_j!}. \quad (5.10)$$

The Schur polynomials $\{p_k(y)\}_{k \geq 0}$ are polynomials such that

$$\exp \left(\sum_{k \geq 1} t^k y_k \right) = \sum_{l \geq 0} p_l(y) t^l, \quad y = y_1, y_2, \dots, \quad (5.11)$$

and given explicitly by

$$p_l(y) = \sum_{\substack{x_1, \dots, x_l \geq 1 \\ x_1 + 2x_2 + \dots = l}} \prod_{j=1}^l \frac{y_j^{x_j}}{x_j!}. \quad (5.12)$$

Comparing with (5.11) yields

$$\widehat{T}(t, t + 1) = \sum_{l \geq 0} q_t^l T_l = \exp \left(\sum_{k \geq 1} q_t^k \frac{b_k}{k} \right). \quad (5.13)$$

We conclude that the transfer matrix is given by

$$\widehat{T}(t, t + 1) = \exp \left(\sum_{k \geq 1} q^{k|t+1/2|} \frac{b_k}{k} \right) \quad (5.14)$$

for $t \in \mathbb{Z}_- = \{-1, -2, \dots\}$, and, by the same reasoning,

$$\widehat{T}(t, t + 1) = \exp \left(\sum_{k \geq 1} q^{k(t+1/2)} \frac{b_{-k}}{k} \right) \quad (5.15)$$

for $t \in \mathbb{Z}_+$.

$\widehat{T}(t, t+1)$ is quadratic in the fermion operators. Hence it is the second quantization of a one-particle operator acting of ℓ_2 . For easier reading second quantization is merely indicated by a “ $\widehat{}$ ”, i.e., for A acting of ℓ_2 we set $\widehat{A} = \Gamma(A)$ as its second quantization. From (5.14), (5.15) we read off

$$T(t, t+1) = \exp\left(\sum_{k \geq 1} \frac{q^{k|t+1/2|}}{k} \alpha_k\right) \quad (5.16)$$

for $t \in \mathbb{Z}_-$, and

$$T(t, t+1) = \exp\left(\sum_{k \geq 1} \frac{q^{k(t+1/2)}}{k} \alpha_{-k}\right) \quad (5.17)$$

for $t \in \mathbb{Z}_+$ with matrices α_k defined through

$$[\alpha_k]_{i,j} = \begin{cases} 1 & \text{if } i - j = k, \\ 0 & \text{otherwise.} \end{cases} \quad (5.18)$$

$T(t, t+1)$ are invertible with the ℓ_2 -norms

$$\begin{aligned} \|T(t, t+1)\| &\leq \exp\left(\frac{q^{|t+1/2|}}{1 - q^{|t+1/2|}}\right), \\ \|T(t, t+1)^{-1}\| &\leq \exp\left(\frac{q^{|t+1/2|}}{1 - q^{|t+1/2|}}\right). \end{aligned} \quad (5.19)$$

For the state at $t = \pm\infty$ all sites in $\mathbb{Z}_- \cup \{0\}$ are filled, those in $\mathbb{Z}_+ \setminus \{0\}$ are empty, which, together with the transfer matrices (5.14), (5.15) determines the Green's functions of an imaginary time (Euclidean) Fermi field. It is inhomogeneous in space-time and uniquely given through the two-point function $\langle a_i^*(t) a_j(t') \rangle$. To compute it correctly one has to employ the standard finite volume approximation. We first restrict all world lines to lie in the spatial interval $[-M, M]$. Thereby the transfer matrix depends on M in the sense that all creation and annihilation operators with index $|k| > M$ are set equal to zero. The state at $\pm\infty$ is $(1, \dots, 1, 0, \dots, 0)^t$ which is $2M+1$ long with the last 1 at site 0. The projector on this state is approximated through

$$\exp[\beta \widehat{N}_M] \quad (5.20)$$

in the limit $\beta \rightarrow \infty$ with $\widehat{N}_M = \sum_{k=-M}^0 a_k^* a_k - \sum_{k=1}^M a_k^* a_k$. We first compute the equal time Green's function through

$$\begin{aligned} \langle a_i^*(t_0) a_j(t_0) \rangle_T &= \\ &= \lim_{M \rightarrow \infty} \lim_{L \rightarrow \infty} \lim_{\beta \rightarrow \infty} \frac{1}{Z_{\beta, M, L}} \text{Tr} \left(e^{\beta \widehat{N}_M} \prod_{t=t_0}^L \widehat{T}_M(t, t+1) a_i^* a_j \prod_{t=-L}^{t_0-1} \widehat{T}_M(t, t+1) \right), \end{aligned} \quad (5.21)$$

where the trace is over the antisymmetric Fock space \mathcal{F} with one-particle space $\ell_2([-M, \dots, M])$. The products are time-ordered increasingly from right to left, which is

indicated by the superscript t at the product symbol \prod . $Z_{\beta, M, L}$ is the normalizing partition function, which is defined through the same trace with $a_i^* a_j$ replaced by $\mathbb{1}$. As explained in Appendix 5.A.1, (5.21) can be expressed in terms of one-particle operators as the limit $M, L, \beta \rightarrow \infty$ of

$$\langle a_i^*(t_0) a_j(t_0) \rangle_{T, \beta M L} = \left[\mathbb{1} + \left(\prod_{t=-L}^{t_0-1} T_M(t, t+1) e^{\beta N_M} \prod_{t=t_0}^L T_M(t, t+1) \right)^{-1} \right]_{j,i}^{-1}. \quad (5.22)$$

Let $P_+ + P_- = \mathbb{1}$ in ℓ_2 with P_+ the projection onto $\mathbb{Z}_+ \setminus \{0\}$ and let

$$e^{G_{\text{right}}(t_0)} = \prod_{t=t_0}^{\infty} T(t, t+1), \quad e^{G_{\text{left}}(t_0)} = \prod_{t=-\infty}^{t_0-1} T(t, t+1), \quad (5.23)$$

and

$$e^{G_{\uparrow}(t_0)} = \prod_{t=-\infty}^{\min(0, t_0)-1} T(t, t+1), \quad e^{G_{\downarrow}(t_0)} = \prod_{t=\max(0, t_0)}^{\infty} T(t, t+1). \quad (5.24)$$

By (5.19) the infinite products are well-defined, as are their inverses. The $T(t, t+1)$'s commute and no time-ordering is required. Hence

$$\begin{aligned} G_{\uparrow}(t_0) &= \sum_{t=-\infty}^{\min(0, t_0)-1} \sum_{r \geq 1} \frac{q^{r|t+1/2|}}{r} \alpha_r = \sum_{r \geq 1} \mu_r(t_0) \alpha_r, \\ G_{\downarrow}(t_0) &= \sum_{t=\max(0, t_0)}^{\infty} \sum_{r \geq 1} \frac{q^{r(t+1/2)}}{r} \alpha_{-r} = \sum_{r \geq 1} \nu_r(t_0) \alpha_{-r} \end{aligned} \quad (5.25)$$

with

$$\mu_r(t_0) = \frac{q^{r/2} q^{-r \min(0, t_0)}}{r(1 - q^r)}, \quad \nu_r(t_0) = \frac{q^{r/2} q^{r \max(0, t_0)}}{r(1 - q^r)}. \quad (5.26)$$

In (5.22) we take limits as indicated in (5.21). Then

$$\langle a_i^*(t_0) a_j(t_0) \rangle_T = \left[e^{G_{\text{left}}(t_0)} P_- (P_- e^{G_{\text{right}}(t_0)} e^{G_{\text{left}}(t_0)} P_- + P_+)^{-1} P_- e^{G_{\text{right}}(t_0)} \right]_{j,i}. \quad (5.27)$$

Let

$$e^{G_-} = \prod_{t=-\infty}^{-1} T(t, t+1), \quad e^{G_+} = \prod_{t=0}^{\infty} T(t, t+1). \quad (5.28)$$

Then $e^{G_{\text{right}}(t_0)} e^{G_{\text{left}}(t_0)} = e^{G_+} e^{G_-} = e^{G_-} e^{G_+}$ and, decomposing $\ell_2 = P_- \ell_2 \oplus P_+ \ell_2$, we have

$$e^{G_-} = \begin{bmatrix} a & 0 \\ c & b \end{bmatrix}, \quad e^{G_+} = \begin{bmatrix} a' & c' \\ 0 & b' \end{bmatrix}. \quad (5.29)$$

Thus

$$P_- (P_- e^{G_{\text{right}}(t_0)} e^{G_{\text{left}}(t_0)} P_- + P_+)^{-1} P_- = \begin{bmatrix} (aa')^{-1} & 0 \\ 0 & 0 \end{bmatrix} \quad (5.30)$$

and, since

$$e^{-G_-} = \begin{bmatrix} a^{-1} & 0 \\ -b^{-1}ca^{-1} & b^{-1} \end{bmatrix}, \quad e^{-G_+} = \begin{bmatrix} (a')^{-1} & -(a')^{-1}c'(b')^{-1} \\ 0 & (b')^{-1} \end{bmatrix}, \quad (5.31)$$

we obtain

$$e^{-G_+} P_- e^{-G_-} = P_- (P_- e^{G_{\text{right}}(t_0)} e^{G_{\text{left}}(t_0)} P_- + P_+)^{-1} P_-. \quad (5.32)$$

Therefore

$$\langle a_i^*(t_0) a_j(t_0) \rangle_T = [e^{G_{\text{left}}(t_0)} e^{-G_+} P_- e^{-G_-} e^{G_{\text{right}}(t_0)}]_{j,i}, \quad (5.33)$$

which rewrites as

$$\langle a_i^*(t_0) a_j(t_0) \rangle_T = [e^{G_{\uparrow}(t_0) - G_{\downarrow}(t_0)} P_- e^{-(G_{\uparrow}(t_0) - G_{\downarrow}(t_0))}]_{j,i}. \quad (5.34)$$

The Fermi field depends on T through $q = 1 - 1/T$. For this reason we keep the index T .

Using the anticommutation relations (5.5) in (5.21) we immediately obtain

$$\langle a_j(t_0) a_i^*(t_0) \rangle_T = [e^{G_{\uparrow}(t_0) - G_{\downarrow}(t_0)} P_+ e^{-(G_{\uparrow}(t_0) - G_{\downarrow}(t_0))}]_{j,i}. \quad (5.35)$$

Thus our final result for the equal time correlations reads

$$\begin{aligned} \langle a_i^*(t_0) a_j(t_0) \rangle_T &= \sum_{l \leq 0} [e^{G_{\uparrow}(t_0) - G_{\downarrow}(t_0)}]_{j,l} [e^{-G_{\uparrow}(t_0) + G_{\downarrow}(t_0)}]_{l,i}, \\ \langle a_j(t_0) a_i^*(t_0) \rangle_T &= \sum_{l > 0} [e^{G_{\uparrow}(t_0) - G_{\downarrow}(t_0)}]_{j,l} [e^{-G_{\uparrow}(t_0) + G_{\downarrow}(t_0)}]_{l,i}. \end{aligned} \quad (5.36)$$

To extend (5.36) to unequal times we have to go through the same limit procedure as before. Since the argument is in essence unchanged, there is no need to repeat. We define the propagator from a to b , $a \leq b$, through

$$e^{G(a,b)} = \prod_{t=a}^{b-1} T(t, t+1), \quad e^{G(a,a)} = \mathbb{1}, \quad e^{G(b,a)} = e^{-G(a,b)}. \quad (5.37)$$

Using the identity

$$e^{-G(0,t_0)} a_m e^{G(0,t_0)} = \sum_{k \in \mathbb{Z}} [e^{G(0,t_0)}]_{m,k} a_k \quad (5.38)$$

for $t \geq t'$, the full two-point function is given by

$$\begin{aligned} \langle a_j^*(t) a_{j'}(t') \rangle_T &= \sum_{l \leq 0} [e^{G_{\uparrow}(0) - G_{\downarrow}(0) + G(0,t')}]_{j',l} [e^{-G_{\uparrow}(0) + G_{\downarrow}(0) - G(0,t)}]_{l,j}, \\ \langle a_j(t) a_{j'}^*(t') \rangle_T &= \sum_{l > 0} [e^{G_{\uparrow}(0) - G_{\downarrow}(0) + G(0,t)}]_{j,l} [e^{-G_{\uparrow}(0) + G_{\downarrow}(0) - G(0,t')}]_{l,j'}. \end{aligned} \quad (5.39)$$

5.2.2 Correlation functions

Moments of the random field $\eta(j, t)$ introduced above can be expressed through fermionic correlations. We consider first equal time correlations. The basic identity is

$$\mathbb{E}_T \left(\prod_{k=1}^n \eta(j_k, t) \right) = \left\langle \prod_{k=1}^n a_{j_k}^*(t) a_{j_k}(t) \right\rangle_T, \quad (5.40)$$

where \mathbb{E}_T is the expectation with respect to the normalized weight (3.112). If $\{j_1, \dots, j_n\}$ are distinct, then, as explained in Appendix 5.A.2, the fermionic expectation is determinantal and

$$\mathbb{E}_T \left(\prod_{k=1}^n \eta(j_k, t) \right) = \text{Det}(R_T(j_k, t; j_l, t))_{1 \leq k, l \leq n}, \quad (5.41)$$

with

$$R_T(i, t; j, t) = \langle a_i^*(t) a_j(t) \rangle_T. \quad (5.42)$$

If coinciding arguments are admitted, then (5.41) still holds with the convention

$$R_T(i, t; j, t) = \begin{cases} \langle a_i^*(t) a_j(t) \rangle_T & \text{for } i \leq j, \\ \langle a_i^*(t) a_j(t) \rangle_T - \delta_{i,j} = -\langle a_j(t) a_i^*(t) \rangle_T & \text{for } i > j. \end{cases} \quad (5.43)$$

(5.40) is easily extended to unequal time correlations. Let us consider n disjoint space-time points $(j_1, t_1), \dots, (j_n, t_n)$ ordered increasingly as $t_1 \leq t_2 \leq \dots \leq t_n$. Then the basic identity is

$$\mathbb{E}_T \left(\prod_{k=1}^n \eta(j_k, t_k) \right) = \langle a_{j_n}^*(t_n) a_{j_n}(t_n) \cdots a_{j_1}^*(t_1) a_{j_1}(t_1) \rangle_T. \quad (5.44)$$

Using (5.38) the left hand side equals

$$\sum_{\substack{k_1, \dots, k_n \\ t_1, \dots, t_n}} \prod_{q=1}^n [e^{-G(0, t_q)}]_{k_q, j_q} [e^{G(0, t_q)}]_{j_q, l_q} \langle a_{k_n}^* a_{l_n} \cdots a_{k_1}^* a_{l_1} \rangle_T. \quad (5.45)$$

Let us set

$$R_T(j, t; j', t') = \begin{cases} \langle a_j^*(t) a_{j'}(t') \rangle_T & \text{for } t \geq t', \\ -\langle a_{j'}(t') a_j^*(t) \rangle_T & \text{for } t < t'. \end{cases} \quad (5.46)$$

Then the unequal time correlations are given by

$$\mathbb{E}_T \left(\prod_{k=1}^n \eta(j_k, t_k) \right) = \text{Det}(R_T(j_k, t_k; j_l, t_l))_{1 \leq k, l \leq n}. \quad (5.47)$$

The identity (5.47) has been derived from left to right. One can read it also from right to left. Then R_T is the defining kernel, resp. Green's function, which is considered to be given and (5.47) defines the moments of some determinantal space-time random field over $\mathbb{Z} \times \mathbb{Z}$. Of course, R_T cannot be chosen arbitrarily, since the right hand side of (5.47) must

be moments of a probability measure. For determinantal random fields over the space coordinate only, compare with (5.41), proper conditions on the defining kernel have been studied in detail [91, 90]. The space-time variant is less well understood, see [46] for a discussion.

The determinantal property is preserved under limits. Thus through bulk and edge scaling further determinantal space-time random fields will be encountered below. One of them is over $\mathbb{Z} \times \mathbb{Z}$ with equal-time given through the sine-kernel. The other is over $\mathbb{Z} \times \mathbb{R}$ with equal-time given through the Airy kernel.

5.3 Limit shape

On the macroscopic scale, in the limit $T \rightarrow \infty$, the random field $\eta(j, t)$ becomes deterministic with a profile given by

$$\rho(\zeta, \tau) = \begin{cases} 1 & \text{for } \zeta \leq b_{\infty}^{-}(\tau), \\ \frac{1}{\pi} \arccos(\cosh(\tau/2) - e^{-\zeta+|\tau|/2}/2) & \text{for } b_{\infty}^{-}(\tau) < \zeta < b_{\infty}(\tau), \\ 0 & \text{for } \zeta \geq b_{\infty}(\tau), \end{cases} \quad (5.48)$$

with

$$b_{\infty}^{-}(\tau) = -2 \ln(1 + e^{-|\tau|/2}), \quad b_{\infty}(\tau) = -2 \ln(1 - e^{-|\tau|/2}). \quad (5.49)$$

More precisely, for all continuous test functions $f : \mathbb{R}^2 \rightarrow \mathbb{R}$ with compact support

$$\lim_{T \rightarrow \infty} \frac{1}{T^2} \sum_{j,t} f(j/T, t/T) \eta(j, t) = \int d\zeta d\tau \rho(\zeta, \tau) f(\zeta, \tau) \quad (5.50)$$

almost surely. (5.50) assumes more spatial averaging than needed. In fact, it suffices to choose a test function whose support on the scale of the lattice diverges as $T \rightarrow \infty$ and to properly normalize.

As a consequence of (5.50) the limit (2.65) holds. h_{ma} can be read off from (5.48) and is given in parametric form through

$$h_{\text{ma}}(u, v) = \begin{cases} 0 & \text{for } (u, v) \in \mathbb{R}_+^2 \setminus \mathcal{D}, \\ \frac{1}{2}(u + v - |\tau|) + \zeta(u, v) & \text{for } (u, v) \in \mathcal{D}, \end{cases} \quad (5.51)$$

where $\tau = v - u$ and where $\zeta(u, v)$ is the unique solution ζ of the equation

$$\frac{1}{2}(u + v - |\tau|) = \int_{b_{\infty}^{-}(\tau)}^{\zeta} (1 - \rho(\zeta', \tau)) d\zeta' - \zeta \quad (5.52)$$

in the interval $[b_{\infty}^{-}(\tau), b_{\infty}(\tau)]$. While the limit (5.50) has been established by Okounkov and Reshetikhin [69], compare also with Section 5.4, the existence of the limit shape has been proved before by Cerf and Kenyon [20]. Instead of (2.64), they used the fixed volume

constraint $V(h) = 2\zeta_R(3)T^3$, resp. $V(h) \leq 2\zeta_R(3)T^3$, with ζ_R the Riemann zeta function. They write the limit shape S_0 , as a set of \mathbb{R}^3 , in the parametric representation

$$S_0 = \{2(f(a, b, c) - \ln a, f(a, b, c) - \ln b, f(a, b, c) - \ln c) \mid a, b, c > 0\} \quad (5.53)$$

with

$$f(a, b, c) = \frac{1}{4\pi^2} \int_0^{2\pi} du \int_0^{2\pi} dv \ln(a + be^{iu} + ce^{iv}). \quad (5.54)$$

Here a, b, c denote the weights for the three orientations of the lozenges and $f(a, b, c)$ is the corresponding free energy per unit area for the lozenge tiling of the plane. As expected from the equivalence of ensembles, the shapes given by (5.51) and (5.53) are identical. This can be seen as follows. Let $z = (z_1, z_2, z_3)$ represent a point on the limit shape. We compare $z_2 - z_1$ and $z_3 - z_1$ (resp. $z_3 - z_2$) for $z_2 \geq z_1$ (resp. $z_2 \leq z_1$) for the parametrizations (5.51) and (5.53). This leads to $a = 1, b = e^{-\tau/2}, c = e^{-\zeta/2}$ for $z_2 \geq z_1$ and to $b = 1, a = e^{-|\tau|/2}, c = e^{-\zeta/2}$ for $z_2 \leq z_1$. Since (5.54) is symmetric in a, b, c , one verifies that indeed

$$\int_{-2\ln(1+e^{-|\tau|/2})}^{\zeta} (1 - \rho(\zeta', \tau)) d\zeta' = 2f(1, e^{-|\tau|/2}, e^{-\zeta/2}) + \zeta. \quad (5.55)$$

According to (5.51), $h_{\text{ma}} = 0$ on $\mathbb{R}_+^2 \setminus \mathcal{D}$. Close to the edge the height vanishes with the power $3/2$. E.g. in the direction $\tau = v - u$ one has

$$h_{\text{ma}}(r, \tau) \simeq \frac{2}{3} \cosh(\tau/4) \pi^{-1} 2^{1/4} r^{3/2} \quad (5.56)$$

with r the distance to the edge. The $3/2$ power is known as Pokrovsky-Talapov law [75].

A limit shape theorem is a law of large numbers. It is available also for related tiling models. A famous case is the Aztec diamond [21]. Cohn, Larsen and Propp [22] consider the 3D-Young diagrams constrained to the box $\alpha N \times \beta N \times \gamma N$ with $\alpha, \beta, \gamma \sim \mathcal{O}(1)$ and compute the limit shape as $N \rightarrow \infty$. In the line-ensemble representation their model corresponds to $q = 1$ with the boundary conditions that at $t = -\alpha N, \beta N$ all lattices sites are occupied except for those in the interval $[1, \gamma N]$. [22] computed the line density and from it the limit shape. Two or higher order point functions are not studied. From our representation we see that higher order correlation functions are determinantal even in this case. However the computation of the two-point function is more complicated, since one cannot rely any more on an expression like (5.34). For a list of further limit shape theorems we refer to the survey [51].

The limit shape can be determined through minimizing the appropriate macroscopic free energy functional. The input is the microscopic surface tension at given slope ∇h . For example in the (111)-frame the surface tension $\sigma_{(111)}(\nabla h)$ is given by (5.54), where a, b, c are defined through the prescribed surface tilt ∇h . $\sigma_{(111)}$ has been computed in [50, 111, 16]. Correspondingly there is a surface tension in the (001)-frame, denoted by $\sigma_{(001)}(\nabla h)$.

To obtain the free energy \mathcal{F} for some macroscopic height profile h over a bounded domain \mathcal{B} , one argues that h is made up of little planar pieces, each one of them having the surface tension at the corresponding local slope. Adding up yields

$$\mathcal{F}(h) = \int_{\mathcal{B}} dudv \sigma_{(001)}(\nabla h(u, v)). \quad (5.57)$$

In our case we have $\mathcal{B} = \mathbb{R}_+^2$, h is decreasing in both variables such that $h(u, v) = 0$ for $(u, v) \rightarrow \infty$, and $V(h) = \int_{\mathcal{B}} dudv h(u, v)$. The minimizer of \mathcal{F} , under these constraints and $V(h) = 2\zeta_R(3)$, is h_{ma} from (5.51). Equivalently one could minimize $\mathcal{F}(h) + V(h)$.

Probabilistically, $\mathcal{F}(h) + V(h)$ can be viewed as a large deviation functional in the sense that in the limit $T \rightarrow \infty$, with respect to the normalized probability $Z^{-1}q^{V(h)}$,

$$\mathbb{P}_T (T^{-1}h_T([uT], [vT]) \simeq h) = \mathcal{O} \left(e^{-T^2(\mathcal{F}(h)+V(h)-\mathcal{F}(h_{\text{ma}})-V(h_{\text{ma}}))} \right) \quad (5.58)$$

for given macroscopic height profile h [20].

Expanding (5.58) to quadratic order in $\delta h = h - h_{\text{ma}}$ yields a heuristic formula for the covariance of the Gaussian shape fluctuations. In spirit it is proportional to $(-\partial_u^2 - \partial_v^2)^{-1}$, hence like a massless Gaussian field. This implies in particular, that on the macroscopic scale shape fluctuations are small, of order $\ln T$ only. Gaussian fluctuations are proved for the Aztec diamond in [45] and for domino tilings of a Temperleyan polyomino in [52].

The limit shape theorem (5.48) implies that also the border step has a deterministic limit. We state a result, which is stronger than what could be deduced from (5.48) and which follows by the transfer matrix techniques to be explained in Section 5.5.

Theorem 5.2. *Let b_T be the border step as defined in (2.66). Then for any $\delta > 0$, $c > 0$, $0 < u_- < u_+ < \infty$ one has*

$$\lim_{T \rightarrow \infty} \mathbb{P} (|T^{-1}b_T([uT]) - b_{\infty}(u)| \geq cT^{-2/3+\delta}, u_- \leq u \leq u_+) = 0. \quad (5.59)$$

5.4 Bulk scaling, local equilibrium

For local equilibrium we zoom to a point $(\zeta_0, \tau_0)T$ with $b_{\infty}^-(\tau_0) < \zeta_0 < b_{\infty}(\tau_0)$ at average density $\rho = \rho(\zeta_0, \tau_0)$, which means to consider the random field

$$\eta_T^{\text{bulk}}(j, t) = \eta([\zeta_0 T] + j, [\tau_0 T] + t) \quad (5.60)$$

with $(j, t) \in \mathbb{Z}^2$ and $[\]$ denoting the integer part. Properly speaking we should keep the reference point (ζ_0, τ_0) in our notation. Since it is fixed throughout, we suppress it for simplicity. In the limit $T \rightarrow \infty$, $\eta_T^{\text{bulk}}(j, t)$ becomes stationary. Then at fixed t , one has to fill the Fermi states up to the density ρ which implies that $\eta_{\infty}^{\text{bulk}}(j, t)$, t fixed, is a determinantal point process on \mathbb{Z} as defined through the discrete sine-kernel. Only at $\tau_0 = 0$, the inhomogeneity of the underlying η -field can still be seen, which, of course, is an artifact of our coordinate system. In the $(1 \ 1 \ 1)$ -projection the line $\tau_0 = 0$ would be just

like any other local slope with a corresponding stationary distribution of lozenges. The case $\tau_0 = 0$ can also be treated. For simplicity we omit it and require $\tau_0 \neq 0$.

Let us define the kernel $S(j, t; j', t')$ by

$$S(j, t; j', t') = \frac{\text{sgn}(t - t')}{2\pi} \int_{I(t, t')} dk \exp [ik(j' - j) + (t' - t) \ln(1 - e^{-|\tau_0|/2} e^{-ik})] \quad (5.61)$$

for $\tau_0 > 0$ and

$$S(j, t; j', t') = \frac{\text{sgn}(t - t')}{2\pi} \int_{I(t, t')} dk \exp [ik(j' - j) - (t' - t) \ln(1 - e^{-|\tau_0|/2} e^{ik})] \quad (5.62)$$

for $\tau_0 < 0$, where

$$I(t, t') = \begin{cases} [-\pi\rho, \pi\rho], & \text{if } t \geq t', \\ [\pi\rho, 2\pi - \pi\rho], & \text{if } t < t', \end{cases}$$

and $\text{sgn}(t - t') = 1$, if $t \geq t'$, and $\text{sgn}(t - t') = -1$, if $t < t'$. In particular at equal times

$$S(i, t; j, t) = \frac{\sin(\rho\pi(i - j))}{\pi(i - j)}, \quad (5.63)$$

which is the sine-kernel. S depends on the reference point (ζ_0, τ_0) . In the particular case of equal times the dependence is only through the local density.

Theorem 5.3. *In the sense of convergence of local distributions we have*

$$\lim_{T \rightarrow \infty} \eta_T^{\text{bulk}}(j, t) = \eta^{\text{sine}}(j, t). \quad (5.64)$$

For $\tau_0 > 0$, $\eta^{\text{sine}}(j, t)$ is the determinantal space-time random field with defining kernel (5.61) and for $\tau_0 < 0$ the one with the kernel (5.62).

Remark: Theorem 5.3 is identical to Theorem 2 of [69]. We use here an integral representation for the defining kernel R_T which differs somewhat from the one of [69] and which turns out to be convenient in the context of the edge scaling.

Proof. We consider the case $\tau_0 > 0$ only, since $\tau_0 < 0$ follows by symmetry. Let us set

$$B_T(j, t; j', t') = e^{g(j) - g(j')} R_T([\zeta_0 T] + j, [\tau_0 T] + t; [\zeta_0 T] + j', [\tau_0 T] + t'), \quad (5.65)$$

where R_T is defined in (5.46) and $g(j) = j|\tau_0|T \ln(1 - 1/T)/2$. The determinant in (5.47) does not change under similarity transformation, in particular not under multiplying by $e^{g(u_i) - g(u_j)}$. Therefore

$$\mathbb{E}_T \left(\prod_{k=1}^m \eta_T^{\text{bulk}}(j_k, t_k) \right) = \text{Det}(B_T(j_k, t_k; j_l, t_l))_{1 \leq k, l \leq m} \quad (5.66)$$

and we need to prove that pointwise

$$\lim_{T \rightarrow \infty} B_T(j, t; j', t') = S(j, t; j', t'). \quad (5.67)$$

First consider $t \geq t'$. For $\tau_0 > 0$ we take T large enough so that $\tau_0 T + t' \geq 0$ (this simplifies (5.72) below). Using (5.47) we obtain

$$\begin{aligned} B_T(j, t; j', t') &= e^{g(j) - g(j')} \\ &\times \sum_{l \leq 0} [e^{G_\uparrow(\tau_0 T) - G_\downarrow(\tau_0 T + t)}]_{\zeta_0 T + j, l} [e^{G_\downarrow(\tau_0 T + t') - G_\uparrow(\tau_0 T)}]_{l, \zeta_0 T + j'}. \end{aligned} \quad (5.68)$$

An explicit expression for the matrix elements of the two-point functions can be found using the translation invariance of the one-particle operators. In Fourier representation they are given by

$$\left[\exp \left(\sum_{r \in \mathbb{Z}} \sigma_r \alpha_r \right) \right]_{n, m} = \frac{1}{2\pi} \int_{-\pi}^{\pi} \exp(-ik(n - m)) \exp \left(\sum_{r \in \mathbb{Z}} \sigma_r e^{ikr} \right) dk \quad (5.69)$$

for $\sigma_r \in \mathbb{R}$. Then using (5.69) and changing l into $-l$, we have

$$\begin{aligned} B_T(j, t; j', t') &= \sum_{l \geq 0} \frac{e^{g(j)}}{2\pi} \int_{-\pi}^{\pi} dk e^{\sigma(k)T} e^{\varphi_q(k, t)} e^{-ik(\zeta_0 T + j)} e^{-ikl} \\ &\times \frac{e^{-g(j')}}{2\pi} \int_{-\pi}^{\pi} dk' e^{-\sigma(k')T} e^{-\varphi_q(k', t')} e^{ik'(\zeta_0 T + j')} e^{ik'l}, \end{aligned} \quad (5.70)$$

where

$$\sigma(k) = (1 - q) \sum_{r \geq 1} \frac{q^{r/2}}{r(1 - q^r)} (e^{ikr} - q^{r\tau_0/(1-q)} e^{-ikr}) \quad (5.71)$$

and

$$\varphi_q(k, t) = \sum_{r \geq 1} \frac{q^{r/2}(1 - q^{rt})}{r(1 - q^r)} q^{r\tau_0/(1-q)} e^{-ikr}. \quad (5.72)$$

To study the asymptotic of integrals as (5.70) we consider the complex k plane and regard the integration in (5.70) as being along the real line from $-\pi$ to π . Such a line integral can be deformed to another path C with the same endpoints. The complex integration along C will be denoted by $\int_C dk \dots$. In the particular case when the path is on the real line, say from a to b , the integral will be denoted by $\int_a^b dk \dots$.

Let us consider the following four paths: $\xi_0 = -\pi \rightarrow \pi$, $\xi_1(p) = -\pi + ip \rightarrow \pi + ip$, $\xi_2 = -\pi \rightarrow -\pi + ip$, and $\xi_3 = \pi + ip \rightarrow \pi$ with $0 \leq p \leq \tau_0$. The factors in (5.70) are integrals along ξ_0 . Their integration contour can be deformed from ξ_0 to $\xi_2 \circ \xi_1 \circ \xi_3$ without changing the integrals, since the integrands are holomorphic. Moreover the integrals on ξ_2 and ξ_3 cancel exactly because of periodicity of the integrands. We transform the integral in k into the integral along $\xi_1(\theta)$ and the one in k' into the integral along $\xi_1(\theta + \varepsilon)$, with

$0 < \varepsilon \ll 1$ and $\theta = -\tau_0 T \ln(1 - 1/T)/2$. θ is chosen such that the exponentially large function in T passes through the critical point of $\sigma(k')$. Consequently we have

$$B_T(j, t; j', t') = \frac{e^{g(j)-g(j')}}{(2\pi)^2} \int_{\xi_1(\theta)} dk' \int_{\xi_1(\theta+\varepsilon)} dk e^{(\sigma(k)-\sigma(k'))T} e^{i\zeta_0 T(k'-k)} \times e^{\varphi_q(k,t)-\varphi_q(k',t')} e^{i(k'j'-kj)} (1 - e^{i(k'-k)})^{-1}. \quad (5.73)$$

As $T \rightarrow \infty$ we obtain

$$\sigma(k) = 2i \sum_{r \geq 1} \frac{e^{-r\tau_0/2}}{r^2} \sin((k - i\tau_0/2)r) + \mathcal{O}(1/T). \quad (5.74)$$

Therefore the terms that increase or decrease exponentially in T in (5.73) are $E(k)$ and $-E(k')$, where

$$E(k) = 2i \sum_{r \geq 1} \frac{e^{-r\tau_0/2}}{r^2} \sin((k - i\tau_0/2)r) - i\zeta_0 k. \quad (5.75)$$

The critical points of $E(k)$ are

$$\pm k_c + i\tau_0/2, \quad k_c = \arccos \left(\cosh(\tau_0/2) - \frac{e^{-\zeta_0 + \tau_0/2}}{2} \right) \in \mathbb{R}. \quad (5.76)$$

For $\text{Im}(k) = \tau_0/2$, $\text{Re}(E(k)) = \zeta_0 \tau_0/2$, the analysis of $\text{Re}(E(k))$ for k close to the line $\text{Im}(k) = \tau_0/2$ shows that, for $\text{Re}(E(k)) \in [-\pi, -k_c] \cup [k_c, \pi]$, it decreases when increasing $\text{Im}(k)$ and, for $\text{Re}(E(k)) \in [-k_c, k_c]$, it decreases when decreasing $\text{Im}(k)$.

Next we transform the integral into a sum of three terms, the first two vanish as $T \rightarrow \infty$ and the third one gives the final result, see Figure 5.1. We have $\int_{I_0} dk' dk \dots = \int_{I_1} dk' dk \dots + \int_{I_2} dk' dk \dots + \int_{I_3} dk' dk \dots$, where the integrand is the one of (5.73). Let us compute the three integrals separately. For the integration along I_3 , first we integrate out k taking the residuum at $k = k'$. Then changing the variable to $z = k' - i\theta$ we obtain

$$\int_{I_3} dk' dk \dots = \frac{1}{2\pi} \int_{-k_c}^{k_c} dz e^{\varphi_q(z+i\theta, t) - \varphi_q(z+i\theta, t')} e^{iz(j'-j)}. \quad (5.77)$$

The asymptotic of $\varphi_q(z + i\theta, t)$ is

$$\varphi(z, t) = \lim_{q \rightarrow 1} \varphi_q(z + i\theta, t) = -t \ln(1 - e^{-\tau_0/2} e^{-iz}). \quad (5.78)$$

The integrals along I_1 and I_2 are treated in the same way. Let us estimate, e.g., the one along I_1 . First we integrate in k . The integral $|\int dk \dots|$, such that the integration avoids the two arcs of circle of radius $\tilde{\varepsilon}$ around the critical points (see Figure 5.1), is bounded by $\mathcal{O}(e^{-a\tilde{\varepsilon}T}/(\tilde{\varepsilon}T))$ for some $a > 0$. $\mathcal{O}(e^{-a\tilde{\varepsilon}T}/T)$ comes from integrating $e^{E(k)T}$ and $\mathcal{O}(1/\tilde{\varepsilon})$ because the minimum of $|k - k'|$ equals $\tilde{\varepsilon}$. The integration through the two arcs around the critical points is bounded by $\mathcal{O}(e^{a'\tilde{\varepsilon}T}/(\tilde{\varepsilon}T))$ for some $a' > 0$, because the integrand is

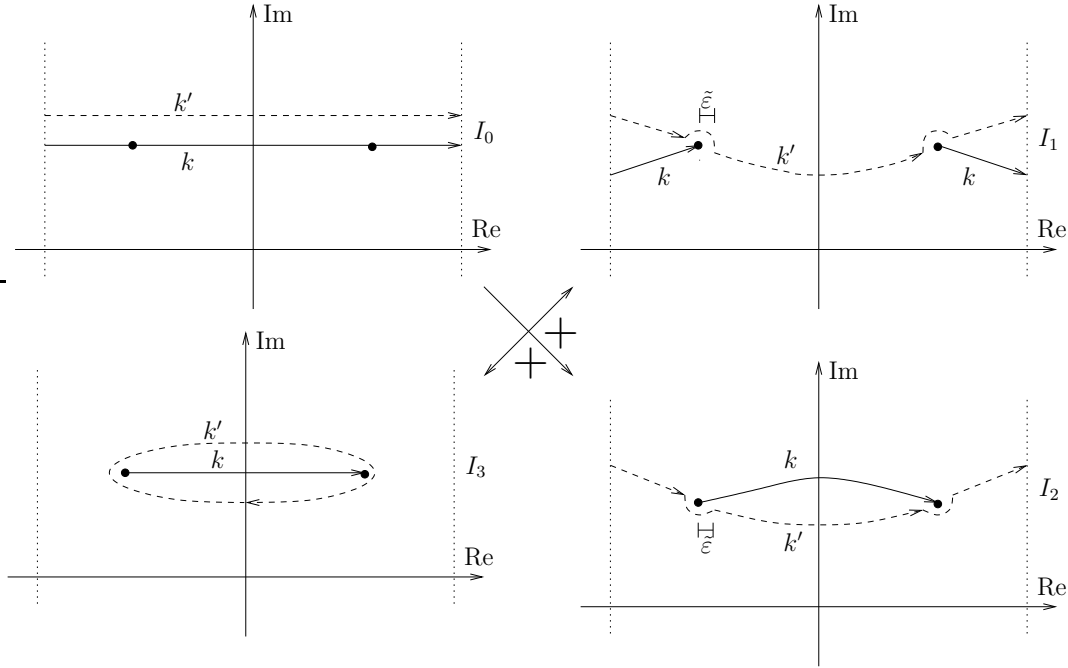


Figure 5.1: Deformation of integration paths. The original integral, along I_0 , is deformed to the sum of integrals along I_1 , I_2 , and I_3 . k is integrated along the dashed lines and k' along the solid lines. The full dots are the critical points of $\sigma(k)$.

at most of $\mathcal{O}(e^{a'\tilde{\varepsilon}T}/\tilde{\varepsilon})$ for some $a' > 0$ and the length of the path of integration is $\mathcal{O}(1/T)$. We choose therefore $\tilde{\varepsilon} = 1/T$, so that $|\int dk \dots| \leq \mathcal{O}(1)$. The integration in k' gives an extra-factor $\mathcal{O}(1/T)$, and

$$\lim_{T \rightarrow \infty} \int_{I_1} dk' dk \dots = 0. \quad (5.79)$$

Summarizing for $t \geq t'$, we have proved that,

$$\lim_{T \rightarrow \infty} B_T(j, t; j', t') = \frac{1}{2\pi} \int_{-\rho\pi}^{\rho\pi} dz e^{\varphi(z, t-t')} e^{iz(j'-j)}, \quad (5.80)$$

where $\rho = k_c/\pi$ and $\varphi(z, t)$ as given in (5.78). In particular for $t = t'$, $\varphi(z, t - t') = 0$, which implies (5.63). The case $t < t'$ is treated in a similar way, leading to

$$\lim_{T \rightarrow \infty} B_T(j, t; j', t') = -\frac{1}{2\pi} \int_{\rho\pi}^{2\pi-\rho\pi} dz e^{\varphi(z, t-t')} e^{iz(j'-j)}. \quad (5.81)$$

Therefore

$$\begin{aligned} \lim_{T \rightarrow \infty} \mathbb{E}_T \left(\prod_{k=1}^m \eta_T^{\text{bulk}}(j_k, t_k) \right) &= \text{Det}(S(j_k, t_k; j_l, t_l))_{1 \leq k, l \leq m} \\ &= \mathbb{E}_b \left(\prod_{k=1}^m \eta^{\text{sine}}(j_k, t_k) \right). \end{aligned} \quad (5.82)$$

The proof for $\tau_0 < 0$ is identical. \square

(5.80), (5.81) define a space-time homogeneous Fermi field. Physically it corresponds to fermions on the lattice \mathbb{Z} in their ground state at density ρ and with kinetic energy

$$E_{\text{kin}}(k) = \ln(1 - e^{-|\tau_0|/2 - ik \operatorname{sgn} \tau_0}). \quad (5.83)$$

E_{kin} is complex reflecting that the fermions have a drift.

The moments (5.82) define a probability measure \mathbb{P}_b on the lozenge tilings of the plane, where the relative fraction of their type depends on the reference point (ζ_0, τ_0) . \mathbb{P}_b is a Gibbs measure in the sense that its conditional expectations satisfy the DLR equations. We refer to [33] of how DLR equations are adjusted in the context of surface models. \mathbb{P}_b is translation invariant with a definite fraction of each type of lozenges. \mathbb{P}_b is even spatially mixing, since truncated correlations decay to zero. One would expect that \mathbb{P}_b is the unique Gibbs measure with these properties. A proof would require that the same limit measure \mathbb{P}_b is obtained when other boundary conditions are imposed, at fixed lozenge chemical potentials. To our knowledge, only for the surface model studied in [33] such a uniqueness property has been established.

5.5 Edge scaling

For the edge scaling one zooms at a macroscopic point lying exactly on the border of the facet, i.e., at $(\zeta_0, \tau_0)T$ with $\zeta_0 = b_\infty(\tau_0)$. For simplicity we set $\tau_0 > 0$. $\tau_0 < 0$ follows by symmetry. Since at the edge the step density is zero, one has to consider a scale coarser than the one for the bulk scaling in Section 5.4. From our study of the PNG droplet we know already that the longitudinal scale is $T^{2/3}$ and the transversal scale is $T^{1/3}$. On that scale the curvature of b_∞ cannot be neglected. Therefore the correct reference points are

$$\begin{aligned} t(s) &= [\tau_0 T + sT^{2/3}], \\ j(r, s) &= [b_\infty(\tau_0)T + b'_\infty(\tau_0)sT^{2/3} + \frac{1}{2}b''_\infty(\tau_0)s^2T^{1/3} + rT^{1/3}]. \end{aligned} \quad (5.84)$$

Note that $(r, s) \in \mathbb{R}^2$. The discrete lattice disappears under edge scaling. Let us abbreviate

$$\begin{aligned} \alpha_1 &= b_\infty(\tau_0) = -2 \ln(1 - e^{-\tau_0/2}), \\ \alpha_2 &= -b'_\infty(\tau_0) = e^{-\tau_0/2}/(1 - e^{-\tau_0/2}), \\ \alpha_3 &= b''_\infty(\tau_0) = e^{-\tau_0/2}/2(1 - e^{-\tau_0/2})^2. \end{aligned} \quad (5.85)$$

Then the edge-scaled random field reads

$$\eta_T^{\text{edge}}(r, s) = T^{1/3} \eta([\alpha_1 T - \alpha_2 sT^{2/3} + \frac{1}{2}\alpha_3 s^2 T^{1/3} + rT^{1/3}], [\tau_0 T + sT^{2/3}]). \quad (5.86)$$

The prefactor $T^{1/3}$ is the volume element for $rT^{1/3}$. Properly speaking we should keep the reference time τ_0 . Since it is fixed throughout, we suppress it in our notation.

Since η_T^{edge} is determinantal, so must be its limit. For the PNG droplet under edge scaling the limit is the Airy random field and, by universality, in our model the steps close

to the facet edge should have the same statistics in the limit $T \rightarrow \infty$. The Airy field is determinantal in space-time with Green's function

$$K^{\text{Airy}}(r, s; r', s') = \text{sgn}(s' - s) \int_{\mathbb{R}} d\lambda \theta(\lambda(s - s')) e^{\lambda(s' - s)} \text{Ai}(r - \lambda) \text{Ai}(r' - \lambda), \quad (5.87)$$

where the step function $\theta(s) = 0$, if $s < 0$, and $\theta(s) = 1$, if $s \geq 0$. The Airy field is stationary in time. In particular, the equal time correlations are given through the Airy kernel

$$\begin{aligned} K^{\text{Airy}}(r, s; r', s) &= \int_{-\infty}^0 d\lambda \text{Ai}(r - \lambda) \text{Ai}(r' - \lambda) \\ &= \frac{1}{r - r'} (\text{Ai}(r) \text{Ai}'(r') - \text{Ai}(r') \text{Ai}'(r)). \end{aligned} \quad (5.88)$$

Theorem 5.4. *Under edge scaling (5.86) the correlation functions have the following limit,*

$$\lim_{T \rightarrow \infty} \mathbb{E}_T \left(\prod_{k=1}^m \eta_T^{\text{edge}}(r_k, s_k) \right) = \mathbb{E} \left(\prod_{k=1}^m \left(\kappa^{-1} \eta^{\text{Airy}} \left(\frac{r_k}{\kappa}, \frac{\kappa}{2} s_k \right) \right) \right) \quad (5.89)$$

uniformly for r_k in a bounded set. Here $\kappa = \sqrt[3]{2b''_\infty(\tau_0)}$. In particular for the process $\eta_T^{\text{edge}}(f, s) = \int dx f(x) \eta_T^{\text{edge}}(x, s)$, smeared over continuous test functions $f : \mathbb{R} \rightarrow \mathbb{R}$ with compact support, one has

$$\lim_{T \rightarrow \infty} \eta_T^{\text{edge}}(f, s) = \int dx f(\kappa x) \eta^{\text{Airy}}(x, s\kappa/2) \quad (5.90)$$

in the sense of the convergence of joint finite-dimensional distributions.

To prove Theorem 5.4 one only has to establish that under edge scaling (5.46) converges to (5.87). We define the rescaled kernel (5.46) as

$$K_T(r, s; r', s') = \frac{e^{-g(r, s)}}{e^{-g(r', s')}} T^{1/3} R_T(j(r, s), t(s); j(r', s'), t(s')) \quad (5.91)$$

where $g(r, s) = -j(r, s)(\tau_0 T \ln(1 - 1/T)/2 + sT^{2/3} \ln(1 - 1/T)/2)$ and $R_T(j, t; j', t')$ from (5.46).

Proposition 5.5. *The edge-scaled kernel (5.91) converges to the Airy kernel*

$$\lim_{T \rightarrow \infty} K_T(r, s; r', s') = \kappa^{-1} K^{\text{Airy}} \left(\frac{r}{\kappa}, \frac{\kappa}{2} s; \frac{r'}{\kappa}, \frac{\kappa}{2} s' \right) \quad (5.92)$$

uniformly for r, r' in bounded sets.

Granted Proposition 5.5 we establish Theorem 5.4.

Proof of Theorem 5.4. From (5.47) and (5.86) it follows that

$$\mathbb{E}_T \left(\prod_{k=1}^m \eta_T^{\text{edge}}(r_k, s_k) \right) = \text{Det} \left(T^{1/3} R_T(j(r_k, s_k), t(s_k); j(r_l, s_l), t(s_l)))_{1 \leq k, l \leq m} \right). \quad (5.93)$$

This determinant does not change when multiplied by the factor $e^{-g(r, s) + g(r', s')}$ and therefore

$$\mathbb{E}_T \left(\prod_{k=1}^m \eta_T^{\text{edge}}(r_k, s_k) \right) = \text{Det}(K_T(r_k, s_k; r_l, s_l))_{1 \leq k, l \leq m}. \quad (5.94)$$

Note that $g(r, s)$ diverges as $T \rightarrow \infty$. On the other hand

$$\mathbb{E} \left(\prod_{k=1}^m \left(\kappa^{-1} \eta^{\text{Airy}} \left(\frac{r_k}{\kappa}, \frac{\kappa}{2} s_k \right) \right) \right) = \text{Det} \left(\kappa^{-1} K^{\text{Airy}} \left(\frac{r_k}{\kappa}, \frac{\kappa}{2} s_k; \frac{r_l}{\kappa}, \frac{\kappa}{2} s_l \right) \right)_{1 \leq k, l \leq m}. \quad (5.95)$$

Theorem 5.4 thus follows from (5.92).

We turn to the proof of Proposition 5.5. As bounded set we fix throughout a centered box $\mathcal{B} \subset \mathbb{R}^d$, where the dimension d depends on the context.

Proof of Proposition 5.5. Let us first consider $s_2 \geq s_1$. By definition of $K_T(r_2, s_2; r_1, s_1)$, (5.39), (5.69), and (5.46), we have

$$\begin{aligned} K_T(r_2, s_2; r_1, s_1) &= \frac{e^{-g(r_1, s_1)}}{e^{-g(r_2, s_2)}} T^{1/3} \times \\ &\times \sum_{l \leq 0} \frac{1}{2\pi} \int_{-\pi}^{\pi} dk e^{-ikj(r_1, s_1)} e^{ikl} e^{\sum_{n \geq 1} (\mu_n e^{ikn} - \nu_n e^{-ikn})} e^{\sum_{n \geq 1} \varphi_n^1 e^{-ikn}} \\ &\times \frac{1}{2\pi} \int_{-\pi}^{\pi} dk' e^{ik'j(r_2, s_2)} e^{-ik'l} e^{-\sum_{n \geq 1} (\mu_n e^{ik'n} - \nu_n e^{-ik'n})} e^{-\sum_{n \geq 1} \varphi_n^2 e^{-ik'n}}, \end{aligned} \quad (5.96)$$

where $\mu_n = q^{n/2}/n(1 - q^n)$, $\nu_n = \mu_n q^{n\tau_0 T}$, and $\varphi_n^i = \nu_n(1 - q^{ns_i T^{2/3}})$. As in Section 5.4 we regard the integrals in (5.96) as complex line integrals and use the notation explained below (5.72).

The integrands in (5.96) are holomorphic away from $\{k \in \mathbb{C} \mid \text{Re}(k) = 0, |\text{Im}(k - i\tau_0/2)| \geq \tau_0/2\}$ and the straight path from $-\pi$ to π can be deformed provided no singularities are touched. In our choice the deformed path has three straight lines, the first one from $-\pi$ to $-\pi + i\beta_i(T)$, the second one from $-\pi + i\beta_i(T)$ to $\pi + i\beta_i(T)$, and the last one from $\pi + i\beta_i(T)$ to π with $\beta_i \in (0, \tau_0)$, see Figure 5.2. To be precise, the path along the real line touches at $k = 0$ the starting point of a branch cut of the term in the exponential, but still the integral remains unchanged by the above deformation. Since the integrands are 2π -periodic along the real axis, the first and the last integrals cancels exactly. $\beta_i(T)$ is determined such that the terms in the exponential are purely imaginary. We obtain

$$\beta_i(T) = -\frac{1}{2} \left(s_i T^{2/3} \ln(1 - 1/T) + \tau_0 T \ln(1 - 1/T) \right), \quad i = 1, 2. \quad (5.97)$$

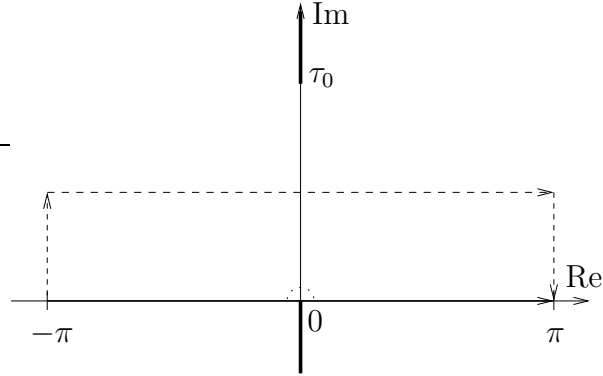


Figure 5.2: Deformation of the integration path. The original integral, from $-\pi$ to π , is deformed along the integral on the dashed path.

We also define $l = LT^{1/3}$. Then the summation goes over $L \in T^{-1/3}(\mathbb{Z}_- \cup \{0\})$ and

$$K_T(r_2, s_2; r_1, s_1) = \frac{e^{-g(r_1, s_1)} T^{1/3}}{e^{-g(r_2, s_2)} 4\pi^2} \sum_{L \in T^{-1/3}(\mathbb{Z}_- \cup \{0\})} \tilde{J}_1(L) \tilde{J}_2(L) e^{\delta_1 - \delta_2}, \quad (5.98)$$

where

$$\delta_i = j(r_i, s_i) \beta_i(T) - \beta_i(T) LT^{1/3} \quad (5.99)$$

and

$$\begin{aligned} \tilde{J}_1(L) &= \int_{-\pi}^{\pi} e^{-ikj(r_1, s_1)} e^{ikLT^{1/3}} \exp \left[2i \sum_{n \geq 1} \mu_n \sin(kn) e^{-\beta_1(T)n} \right] dk, \quad (5.100) \\ \tilde{J}_2(L) &= \int_{-\pi}^{\pi} e^{ik'j(r_2, s_2)} e^{-ik'LT^{1/3}} \exp \left[-2i \sum_{n \geq 1} \mu_n \sin(k'n) e^{-\beta_2(T)n} \right] dk'. \end{aligned}$$

Finally defining $J_i(L) = T^{1/3} \tilde{J}_i(L)$, we have

$$K_T(r_2, s_2; r_1, s_1) = \sum_{L \in T^{-1/3}(\mathbb{Z}_- \cup \{0\})} (4\pi^2 T^{1/3})^{-1} e^{\frac{1}{2}L(s_2 - s_1)(1 + \mathcal{O}(T^{-1}))} J_1(L) J_2(L). \quad (5.101)$$

For the case $s_2 < s_1$ the result is

$$K_T(r_2, s_2; r_1, s_1) = - \sum_{L \in T^{-1/3}(\mathbb{Z}_+ \setminus \{0\})} (4\pi^2 T^{1/3})^{-1} e^{\frac{1}{2}L(s_2 - s_1)(1 + \mathcal{O}(T^{-1}))} J_1(L) J_2(L). \quad (5.102)$$

Now we proceed as follows. First we prove that, as $T \rightarrow \infty$, $J_i(L) \rightarrow \frac{2\pi}{\kappa} \text{Ai}\left(\frac{r_i - L}{\kappa}\right)$ for $L \in \mathcal{B}$, by using the steepest descent curve for the term which is exponentially small in T . Secondly we consider separately $s_2 < s_1$ and $s_2 \geq s_1$. In the latter case, for large L , we need the steepest descent curve for the whole integrand. The same strategy has been

used in [35]. In the case $s_2 < s_1$, for large L , the steepest descend curve does not exist anymore. On the other hand the term $e^{-L(s_1-s_2)}$ serves as a convergence factor and we only need to find bounds for the $J_i(L)$.

Convergence for L in a bounded set

Let $L \in \mathcal{B}$. The integral $J_1(L)$ is written as

$$J_1(L) = T^{1/3} \int_{-\pi}^{\pi} e^{T\psi_{1,T}(k)} e^{ikLT^{1/3}} dk, \quad (5.103)$$

where

$$\psi_{1,T}(k) = -ikT^{-1}j(r_1, s_1) + 2i \sum_{n \geq 1} \frac{\mu_n}{T} e^{-\beta_1 n} \sin(kn). \quad (5.104)$$

We make a saddle point approximation by using a curve which, for small k , is very close to the steepest descend curve for $\psi(k)$, where

$$\psi(k) = \lim_{T \rightarrow \infty} (ikLT^{1/3} + \psi_{1,T}(k))/T \quad (5.105)$$

and the convergence is uniform for $(s_1, r_1, L) \in \mathcal{B}$. For the limit we obtain

$$\psi(k) = \psi_0(k) + 2ik \ln(1 - e^{-\tau_0/2}), \quad (5.106)$$

where

$$\psi_0(k) = \sum_{n \geq 1} 2i \sin(kn) \frac{e^{-n\tau_0/2}}{n^2}. \quad (5.107)$$

In particular $\psi(k)$ is holomorphic in $\mathbb{C} \setminus \{k = x + iy \in \mathbb{C} \mid x = 0, |y| \geq \tau_0/2\}$ and the whole integrand is 2π -periodic along the real axis.

Instead of integrating along the straight path $-\pi \rightarrow \pi$ we integrate along $C = \{k = x + iy, y = -|x|/\sqrt{3}\}$, see Figure 5.3. For x small this path is almost at steepest descend. The real part of $\psi(k)$ reaches its maximum at $k = 0$. To evaluate the errors for x away from zero we prove that the real part of $\psi(k)$ is strictly decreasing for $|x|$ increasing. By symmetry we consider only $x \in [0, \pi]$. A simple computation gives

$$\frac{d\psi(k)}{dx} = -(i + 1/\sqrt{3}) \ln(Q) \quad (5.108)$$

with

$$Q = \frac{(1 - e^{ix+x/\sqrt{3}-\tau_0/2})(1 - e^{-ix-x/\sqrt{3}-\tau_0/2})}{(1 - e^{-\tau_0/2})^2} \quad (5.109)$$

and

$$\begin{aligned} \operatorname{Re}Q &= \frac{\cosh(\tau_0/2) - \cosh(x/\sqrt{3}) \cos(x)}{2 \sinh^2(\tau_0/4)}, \\ \operatorname{Im}Q &= -\frac{\sin(x) \sinh(x/\sqrt{3})}{2 \sinh^2(\tau_0/4)}. \end{aligned} \quad (5.110)$$

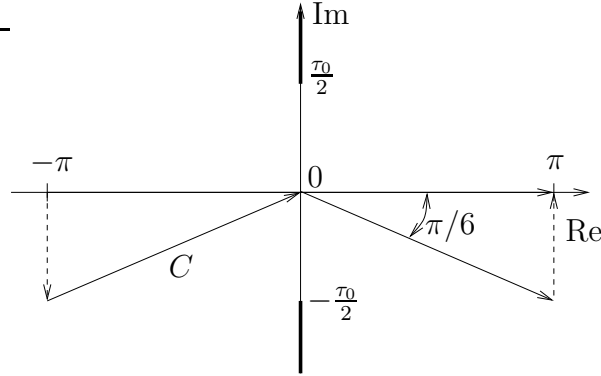


Figure 5.3: Deformation of the integration path. The path from $-\pi$ to π is deformed into C plus the dashed ones.

Using that $\cosh(x/\sqrt{3}) \cos(x) \leq 1$ and is maximal at $x = 0$, we have $\operatorname{Re}Q(x) \geq \operatorname{Re}Q(0) = 1$, the inequality being strict if $x \neq 0$. Obviously $\operatorname{Im}Q \leq 0$. Therefore

$$\operatorname{Re} \left(\frac{d\psi(k)}{dx} \right) = -\frac{1}{2\sqrt{3}} \ln((\operatorname{Re}Q)^2 + (\operatorname{Im}Q)^2) + \arctan(\operatorname{Im}Q/\operatorname{Re}Q) \leq 0 \quad (5.111)$$

for all $x \in [0, \pi]$ and for all $\tau_0 \in (0, \infty)$. The inequality is strict if $x \neq 0$. Since $\frac{d\operatorname{Re}(\psi(k))}{dx} = \operatorname{Re} \left(\frac{d\psi(k)}{dx} \right)$ and by (5.111), $\operatorname{Re}\psi(k)$ is maximal at $k = 0$, $\psi(0) = 0$, and is strictly decreasing for $|x|$ increasing.

Let us fix ε , $0 < \varepsilon \ll 1$, and let C_ε be the part of C with $x \in [-\varepsilon, \varepsilon]$. Then the contribution at $J_1(L)$ coming from $C \setminus C_\varepsilon$ is exponentially small in T .

Lemma 5.6. For some $\delta > 0$,

$$J_1(L) = \mathcal{O}(e^{-\delta T}) + T^{1/3} \int_{C_\varepsilon} e^{\psi_{1,T}(k)T} e^{ikLT^{1/3}} dk. \quad (5.112)$$

Proof. Let \tilde{C}_ε^+ be the part of C with $x \in [\varepsilon, \pi]$ and \tilde{C}_ε^- the one with $x \in [-\pi, -\varepsilon]$. For $x \geq \varepsilon$, $\operatorname{Re}\psi(k) \leq \operatorname{Re}\psi(0) - 2\delta < 0$ for suitable $\delta = \delta(\varepsilon) > 0$. In addition

$$\psi_{1,T}(k)T + ikLT^{1/3} = \psi(k)T + \mathcal{O}((L - r_1)T^{1/3} + s_1T^{2/3}). \quad (5.113)$$

Then

$$\left| \int_{\tilde{C}_\varepsilon^+} e^{\psi_{1,T}(k)T} e^{ikLT^{1/3}} dk \right| \leq e^{-\delta T} \int_\varepsilon^\pi \frac{2}{\sqrt{3}} e^{(\operatorname{Re}\psi(k) - \delta)T} e^{\mathcal{O}((L - r_1)T^{1/3} + s_1T^{2/3})} dx. \quad (5.114)$$

For $(L, s_1, r_1) \in \mathcal{B}$, the integral on the right side is uniformly bounded and therefore

$$\left| \int_{\tilde{C}_\varepsilon^+} e^{\psi_{1,T}(k)T} e^{ikLT^{1/3}} dk \right| = \mathcal{O}(e^{-\delta T}). \quad (5.115)$$

Similarly for the integral along \tilde{C}_ε^- . □

Lemma 5.7. *Uniformly for $(L, r_1, s_1) \in \mathcal{B}$, one has*

$$J_1(L) = \mathcal{O}(e^{-\delta T}) + \mathcal{O}(T^{-1/3}) + \frac{2\pi}{\kappa} \text{Ai}\left(\frac{r_1 - L}{\kappa}\right) \quad (5.116)$$

for large T , with $\kappa = \sqrt[3]{2\alpha_3}$.

Proof. By Lemma 5.6 we have to evaluate the contribution of the integral along C_ε . For k close to 0 we have

$$\begin{aligned} \psi_{1,T}(k)T + ikLT^{1/3} &= -\frac{2}{3}i\alpha_3 k^3 T - ikT^{1/3}(r_1 - L) \\ &+ \mathcal{O}(s_1^2 k + s_1 k^3 T^{2/3} + k^5 T). \end{aligned} \quad (5.117)$$

Let C_ε^+ be the part of C with $x \in [0, \varepsilon]$ and C_ε^- the one with $x \in [-\varepsilon, 0]$. Then $\int_{C_\varepsilon} \cdots = \int_{C_\varepsilon^+} \cdots + \int_{C_\varepsilon^-} \cdots$. We consider explicitly only one of the two integrals, the second being evaluated in the same fashion,

$$\begin{aligned} T^{1/3} \int_{C_\varepsilon^+} e^{\psi_{1,T}(k)T + ikLT^{1/3}} dk &= T^{1/3} \int_{C_\varepsilon^+} e^{-\frac{2}{3}i\alpha_3 k^3 T} e^{-ikT^{1/3}(r_1 - L)} e^{\mathcal{O}(s_1^2 k + s_1 k^3 T^{2/3} + k^5 T)} dk \\ &= T^{1/3} \int_{C_\varepsilon^+} e^{-\frac{2}{3}i\alpha_3 k^3 T} e^{-ikT^{1/3}(r_1 - L)} dk + E_1(L). \end{aligned} \quad (5.118)$$

The error term is the integral along C_ε^+ with integrand

$$\begin{aligned} T^{1/3} e^{-\frac{2}{3}i\alpha_3 k^3 T} e^{-ikT^{1/3}(r_1 - L)} (e^{\mathcal{O}(s_1^2 k + s_1 k^3 T^{2/3} + k^5 T)} - 1) \\ = T^{1/3} e^{-\frac{2}{3}i\alpha_3 k^3 T} e^{-ikT^{1/3}(r_1 - L)} e^{\mathcal{O}(s_1^2 k + s_1 k^3 T^{2/3} + k^5 T)} \mathcal{O}(s_1^2 k + s_1 k^3 T^{2/3} + k^5 T). \end{aligned} \quad (5.119)$$

The term in the exponential is $-\frac{2}{3}i\alpha_3 k^3 T(1 + \chi_1) - ikT^{1/3}(r_1 - L)(1 + \chi_2)$, where χ_1 and χ_2 can be made arbitrarily small by taking ε small enough (s_1 is bounded). With the change of variable $z = kT^{1/3}$ we obtain

$$E_1(L) = \frac{1}{T^{1/3}} \int_{T^{1/3}C_\varepsilon^+} e^{-i\frac{2}{3}\alpha_3(1+\chi_1)z^3 - i(1+\chi_2)(r_1 - L)z} \mathcal{O}(s_1^2 z + s_1 z^3 + z^5 T^{-1/3}) dz. \quad (5.120)$$

Remark that at the boundary of the integration, the real part of the integrand behaves as $e^{-\frac{2}{3}\alpha_3 \varepsilon^3 T}$. This integral is uniformly bounded in T for $(L, r_1, s_1) \in \mathcal{B}$. The same holds for the integral on C_ε^- . Consequently $E_1(L) = \mathcal{O}(T^{-1/3})$.

Next we extend the integration from C_ε to $-\pi T^{1/3}(1, \cos(\pi/6))$ and $\pi T^{1/3}(1, -\cos(\pi/6))$, obtaining the path D_1 . In this way we add an error of $\mathcal{O}(e^{-\delta'(\varepsilon)T})$ with $\delta'(\varepsilon) \sim \varepsilon^3$. Similarly we can complete the path up to $x = \pm N\pi T^{1/3}$, $y = -N\pi T^{1/3}/\sqrt{3}$ by straight lines. The integral is equal to the integration from $-N\pi T^{1/3}$ to $N\pi T^{1/3}$, since the function is $2\pi T^{1/3}$ periodic in the real direction and the

error added by completing the integral is exponentially small in T , for all N . Therefore we may take the limit $N \rightarrow \infty$.

Finally we obtain (5.116), since

$$\int_{-\infty}^{\infty} e^{-i\frac{2}{3}\alpha_3 z^3 - iz(r_1-L)} dz = \frac{2\pi}{\kappa} \text{Ai}\left(\frac{r_1-L}{\kappa}\right) \quad (5.121)$$

with $\kappa = \sqrt[3]{2\alpha_3}$. □

Convergence of $K_T(r_2, s_2; r_1, s_1)$ with $s_2 < s_1$

Lemma 5.8. *Uniformly for $(r_i) \in \mathcal{B}$, $i = 1, 2$,*

$$\lim_{T \rightarrow \infty} K_T(r_2, s_2; r_1, s_1) = - \int_0^{\infty} e^{\frac{1}{2}L(s_2-s_1)} \text{Ai}\left(\frac{r_1-L}{\kappa}\right) \text{Ai}\left(\frac{r_2-L}{\kappa}\right) \frac{dL}{\kappa^2} \quad (5.122)$$

with $\kappa = \sqrt[3]{2\alpha_3}$.

Proof. Since $(r_1, r_2) \in \mathcal{B}$, let us set L_0 such that $L_0 \leq 2(|r_1| + |r_2| + 1)$ for all r_1, r_2 . K_T can be transformed into an integral adding an error $\mathcal{O}(T^{-1/3})$. Let us fix an ε with $0 < \varepsilon \ll 1$. Then

$$\begin{aligned} -K_T(r_2, s_2; r_1, s_1) &= \int_0^{L_0} J_1(L)J_2(L) \frac{e^{-LX}}{4\pi^2} dL + \int_{L_0}^{\varepsilon T^{2/3}} J_1(L)J_2(L) \frac{e^{-LX}}{4\pi^2} dL \\ &\quad + \int_{\varepsilon T^{2/3}}^{\infty} J_1(L)J_2(L) \frac{e^{-LX}}{4\pi^2} dL + \mathcal{O}(T^{-1/3}) \end{aligned} \quad (5.123)$$

with $X = \frac{1}{2}(s_1 - s_2)(1 + \mathcal{O}(1/T)) > 0$. Since $|J_i(L)| \leq T^{1/3}$, $i = 1, 2$, the third term is bounded by $T^{2/3}e^{-\varepsilon T^{2/3}X}/X \rightarrow 0$ as $T \rightarrow \infty$. By Lemma 5.7 the first term converges, uniformly for $(u_i, s_i) \in \mathcal{B}$, to

$$\int_0^{L_0} \text{Ai}\left(\frac{r_1-L}{\kappa}\right) \text{Ai}\left(\frac{r_2-L}{\kappa}\right) e^{L\frac{s_2-s_1}{2}} \frac{1}{\kappa^2} dL \quad (5.124)$$

as $T \rightarrow \infty$.

We consider the second term. We have already established the pointwise convergence of $J_i(L)$ to $\frac{2\pi}{\kappa} \text{Ai}\left(\frac{r_i-L}{\kappa}\right)$. If we obtain that for large T , $|J_i(L)| \leq G$ with a constant G independent of r_i, s_i and $L \in [L_0, \varepsilon T^{2/3}]$, then by dominated convergence

$$\lim_{T \rightarrow \infty} \int_{L_0}^{\varepsilon T^{2/3}} J_1(L)J_2(L) e^{-LX} dL = \int_{L_0}^{\infty} \text{Ai}\left(\frac{r_1-L}{\kappa}\right) \text{Ai}\left(\frac{r_2-L}{\kappa}\right) \frac{e^{\frac{1}{2}L(s_2-s_1)}}{\kappa^2} dL \quad (5.125)$$

uniformly for $(r_i) \in \mathcal{B}$. This property is proven in the following lemma. □

Lemma 5.9. *For $L \in [L_0, \varepsilon T^{2/3}]$, $|J_i(L)| \leq G$ with the constant G independent of s_i, r_i , and L , provided $0 < \varepsilon \ll 1$ and T large enough.*

Proof. The exponential terms in (5.103) are purely imaginary for k real. Let us set

$$\psi_1^I(k) = \frac{1}{i}(ikLT^{-2/3} + \psi_{1,T}(k)), \quad (5.126)$$

then

$$J_1(L) = T^{1/3} \int_{-\pi}^{\pi} e^{i\psi_1^I(k)T} dk. \quad (5.127)$$

In particular for k close to 0,

$$\psi_1^I(k) = -\frac{2}{3}\alpha_3 k^3 (1 + \mathcal{O}(k^2 + s_1 T^{-1/3})) - k(r_1 - L)T^{-2/3} (1 + \mathcal{O}(s_1^2 T^{-1/3})). \quad (5.128)$$

Since $(r_1 - L)T^{-2/3} \sim \mathcal{O}(\varepsilon)$ at most, we set $\tilde{L} = (L - r_1)T^{-2/3}$. $\psi_1^I(k)$ has two local extrema at $\pm k(\tilde{L})$ with

$$k(\tilde{L}) = \sqrt{\tilde{L}}c_0 (1 + \mathcal{O}(\tilde{L} + s_1^2 T^{-1/3})) \quad (5.129)$$

and $c_0 = (2\alpha_3)^{-1/2}$. Moreover for $|k| \geq 2k(\tilde{L})$, $\psi_1^I(k)$ is strictly decreasing. $J_1(L) = \int_{-\pi}^{\pi} \dots = \sum_{i=1}^4 \int_{I_i} \dots$ where $I_1 = [-\pi, -2c_0\sqrt{\tilde{L}}]$, $I_2 = [-2c_0\sqrt{\tilde{L}}, 0]$, $I_3 = [0, 2c_0\sqrt{\tilde{L}}]$, and $I_4 = [2c_0\sqrt{\tilde{L}}, \pi]$. The integrals along I_1 and I_4 are evaluated similarly and so are the integrals along I_2 and I_3 . We present in detail only the integration along I_3 and I_4 . Let $\gamma = \sqrt{\tilde{L}}$. Then

$$\int_{I_4} \dots = T^{1/3} \int_{2c_0\gamma}^{\pi} e^{i\psi_1^I(k)T} dk = T^{1/3} \int_{u(2c_0\gamma)}^{u(\pi)} f(u)e^{iuT} du \quad (5.130)$$

where $u = \psi_1^I(k)$ and $f(u) = \frac{dk(u)}{du}$. Integrating by parts we obtain

$$T^{-1/3} \int_{I_4} \dots = f(u) \frac{e^{iuT}}{iT} \Big|_{u(2c_0\gamma)}^{u(\pi)} - \int_{u(2c_0\gamma)}^{u(\pi)} \frac{df(u)}{du} \frac{e^{iuT}}{iT} du. \quad (5.131)$$

For $k \in I_4$ with $|k| \leq \varepsilon$ follows from (5.128) that $\frac{du}{dk} < 0$ and $\frac{d^2u}{dk^2} \geq 0$. For $k > \varepsilon$,

$$\frac{du}{dk} = \tilde{L} - \ln \left(\frac{1 + e^{-\tau_0} - 2e^{-\tau_0/2} \cos(k)}{1 + e^{-\tau_0} - 2e^{-\tau_0/2}} \right) + \mathcal{O}(s_1 T^{-1/3}). \quad (5.132)$$

Then for $k \in I_4$ with $k > \varepsilon$, $\frac{du}{dk} < 0$ and $\frac{d^2u}{dk^2} \geq 0$. Therefore $\frac{df(u)}{du} = -\left(\frac{du}{dk}\right)^{-3} \frac{d^2u}{dk^2}$ where $\frac{du}{dk} < 0$ and $\frac{d^2u}{dk^2} \geq 0$ for every point in I_4 . Thus $\frac{df(u)}{du}$ does not change sign along I_4 , and

$$\left| \int_{I_4} \dots \right| \leq \frac{2}{T^{2/3}} (|f(u(\pi))| + |f(u(2c_0\gamma))|). \quad (5.133)$$

Using (5.132), for T sufficiently large,

$$\begin{aligned} |f(u(\pi))| &= \left| 2\ln(1 - e^{-\tau_0/2}) - 2\ln(1 + e^{-\tau_0/2}) + \gamma^2 + \mathcal{O}(s_1 T^{-1/3}) \right|^{-1} \\ &\leq \left| \ln(1 - e^{-\tau_0/2}) - \ln(1 + e^{-\tau_0/2}) \right|^{-1} = G_1, \end{aligned} \quad (5.134)$$

provided ε small enough (which implies γ sufficiently small). The second term is bounded by

$$|f(u(2c_0\gamma))| = \left| \frac{1 + \mathcal{O}(\gamma^2 + s_1 T^{-1/3})}{-\gamma^2} \right| \leq 2/\gamma^2 \quad (5.135)$$

for ε small and $s_1 \in \mathcal{B}$. Therefore we have, uniformly in $(r_1, s_1) \in \mathcal{B}$,

$$\left| \int_{I_4} \cdots \right| = \left| \int_{I_1} \cdots \right| \leq \frac{2G_1}{T^{2/3}} + \frac{2}{(L - r_1)} \leq \frac{2G_1}{T^{2/3}} + \frac{2}{(L_0 - r_1)}. \quad (5.136)$$

Next we estimate $\left| \int_{I_3} \cdots \right|$.

$$\int_{I_3} \cdots = T^{1/3} \int_0^{2c_0\gamma} e^{i\psi_1^I(k)T} dk = T^{1/3} \int_{-c_1\gamma}^{c_2\gamma} e^{i\tilde{\psi}(k)T} dk \quad (5.137)$$

where $\tilde{\psi}(k) = \psi_1^I(k - k(\tilde{L}))$, $c_1 = c_0(1 + \mathcal{O}(\gamma))$ and $c_2 = c_0(1 + \mathcal{O}(\gamma))$. Let us define the paths $\xi_0 = \{k = x, x : -c_1\gamma \rightarrow c_2\gamma\}$, $\xi_1 = \{k = -c_1\gamma e^{-i\varphi}, \varphi : 0 \rightarrow \pi/4\}$, $\xi_2 = \{k = e^{-i\pi/4}x, x : -c_1\gamma \rightarrow c_2\gamma\}$, $\xi_3 = \{k = c_2\gamma e^{i\varphi}, \varphi : \pi/4 \rightarrow 0\}$. Then $\int_{I_3} \cdots = \int_{\xi_0} \cdots = \sum_{i=1}^3 \int_{\xi_i} \cdots$. The integrals along ξ_1 and ξ_3 are estimated in the same way.

$$T^{1/3} \int_{\xi_1} e^{i\tilde{\psi}(k)T} dk = T^{1/3} \int_0^{\pi/4} e^{i\varphi} e^{i\tilde{\psi}(k(\varphi))T} i c_0 \gamma (1 + \mathcal{O}(\gamma)) d\varphi \quad (5.138)$$

and therefore

$$\left| T^{1/3} \int_{\xi_1} e^{i\tilde{\psi}(k)T} dk \right| \leq 2T^{1/3} \gamma c_0 \int_0^{\pi/4} e^{-T\text{Im}(\tilde{\psi}(k(\varphi)))} d\varphi. \quad (5.139)$$

Since $\tilde{\psi}(k(\varphi)) = \tilde{\psi}(0) + \frac{1}{2}\tilde{\psi}''(0)k(\varphi)^2(1 + \delta_1(\varphi))$ with $\delta_1(\varphi) \rightarrow 0$ as $\varepsilon \rightarrow 0$ and $k(\varphi)^2 = c_0^2\gamma^2(1 + \mathcal{O}(\gamma))e^{-2i\varphi}$, one has

$$\text{Im}\tilde{\psi}(k(\varphi)) = -\frac{1}{2}\tilde{\psi}''(0)(k(\varphi))^2(1 + \delta_2(\varphi))c_0^2\gamma^2(1 + \mathcal{O}(\gamma))\sin(2\varphi) \quad (5.140)$$

with $\delta_2(\varphi) \rightarrow 0$ as $\varepsilon \rightarrow 0$. Moreover, for ε small enough, $\sin(2\varphi)(1 + \delta_2(\varphi))(1 + \mathcal{O}(\gamma)) \geq \varphi$. From this it follows

$$\begin{aligned} \left| T^{1/3} \int_{\xi_1} e^{i\tilde{\psi}(k)T} dk \right| &\leq 2T^{1/3} c_0 \gamma \int_0^{\pi/4} e^{T c_0^2 \gamma^2 \tilde{\psi}''(0) \varphi / 2} d\varphi \\ &\leq 2T^{1/3} c_0 \gamma \int_0^\infty e^{T c_0^2 \gamma^2 \tilde{\psi}''(0) \varphi / 2} d\varphi = \frac{4T^{1/3} c_0 \gamma}{T c_0^2 \gamma^2 \left| \tilde{\psi}''(0) \right|}. \end{aligned} \quad (5.141)$$

We compute $\tilde{\psi}''(0) = -2\gamma c_0^{-1} (1 + \mathcal{O}(\gamma^2 + s_1 T^{-1/3}))$. Therefore for $s_1 \in \mathcal{B}$ and T large enough,

$$\left| T^{1/3} \int_{\xi_1} e^{i\tilde{\psi}(k)T} dk \right| \leq \frac{4}{(L - r_1)} \leq \frac{4}{(L_0 - r_1)}. \quad (5.142)$$

Next we need to evaluate the integral along ξ_2 ,

$$T^{1/3} \int_{\xi_2} e^{i\tilde{\psi}(k)T} dk = T^{1/3} e^{-i\pi/4} e^{iT\tilde{\psi}(0)} \int_{-c_1\gamma}^{c_2\gamma} e^{T\tilde{\psi}''(0)x^2/2(1+\mathcal{O}(x))} dx. \quad (5.143)$$

Then for sufficiently small δ ,

$$\begin{aligned} \left| T^{1/3} \int_{\xi_2} e^{i\tilde{\psi}(k)T} dk \right| &\leq T^{1/3} \int_{-c_1\gamma}^{c_2\gamma} e^{T\tilde{\psi}''(0)x^2(1+\delta)/2} dx \\ &\leq T^{1/3} \int_{-\infty}^{\infty} e^{T\tilde{\psi}''(0)x^2/4} dx \leq T^{1/3} \int_{-\infty}^{\infty} e^{-x^2 T\gamma/c_0} dx \\ &= \frac{\sqrt{\pi}\sqrt{c_0}}{\sqrt[4]{L - r_1}} = \frac{\sqrt{\pi}\sqrt{c_0}}{\sqrt[4]{L_0 - r_1}}. \end{aligned} \quad (5.144)$$

Thus we have, uniformly for $s_1 \in \mathcal{B}$ and T large enough,

$$\left| \int_{I_3} \dots \right| \leq \frac{8}{(L_0 - r_1)} + \frac{\sqrt{\pi}\sqrt{c_0}}{\sqrt[4]{L_0 - r_1}}. \quad (5.145)$$

Therefore $J_i(L)$ is bounded by

$$|J_i(L)| \leq \frac{4G_1}{T^{2/3}} + \frac{20}{(L_0 - r_i)} + \frac{2\sqrt{\pi}}{\sqrt[4]{2\alpha_3(L_0 - r_i)}}. \quad (5.146)$$

Since $L_0 - r_i \geq 2$ and $X > 0$, it follows that $J_1(L)J_2(L)e^{-LX}$ is bounded by an integrable function on $[L_0, \varepsilon T^{2/3}]$ for $0 < \varepsilon \ll 1$ and T large enough. \square

Convergence of $K_T(r_2, s_2; r_1, s_1)$ with $s_2 \geq s_1$

Lemma 5.10. *Uniformly for $(s_i, r_i) \in \mathcal{B}$, $i = 1, 2$,*

$$\lim_{T \rightarrow \infty} K_T(r_2, s_2; r_1, s_1) = \int_{-\infty}^0 e^{\frac{1}{2}L(s_2 - s_1)} \text{Ai}\left(\frac{r_1 - L}{\kappa}\right) \text{Ai}\left(\frac{r_2 - L}{\kappa}\right) \frac{dL}{\kappa^2} \quad (5.147)$$

with $\kappa = \sqrt[3]{2\alpha_3}$.

Proof. Let us set L_0 such that $L_0 \geq 2(|r_1| + |r_2| + 1)$ for all $(r_1, r_2) \in \mathcal{B}$. Then the sum in K_T can be approximated by an integral at the expense of an error $\mathcal{O}(T^{-1/3})$. Let us fix ε , $0 < \varepsilon \ll 1$. Then

$$\begin{aligned} K_T(r_2, s_2; r_1, s_1) &= \int_{-L_0}^0 J_1(L)J_2(L) \frac{e^{LX}}{4\pi^2} dL + \int_{-\varepsilon T^{2/3}}^{-L_0} J_1(L)J_2(L) \frac{e^{LX}}{4\pi^2} dL \\ &+ \int_{-\infty}^{-\varepsilon T^{2/3}} J_1(L)J_2(L) \frac{e^{LX}}{4\pi^2} dL + \mathcal{O}(T^{-1/3}), \end{aligned} \quad (5.148)$$

with $X = \frac{1}{2}(s_2 - s_1)(1 + \mathcal{O}(1/T)) \geq 0$. The convergence of the first term has already been proved. Let us set $\tilde{L} = -(L - r_1)T^{-2/3}$. In the remainder of the proof we set

$$\psi(k) = \frac{1}{i}\psi_{1,T}(k) - k\tilde{L}. \quad (5.149)$$

First consider $\tilde{L} \geq \varepsilon$.

$$J_1(L) = T^{1/3} \int_{-\pi}^{\pi} e^{\psi(k)T} dk. \quad (5.150)$$

With the change of variable $u = \psi(k)$, $f(u) = \frac{dk(u)}{du}$, and integration by parts, we have

$$|J_1(L)| \leq T^{1/3} \frac{2\psi(\pi)}{T} \max_{k \in [\psi(-\pi), \psi(\pi)]} \left| \frac{df(u)}{du} \right|. \quad (5.151)$$

To compute $\left| \frac{df(u)}{du} \right|$ we use $\frac{df(u)}{du} = -\left(\frac{du}{dk}\right)^{-3} \frac{d^2u}{dk^2}$. $\left| \frac{du}{dk} \right|$ is (5.132) with \tilde{L} replaced by $-\tilde{L}$. It is easy then to see that uniformly for $s_1 \in \mathcal{B}$, $\max_{k \in [\psi(-\pi), \psi(\pi)]} \left| \frac{df(u)}{du} \right| \leq G_1 \tilde{L}^{-1}$ for $G_1 = 2/(\sinh(\tau_0/2)\varepsilon)^2 < \infty$. Then for a suitable constant $G_2 < \infty$,

$$|J_1(L)| \leq G_2(r_1 - L)^{-1}. \quad (5.152)$$

The same holds for J_2 , therefore the third term in (5.148) is bounded by

$$\int_{-\infty}^{-\varepsilon T^{2/3}} \frac{G_2^2}{(L + |r_1| + |r_2|)^2} dL, \quad (5.153)$$

which is convergent for T finite and vanishes for $T \rightarrow \infty$.

Finally we consider $0 < \tilde{L} \leq \varepsilon$. Let us set $\beta = \sqrt{2(\cosh(\tau_0/2) - 1)}$. We integrate over $C = \left\{ k = x + iy(x), y(x) = -\sqrt{y(0)^2 + x^2/3} \right\}$, with $iy(0)$ the stationary point of $\psi(\cdot, \tilde{L})$, see Figure 5.4. $y(0) = -\beta\sqrt{\tilde{L}} + \mathcal{O}(\tilde{L}^{3/2})$ and C is almost the steepest descend curve for x small. This path has the property that the real part of $\psi(k)$ is strictly decreasing as $|x|$ increases and

$$\psi(iy(0)) = -\frac{2}{3}\beta\tilde{L}^{3/2} \left(1 + \mathcal{O}\left(s_1^2 T^{-1/3} + \tilde{L}\right) \right). \quad (5.154)$$

We divide the integral in the part with $|x| \leq \varepsilon$ and the remainder,

$$J_1(L) = T^{1/3} \int_{-\pi}^{\pi} e^{\psi(k)T} dk = T^{1/3} \int_C e^{\psi(k)T} dk = T^{1/3} \int_{C_\varepsilon} e^{\psi(k)T} dk + E_2(L), \quad (5.155)$$

where

$$E_2(L) = T^{1/3} \int_{C \setminus C_\varepsilon} e^{\psi(k)T} dk = \mathcal{O}\left(e^{-\delta T} e^{\psi(x=0)T}\right) = \mathcal{O}\left(e^{-\delta T} e^{-\frac{2}{3}\beta(r_1 - L)^{3/2}}\right). \quad (5.156)$$

We then need to integrate only close to $x = 0$. We first establish some properties of $\psi(k)$ for $x = 0$.

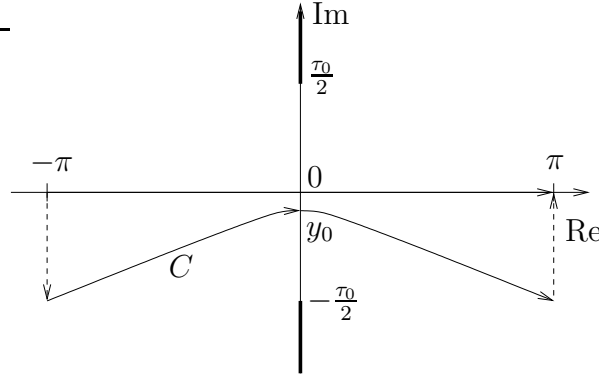


Figure 5.4: Deformation of the integration path. The path from $-\pi$ to π is deformed into C plus the dashed ones.

Lemma 5.11.

$$\begin{aligned}
 i) \quad \psi(iy(0), \tilde{L}) &= -\frac{2}{3}\beta\tilde{L}^{3/2} + \mathcal{O}\left(\tilde{L}^{5/2} + \tilde{L}^{3/2}s_1^2T^{-1/3}\right), \\
 ii) \quad \frac{d\psi(k, \tilde{L})}{dk}\Big|_{k=iy(0)} &= 0, \\
 iii) \quad \frac{d^2\psi(k, \tilde{L})}{dk^2}\Big|_{k=iy(0)} &= -\frac{2}{\beta}\sqrt{\tilde{L}} + \mathcal{O}\left(\tilde{L} + \sqrt{\tilde{L}}s_1T^{-1/3}\right), \\
 iv) \quad \frac{d^3\psi(k, \tilde{L})}{dk^3}\Big|_{k=iy(0)} &= -\frac{2}{\beta^2}i + \mathcal{O}\left(\tilde{L} + s_1T^{-1/3}\right).
 \end{aligned} \tag{5.157}$$

Proof. i) follows from Equation (5.154) and ii) because $k = iy(0)$ is a stationary point of $\psi(\cdot, \tilde{L})$. iv) follows from (5.117) because $2\alpha_3 = 1/\beta^2$. Finally let $\lambda = \sqrt{\tilde{L}}$. Then

$$\frac{d}{d\lambda} \frac{d^2\psi(k, \tilde{L})}{dk^2} = \frac{d^3\psi(k, \tilde{L})}{dk^3} \frac{dk}{d\lambda} \tag{5.158}$$

and evaluating at $k = iy(0)$ and $\lambda = 0$ we obtain iii). \square

With these properties

$$\begin{aligned}
 J_1(L) - E_2(L) &= T^{1/3} \int_{C_\varepsilon} e^{\psi(k)T} dk \\
 &= e^{-\frac{2}{3}\beta\tilde{L}^{3/2}T} e^{\mathcal{O}(\tilde{L}^{5/2}T + \tilde{L}^{3/2}s_1^2T^{2/3})} T^{1/3} \int_{C_\varepsilon} dk e^{-\frac{1}{\beta}\sqrt{\tilde{L}}(k-iy(0))^2T} e^{-\frac{i}{3\beta^2}(k-iy(0))^3T} \\
 &\quad \times e^{\mathcal{O}\left(\tilde{L}(k-iy(0))^2T + \sqrt{\tilde{L}}(k-iy(0))^2s_1T^{2/3} + \tilde{L}(k-iy(0))^3T + (k-iy(0))^3s_1T^{2/3} + (k-iy(0))^4T\right)}.
 \end{aligned} \tag{5.159}$$

Let $\gamma = \sqrt{r_1 - \tilde{L}}$, then $\sqrt{\tilde{L}} = \gamma T^{-1/3}$. Let $k' = k - iy(0)$, then the integration is along $C'_\varepsilon = C_\varepsilon + iy(0)$.

$$\begin{aligned}
 J_1(L) - E_2(L) &= e^{-\frac{2}{3}\beta\gamma^3} e^{\mathcal{O}(\gamma^5T^{-2/3} + \gamma^3s_1^2T^{-1/3})} T^{1/3} \int_{C'_\varepsilon} dk e^{-\frac{\gamma}{\beta}k^2T^{2/3}} e^{-\frac{i}{3\beta^2}k^3T} \\
 &\quad \times \exp[\mathcal{O}(\gamma^2k^2T^{1/3} + \gamma s_1k^2T^{1/3} + \gamma^2k^3T^{1/3} + k^3s_1T^{2/3} + k^4T)].
 \end{aligned} \tag{5.160}$$

Since \tilde{L} can be made arbitrarily small, for $s_1 \in \mathcal{B}$ the exponent of the term in the integral can be written as

$$-\frac{\gamma}{\beta}k^2T^{2/3}(1+\chi_1) - \frac{i}{3\beta^2}k^3T(1+\chi_2), \quad (5.161)$$

where the χ_i can be made as small as desired by choosing ε small enough. After the change of variable $kT^{1/3} = z$ the integral becomes

$$\int_{C'_\varepsilon T^{1/3}} dz e^{-\frac{\gamma}{\beta}z^2(1+\chi_1)} e^{-\frac{i}{3\beta^2}z^3(1+\chi_2)}. \quad (5.162)$$

The integration is taken along a contour, symmetric with respect to the imaginary axis and such that for $\operatorname{Re}(z) \geq 0$, $\arg(z) \in [-\pi/6, 0]$. This implies that the integral is uniformly bounded.

Replacing the term in front of the integral (5.160) by one, the error can be estimated as

$$e^{-\frac{2}{3}\beta\gamma^3} \left(e^{\mathcal{O}(\gamma^5 T^{-2/3} + \gamma^3 s_1^2 T^{-1/3})} - 1 \right), \quad (5.163)$$

since the integral in (5.160) is bounded. For $\tilde{L} \leq \varepsilon$,

$$(r_1 - L)^{5/2} T^{-2/3} + (r_1 - L)^3 T^{-1/3} \leq (r_1 - L)^{3/2} \varepsilon + (r_1 - L) \sqrt{\varepsilon}. \quad (5.164)$$

As a consequence

$$\begin{aligned} e^{-\frac{2}{3}\beta\gamma^3} \left(e^{\mathcal{O}(\gamma^5 T^{-2/3} + \gamma^3 s_1^2 T^{-1/3})} - 1 \right) &\leq \mathcal{O} \left(e^{-\frac{\beta}{2}\gamma^3} (\gamma^5 T^{-2/3} + \gamma^3 s_1^2 T^{-1/3}) \right) \\ &\leq \mathcal{O} \left(T^{-1/3} e^{-\frac{\beta}{2}(r_1 - L)^{3/2}} \right). \end{aligned} \quad (5.165)$$

After this step we can also remove the error inside the integral (5.160). As in the case of $L \in \mathcal{B}$, the removal of this error leads to an additional error of $T^{-1/3}$ with the prefactor $e^{-\frac{2}{3}\beta(r_1 - L)^{3/2}}$. Consequently we have obtained

$$\begin{aligned} J_1(L) &= e^{-\frac{2}{3}\beta(r_1 - L)^{3/2}} \int_{C'_\varepsilon T^{1/3}} dz e^{-\frac{\gamma}{\beta}z^2} e^{-\frac{i}{3\beta^2}z^3} + \mathcal{O} \left(T^{-1/3} e^{-\frac{2}{3}\beta(r_1 - L)^{3/2}} \right) \\ &+ \mathcal{O} \left(T^{-1/3} e^{-\frac{1}{2}\beta(r_1 - L)^{3/2}} \right) + \mathcal{O} \left(e^{-\delta T} e^{-\frac{2}{3}\beta(r_1 - L)^{3/2}} \right). \end{aligned} \quad (5.166)$$

Next we change to the variable $z = w + i\beta\sqrt{r_1 - L}$. The integral becomes

$$\int_{C'_\varepsilon T^{1/3} + i\beta\gamma} e^{-\frac{i}{3\beta^2}w^3 - i(r_1 - L)w} dw. \quad (5.167)$$

Finally completing the contour of the integration such that it goes to infinity in the directions $\arg(w) = \varphi_\pm$ with $\varphi_+ = -\pi/6$ and $\varphi_- = -5\pi/6$ leads to an exponentially small error. Using that $2\alpha_3 = 1/\beta^2$, the main term goes to $\frac{2\pi}{\kappa} \operatorname{Ai} \left(\frac{r_1 - L}{\kappa} \right)$. Since the errors are integrable in L and go to zero as $T \rightarrow \infty$, we obtain, for $s_2 \geq s_1$,

$$\lim_{T \rightarrow \infty} K_T(r_2, s_2; r_1, s_1) = \int_{-\infty}^0 e^{\frac{1}{2}L(s_2 - s_1)} \operatorname{Ai} \left(\frac{r_1 - L}{\kappa} \right) \operatorname{Ai} \left(\frac{r_2 - L}{\kappa} \right) \frac{dL}{\kappa^2} \quad (5.168)$$

with $\kappa = \sqrt[3]{2\alpha_3}$. \square

With the change of variable $\lambda = L/\kappa$, (5.168) is rewritten as

$$\begin{aligned} \lim_{T \rightarrow \infty} K_T(r_2, s_2; r_1, s_1) &= \kappa^{-1} \int_{-\infty}^0 e^{\frac{1}{2}\lambda(s_2-s_1)\kappa} \text{Ai}\left(\frac{r_1}{\kappa} - \lambda\right) \text{Ai}\left(\frac{r_2}{\kappa} - \lambda\right) d\lambda \\ &= \kappa^{-1} K^{\text{Airy}}\left(\frac{r_2}{\kappa}, \frac{\kappa}{2}s_2; \frac{r_1}{\kappa}, \frac{\kappa}{2}s_1\right). \end{aligned} \quad (5.169)$$

5.6 Proof of Theorem 5.1

Now we have all the elements to prove our main theorem.

Proof of Theorem 5.1. Let f_i be the indicator function of (a_i, ∞) . Then (5.4) corresponds to

$$\lim_{T \rightarrow \infty} \mathbb{P}_T\left(\bigcap_{i=1}^m \{\eta_T^{\text{edge}}(f_i, s_i) = 0\}\right) = \mathbb{P}\left(\bigcap_{i=1}^m \{\eta^{\text{Airy}}(f_i/\kappa, s_i\kappa/2) = 0\}\right). \quad (5.170)$$

We choose a large enough and split $f_i = f_i^a + g^a$ with f_i^a the indicator function of $(a_i, a]$ and g^a the one of (a, ∞) . Then

$$\begin{aligned} \left| \mathbb{P}_T\left(\bigcap_{i=1}^m \{\eta_T^{\text{edge}}(f_i, s_i) = 0\}\right) - \mathbb{P}_T\left(\bigcap_{i=1}^m \{\eta_T^{\text{edge}}(f_i^a, s_i) = 0\}\right) \right| &\leq \\ &\leq \sum_{i=1}^m \mathbb{P}_T\left(\eta_T^{\text{edge}}(g^a, s_i) \geq 1\right). \end{aligned} \quad (5.171)$$

The term

$$\mathbb{P}_T\left(\bigcap_{i=1}^m \{\eta_T^{\text{edge}}(f_i^a, s_i) = 0\}\right) \quad (5.172)$$

converges to

$$\mathbb{P}\left(\bigcap_{i=1}^m \{\eta^{\text{Airy}}(f_i^a/\kappa, s_i\kappa/2) = 0\}\right) \quad (5.173)$$

which yields the right hand side of (5.4) as $a \rightarrow \infty$.

The terms in the sum of the right hand side of (5.171) are bounded by

$$\mathbb{P}_T\left(\eta_T^{\text{edge}}(g^a, s_i) \geq 1\right) \leq \mathbb{E}_T\left(\eta_T^{\text{edge}}(g^a, s_i)\right) = \int_a^\infty \mathbb{E}_T\left(\eta_T^{\text{edge}}(r, s_i)\right) dr. \quad (5.174)$$

From (5.101),

$$\mathbb{E}_T\left(\eta_T^{\text{edge}}(r, s_i)\right) \simeq \int_0^\infty \frac{1}{4\pi^2} J_1(-L)^2 dL. \quad (5.175)$$

$J_1(-L)$ is indeed a function of $r+L$, which asymptotics has been studied already for $r+L$ large, but bounded by $r+L \leq \varepsilon T^{2/3}$, with the result (5.166). Therefore the integrals in (5.174), (5.175) converge for $r+L \leq \varepsilon T^{2/3}$.

Next consider $r+L > \varepsilon T^{2/3}$. Let $\tilde{L} = (r+L)T^{-2/3}$. With the change of variable $u = \psi(k)$ and integrating twice by parts, we obtain

$$|J_1(-L)| \leq T^{1/3} \frac{2\psi(\pi)}{T^2} \max_{k \in [\psi(-\pi), \psi(\pi)]} \left| \frac{d^3 k(u)}{du^3} \right|. \quad (5.176)$$

Similarly as for (5.152) we have,

$$\max_{k \in [\psi(-\pi), \psi(\pi)]} \left| \frac{d^3 k(u)}{du^3} \right| \leq G_1 \tilde{L}^{-2}, \quad (5.177)$$

for a suitable constant $G_1 < \infty$, which yields

$$|J_1(-L)| \leq G_2 (r+L)^{-2} T^{-1/3} \quad (5.178)$$

for some constant $G_2 < \infty$. Therefore the integrals in (5.174), (5.175) have a bound $G(a)$ uniform in T which vanishes as $a \rightarrow \infty$

5.A Appendix: fermionic correlations

5.A.1 Two-point function

Let $\hat{A} = \sum_{k,l \in \mathbb{Z}} A_{k,l} a_k^* a_l$ be the second quantization of the one-particle matrix A . It is assumed that $e^{-\hat{A}}$ is trace class and $\text{Det}(1 + e^A) \neq 0$ (see [85], Chap. XIII). We use the identities

$$e^{-\hat{A}} a_i^* e^{\hat{A}} = \sum_{j \in \mathbb{Z}} a_j^* [e^{-A}]_{j,i}, \quad e^{-\hat{A}} a_i e^{\hat{A}} = \sum_{j \in \mathbb{Z}} [e^A]_{i,j} a_j. \quad (5.179)$$

Then

$$\begin{aligned} \langle a_i^* a_j \rangle &= \frac{1}{\mathcal{Z}} \text{Tr}(e^{-\hat{A}} a_i^* a_j) = \sum_{n \in \mathbb{Z}} \frac{1}{\mathcal{Z}} \text{Tr}(a_n^* [e^{-A}]_{n,i} e^{-\hat{A}} a_j) \\ &= \sum_{n \in \mathbb{Z}} [e^{-A}]_{n,i} (-\langle a_n^* a_j \rangle + \delta_{j,n}) = [e^{-A}]_{j,i} - \sum_{n \in \mathbb{Z}} \langle a_n^* a_j \rangle [e^{-A}]_{n,i}, \end{aligned} \quad (5.180)$$

and

$$\sum_{n \in \mathbb{Z}} \langle a_n^* [\mathbb{1} + e^{-A}]_{n,i} a_j \rangle = [e^{-A}]_{j,i}. \quad (5.181)$$

Finally multiplying this expression by $\sum_{i \in \mathbb{Z}} [(\mathbb{1} + e^{-A})^{-1}]_{i,m}$ we obtain

$$\langle a_m^* a_j \rangle = [(\mathbb{1} + e^A)^{-1}]_{j,m}. \quad (5.182)$$

5.A.2 Proof of (5.41)-(5.43)

We prove recursively that

$$\langle a_{i_1}^* a_{j_1} \cdots a_{i_n}^* a_{j_n} \rangle = \text{Det}(R(i_k, j_l))_{1 \leq k, l \leq n}, \quad (5.183)$$

where

$$R(i_k, j_l) = \begin{cases} \langle a_{i_k}^* a_{j_l} \rangle & \text{if } k \leq l, \\ -\langle a_{j_l} a_{i_k}^* \rangle & \text{if } k > l. \end{cases} \quad (5.184)$$

Then, taking $i_k = j_k$ for all k , the result (5.41)-(5.43) is obtained. For $n = 1$ the formula holds by definition. Suppose the formula (5.183) has been established for some n , i.e.

$$\langle a_{i_1}^* a_{j_1} \cdots a_{i_n}^* a_{j_n} \rangle = \begin{vmatrix} \langle a_{i_1}^* a_{j_1} \rangle & \langle a_{i_1}^* a_{j_2} \rangle & \cdots & \langle a_{i_1}^* a_{j_n} \rangle \\ -\langle a_{j_2} a_{i_1}^* \rangle & \langle a_{i_2}^* a_{j_2} \rangle & \cdots & \langle a_{i_2}^* a_{j_n} \rangle \\ \vdots & \vdots & \ddots & \vdots \\ -\langle a_{j_n} a_{i_1}^* \rangle & -\langle a_{j_n} a_{i_2}^* \rangle & \cdots & \langle a_{i_n}^* a_{j_n} \rangle \end{vmatrix}. \quad (5.185)$$

We will need one more expression for $\langle \cdots \rangle$ such that in the first k pairs the annihilation operator precedes the creation operator,

$$\begin{aligned} & \langle a_{j_1} a_{i_1}^* \cdots a_{j_k} a_{i_k}^* a_{i_{k+1}}^* a_{j_{k+1}} \cdots a_{i_n}^* a_{j_n} \rangle = \\ & = (-1)^k \begin{vmatrix} -\langle a_{j_1} a_{i_1}^* \rangle & \cdots & \langle a_{i_1}^* a_{j_k} \rangle & \langle a_{i_1}^* a_{j_{k+1}} \rangle & \cdots & \langle a_{i_1}^* a_{j_n} \rangle \\ \vdots & \ddots & \vdots & \vdots & \ddots & \vdots \\ -\langle a_{j_k} a_{i_1}^* \rangle & \cdots & -\langle a_{j_k} a_{i_k}^* \rangle & \langle a_{i_k}^* a_{j_{k+1}} \rangle & \cdots & \langle a_{i_k}^* a_{j_n} \rangle \\ -\langle a_{j_{k+1}} a_{i_1}^* \rangle & \cdots & -\langle a_{j_{k+1}} a_{i_k}^* \rangle & \langle a_{i_{k+1}}^* a_{j_{k+1}} \rangle & \cdots & \langle a_{i_{k+1}}^* a_{j_n} \rangle \\ \vdots & \ddots & \vdots & \vdots & \ddots & \vdots \\ -\langle a_{j_n} a_{i_1}^* \rangle & \cdots & -\langle a_{j_n} a_{i_k}^* \rangle & -\langle a_{j_n} a_{i_{k+1}}^* \rangle & \cdots & \langle a_{i_n}^* a_{j_n} \rangle \end{vmatrix}. \end{aligned} \quad (5.186)$$

Let us prove this formula. For $k = 0$, it agrees with (5.185). Suppose it to be true for some k . Let us then prove that the formula (5.186) holds for $k + 1$,

$$\begin{aligned} & \langle a_{j_1} a_{i_1}^* \cdots a_{j_{k+1}} a_{i_{k+1}}^* a_{i_{k+2}}^* a_{j_{k+2}} \cdots a_{i_n}^* a_{j_n} \rangle = \\ & = -\langle a_{j_1} a_{i_1}^* \cdots a_{j_k} a_{i_k}^* a_{i_{k+1}}^* a_{j_{k+1}} \cdots a_{i_n}^* a_{j_n} \rangle \\ & \quad + \delta_{i_{k+1}, j_{k+1}} \langle a_{j_1} a_{i_1}^* \cdots a_{j_k} a_{i_k}^* a_{i_{k+2}}^* a_{j_{k+2}} \cdots a_{i_n}^* a_{j_n} \rangle. \end{aligned} \quad (5.187)$$

Using the expression (5.186) and considering the expansion of the determinant in the $(k + 1)^{\text{th}}$ column (or row), it is easy to see that (5.187) corresponds, up to a factor of -1 , to the expression (5.186) but with the diagonal term $a_{i_{k+1}}^* a_{j_{k+1}}$ replaced by $-a_{j_{k+1}} a_{i_{k+1}}^*$. Therefore (5.186) holds for $k + 1$, too.

Now we prove (5.185) for $n + 1$ by using (5.185) for n and (5.186) for n and $k \leq n$,

$$\begin{aligned}
\langle a_q^* a_{j_1} \cdots a_{i_{n+1}}^* a_{j_{n+1}} \rangle &= \frac{1}{Z} \text{Tr}(e^{-\hat{A}} a_q^* a_{j_1} \cdots a_{i_{n+1}}^* a_{j_{n+1}}) \\
&= \sum_{m \in \mathbb{Z}} \frac{1}{Z} [e^{-A}]_{m,q} \text{Tr}(e^{-\hat{A}} a_{j_1} \cdots a_{i_{n+1}}^* a_{j_{n+1}} a_m^*) \\
&= - \sum_{m \in \mathbb{Z}} [e^{-A}]_{m,q} \langle a_m^* a_{j_1} \cdots a_{i_{n+1}}^* a_{j_{n+1}} \rangle \\
&\quad + \sum_{p=2}^{n+1} [e^{-A}]_{j_p,q} \langle a_{j_1} a_{i_2}^* \cdots a_{j_{p-1}} a_{i_p}^* a_{i_{p+1}}^* a_{j_{p+1}} \cdots a_{i_{n+1}}^* a_{j_{n+1}} \rangle \\
&\quad + [e^{-A}]_{j_1,q} \langle a_{i_2}^* a_{j_2} \cdots a_{i_{n+1}}^* a_{j_{n+1}} \rangle.
\end{aligned} \tag{5.188}$$

We take the term with the sum over $m \in \mathbb{Z}$ together with the first one and multiply the whole expression by $\sum_{q \in \mathbb{Z}} [(\mathbb{1} + e^{-A})^{-1}]_{q,i_1}$ to obtain

$$\begin{aligned}
\langle a_{i_1}^* a_{j_1} \cdots a_{i_{n+1}}^* a_{j_{n+1}} \rangle &= \langle a_{i_1}^* a_{j_1} \rangle \langle a_{i_2}^* a_{j_2} \cdots a_{i_{n+1}}^* a_{j_{n+1}} \rangle \\
&\quad + \sum_{p=2}^{n+1} \langle a_{i_1}^* a_{j_p} \rangle \langle a_{j_1} a_{i_2}^* \cdots a_{j_{p-1}} a_{i_p}^* a_{i_{p+1}}^* a_{j_{p+1}} \cdots a_{i_{n+1}}^* a_{j_{n+1}} \rangle.
\end{aligned} \tag{5.189}$$

Using (5.185) and (5.186) for n terms we see that this last expression is nothing else than the expansion with respect to the first row of (5.185) with n substituted by $n + 1$.

Appendix

A.1 Equilibrium crystal shape geometry

As illustrated in Figure A.5, we define

$$x = x_0 + \delta, \quad y = y_0 + f'(x_0)\delta - \varepsilon \quad (\text{A.1})$$

and

$$\tilde{x} = x - x_0, \quad \tilde{y} = y - y_0. \quad (\text{A.2})$$

If $z(\varepsilon, \delta) \cong -\frac{2}{3}\gamma_{PT}\varepsilon^{3/2}$, then

$$z(\tilde{x}, \tilde{y}) \cong -\frac{2}{3}\gamma_{PT}(f'(x_0)\tilde{x} - \tilde{y})^{3/2}. \quad (\text{A.3})$$

Let $p_x = \partial_x z$, $p_y = \partial_y z$, and θ the angle between the x -axis and the outer normal to the facet. Then $f'(x_0) = -\text{ctan } \theta$. The surface profile and the free-energy density (surface tension) per unit projected are the Legendre transform one of the other [8]

$$z(x, y) = \ell \hat{f}(x/\ell, y/\ell), \quad f(p_x, p_y) = \ell^{-1}(z - xp_x - yp_y). \quad (\text{A.4})$$

Close to the flat surface, some algebra leads to

$$f(|\mathbf{p}|) = \gamma(\theta)|\mathbf{p}| + B(\theta)|\mathbf{p}|^3 \quad (\text{A.5})$$

with

$$\gamma(\theta) = \frac{\text{ctan}(\theta)x_0 - y_0}{\ell\sqrt{1 + \text{ctan}(\theta)^2}}, \quad B(\theta) = \frac{1}{3\ell\gamma_{PT}^2(1 + \text{ctan}(\theta)^2)^{3/2}}. \quad (\text{A.6})$$

Defining $\kappa = f''(x_0)$ it follows that $\frac{dx_0}{d\theta} = (1 + \text{ctan}(\theta)^2)\kappa^{-1}$ and $\frac{dy_0}{d\theta} = -\text{ctan}(\theta)(1 + \text{ctan}(\theta)^2)\kappa^{-1}$. The stiffness $\tilde{\gamma}$ is then

$$\tilde{\gamma}(\theta) = \gamma(\theta) + \gamma''(\theta) = \frac{(1 + \text{ctan}(\theta)^2)^{3/2}}{\kappa\ell}, \quad (\text{A.7})$$

therefore

$$\tilde{\gamma}(\theta)B(\theta) = \frac{1}{3\ell^2\kappa\gamma_{PT}^2} = \frac{\pi^2}{6}, \quad (\text{A.8})$$

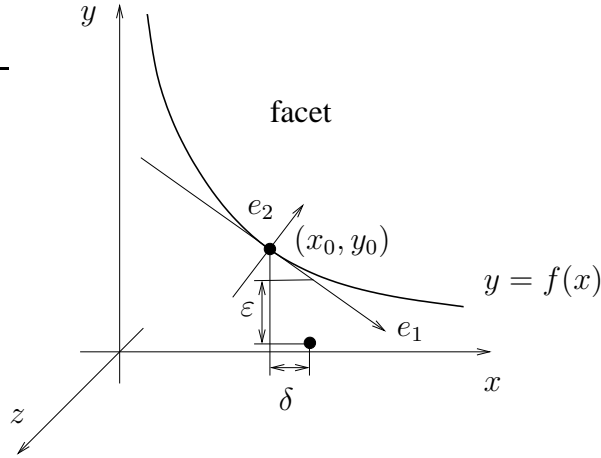


Figure A.5: The facet in the $x - y$ plane goes into the rounded surface in the negative z .

where the last equality in (A.7) comes from thermodynamics [4]. γ_{PT} , κ , and σ^2 are the PT coefficient, the second derivative of the border line, and the local wandering coefficient in the (x, y, z) coordinate axis. The change of coordinate from (x, y) to (e_1, e_2) leads to the PT coefficient, the curvature, and the local wandering coefficient in the orthogonal coordinate axis, $\gamma_{PT,\perp}$, κ_\perp , and σ_\perp^2 namely

$$\begin{aligned}\kappa_\perp(\theta) &= \kappa(1 + \cotan(\theta)^2)^{-3/2}, \\ \gamma_{PT,\perp}(\theta) &= \gamma_{PT}(1 + \cotan(\theta)^2)^{3/4}, \\ \sigma_\perp^2(\theta) &= \sigma^2(1 + \cotan(\theta)^2)^{-3/2}.\end{aligned}\tag{A.9}$$

A.2 Fredholm determinant and Fredholm Pfaffian

A.2.1 Preliminaries

These notions are taken from [83], Chapter VI. Let \mathcal{H} be a separable Hilbert space. Denote by $\mathcal{L}(\mathcal{H})$ the set of all bounded linear operator from \mathcal{H} to \mathcal{H} . Let $\{\varphi_n\}_{n=1}^\infty$ be an orthonormal basis of \mathcal{H} . Then, for any positive operator $A \in \mathcal{L}(\mathcal{H})$, the *trace* is defined by $\text{Tr}(A) = \sum_{n=1}^\infty \langle \varphi_n, A\varphi_n \rangle$.

An operator $A \in \mathcal{L}(\mathcal{H})$ is called *trace class* if and only if $\text{Tr}(|A|) < \infty$, where $|A| = \sqrt{A^*A}$.

An operator $A \in \mathcal{L}(\mathcal{H})$ is called *Hilbert-Schmidt* if and only if $\text{Tr}(A^*A) < \infty$. These operators can be expressed via an integral kernel. Let (M, μ) be a measurable space and $\mathcal{H} = L^2(M, \mu)$. Then $A \in \mathcal{L}(\mathcal{H})$ is Hilbert-Schmidt if and only if there is a function (the

kernel) $K \in L^2(M \times M, \mu \otimes \mu)$ with

$$(Af)(x) = \int_M K(x, y)f(y)d\mu(y). \quad (\text{A.10})$$

Moreover, $\|A\|_2^2 = \int_M |K(x, y)|^2 d\mu(x)d\mu(y)$.

The notions in the following part are taken from [85], Chapter XIII. Let \mathcal{H} be an Hilbert space, then $\bigotimes^n \mathcal{H}$ is defined as the vector space of multilinear functionals on \mathcal{H} : for given $\varphi_1, \dots, \varphi_n \in \mathcal{H}$, $\varphi_1 \otimes \dots \otimes \varphi_n \in \bigotimes^n \mathcal{H}$ by

$$(\varphi_1 \otimes \dots \otimes \varphi_n)(\langle \eta_1, \dots, \eta_n \rangle) = (\varphi_1, \eta_1) \cdots (\varphi_n, \eta_n) \quad (\text{A.11})$$

for any $\langle \eta_1, \dots, \eta_n \rangle \in \mathcal{H} \times \dots \times \mathcal{H}$. The inner-product is defined by

$$(\varphi_1 \otimes \dots \otimes \varphi_n)(\eta_1 \otimes \dots \otimes \eta_n) = (\varphi_1, \eta_1) \cdots (\varphi_n, \eta_n), \quad (\text{A.12})$$

and for any operator $A \in \mathcal{L}(\mathcal{H})$ there is an operator $\Gamma_n(A) \in \mathcal{L}(\bigotimes^n \mathcal{H})$ with

$$\Gamma_n(A)(\varphi_1 \otimes \dots \otimes \varphi_n) = A\varphi_1 \otimes \dots \otimes A\varphi_n. \quad (\text{A.13})$$

It satisfies $\Gamma_n(AB) = \Gamma_n(A)\Gamma_n(B)$.

Next we consider the antisymmetric subspace of $\bigotimes^n \mathcal{H}$, denoted by $\bigwedge^n \mathcal{H}$. Let \mathcal{S}_n denote the permutation group of $\{1, \dots, n\}$, then $\bigwedge^n \mathcal{H}$ is the space spanned by the elements

$$\varphi_1 \wedge \dots \wedge \varphi_n = \frac{1}{\sqrt{n!}} \sum_{\sigma \in \mathcal{S}_n} (-1)^{\text{sgn}(\sigma)} \varphi_{\sigma(1)} \otimes \dots \otimes \varphi_{\sigma(n)}. \quad (\text{A.14})$$

The operator $\Gamma_n(A)$ restricted to $\bigwedge^n \mathcal{H}$ is denoted by $\bigwedge^n(A)$.

A.2.2 Fredholm determinant

Determinant of a trace class operator

If the Hilbert space \mathcal{H} has finite dimension n , then $\bigwedge^n(A)$ is the operator multiplication by $\text{Det}(A)$ (the usual determinant). The Fredholm determinant extends the notion of determinant to infinite dimensional Hilbert spaces. For all trace class operators A acting on a finite-dimensional space \mathcal{H} with dimension n , one can see that

$$\text{Det}(\mathbb{1} + A) = \sum_{k=0}^n \text{Tr}(\bigwedge^k(A)), \quad (\text{A.15})$$

where the term $k = 0$ is by definition set to be 1. In the case $\dim \mathcal{H} = \infty$, $\text{Det}(\mathbb{1} + A)$ is defined by (A.15) with n replaced with ∞ . The sum converges because A is trace class.

In particular, consider the case of an integral operator on $\mathcal{H} = L^2(M, \mu)$ given by a kernel K , i.e.,

$$(Af)(x) = \int_M K(x, y)f(y)d\mu(y). \quad (\text{A.16})$$

If A is trace class and the kernel K is continuous, then

$$\mathrm{Tr} \left(\bigwedge^n (A) \right) = \frac{1}{n!} \int_{M^n} \mathrm{Det} \left(K(x_i, x_j) \right)_{1 \leq i, j \leq n} d\mu(x_1) \cdots d\mu(x_n). \quad (\text{A.17})$$

The determinant (A.15) then writes

$$\mathrm{Det}(\mathbb{1} + A) = \sum_{n=0}^{\infty} \frac{1}{n!} \int_{M^n} \mathrm{Det} \left(K(x_i, x_j) \right)_{1 \leq i, j \leq n} d\mu(x_1) \cdots d\mu(x_n). \quad (\text{A.18})$$

(A.18) is called Fredholm determinant on $\mathcal{H} = L^2(M, \mu)$.

Determinant of a kernel

The Fredholm determinant can also be defined for a kernel K without passing by the operators, as explained e.g. in [7]. Let (M, μ) be a measure space and $A(x)$ be a positive continuous function on M such that $1/A(x) \in L^2(M, \mu)$. We say that a measurable set $S \subset M \times M$ is thin if for all $x_0, y_0 \in M$ the sets

$$\{x \in M \mid (x, y_0) \in S\}, \quad \{x \in M \mid (x_0, y) \in S\}, \quad \{x \in M \mid (x, x) \in S\} \quad (\text{A.19})$$

are of μ -measure zero. A thick subset of $M \times M$ is defined as the complement of a thin subset.

A function $K(x, y)$ on $M \times M$ is a *kernel* if:

- 1) $K(x, y)$ is measurable,
- 2) for some thick open subset $U \subset M \times M$, $K(x, y)$ is continuous on U ,
- 3) $\|K\|_A = \sup_{(x,y) \in M \times M} A(x)A(y)|K(x,y)| < \infty$.

The class of kernels form a vector space with the norm $\|\cdot\|_A$.

For any kernel $K(x, y)$ and $n > 0$ define

$$\Delta_n(K) = \int_{M^n} d\mu(x_1) \cdots d\mu(x_n) \mathrm{Det}[K(x_i, x_j)]_{i,j=1,\dots,n} \quad (\text{A.20})$$

and $\Delta_0(K) = 1$. One can show that

$$\int_{M^n} d\mu(x_1) \cdots d\mu(x_n) |\mathrm{Det}[K(x_i, x_j)]_{i,j=1,\dots,n}| \leq C^n \|K\|_A^n n^{n/2} \quad (\text{A.21})$$

with a constant $C > 0$ (depending on A). Thus $\Delta_n(K)$ is well-defined and the Fredholm determinant attaced to the kernel K is defined by

$$\Delta(K) = \sum_{n=0}^{\infty} \frac{(-1)^n}{n!} \Delta_n(K). \quad (\text{A.22})$$

A.2.3 Fredholm Pfaffian

As for the Fredholm determinant, also the Fredholm Pfaffian of a kernel is defined via series. Consider a kernel a 2×2 matrix kernel K on a measurable space (M, μ) . Assume that K is *antisymmetric*, i.e., $K(x, y) = -K^t(y, x)$. This means

$$K_{1,2}(x, y) = -K_{2,1}(y, x), \quad K_{i,i}(x, y) = -K_{i,i}(y, x) = 0, \quad i = 1, 2. \quad (\text{A.23})$$

Define another kernel J as the 2×2 matrix

$$J(x, y) = \delta_{x,y} \begin{pmatrix} 0 & 1 \\ -1 & 0 \end{pmatrix}. \quad (\text{A.24})$$

The Fredholm Pfaffian is defined in Rains's paper [82]. Denote $\Gamma = \bigcup_{n=0}^{\infty} M^n$, let $S = \{x_1, \dots, x_n\} \subset \Gamma$ and denote by $K(S) = [K(x_i, x_j)]_{i,j=1,\dots,n}$. Then, since K is antisymmetric,

$$\begin{aligned} \text{Pf}[(J + K)(S)] &= \text{Pf}[J(x_i, x_j) + K(x_i, x_j)]_{i,j=1,\dots,n} \\ &= \sum_{S' \subset S} \text{Pf}[K(S')] = \sum_{m=0}^n \sum_{i_1 \neq \dots \neq i_m} \text{Pf}[K(x_{i_k}, x_{i_l})]_{l,k=1,\dots,m}. \end{aligned} \quad (\text{A.25})$$

The Fredholm Pfaffian on the measurable space (M, μ) is defined by

$$\begin{aligned} \text{Pf}(J + K) &= \int_{S \subset \Gamma} \text{Pf}(K(S)) d\mu(S) \\ &= \sum_{n=0}^{\infty} \frac{1}{n!} \int_{M^n} d\mu(x_1) \dots d\mu(x_n) \text{Pf}[K(x_i, x_j)]_{i,j=1,\dots,n}. \end{aligned} \quad (\text{A.26})$$

It is also shown that the connection with the Fredholm determinant is

$$\text{Pf}(J + K)^2 = \text{Det}(\mathbb{1} - JK). \quad (\text{A.27})$$

A.3 Real quaternionic matrices

A quaternion is a linear combination of the basis quaternions $\{e_0 \equiv 1, e_1, e_2, e_3\}$, which satisfy $e_1^2 = e_2^2 = e_3^2 = -1$ and $e_1 e_2 e_3 = -1$. A $N \times N$ quaternionic matrix Q is then $Q = Q^0 + Q^1 e_1 + Q^2 e_2 + Q^3 e_3$ with Q^μ some $N \times N$ matrices. The quaternion of basis e_μ can be represented as 2×2 matrices \hat{e}_μ

$$\hat{e}_0 = \begin{pmatrix} 1 & 0 \\ 0 & 1 \end{pmatrix}, \quad \hat{e}_1 = \begin{pmatrix} i & 0 \\ 0 & -i \end{pmatrix}, \quad \hat{e}_2 = \begin{pmatrix} 0 & 1 \\ -1 & 0 \end{pmatrix}, \quad \hat{e}_3 = \begin{pmatrix} 0 & i \\ i & 0 \end{pmatrix}. \quad (\text{A.28})$$

Therefore the $N \times N$ matrix Q can be represented by a $2N \times 2N$ matrix \hat{Q} . A quaternion is called *real* if the coefficients of Q are real: $q_{j,k}^\mu \in \mathbb{R}$, $\mu = 0, \dots, 3$, $j, k = 1, \dots, N$. The *quaternion conjugate* of a quaternion $q = q_0 + q_1 e_1 + q_2 e_2 + q_3 e_3$ is

$$\bar{q} = q_0 - q_1 e_1 - q_2 e_2 - q_3 e_3, \quad (\text{A.29})$$

the *complex conjugate* of q is

$$q^* = q_0^* + q_1^* e_1 + q_2^* e_2 + q_3^* e_3, \quad (\text{A.30})$$

and the *Hermite conjugate* is

$$q^\dagger = \bar{q}^* = q_0^* - q_1^* e_1 - q_2^* e_2 - q_3^* e_3. \quad (\text{A.31})$$

For real quaternion the modulus of q is given by $|q|^2 = \bar{q}q = q\bar{q} = q_0^2 + q_1^2 + q_2^2 + q_3^2$.

Consider the $2N \times 2N$ representation \hat{Q} of a quaternion matrix Q with elements $Q_{j,k}$, $j, k = 1, \dots, N$. The operations on \hat{Q} reflect to Q as follows. The transposition gives $(Q^T)_{j,k} = -e_2 \bar{q}_{k,j} e_2$, the Hermitian conjugation $(Q^\dagger)_{j,k} = (q_{k,j})^\dagger$, and the time reversal $(Q^R)_{j,k} = e_2 (Q^T)_{j,k} e_2^{-1} = \bar{q}_{k,j}$.

An hermitian matrix, $Q^\dagger = Q$, which is at the same time quaternionic real must satisfy $q_{j,k}^\dagger = \bar{q}_{j,k} = q_{k,j}$, therefore $q_{j,k}^0$ must form a real symmetric matrix and $q_{j,k}^\mu$ real antisymmetric matrices for $\mu = 1, 2, 3$. Consequently the number of independent variables of such matrices is $N + 4N(N-1)/2 = N(2N-1)$.

A $2N \times 2N$ real quaternionic matrix \hat{Q} is diagonalized by a unitary matrix U such that $UU^R = U^R U = \mathbb{1}$. These matrices compose a group, the *unitary symplectic* group $USp(2N)$. Each eigenvalue of \hat{Q} is twice degenerate and each couple corresponds to an eigenvalue of Q (Kramers degeneracy).

A.4 Gaussian ensembles via variational principle

Let $S(p) = -\int p(H) \ln p(H) dH$ be the entropy for the joint distribution function on random matrices p . We want to maximize $S(p)$ under the constraint $C = \int p(H) \text{Tr}(H^2) dH$ be fixed and the constraint of the normalization. Let $B = -\ln(A) - 1$ and λ be the Lagrange multiplier, i.e.,

$$\begin{aligned} S(p) &= -\int p(H) \ln p(H) dH - \lambda \left(\int p(H) \text{Tr}(H^2) dH - C \right) \\ &\quad + (\ln A + 1) \left(\int p(H) dH - 1 \right). \end{aligned} \quad (\text{A.32})$$

Let p_0 be the distribution which maximize $S(p)$, then at first order in δp , $\delta S(p_0) = S(p_0 + \delta p) - S(p_0) = 0$, i.e.,

$$-1 - \ln(p_0) - \lambda \text{Tr}(H^2) + \ln A + 1 = 0, \quad (\text{A.33})$$

which implies $p(H) = A \exp(-\lambda \text{Tr}(H^2))$. The normalization condition fixes the value of A ,

$$A^{-1} = \int e^{-\lambda \text{Tr}(H^2)} dH \equiv a(\lambda). \quad (\text{A.34})$$

The second constraint writes

$$C = \frac{1}{a(\lambda)} \int \text{Tr}(H^2) e^{-\lambda \text{Tr}(H^2)} dH = -\frac{1}{a(\lambda)} \frac{da(\lambda)}{d\lambda}. \quad (\text{A.35})$$

Let us estimate $a(\lambda)$. With the change of variable $X = H\sqrt{\lambda}$, we obtain

$$a(\lambda) = \lambda^{-n/2} \int e^{-\text{Tr}(X^2)} dX \quad (\text{A.36})$$

where n is the dimension of the space where the integral is made, i.e., the number of independent elements of the matrix. The integral over dX being finite and independent of λ , it follows that

$$\frac{da(\lambda)}{d\lambda} = a(\lambda) \frac{-n}{2\lambda}, \quad (\text{A.37})$$

and finally $\lambda = \frac{n}{2C}$. Since we want $\lambda = 1/2N$, it follows that

$$C = nN, \quad n = N + \frac{1}{2}\beta N(N-1). \quad (\text{A.38})$$

A.5 Hermite polynomials

The Hermite polynomials $\{p_k^H\}$ are orthogonal with respect to the weight e^{-x^2} on \mathbb{R} , i.e.,

$$\int_{\mathbb{R}} p_k^H(x) p_l^H(x) e^{-x^2} dx = \begin{cases} 0 & \text{if } k \neq l, \\ \sqrt{\pi} 2^k k! & \text{if } k = l. \end{cases} \quad (\text{A.39})$$

They satisfy the recursion relations

$$\begin{aligned} p_0^H(x) &= 1, \\ p_1^H(x) &= 2x, \\ p_k^H(x) &= 2x p_{k-1}^H(x) - 2(k-1) p_{k-2}^H(x), \quad k \geq 2, \end{aligned} \quad (\text{A.40})$$

thus the leading coefficient of $p_k^H(x)$ is $u_k = 2^k$. Another representation of Hermite polynomials is

$$p_k^H(x) = e^{x^2} \frac{d^k}{dx^k} e^{-x^2}. \quad (\text{A.41})$$

An asymptotics of Hermite polynomial relevant for our purpose is the following [99]. For $x = (2n+1)^{1/2} - 2^{-1/2} n^{-1/6} t$, t bounded,

$$e^{-x^2/2} p_n^H(x) = (2\pi)^{1/4} 2^{n/2} (n!)^{1/2} n^{-1/12} (\text{Ai}(t) + \mathcal{O}(n^{-2/3})), \quad (\text{A.42})$$

and for $x = (2n+1)^{1/2} \cos \psi$, with $\psi \in (0, \pi)$,

$$e^{-x^2/2} p_n^H(x) = \frac{2^{n/2} (n!)^{1/2}}{(\pi n/2)^{1/4}} \frac{1}{\sqrt{\sin \psi}} \left(\sin \left[\left(\frac{1}{2}n + \frac{1}{4} \right) (\sin(2\psi) - 2\psi) + \frac{3}{4}\pi \right] + \mathcal{O}(n^{-1}) \right). \quad (\text{A.43})$$

In all these formulas the \mathcal{O} -terms hold uniformly.

A.6 Kernel for $\beta = 2$ Dyson's Brownian motion

First of all we develop the transition function Φ defined in (3.86) in terms of orthogonal polynomials involving the Hermite polynomials p_k^H . Let us define

$$f_k(x) = (\sqrt{2\pi N} 2^k k!)^{-1/2} p_k^H(x/\sqrt{2N}) e^{-x^2/4N}, \quad (\text{A.44})$$

then, for $t' > t$,

$$\Phi_{t,t'}(x, x') = \sum_{k=0}^{\infty} f_k(x) f_k(x') q(t' - t)^k. \quad (\text{A.45})$$

Consider $t_0 < t_1 < t_2 < t_3$ with $t_1 - t_0 \gg 1$ and $t_3 - t_2 \gg 1$. Denote by $Q_1 = e^{-(t_1 - t_0)/2N}$, $q = e^{-(t_2 - t_1)/2N}$, and $Q_2 = e^{-(t_3 - t_2)/2N}$. We want the expression of the kernel in the limit $t_0 \rightarrow -\infty$ and $t_3 \rightarrow \infty$, i.e., $Q_1 \rightarrow 0$ and $Q_2 \rightarrow 0$.

First we derive $K_N(x, t_2; x', t_1)$. We can write it as product of matrices as follows. Let

$$\begin{aligned} u &= [f_i(x) Q_2^i]_{i=0, \dots, \infty}, & R &= [f_i(x_j^3)]_{\substack{i=0, \dots, \infty, \\ j=0, \dots, N-1}}, \\ v^t &= [f_j(x') Q_1^j]_{j=0, \dots, \infty}, & L &= [f_j(x_i^0)]_{\substack{i=0, \dots, N-1, \\ j=0, \dots, \infty}}, \\ D &= [(Q_1 Q_2 q)^i \delta_{i,j}]_{i,j=0, \dots, \infty}. \end{aligned} \quad (\text{A.46})$$

The $N \times N$ matrix to be inverted writes $A = LDR$ and the kernel $K_N = uRA^{-1}Lv$. Dividing the indices as follows $\{0, \dots, \infty\} = \{0, \dots, N-1\} \cup \{N, \dots, \infty\}$ we write the matrices as blocks. The index 1 refers to the set $\{0, \dots, N-1\}$ and the index 2 to the set $\{N, \dots, \infty\}$, explicitly

$$\begin{aligned} K_N &= [u_1 \ u_2] [R_{1,1} \ R_{2,1}]^t A^{-1} [L_{1,1} \ L_{1,2}] [v_1 \ v_2]^t, \\ A &= [L_{1,1} \ L_{1,2}] \begin{bmatrix} D_{1,1} & 0 \\ 0 & D_{2,2} \end{bmatrix} [R_{1,1} \ R_{2,1}]^t. \end{aligned} \quad (\text{A.47})$$

The inverse of A can be well approximated by $B = R_{1,1}^{-1} D_{1,1}^{-1} L_{1,1}^{-1}$. The inverse $D_{1,1}$ obviously exists. $L_{1,1}$ and $R_{1,1}$ are also invertible provided that both the initial positions x_i^0 and the final positions x_i^3 are distinct. In fact their determinants are Vandermonde determinants. A simple computation shows $AB = \mathbb{1} + Q_1 Q_2 q \mathcal{O}(1)$, $\mathcal{O}(1)$ meaning a matrix with coefficients of order one. Thus $A^{-1} = B(\mathbb{1} + Q_1 Q_2 q \mathcal{O}(1))$. Then

$$\begin{aligned} K_N &= (u_1 R_{1,1} + u_2 R_{2,1}) R_{1,1}^{-1} D_{1,1}^{-1} L_{1,1}^{-1} (\mathbb{1} + Q_1 Q_2 q \mathcal{O}(1)) (L_{1,1} v_1 + L_{1,2} v_2) \\ &= u_1 D_{1,1}^{-1} v_1 (1 + \mathcal{O}(Q_1 Q_2 q)) + u_1 D_{1,1}^{-1} L_{1,1}^{-1} (\mathbb{1} + Q_1 Q_2 q \mathcal{O}(1)) L_{1,2} v_2 \end{aligned} \quad (\text{A.48})$$

$$+ u_2 R_{2,1} R_{1,1}^{-1} (\mathbb{1} + Q_1 Q_2 q \mathcal{O}(1)) D_{1,1}^{-1} v_2 + u_2 \cdots D_{1,1}^{-1} v_2. \quad (\text{A.49})$$

Since

$$u_1 D_{1,1}^{-1} = [f_0(x) \ f_1(x) (Q_2 q)^{-1} \ \cdots \ f_{N-1}(x) (Q_2 q)^{N-1}] \quad (\text{A.50})$$

and

$$v_2 = Q_2^N [f_N(x') \ f_{N+1}(x') Q_2 \ \cdots]^t, \quad (\text{A.51})$$

the second term is of order Q_2 . Similarly the third term is of order Q_1 . The fourth term is of order $Q_1 Q_2$. Thus in the limit $Q_1 \rightarrow 0$ and $Q_2 \rightarrow 0$ the kernel is

$$K_N(x, t_2; x', t_1) = u_1 D_{1,1}^{-1} v_1 = \sum_{k=0}^{N-1} f_k(x) f_k(x') q^{-k}. \quad (\text{A.52})$$

The derivation formula for $K_N(x, t_1; x', t_2)$ is deduced in an analogous way. To obtain the term with the double sum we need only to remark that in this case $D = [(Q_1 Q_2 / q)^i \delta_{i,j}]_{i,j=0,\dots,\infty}$ because the intervals $[t_0, t_2]$ and $[t_1, t_3]$ intersect. Thus

$$K_N(x, t_1; x', t_2) = - \sum_{k=0}^{\infty} f_k(x) f_k(x') q^k + \sum_{k=0}^{N-1} f_k(x) f_k(x') q^k = - \sum_{k=N}^{\infty} f_k(x) f_k(x') q^k. \quad (\text{A.53})$$

A.7 Convergence of the extended Hermite kernel to the extended Airy kernel

Recently new bounds on the Hermite polynomials are obtained by Krasikov [55]. They implies

$$\max_{x \in \mathbb{R}} (|p_k^H(x/\sqrt{2N})| e^{-x^2/4N}) \leq \begin{cases} C 2^{2/k} \sqrt{k!} k^{-1/12}, & k \geq 1, \\ C, & k = 0 \end{cases} \quad (\text{A.54})$$

for some constant $C > 0$.

With this estimate we obtain that the rescaled Hermite kernel is uniformly bounded in the spatial arguments.

Lemma A.12.

$$\lim_{N \rightarrow \infty} N^{1/3} K_N^H(x = 2N + uN^{1/3}, 2sN^{2/3}; y = 2N + u'N^{1/3}, 2s'N^{2/3}) = A(u, v; u', v') \quad (\text{A.55})$$

uniformly in $u, u' \in \mathbb{R}$.

Proof. First we want to show that

$$N^{1/3} K_N^H(x = 2N + uN^{1/3}, 2sN^{2/3}; y = 2N + u'N^{1/3}, 2s'N^{2/3}) \quad (\text{A.56})$$

is uniformly bounded in $u, u' \in \mathbb{R}$ for N large enough. Consider first the case $s - s' = \Delta s > 0$. Then

$$\begin{aligned} (\text{A.56}) &= \sum_{k=-N}^{-1} e^{\Delta s k N^{-1/3}} N^{1/3} \frac{p_{N+k}^H(x/\sqrt{2N}) e^{-x^2/4N} p_{N+k}^H(y/\sqrt{2N}) e^{-y^2/4N}}{\sqrt{2\pi N} 2^{N+k} (N+k)!} \\ &= \frac{1}{N^{1/3}} \sum_{\kappa \in I} e^{\kappa \Delta s} N^{2/3} \frac{p_{N+\kappa N^{1/3}}^H(x/\sqrt{2N}) e^{-x^2/4N} p_{N+\kappa N^{1/3}}^H(y/\sqrt{2N}) e^{-y^2/4N}}{\sqrt{2\pi N} 2^{N+\kappa N^{1/3}} (N+\kappa N^{1/3})!} \end{aligned}$$

where $I = \{-N, \dots, -1\}N^{-1/3}$. This last sum can be written as an integral of a function $f_N(u, u', \Delta s)$ which is constant on intervals of width $N^{-1/3}$. If we prove that $|f_N|$ is bounded by an integrable function, then by dominated convergence we can exchange the limit and the integral. (A.43) implies that this function converges pointwise to the integrand of the extended Airy kernel. Thus the limit will be the desired one.

In what follow the C_i are positive constant which do not depend on u, u' . Using (A.54) we obtain

$$\begin{aligned}
|(A.56)| &\leq C + C_2 \frac{1}{N^{1/3}} \sum_{\kappa \in J} e^{\kappa \Delta s} N^{2/3} \frac{1}{(1 + \kappa N^{-1/3})^{1/6}} \\
&\leq C + C_3 \int_{-N^{2/3}}^{-N^{1/3}} d\kappa e^{\kappa \Delta s} N^{1/18} + C_3 \int_{-N^{1/3}}^{-N^{-1/3}} d\kappa e^{\kappa \Delta s} (1 - N^{-1/3})^{-1/6} \\
&\leq C + C_4 N^{1/18} \frac{e^{-N^{1/3} \Delta s}}{\Delta s} + \frac{1 - e^{-N^{1/3} \Delta s}}{\Delta s} \tag{A.57}
\end{aligned}$$

with $J = \{-N + 1, \dots, -1\}N^{-1/3}$.

In the case $\Delta s < 0$ is similar. In the same way we get

$$\begin{aligned}
|(A.56)| &\leq C_5 \frac{1}{N^{1/3}} \sum_{\kappa \in L} e^{\kappa \Delta s} N^{2/3} \frac{1}{(1 + \kappa N^{-1/3})^{1/6}} \\
&\leq C_6 \int_0^\infty d\kappa e^{\kappa \Delta s} \leq \frac{C_6}{|\Delta s|} \tag{A.58}
\end{aligned}$$

with $L = N^{-1/3}\mathbb{N}$. □

A.8 Numerical analysis

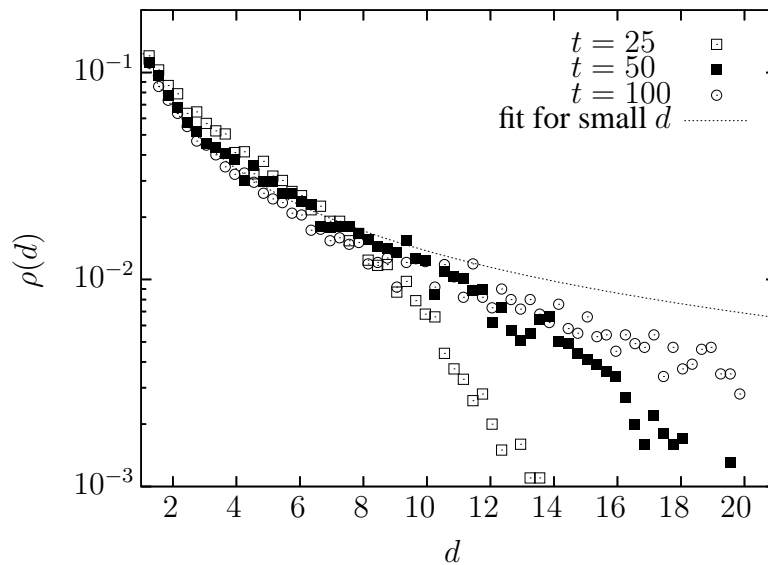


Figure A.6: Probability density of the distribution of the distance d for $t = 25, 50, 100$. The fit is $\rho = 2.2d(1 + 16d^2)^{-1} \simeq 0.14/d$.

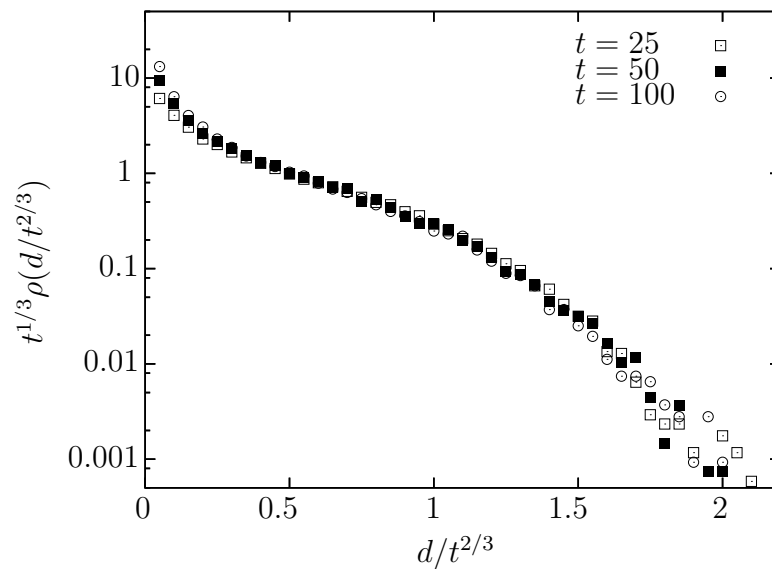


Figure A.7: Rescaled probability density of the distribution of the distance d for $t = 25, 50, 100$.

t	$\mathbb{E}(\text{deg})$	$\mathbb{E}(d)/t^{1/3}$	$\text{Var}(d(t))/t$
25	2.42	0.57 ± 0.027	0.24 ± 0.018
50	2.43	0.52 ± 0.028	0.22 ± 0.022
100	2.38	0.57 ± 0.034	0.26 ± 0.027
150	2.43	0.56 ± 0.033	0.20 ± 0.022
200	2.36	0.54 ± 0.036	0.22 ± 0.026
300	2.48	0.56 ± 0.039	0.22 ± 0.028
400	2.31	0.52 ± 0.040	0.22 ± 0.029
500	2.41	0.51 ± 0.039	0.19 ± 0.026
600	2.48	0.61 ± 0.047	0.26 ± 0.034
700	2.42	0.57 ± 0.045	0.23 ± 0.032
800	2.36	0.60 ± 0.050	0.27 ± 0.043
1000	2.37	0.54 ± 0.049	0.24 ± 0.037
Mean	2.40	0.56	0.23

Table A.1: Results of the simulations for different values of t and 1000 runs each.

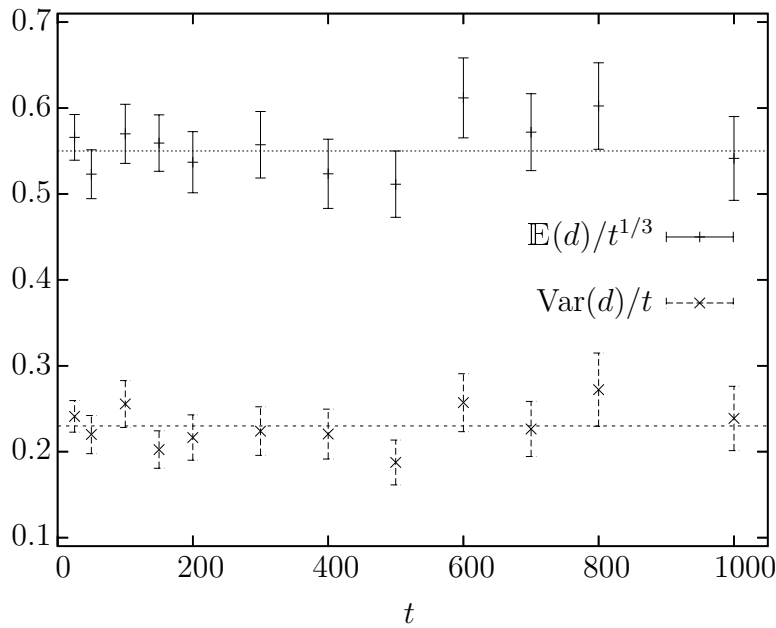


Figure A.8: Mean and variance for values of t up to 1000. For each t the simulation consists in 1000 runs.

Bibliography

- [1] M. Abramowitz and I.A. Stegun, *Pocketbook of Mathematical Functions*, Verlag Harri Deutsch, Thun-Frankfurt am Main, 1984.
- [2] M. Adler and P. van Moerbeke, *PDE's for the joint distribution of the Dyson, Airy and Sine processes*, arXiv:math.PR/0403504, to appear in Ann. Probab. (2005).
- [3] Y. Akutsu and N. Akutsu, *Relationship between the anisotropic interface tension, the scaled interface width and the equilibrium shape in two dimensions*, J. Phys. A: Math. Gen. **19** (1986), 2813–2820.
- [4] Y. Akutsu, N. Akutsu, and T. Yamamoto, *Universal jump of Gaussian curvature at the facet edge of a crystal*, Phys. Rev. Lett. **61** (1988), 424–427.
- [5] D.J. Aldous and P. Diaconis, *Hammersley's interacting particle process and longest increasing subsequences*, Probab. Theory Relat. Fields **103** (1995), 199–213.
- [6] D.J. Aldous and P. Diaconis, *Longest increasing subsequences: from patience sorting to the Baik-Deift-Johansson theorem*, Bull. Amer. Math. Soc. **36** (1999), 413–432.
- [7] G. Anderson and O. Zeitouni, *Lecture notes on random matrices*, 2003.
- [8] A.F. Andreev, Sov. Phys. JETP **53** (1981), 1063.
- [9] R.M. Baer and P. Brock, *Natural sorting over permutation spaces*, Math. Comp. **22** (1968), 385–510.
- [10] J. Baik, P.A. Deift, and K. Johansson, *On the distribution of the length of the longest increasing subsequence of random permutations*, J. Amer. Math. Soc. **12** (1999), 1119–1178.
- [11] J. Baik and E.M. Rains, *Limiting distributions for a polynuclear growth model with external sources*, J. Stat. Phys. **100** (2000), 523–542.
- [12] J. Baik and E.M. Rains, *The asymptotics of monotone subsequences of involutions*, Duke Math. J. **109** (2001), 205–281.

-
- [13] J. Baik and E.M. Rains, *Symmetrized random permutations*, Random Matrix Models and Their Applications, vol. 40, Cambridge University Press, 2001, pp. 1–19.
- [14] R. Balian, *Random matrices and information theory*, Nuovo Cimento **57** (1968), 183–193.
- [15] A.L. Barabási and H.E. Stanley, *Fractal concepts in surface growth*, Cambridge University Press, Cambridge, 1995.
- [16] H.W.J. Blöte and H.J. Hilhorst, *Roughening transitions and the zero-temperature triangular Ising antiferromagnet*, J. Phys. A: Math. Gen. **15** (1982), L631–L637.
- [17] H.W.J. Blöte, H.J. Hilhorst, and B. Nienhuis, *Triangular SOS models and cubic-crystal shapes*, J. Phys. A: Math. Gen. **17** (1984), 3559–3581.
- [18] A. Borodin, *Biorthogonal ensembles*, Nuclear Phys. B **536** (1999), 704–732.
- [19] A. Borodin and G. Olshanski, *Continuous time Markov chains related to Plancherel measure (announcement of results)*, arXiv:math-ph/0402064 (2004).
- [20] R. Cerf and R. Kenyon, *The low-temperature expansion of the Wulff crystal in the 3D-Ising model*, Comm. Math. Phys. **222** (2001), 147–179.
- [21] H. Cohn, N. Elkies, and J. Propp, *Local statistics for random domino tilings of the Aztec diamond*, Duke Math. J. **85** (1996), 117–166, arXiv:math.CO/0008243.
- [22] H. Cohn, M. Larsen, and J. Propp, *The shape of a typical boxed plane partition*, New York J. Math. **4** (1998), 137–165.
- [23] F.J. Dyson, *A Brownian-motion model for the eigenvalues of a random matrix*, J. Math. Phys. **3** (1962), 1191–1198.
- [24] F.J. Dyson, *The three fold way. Algebraic structure of symmetry groups and ensembles in quantum mechanics*, J. Math. Phys. **3** (1962), 1199–1215.
- [25] T.L. Einstein and O. Pierre-Louis, *Implications of random-matrix theory for terrace-width distributions on vicinal surfaces: improved approximations and exact results*, Surf. Sci. **424** (1999), L299–L308.
- [26] T.L. Einstein, H.L. Richards, S.D. Cohen, and O. Pierre-Louis, *Terrace-width distributions and step-step repulsions on vicinal surfaces: symmetries, scaling, simplifications, subtleties, and Schrödinger*, Surf. Sci. **493** (2001), 460–474.
- [27] B. Eynard and M.L. Mehta, *Matrices couples in a chain. I. Eigenvalues correlations*, J. Phys. A: Math. Gen. **31** (1998), 4449–4456.
- [28] P.L. Ferrari, *Polynuclear growth on a flat substrate and edge scaling of GOE eigenvalues*, math-ph/0402053 (2004), Comm. Math. Phys. (online first).

- [29] P.L. Ferrari, M. Prähofer, and H. Spohn, *Fluctuations of an atomic ledge bordering a crystalline facet*, Phys. Rev. E, Rapid Communications **69** (2004), 035102(R).
- [30] P.L. Ferrari and H. Spohn, *Last branching in directed last passage percolation*, Markov Process. Related Fields **9** (2003), 323–339.
- [31] P.L. Ferrari and H. Spohn, *Step fluctuations for a faceted crystal*, J. Stat. Phys. **113** (2003), 1–46.
- [32] P.J. Forrester, T. Nagao, and G. Honner, *Correlations for the orthogonal-unitary and symplectic-unitary transitions at the hard and soft edges*, Nuclear Phys. B **553** (1999), 601–643.
- [33] T. Funaki and H. Spohn, *Motion by mean curvature from the Ginzburg-Landau $\nabla\varphi$ interface model*, Comm. Math. Phys. **185** (1997), 1–36.
- [34] I.C. Gohberg and M.G. Krein, *Introduction to the theory of nonselfadjoint operators*, Transl. Math. Monogr., vol. 35, Providence, RI, 1969.
- [35] J. Gravner, C.A. Tracy, and H. Widom, *Limit theorems for height fluctuations in a class of discrete space and time growth models*, J. Stat. Phys. **102** (2001), 1085–1132.
- [36] C. Greene, *An extension of Schensted’s theorem*, Adv. Math. **14** (1974), 254–265.
- [37] E.E. Gruber and W.W. Mullins, *On the theory of anisotropy of crystalline surface tension*, J. Phys. Chem. Solids **28** (1967), 875–887.
- [38] J. Gustavsson, *Gaussian fluctuations of eigenvalues in the GUE*, arXiv:math.PR/0401076 (2004).
- [39] J.M. Hammersley, *A few seedlings of research*, Proc. Sixth Berkeley Symp. Math. Statist. and Probability (University of California Press, ed.), vol. 1, 1972, pp. 345–394.
- [40] T. Imamura and T. Sasamoto, *Fluctuations of a one-dimensional polynuclear growth model in a half space*, J. Stat. Phys. **115** (2004), 749–803.
- [41] K. Johansson, *The longest increasing subsequence in a random permutation and a unitary random matrix model*, Math. Res. Lett. **5** (1998), 63–82.
- [42] K. Johansson, *On fluctuations of eigenvalues of random Hermitian matrices*, Duke Math. J. **91** (1998), 151–2003.
- [43] K. Johansson, *Shape fluctuations and random matrices*, Comm. Math. Phys. **209** (2000), 437–476.

- [44] K. Johansson, *Transversal fluctuations for increasing subsequences on the plane*, Probab. Theory Related Fields **116** (2000), 445–456.
- [45] K. Johansson, *Non-intersecting paths, random tilings and random matrices*, Probab. Theory Related Fields **123** (2002), 225–280.
- [46] K. Johansson, *Discrete polynuclear growth and determinantal processes*, Comm. Math. Phys. **242** (2003), 277–329.
- [47] K. Johansson, *The arctic circle boundary and the Airy process*, arXiv:math.PR/0306216, to appear in Ann. Probab. **33** (2005).
- [48] K. Kardar, G. Parisi, and Y.Z. Zhang, *Dynamic scaling of growing interfaces*, Phys. Rev. Lett. **56** (1986), 889–892.
- [49] S. Karlin and L. McGregor, *Coincidence probabilities*, Pacific J. **9** (1959), 1141–1164.
- [50] P.W. Kasteleyn, *Dimer statistics and phase transitions*, J. Math. Phys. **4** (1963), 287–293.
- [51] R. Kenyon, *The planar dimer model with boundary: a survey*, Directions in mathematical quasicrystals, CRM Monogr. Ser. **13** (2000), 307–328.
- [52] R. Kenyon, *Dominos and Gaussian free field*, Ann. Probab. **29** (2001), 1128–1137.
- [53] R. Kenyon, A. Okounkov, and S. Sheffield, *Dimers and amoebae*, arXiv:math-ph/0311005, to appear in Ann. Math. (2003).
- [54] W. König, *Orthogonal polynomial ensembles in probability theory*, arXiv:math.PR/0403090 (2004).
- [55] I. Krasikov, *New bounds on the Hermite polynomials*, arXiv:math.CA/0401310 (2004).
- [56] H. Kunz, *Matrices aléatoires en physique*, Presse Polytechniques et Universitaires Romandes, Lausanne, 1998.
- [57] L.J. Landau, *Bessel functions: monotonicity and bounds*, J. London Math. Soc. **61** (2000), 197–215.
- [58] A. Lenard, *Correlation functions and the uniqueness of the state in classical statistical mechanics*, Comm. Math. Phys. **30** (1973), 35–44.
- [59] A. Lenard, *States of classical statistical mechanical system of infinitely many particles II*, Arch. Rational Mech. Anal. **59** (1975), 240–256.

- [60] C. Licea, C.M. Newman, and M.S.T. Piza, *Superdiffusivity in first-passage percolation*, Probab. Theory Related Fields **106** (1996), 559–591.
- [61] B.F. Logan and L.A. Shepp, *A variational problem for random Young tableaux*, Adv. Math. **26** (1977), 206–222.
- [62] M.L. Mehta, *Random Matrices*, 2nd ed., Academic Press, San Diego, 1991.
- [63] T. Michely and J. Krug, *Islands, mounds and atoms*, Springer Verlag, 2004.
- [64] J. Neveu, *Processus ponctuels*, *École d’été de Saint Flour*, Lecture Notes in Mathematics, vol. 598, Springer-Verlag, 1976, pp. 249–445.
- [65] C.M. Newman and M.S.T. Piza, *Divergence of shape fluctuations in two dimensions*, Ann. Probab. **23** (1995), 977–1005.
- [66] M. Nowicki, C. Bombis, A. Emundts, and H.P. Bonzel, *Absolute surface free energies of Pb*, Surf. Sci. **511** (2002), 83–96.
- [67] M. Nowicki, C. Bombis, A. Emundts, H.P. Bonzel, and P. Wynblatt, *Universal exponents and step-step interactions on vicinal Pb (111) surfaces*, Europhys. Lett. **59** (2002), 239–244.
- [68] A.M. Odlyzko and E.M. Rains, *On longest increasing subsequences in random permutations*, Analysis, Geometry, Number Theory: The Mathematics of Leon Ehrenpreis (E.L. Grinberg, S. Berhanu, M. Knopp, G. Mendoza, and E.T. Quinto, eds.), Contemporary Math., vol. 251, Amer. Math. Soc., 2000, pp. 439–451.
- [69] A. Okounkov and N. Reshetikhin, *Correlation function of Schur process with application to local geometry of a random 3-dimensional Young diagram*, J. Amer. Math. Soc. **16** (2003), 581–603.
- [70] B.K. Øksendal, *Stochastic differential equations*, 5th ed., Springer Verlag, Berlin, 1998.
- [71] L. Pastur, *Random matrices as paradigm*, Mathematical Physics 2000 (Singapore), World Scientific, 2000, pp. 216–266.
- [72] L. Pastur and A. Lejay, *Matrices aléatoires: statistique asymptotique des valeurs propres*, *Séminaire de probabilités XXXVI*, Lecture Notes in Mathematics, vol. 1801, Springer-Verlag, 2003, pp. 135–164.
- [73] A. Pimpinelli and J. Villain, *Physics of Crystal Growth*, Cambridge University Press, Cambridge, 1998.
- [74] M.S.T. Piza, *Directed polymers in a random environment: some results on fluctuations*, J. Stat. Phys. **89** (1997), 581–603.

- [75] V.L. Pokrovsky and A.L. Talapov, *Ground state, spectrum, and phase diagram of two-dimensional incommensurate crystals*, Phys. Rev. Lett. **42** (1978), 65–68.
- [76] M. Prähofer, *Stochastic Surface Growth*, Ph.D. thesis, Ludwig-Maximilians-Universität, München, <http://edoc.ub.uni-muenchen.de/archive/00001381/>, 2003.
- [77] M. Prähofer and H. Spohn, *Universal distributions for growth processes in $1 + 1$ dimensions and random matrices*, Phys. Rev. Lett. **84** (2000), 4882–4885.
- [78] M. Prähofer and H. Spohn, *Current fluctuations for the totally asymmetric simple exclusion process*, In and out of equilibrium (V. Sidoravicius, ed.), Progress in Probability, Birkhäuser, 2002.
- [79] M. Prähofer and H. Spohn, *Exact scaling function for one-dimensional stationary KPZ growth*, J. Stat. Phys. **115** (2002), 255–279.
- [80] M. Prähofer and H. Spohn, *Exact scaling function for one-dimensional stationary KPZ growth*, <http://www-m5.ma.tum.de/KPZ/> (2002).
- [81] M. Prähofer and H. Spohn, *Scale invariance of the PNG droplet and the Airy process*, J. Stat. Phys. **108** (2002), 1071–1106.
- [82] E.M. Rains, *Correlation functions for symmetrized increasing subsequences*, arXiv:math.CO/0006097 (2000).
- [83] M. Reed and B. Simon, *Methods of Modern Mathematical Physics I: Functional analysis*, Academic Press, New York, 1978.
- [84] M. Reed and B. Simon, *Methods of Modern Mathematical Physics II: Fourier analysis, self-adjointness*, Academic Press, New York, 1978.
- [85] M. Reed and B. Simon, *Methods of Modern Mathematical Physics IV: Analysis of Operators*, Academic Press, New York, 1978.
- [86] L.C.G. Roger and Z. Shi, *Interacting Brownian particles and the Wigner law*, Probab. Theory Related Fields **95** (1993), 555–570.
- [87] D. Ruelle, *Statistical mechanics, rigorous results*, Benjamin, New York, 1969.
- [88] C. Schensted, *Longest increasing and decreasing subsequences*, Canad. J. Math. **16** (1961), 179–191.
- [89] T. Seppäläinen, *Hydrodynamic scaling, convex duality and asymptotic shapes of growth models*, Markov Process. Related Fields **4** (1998), 1–26.
- [90] T. Shirai and Y. Takahashi, *Random point fields associated with certain Fredholm determinants I: Fermion, Poisson and Boson point processes*, J. Funct. Anal. **211** (2004), 424–456.

-
- [91] A. Soshnikov, *Determinantal random point fields*, Russian Math. Surveys **55** (2000), 923–976.
- [92] A. Soshnikov, *Janossy densities II. Pfaffian ensembles*, J. Stat. Phys. **113** (2003), 611–622.
- [93] H. Spohn, *Tracer dynamics in Dyson’s model of interacting Brownian particles*, J. Stat. Phys. **47** (1987), 669–680.
- [94] H. Spohn, *Fixed points of functional renormalization group for critical wetting*, Europhys. Lett. **14** (1991), 689–692.
- [95] H. Spohn, *Dyson’s model of interacting Brownian motions at arbitrary coupling strength*, Markov Processes Relat. Fields **4** (1998), 649–661.
- [96] J.R. Stembridge, *Nonintersecting paths, Pfaffians, and plane partitions*, Adv. Math. **83** (1990), 96–131.
- [97] S. Surnev, P. Coenen, B. Voigtländer, H.P. Bonzel, and P. Wynblatt, *Flatness and shape of (111) facets of equilibrated Pb crystals*, Phys. Rev. B **56** (1997), 12131–12134.
- [98] B. Sutherland, *Quantum many-body problem in one dimension: ground state*, J. Math. Phys. **12** (1970), 246–250.
- [99] G. Szegő, *Orthogonal Polynomials*, 3th ed., American Mathematical Society Providence, Rhode Island, 1967.
- [100] C.A. Tracy and H. Widom, *Level-spacing distributions and the Airy kernel*, Comm. Math. Phys. **159** (1994), 151–174.
- [101] C.A. Tracy and H. Widom, *On orthogonal and symplectic matrix ensembles*, Comm. Math. Phys. **177** (1996), 727–754.
- [102] C.A. Tracy and H. Widom, *Correlation functions, cluster functions, and spacing distributions for random matrices*, J. Stat. Phys. **92** (1998), 809–835.
- [103] C.A. Tracy and H. Widom, *Distribution functions for largest eigenvalues and their applications*, Proceedings of ICM 2002, vol. 3, 2002.
- [104] C.A. Tracy and H. Widom, *A system of differential equations for the Airy process*, Elect. Comm. in Probab. **8** (2003), 93–98.
- [105] C.A. Tracy and H. Widom, *Matrix kernel for the Gaussian orthogonal and symplectic ensembles*, arXiv:math-ph/0405035 (2004).

- [106] S.M. Ulam, *Monte Carlo calculations in problems of mathematical physics*, Modern Mathematics for the Engineer (E.F.Beckenbach, ed.), vol. II, McGraw-Hill, New York, Toronto, London, 1961, pp. 261–277.
- [107] H. van Beijeren and I. Nolden, *The roughening transition*, Structure and Dynamics of Surfaces II (W. Schommers and P. von Blackenhagen, eds.), Springer Verlag, 1987, pp. 259–300.
- [108] A.M. Vershik and S.V. Kerov, *Asymptotics of Plancherel measure of symmetric group and the limiting form of Young tables*, Sov. Math. Dokl. **18** (1977), 527–531.
- [109] J. Villain and P. Bak, *Two-dimensional Ising model with competing interactions: floating phase, walls and dislocations*, J. Physique **42** (1981), 657–658.
- [110] H. Widom, *On asymptotic for the Airy process*, J. Stat. Phys. **115** (2004), 1129–1134.
- [111] F.Y. Wu, *Remarks on the modified potassium dihydrogen phosphate model of a ferroelectric*, Phys. Rev. **168** (1968), 539–543.